ACID DIVERSION IN CARBONATE RESERVOIRS USING POLYMER-BASED IN-SITU GELLED ACIDS

Dissertation

by

AHMED MOHAMED MOHAMED GOMAA

Submitted to the Office of Graduate Studies of
Texas A&M University
in partial fulfillment of the requirements for the degree of

DOCTOR OF PHILOSOPHY

May 2011

Major Subject: Petroleum Engineering

ACID DIVERSION IN CARBONATE RESERVOIRS USING POLYMER-BASED IN-SITU GELLED ACIDS

Dissertation

by

AHMED MOHAMED MOHAMED GOMAA

Submitted to the Office of Graduate Studies of
Texas A&M University
in partial fulfillment of the requirements for the degree of

DOCTOR OF PHILOSOPHY

Approved by:

Chair of Committee,	Hisham A. Nasr-El-Din
Committee Members,	A. Daniel Hill
	Jerome J. Schubert
	Mahmoud El-Halwagi
Head of Department,	Stephen A. Holditch

May 2011

Major Subject: Petroleum Engineering

ABSTRACT

Acid Diversion in Carbonate Reservoirs Using Polymer-Based In-Situ Gelled Acids.

(May 2011)

Ahmed Mohamed Mohamed Gomaa, B.S., Cairo University;

M.S., Cairo University

Chair of Advisory Committee: Dr. Hisham A. Nasr-El-Din

Diversion in carbonates is more difficult than in sandstones because of the ability of acid to significantly increase the permeability in carbonates as it reacts in the pore spaces and flow channels of matrix. In-situ gelled acids that are based on polymers have been used in the field for several years and were the subject of many lab studies. An extensive literature survey reveals that there are conflicting opinions about using these acids. On one hand, these acids were used in the field with mixed results. Recent lab work indicated that these acids can cause damage under certain conditions. There is no agreement on when this system can be successfully applied in the field. Therefore, this study was conducted to better understand this acid system and determine factors that impact its performance.

Lab test of polymer-based in-situ gelled acids reveal that polymer and other additives separate out of the acid when these acids are prepared in high salinity water. In coreflood tests, in-situ gelled acid formed a gel inside 20” long core samples, and the

acid changed its direction several times. Unexpectantly, the core's permeability was reduced at low shear rate.

Wormhole length increased as the shear rate was increased; while the diameter of the wormhole increased as the acid cumulative injected volume was increased. CT scan indicated the presence of gel residue inside and around the wormhole. Gel residue increased at low shear rates. Material balance on the cross-linker indicated that a significant amount of the crosslinker was retained in the core.

Based on the results obtained from this study the in-situ gelled acids should be used only at low HCl concentrations (5 wt% HCl). Acid should be prepared in low salinity water and the acid injection rate should be determined based on the expected shear rate in the formation. A core flood experiment is recommended to confirm optimum injected rate. Well flow back is needed to minimize the residual gel inside the formation. The data obtained in this study can be used as a guideline for injection rate selection.

DEDICATION

This dissertation is dedicated to my parents, my wife, and my little baby.

ACKNOWLEDGEMENTS

I would like to take this opportunity to express my deepest gratitude and appreciation to my advisor and committee chair, Dr. Hisham A. Nasr-El-Din, for his continuous encouragement and especially for his academic guidance.

Appreciation is extended to the members of my committee, Dr. A. Daniel Hill, Dr. Jerome J. Schubert, Dr. Mahmoud El-Halwagi, for their help.

I also would like thank my colleagues, Mohamed Mahmoud and Ahmed Rabie, for their friendship and help during my graduate study.

Finally, I would like to acknowledge the financial support of the Texas A&M U., the Texas Engineering Experiment Station of Texas A&M University and Crisman Institute for Petroleum Research. Also, I wish to thank Saudi Aramco Company for partially funding this work. The facilities and resources provided by the Harold Vance Department of Petroleum Engineering of Texas A&M University are gratefully acknowledged.

TABLE OF CONTENTS

Page

Page

LIST OF FIGURES

Page

Page

Page

Page

LIST OF TABLES

Page

Page

1. INTRODUCTION

Unlike matrix stimulation of sandstone, carbonate acidizing provides an opportunity to improve permeability around wellbore by creating large flow channels (wormholes). Unless effectively diverted, the treated region eventually becomes the sink for the acid and leaving other regions not adequately acidized. Therefore, acid placement will affect the success or failure of a matrix acid treatment.

Effective diversion of live acids is necessary for the successful matrix acid treatments. When injected, the acid tends to follow the path of least resistance that is to the higher permeability and/or the least damaged zones. Since damage must be removed or bypassed from the entire producing interval, effective diversion techniques must be employed.

Diversion in carbonates is generally more difficult than in sandstones because of the ability of the highly reactive HCl to increase permeability in carbonate rocks as the acid reacts with the rock and generates new flow channels. Apart from particulate diverters, a number of methods and techniques are commonly used for acid diversion in matrix treatments including: mechanical (packers, bridge plugs, ball sealers, coiled tubing); and chemical methods (gelled acids based on polymers or viscoelastic surfactants, emulsified acids and foams) (Chang et al. 2008).

Hill and Rossen (1994) mentioned that the techniques that have been applied to improve acid coverage: mechanical (mechanical zone isolation (packers), ball sealers,

---

This dissertation follows the style of *SPE Production and Operations Journal*.

coiled tubing), and chemical (foam, particulate diverting agents, and viscosified acids). Chang et al. (2007) showed that mechanical techniques are more expensive and time consuming than chemical techniques and they are often not applicable nor effective in open-holes. They stated that acid placement should have the characteristics:

1. Must not cause formation damage.
2. Must be compatible with the treating fluids (overflush or displacement fluids) and formation brines.
3. Must clean-up rapidly and completely when the well is put back on production.
4. Must be stable at the bottom hole treating conditions.

1.1 History of Polymer

Gelation of hydrochloric acid (HCl) for use in the oil industry started in the mid of 1970's. A lot of problems were achieved like: lumping or "fisheyes" due to incomplete hydration, safety in handling the addition of polymer powders to strong acid, and time to reach final viscosity (possible several hours). Over the years, the industry has made changes in the polymers and the methods of incorporating them into acid systems. A big improvement was the use of emulsion polymers, in which the polymer was held in an emulsion until mixed with the acid and then an internal activator would invert the emulsion exposing the polymer to acid and allow hydration to occur, Metcalf et al. (2000).

Conventional emulsion polymers generally appear to be white viscous liquids composed of an organic solvent, water, surfactants, and a polymer emulsified in an oil

external emulsion. Oil external emulsions, although dependent on the ratios of organic solvent to water, are inherently high in viscosity. These high viscosities are necessary to develop a stable system that will not degrade over time, Woo et al. (1999). The conventional emulsion polymers contain surfactant(s) or de-emulsifier(s) which when mixed in an aqueous fluid such as acid or water, will rapidly invert the emulsion releasing the polymer for hydration. Therefore, during gelling on location, a high shear rate is necessary to prevent the formation of un-hydrated masses (fisheyes), Woo et al. (1999).

A new emulsion polymer, has been used by Metcalf et al. (2000), was composed of a highly specific micro-sized Polymer. The micelles of this emulsion were $1/15^{th}$ the size of previous materials. The micelles were so minute that the solution appears to be a transparent amber color rather than a turbid mixture. The potential for the formation of un-hydrated masses or “fisheyes” on even the micro level is significantly depressed. The fluid also achieves a more complete hydration yielding consistent optimum base gel viscosities.

1.2 Mechanism of Viscosity Build-Up

According to Hill (2005), suitable polymers can be any polymer that is stable in aqueous acid solutions and that can be crosslinked in the presence of ferric or zirconium ions at a pH of about 2 or greater. The polymer should be containing carboxyl groups, such polymers include polyacrylamide copolymers. Initial spending of the live acid, during leak-off and wormholing, produces a rise in pH to a value of above about 2,

which initiates cross-linking of the polymer and a rapid increase in the viscosity of the partially spent acid. This increase in viscosity diverts the acid from high permeability streaks into the matrix. The highly viscous acid will plug off the treated zones, forcing the following stages of live acid into the untreated zones. The lower viscosity of the fresh acid allows penetration into other areas, until the reaction of the acid increases the pH value and causes cross-linking, thereby diverting the following acid stages into other portions of the target zone. Fresh acid in the wellbore and from subsequent treatment stages will keep the pH sufficiently low therefore the viscosity will be maintained until the end of the treatment, at that time the acid is allowed to spend completely.

Hill (2005) stated that as the in-situ gelled acid spends further, the pH continues to increase. For polymer that is crosslinked by ferric ions, this polymer does not cross-link by ferrous ions. As the acid spends further and the pH continues to rise, the reducing agent converts the ferric to ferrous ions. The gel structure will collapse and the acid system reverts back to a low viscosity fluid. Further pH increases to nearly 3.5 will reduce the viscosity to that of an uncross-linked polymer thickened fluid at the well temperature. It has been observed that the retention of some viscosity after spending assists in maintaining the formation fines in suspension and facilitates cleanup (if the reservoir is not too depleted).

Hill (2005) examined the effectiveness of various gel breakers, including sodium erythorbate (a reducing agent), but was found to be too active in live acids; a significant amount of ferric ion was reduced even at low temperatures. That will lead to poor

gelling in the formation. Therefore, the preferred reducing agent can be hydrazine sulfate or hydroxylamine hydrochloride, which doesn't reduce ferric ion in live acids.

For polymers that are cross-linked by zirconium ions (Boles et al. 1996), the cross-linker is preferably zirconium or titanium compounds with poly-functional organic acids. Gel breakers used with these fluids are formed from materials capable of complexing with the organo-metallic cross-linkers like fluoride. Boles et al. (1996) stated that fluoride reacts readily when introduced into the cross-linked polymer gel. The breaker, however, should be coated with a water-insoluble resin. This coating controls the release of the fluoride into the system.

1.3 Previous Work

The use of chemical diversion systems has also recently received increased attention. Initially, the industry concentrated on particulate systems, which have been widely used in vertical perforated wells (Schechter, 1992). Acids viscosified by polymer are probably applicable to all completion types. They are of particular benefit in horizontal, openhole, and gravel-packed wells, where many other diversion and selective placement techniques cannot be applied. The viscous fluid can be placed efficiently along the treatment interval because it can first limit fluid loss into the formation and then divert itself from regions of high to low injectivity as it is injected into the formation (Jones et al., 1996). Jones and Davies (1996) compared using a simulator between a gelled acid with a viscosity of 70 cp at a shear rate of 100 s^{-1} and conventional low-viscosity acids based on the coverage obtained over the wellbore

interval. They showed that in many cases, viscosifying the fluid can dramatically improve the placement over the wellbore interval.

De Rozieres et al. (1994) show that increasing the viscosity of acids will reduce the diffusion coefficient of the hydrogen ion (H+) and, as a result, the rate of mass transfer of the acid into the rock surface will decrease. The polymer and/or the generated gel forms an external filter cake that can reduce the leak-off rate of the acid during acid fracturing treatments. Mirza and Turton (1995) showed that polymer-based systems were firstly used for blocking zones to help the gel plug reach to the desired stiffness and the required isolation between intervals. Polymer Gel Diverter (PGD) had been used on field for many injection wells, which help in reducing the skin factor from +1 to –2.5.

Yeager and Shuchart (1997) demonstrated that in-situ gelled acids that are cross-linked by iron(III) formed a gel at a pH value of nearly 2. Woo et al. (1999) stated that there is a need for proper fluid diversion to enhance the outcome of matrix acid treatments. One way to enhance diversion is to increase the viscosity of the acid. Conway et al. (1999) stated that the in-situ gelled acid that they tested was very viscous, especially in the pH range of 2-4. This viscosity will reduce the diffusion coefficient of the hydrogen ion (H^+) and, as a result, the rate of mass transfer of the acid into the rock surface will decrease.

Mohamed et al. (1999) examined matrix acid treatments of a large number of seawater injectors. Field data indicated that this acid system can cause loss of well injectivity in some cases. They indicated that the volume of in-situ gelled acid should not exceed nearly 30 vol% of the total volume of acids used in typical matrix acid

treatments. a poor field results when in-situ gelled acids were used to stimulate power water injectors with tight carbonate zones.

One of the concerns raised about in-situ gelled acid is the presence of ferric ion in the system. It is well known that iron can precipitate in the formation and cause formation damage. For example, Taylor et al. (1999) showed that the type of iron precipitate depends on the level of hydrogen sulfide present. In sweet wells (no hydrogen sulfide) hydrated iron hydroxides will precipitate at pH values of 1-2. Crowe (1985) and Brezinski (1999) showed that in sour wells, however, iron sulfide species will precipitate at pH value of 1.9. The presence of ferric ion can enhance sludge formation with heavy oils and increase corrosion rate.

Polymer-based acids had been used in the field for several years as gelled acid for acid retardation or in-situ gelled acids for acid diversion. Gelled acids were developed primarily for fracturing but have found some applications in matrix acidizing. They are used in acid fracturing to increase the viscosity and decrease the leak off rate. The same principle applies to matrix acidizing conditions in fissured or vugular formations with low primary porosity. In this case, gelled acids are used mainly to clean up the high-permeability channels and minimize fluid loss in the lower permeability matrix. Gelled acids can also be used as a carrier fluid for ball sealers or particulate diverters. Since gelled acid is a shear-thinning (non-Newtonian) fluid, its viscosity increases further away from the wellbore, thereby blocking the following acid and diverting it to other, less permeable zones (Economides, 2000). Gelling agents reduce acid consumption because of a lower diffusion coefficient and a lower leak off rate

through the wormhole walls. The net result of these two effects is expected to be a higher wormhole propagation velocity. However, a potential problem with polymer gelling agents is filter-cake formation near the core surface which hinders the wormhole formation (Bazin et al., 1999).

Chang et al. (2001) showed that the in-situ gelled acid combines the capabilities of stimulation and diversion in one process, which significantly reduces the operational complexity. The apparent viscosity of the in-situ gelled acid is a preferred mechanism in diversion because it creates a viscosity differential in treated and untreated zones. Also, they noted that in-situ gelled acids caused loss of core permeability in tight carbonate cores. Permeability loss was attributed to polymer retention in the core and on the injection face of the core. A similar observation was noted by Taylor and Nasr-El-Din (2002).

Lynn and Nasr-El-Din (2001) investigated in-situ gelled acids at high temperature conditions. They noted that polymer residue attached to the walls of the wormholes created by the acid. Also, the iron cross-linker precipitated on the surfaces of the wormholes. Precipitation of iron and polymer residue can reduce the outcome of acid treatments. The in-situ gelled acids enhanced the permeability of the reservoir cores by a factor that depended on the acid injection rate. Lynn and Nasr-El-Din (2001) showed that there were polymer residue and crosslinker precipitation, which can potentially plug the face of the wormholes. Flow back of wells can reduce the damage due to the external filter cake that can be formed by the polymer.

Nasr-El-Din et al. (2002a) showed that there was polymer residue on the injection side of the cores. Flow back will be required to reduce the damage due to polymer residue. They also highlighted various negative interactions of this system in the presence of hydrogen sulfide, even in the presence of iron control agents. One of the noted disadvantages of this system was the precipitation of the cross-linker in some cases.

Taylor and Nasr-El-Din (2003) tested three different in-situ gelled acid systems based on polymer at different temperatures. They found the reaction of all three of the in-situ gelled acids was significantly retarded compared to the corresponding regular HCl acid. The primary cause of this reduction in the acid reaction rate was the polymer present in each of the acid formulae. Core flood studies showed that the polymer and cross-linker component of in-situ gelled acids irreversibly reduced the permeability of carbonate reservoir rock. Also, viscosity of some of these systems did not behave with the pH as claimed by some vendors. Therefore, testing of in-situ gelled acids in the lab before field application is recommended.

Halder et al (2004) concluded that field application of polymer-based in-situ gelled acids demonstrated an effective diversion in high permeable heterogeneous reservoirs. Based on lab results and field data, these systems can be applied as diversion agents for multi-layered wells in carbonate reservoirs up to 120°C. Amro (2006) noted that viscosity of the polymer-based in-situ gelled acids depends on shear rate, salinity, temperature, acid, and polymer concentration.

Abdel Fatah et al. (2008) found that in-situ gelled acids that are based on aluminum formed a gel at pH higher than that noted with iron-based cross-linkers. Also, corrosion inhibitor affected the pH at gelation: it reduced the pH at gelation for the iron cross-linker; whereas it increased the pH at gelation for the aluminum cross-liker. Mutual solvent did help in removing polymer residue from the cores. Kalfayan and Martin (2009) stated that there is still no universally applicable acid placement or diversion method. Therefore, more work is needed to better formulate acid systems.

1.4 Objectives

Literature review indicated that there is conflicting opinions regarding this system. Therefore, the aim of this study is to further examine this acid system and determine when it can be used in the field. Four main studies were conducted:

Viscosity measurements: Acid systems are sometimes prepared in the field using fresh water, seawater or any other available water. The objective of the present study is to determine the impact of the salinity of field mixing water on the viscosity of in-situ gelled acids that are based on polymers. A second objective is to assess the effect of iron contamination on the gelation process of these acid systems.

Rheological study: To the best of our knowledge, the rheological properties of the gelled and in-situ gelled acids were not considered before, especially the impact of pH on the elastic and viscous modulii. Therefore, this objectives of this study are to: (1) measure the rheological properties (G" and G") of in-situ gelled acids, (2) determine the effect of pH value on these properties, (3) predict these properties using available

models for viscoelastic fluids (mainly Maxwell; Kelvin and Voigt), and (4) develop new models to predict these properties if needed.

Also, no previous studies were done to examine the differences between the behaviors of Gelled and In-situ gelled acids. Therefore, the objective of this work is to study the viscoelastic properties of gelled acids and in-situ gelled acids and examine the effect of these properties on the acid diversion inside the formation.

Core flood study: The aim of this part of study is to further examine in-situ gelled acid during 20-in. long cores as a first time in literature. Previous studies used only using 2-6-in. long cores. Effect of the pours media shear rate was main parameter that what examined using single core test. Material balance was conducted to determine the percentage of the iron crosslinker that remain inside the core.

A second objective of the coreflood study is to evaluate the impact of an in-situ gelled acid stage volume on the propagation of regular HCl acid in carbonate cores. Two different injection rats and two different in-situ gelled acid stages volume were selected to represent high and low shear rate conditions.

Another objective of this study is to determine the wormhole propagation rate of gelled and in-situ gelled acids. Also, effects of temperature, initial permeability, and acid type on the wormhole propagation rate were considered in this work.

Finally, study the ability of in-situ gelled acid to divert regular acid into low permeability cores using parallel core flood setup. Also, the impact of initial permeability contrast on the effectiveness of in-situ gelled acid to divert regular acids into low permeability cores was tested.

Reaction rate study: Studying in details the reaction of in-situ gelled acid with carbonate rocks and to investigate the effect of parameters such s temperature, rotational speed, and the presence of crosslinker on the speed of reaction.

2. NEW INSIGHTS INTO THE VISCOSITY OF POLYMER-BASED IN-SITU-GELLED ACIDS*

Diversion techniques must be employed to remove all the damage from the entire producing interval. Diversion in carbonates is more difficult than in sandstones because of the ability of acid to significantly increase the permeability in carbonates as it reacts in the pore spaces and flow channels of matrix. The apparent viscosity of the in-situ gelled acid based on polymer plays a key role in diversion because it creates a viscosity differential in treated and untreated zones. An extensive literature survey and field data show that there is no agreement on the effectiveness of this acid system. Therefore, this study was conducted to better understand this acid system and determine factors that impact its viscosity buildup. Three commercially available in-situ acids were examined.

The effect of salts and iron (III) [Fe(III)] contamination on the apparent viscosity of these acids was examined in detail. Several new findings were identified, including that polymer and other additives were separated out of the acid when these acids were prepared in high-salinity water. Preparing the in-situ gelled acid with saline water decreased the viscosity of the acid in live and neutralized conditions.

Concentrated hydrochloric acid (HCl) solutions produced high concentrations of calcium ion that reduced the viscosity of the in-situ-gelled acid system. A brown precipitate was noted during the neutralization of acid systems that contained Fe (III), even in the presence of the recommended concentration of iron-control agents.

2.1 Introduction

The present study will focus on acid diversion using in-situ-gelled acids that are based on polymers. Acid systems are sometimes prepared in the field using fresh water, seawater, or any other available water. The objective of the present study is to determine the impact of the salinity of field mixing water on the viscosity of in-situ-gelled acids that are based on polymers. A second objective is to assess the effect of iron contamination on the gelation process of these acid systems.

2.2 Experimental Studies

Materials: HCl (ACS reagent grade) was titrated using 1N sodium hydroxide solution to determine its concentration, which was found to be 36.8 wt%. Calcium carbonate powder and sodium hydroxide pellets (ACS grade) were used to neutralize live acids. Sodium chloride, calcium chloride, and anhydrous iron (III) chloride (ACS grade) were used as a source of mono-, di-, and tri-covalent cations. Deionized water was obtained from a water-purification system (BARNSTEAD EASYpure PoDi-model D13321) that had a resistively of 18.2 MΩ·cm at room temperature. Polymer and other additives were all oilfield chemicals and were used without further purification.

Measurements: Viscosity measurements of live and partially spent acids were made using an M3600 viscometer. To resist corrosion by acids, both the rotor (R1) and the bob (B1) of the viscometer were made of Hastelloy C. The viscosity was measured as a function of shear rate (from 0.1 to 1020 s^{-1}). Measurements were conducted at atmospheric pressure and ambient temperature. pH values were measured using a 950 ROSS FASTQC.

Procedures: **Table 2.1** lists the formulae of the three in-situ acid systems (A, B, and C) examined in the present work. The three in-situ-gelled acids contained acid, a polymer, a crosslinker, a breaker, and a corrosion inhibitor. The study also included three gelled acids (D, E, and F). The formulae of the gelled acids were similar to those reported in **Table 2.1**, but without the crosslinker and the breaker. Gelled acids are used to minimize the acid leakoff, whereas in-situ-gelled acids are used for diversion. Acids A and C were crosslinked using Fe (III), while Acid B was crosslinked using zirconium (IV). The effect of salts on the viscosity of gelled and in-situ-gelled acids was examined in detail. Salts examined included NaCl (0, 3.5, and 6 wt%) and $CaCl_2$ at same salt concentrations, and $FeCl_3$ at 1 and 3.5 wt%.

To study the behavior of the in-situ-gelled acids, Acids A, B, and C were prepared with all acid additives as described in **Table 2.1**. The prepared acids were examined in live and partially spent conditions. The impact of salts and iron concentration on the viscosity of gelled and in-situ-gelled acids was examined. Polymer-based acids were prepared as follows:

1. Deionized water was mixed with a predetermined amount of NaCl, $CaCl_2$, or $FeCl_3$ for 5 minutes.
2. HCl, polymer, and corrosion inhibitor (and crosslinker and breaker, in case of in-situ-gelled acids) were added to the water and mixed according to the mixing procedure provided by each service company.

TABLE 2.1—IN-SITU GELLED ACID FORMULA A, B, AND C

	A	B	C
Acid	5 wt% HCl	5 wt% HCl	5 wt% HCl
Acid gelling agent	24 gal/Mgal of polymer (10-30 wt%).	20 gal/Mgal of polymer	20 gal/Mgal of (10-30 wt).
Corrosion inhibitor	5 Gal/Mgal of a mixture of Aliphatic amide (10-30 wt%), Methanol (10-30 wt%).	5 Gal/Mgal of a mixture of Methanol (1-5 wt%), Isopropanol (1-5 wt%), Formic acid (30-60 wt%).	5 Gal/Mgal of a mixture of Methanol (30-60 wt%), Propargyl alcohol (5-10 wt%)
Cross-linker:	5 gal/Mgal of Iron trichloride (30-60 wt%) in water, Specific gravity 1.45.	10 gal/Mgal of a mixture of zirconium and aluminum salts in water	10 gal/Mgal of Ferric chloride (37-45 wt%)
Breaker	-	20 lb/Mgal of resin-coated inorganic salt, 85 to 90 wt% calcium fluoride and 10 to 15 wt% resin.	20 lb/Mgal of isoascorbic acid, sodium salt (60 to 100 wt%)
Other additives	-	2 gal/Mgal of akoxylated alcohols	2 gal/Mgal of hydroxyacetic acid (30-60 wt%)

3. The acids with additives were mixed for 30 minutes using an overhead mixer at a rotational speed of 350 rev/min, and after that were centrifuged for 20 minutes at a rotational speed 2,500 rev/min to remove air bubbles from acid solutions.

4. Live acids were gradually neutralized by adding calcium carbonate powder while the pH was monitored. Live acids were neutralized using NaOH pellets in one set of experiments. This was done to examine the effect of cation type on the apparent viscosity of partially neutralized acids. All acids were mixed continuously during the experiments to ensure that acid was neutralized to the required pH values.
5. The apparent viscosity was measured at 28°C using the M3600 viscometer for live and partially spent acids.
6. The apparent viscosity was measured as a function of equilibrium pH value, which was achieved when the pH value of the partially neutralized acid became constant with respect to time.

2.3 Results and Discussion

2.3.1 Compatibility tests of gelled acids

Ferric ions have three positive charges and can crosslink the polymer that was used to prepare gelled and in-situ-gelled acids. Acids are usually contaminated with ferric iron because of dissolution of rust from well tubulars and mixing tanks (Nasr-El-Din et al. 2002b). Because of surface contamination, the concentration of ferric ions in live acids can reach up to 10,000 ppm in some cases (Al-Nakhli et al. 2008). Gelled acids (D, E, and F) similar to Acids A, B, and C, but without the crosslinker and breakers, were prepared and doped with 1 wt% $FeCl_3$. No phase separation was noted in the case of Gelled Acid D**,** while polymers of Acids E and F were separated from the

solution **(Fig. 2.1).** The polymer for Acid D separated out of solution in the presence of 4 wt% NaCl and 1 wt% $FeCl_3$.

Acids D, E, and F were prepared with 10 wt% NaCl. The polymers and the corrosion inhibitor separated out from the live acids. On the basis of these results, it is recommended to minimize the iron contamination in live acids by cleaning the mixing tank and pickling well tubulars or coiled tubing before pumping the acid. Also, the acid should be prepared using low-salinity water. High salt concentrations reduced the solubility of these polymers in live acids.

Acid A (1 wt% $FeCl_3$ + 4wt% NaCl)

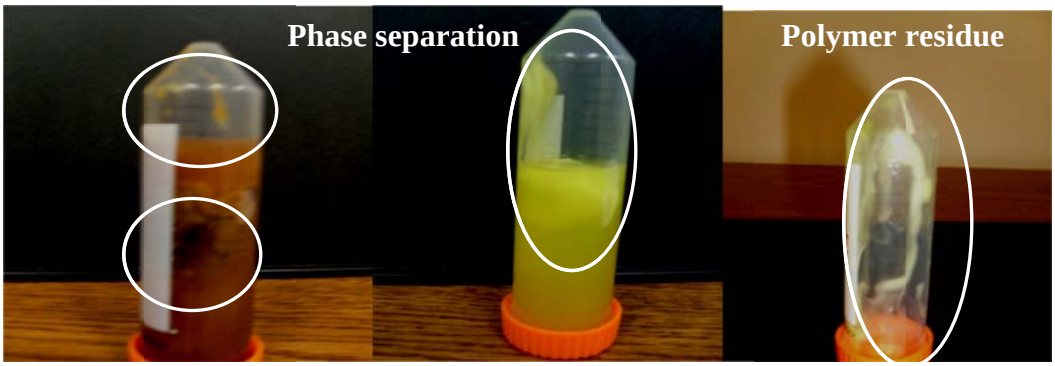

Acid A (1 wt% $FeCl_3$ Acid B (1 wt% $FeCl_3$) Acid B (1 wt% $FeCl_3$)

Fig. 2.1—Phase separation of polymer in the live condition due to high salt concentration, 5 wt% HCl, 28 ºC.

2.3.2 Effect of salts

Live Acids, Gelled Acids: The viscosity behavior of live in-situ-gelled acids was examined at an initial HCl concentration of 5 wt%, a temperature of 28°C, and atmospheric pressure. It is desirable to have live gelled acids with low viscosity to allow pumping of the acid into the formation. This is an important issue when stimulating deep vertical wells or horizontal wells with extended reach. Acid D was used at 5 wt% HCl, and NaCl, $CaCl_2$, or $FeCl_3$ was added at different concentrations. The apparent viscosity was measured as a function of shear rate. **Fig. 2.2** shows the effect of NaCl, $CaCl_2$, and $FeCl_3$, on the apparent viscosity of this gelled acid. The apparent viscosity of the live acid significantly decreased as the salt concentration was increased. The viscosity/shear-rate relationship for all acid systems examined was described by the power-law model:

$$\mu = k\,\gamma^{n-1}, \qquad (2.1)$$

where μ is the fluid viscosity, mPa·s; k is the power-law constant, mPa·s^n; γ is the shear rate, s^{-1}; and n is the power-law index, dimensionless. Power-law constants for the acids examined are given in **Table 2.2.**

TABLE 2.2—POWER-LAW PARAMETERS OF 5 WT% HCL, CORROSION INHIBITOR, AND POLYMER OF LIVE ACID A AT DIFFERENT SALT CONCENTRATIONS (28 °C)				
Salt, wt %	**Salt Type**	**K, mPa.s^n**	**n**	**R^2**
0	0	506.0	0.601	0.998
3.5	NaCl	319.4	0.606	0.997
6	NaCl	124.2	0.539	0.973
3.5	$CaCl_2$	151.3	0.557	0.983
6	$CaCl_2$	78.2	0.551	0.980
1	$FeCl_3$	258.2	0.428	0.989
3.5	$FeCl_3$	180.1	0.300	0.988

Salts have different effects on the viscosity of live acids. NaCl had less effect on the viscosity of live acid than $CaCl_2$ or $FeCl_3$. A similar behavior was noted with Acids E and F; the results are given in **Table 2.3.** The results discussed thus far indicate that salts reduced the apparent viscosity of live acids, and this trend increased with salt concentration. Also, the viscosity decreased with the number of positive charges of the cation used. It is important to note that the carboxylate groups of the polymer are not protonated in live acids. On the basis of these results, it appears that salts affect the configuration of the polymer in such a way that its size was reduced, which resulted in this viscosity decrease. The polymer separated out of solution in an untimely way, indicating that solutions of live acids that contain high salt content become poor solvents to these polymers.

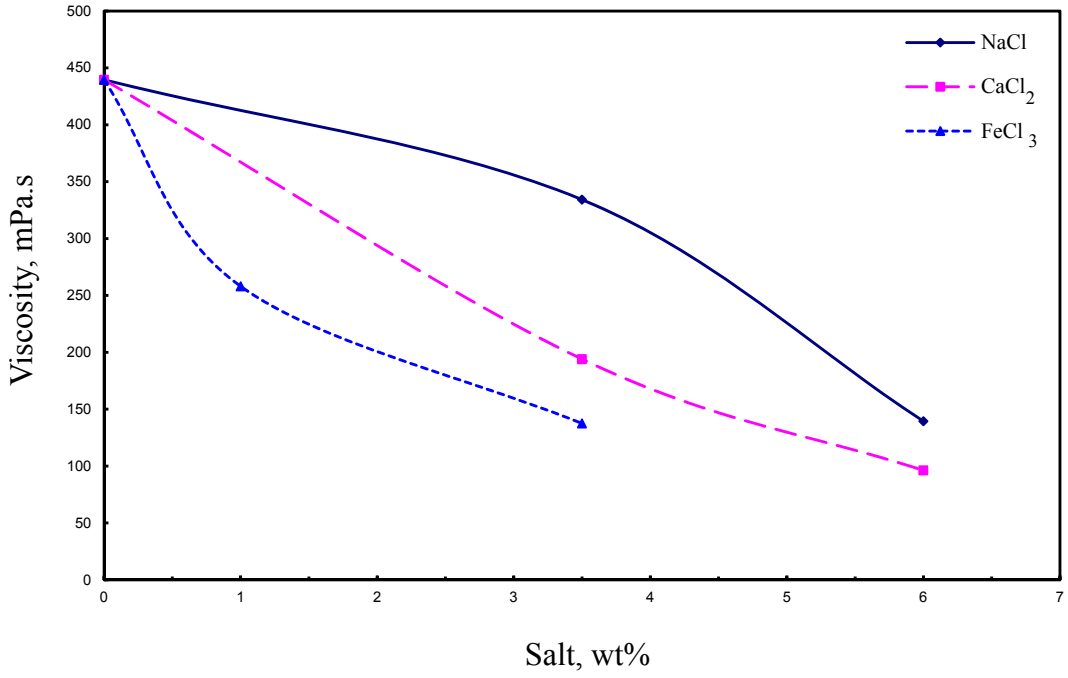

Fig. 2.2—Effect of NaCl, $CaCl_2$, and $FeCl_3$ on the apparent viscosity of live acid: 5 wt% HCl, corrosion inhibitor, and polymer of live Acid A (Table 2.1 - no cross-liker, no breaker, and no additives), (shear rate = 1 s^{-1}, 28 ºC).

TABLE 2.3—POWER-LAW PARAMETERS OF 5 WT% HCL, CORROSION INHIBITOR, AND POLYMER OF LIVE ACIDS B & C (TABLE 2.1, NO CROSS-LIKER, NO BREAKER, AND NO ADDITIVES) AT DIFFERENT SALT CONCENTRATIONS (28 ºC)

Acid Type	Salt, wt %	Salt Type	K, mPa.s^n	n	R^2
B	0	0	997.3	0.527	0.993
	3.5	NaCl	590.2	0.609	0.997
	10 gal/Mgal	Zr Salts	426.8	0.635	0.995
C	0	0	889.6	0.457	0.999
	3.5	NaCl	595.9	0.497	0.999
	10 gal/Mgal	Ferric Salts	426.7	0.635	0.995

Spent Acids Gelled Acids: Acid D was prepared and reacted with increasing amounts of calcium carbonate to simulate spending of the acid with carbonate rocks. The

apparent viscosity of this acid was measured as a function of shear rate at each equilibrium pH, and the data were fitted using the power-law model. **Table 2.4** gives the power-law parameters at each pH value. The viscosity increased at pH 1.4 and reached a maximum value of 800 mPa·s at pH of 2. The viscosity remained constant as the pH value was increased further. Acids E and F exhibited a similar behavior when neutralized by calcium carbonate powder **(Table 2.5).**

TABLE 2.4—POWER-LAW PARAMETERS OF 5 WT% HCL, CORROSION INHIBITOR, AND POLYMER OF LIVE ACID A (TABLE 2.1 - NO CROSS-LIKER, NO BREAKER, AND NO ADDITIVES) AT DIFFERENT PH VALUES NEUTRALIZED BY $CACO_3$, AND NAOH (28 ºC)

	pH	K, mPa.s^n	n	R^2
Neutralization by				
	live acid	506.0	0.601	0.998
$CaCO_3$	0.18	576.5	0.583	0.998
	2.4	826.5	0.558	0.999
	4.89	807.0	0.562	0.998
NaOH	0.92	393.6	0.609	0.991
	4.1	309.4	0.617	0.987

TABLE 2.5—POWER-LAW PARAMETERS OF 5 WT% HCL, CORROSION INHIBITOR, AND POLYMER OF LIVE ACIDS B, AND C (TABLE 2.1, NO CROSS-LIKER, NO BREAKER, AND NO ADDITIVES) AT DIFFERENT PH VALUES NEUTRALIZED BY $CACO_3$ (28 ºC)

Type	Equilibrium pH	K, mPa.s^n	n	R^2
B	live acid	997.3	0.527	0.993
	1.5	1,739.4	0.443	0.997
	2.1	1,904.1	0.428	0.994
	3.9	2,055.8	0.414	0.991
	6	706.2	0.577	0.994
C	live acid	748.1	0.418	0.981
	1.8	860.3	0.469	0.975
	2.5	903.3	0.489	0.990
	3.5	910.2	0.498	0.992
	5	915.5	0.489	0.992

The increase in the viscosity of Gelled Acid D with pH was interesting because there was no crosslinker used. The carboxylate groups will be protonated at pH values greater than nearly 2. It appears from these results that the calcium ions with two positive charges interacted with the negatively charged carboxylate groups and increased the viscosity of the acid. To confirm this explanation, live Acid D was prepared and then neutralized using sodium hydroxide (NaOH). Sodium ion has one positive charge, which has minimum interaction with the polymer molecules. **Table 2.4** gives the power-law constants obtained with NaOH. The viscosity of this acid decreased as the pH was increased **(Fig. 2.3).** This decrease in viscosity was because of the charge screening effects of sodium ions. These results indicated that calcium ions interacted with the polymer molecules in a different way, which resulted in the aforementioned viscosity increase.

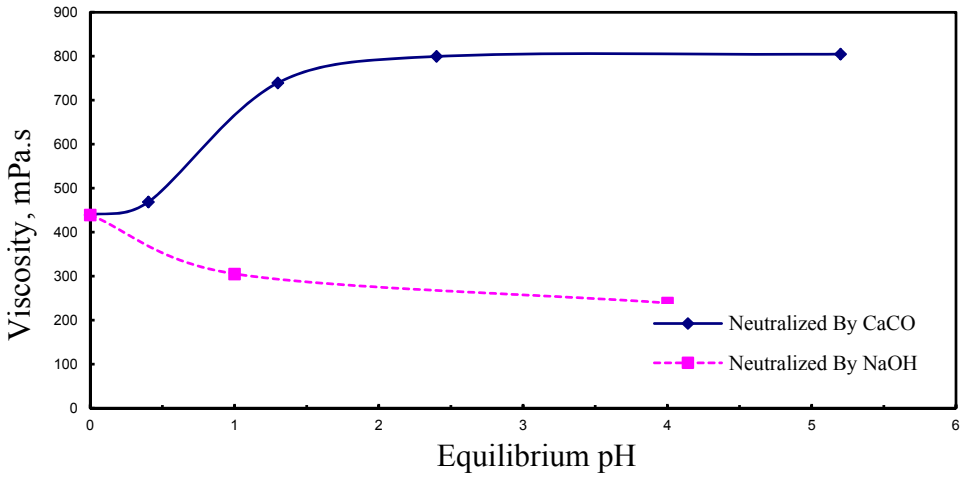

Fig. 2.3—Apparent viscosity of 5 wt% HCl, corrosion inhibitor, and polymer of live Acid A (Table 2.1 - no cross-liker, no breaker, and no additives). Acid was neutralized to various pH values using $CaCO_3$, and NaOH (shear rate = 1 s^{-1}, 28 ºC).

Spent Acids, In-Situ-Gelled Acids: The effects of salts on the apparent viscosity of live and spent acids, without the crosslinker, highlighted the complexity of this system. It is of interest to investigate the combined effects of NaCl (added to the system), $CaCl_2$ (produced from acid reaction with calcium carbonate), and $FeCl_3$ (surface contamination) on the viscosity of partially spent acids.

Fig. 2.4 shows the apparent viscosity of partially spent Acid A solutions that were prepared in deionized water and in the presence of 4 wt% NaCl. The viscosity of Acid A prepared in deionized water increased at nearly pH 2, which was similar to the results obtained by Taylor and Nasr-El-Din (2003). However, in the presence of 4 wt% NaCl, the viscosity increased at pH of 2.5, and the maximum value was 1400 mPa·s, which was reached at pH 3.3; then, the viscosity remained constant. The maximum viscosity reached in the presence of NaCl was significantly less than that obtained when the acid was prepared in deionized water. NaCl had a very detrimental effect on the apparent viscosity of partially spent Acid A. A similar trend was noted with Acid B **(Fig. 2.5).** The addition of 4 wt% NaCl to Acid C reduced the apparent viscosity at all pH values examined **(Fig. 2.6).** It is important to mention that this system contained $CaCl_2$, from the acid reaction with calcium carbonate, and ferric chloride or zirconium salts, as a crosslinker. These salts reduced the viscosity of live acids. $CaCl_2$ increased the viscosity of partially spent acid without the crosslinker. The results shown in **Figs. 2.4, 2.5, and 2.6** and **Table 2.6** indicate that the polymer did crosslink with ferric or zirconium ions. NaCl present in the system at pH 0 changed the configuration of the polymer in such a way that reduced the accessibility of the carboxylate groups to ferric,

or zirconium, ions; as a result, the viscosity was much less than that noted when the acid was prepared in deionized water.

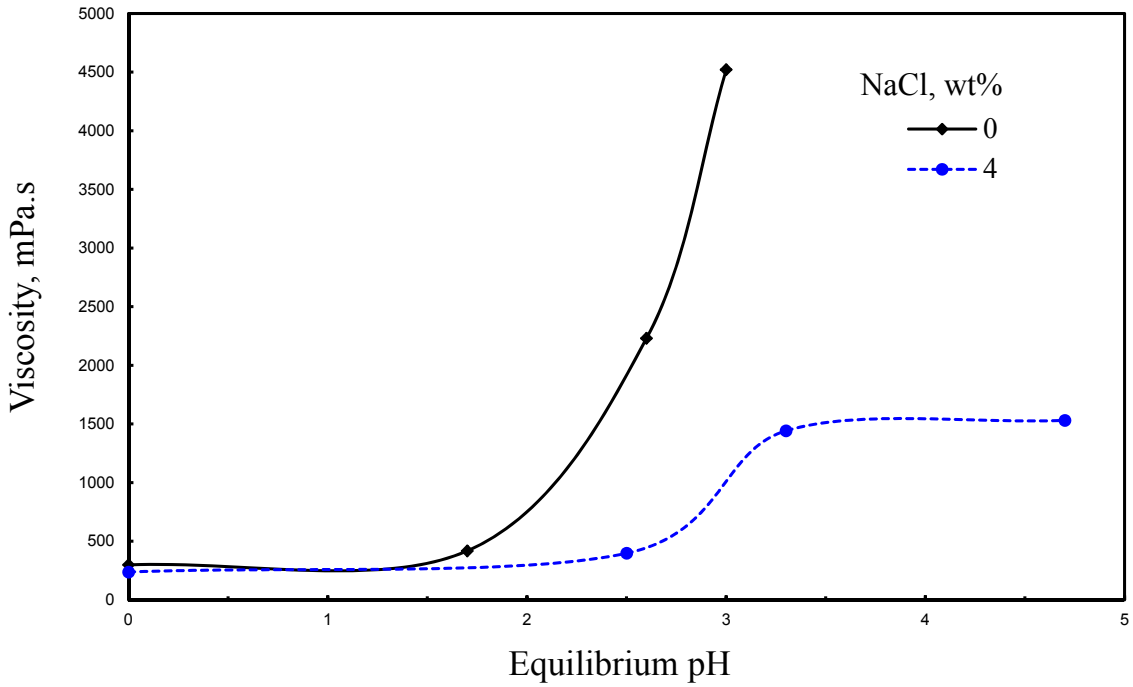

Fig. 2.4—Viscosity decrease of Acid A (Table 2.1) when it was mixed with 4 wt% NaCl (shear rate = 1 s^{-1}, 5 wt% HCl, 28 ºC).

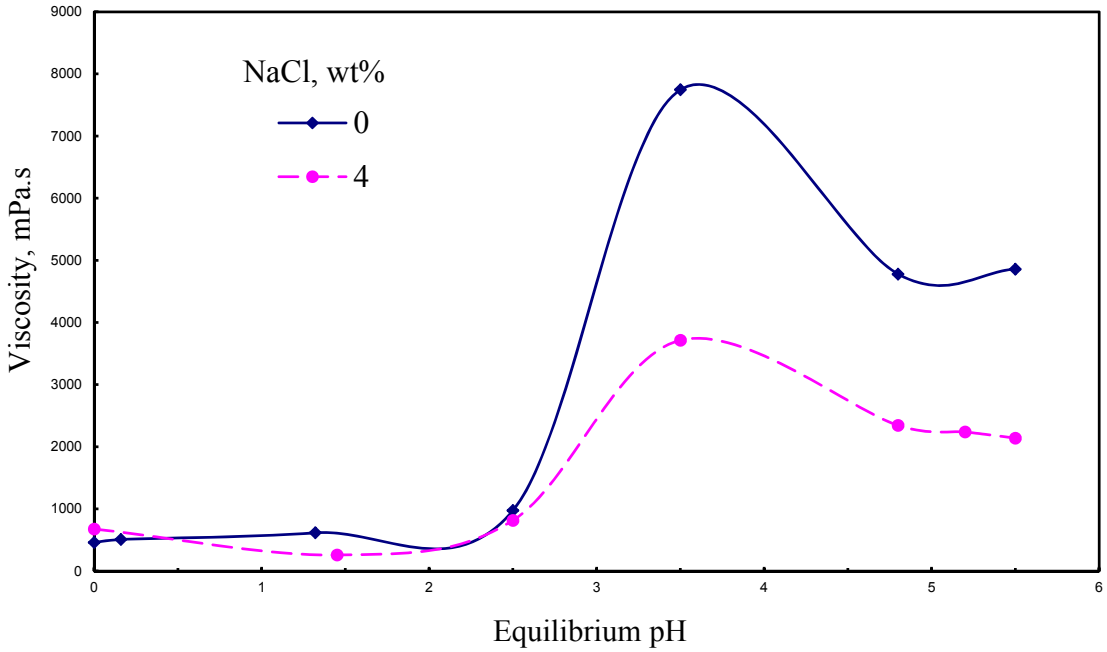

Fig. 2.5—Viscosity decrease of Acid B (Table 2.1) when it was mixed with 4 wt% NaCl (shear rate = 1 s^{-1}, 5 wt% HCl, 28 ºC).

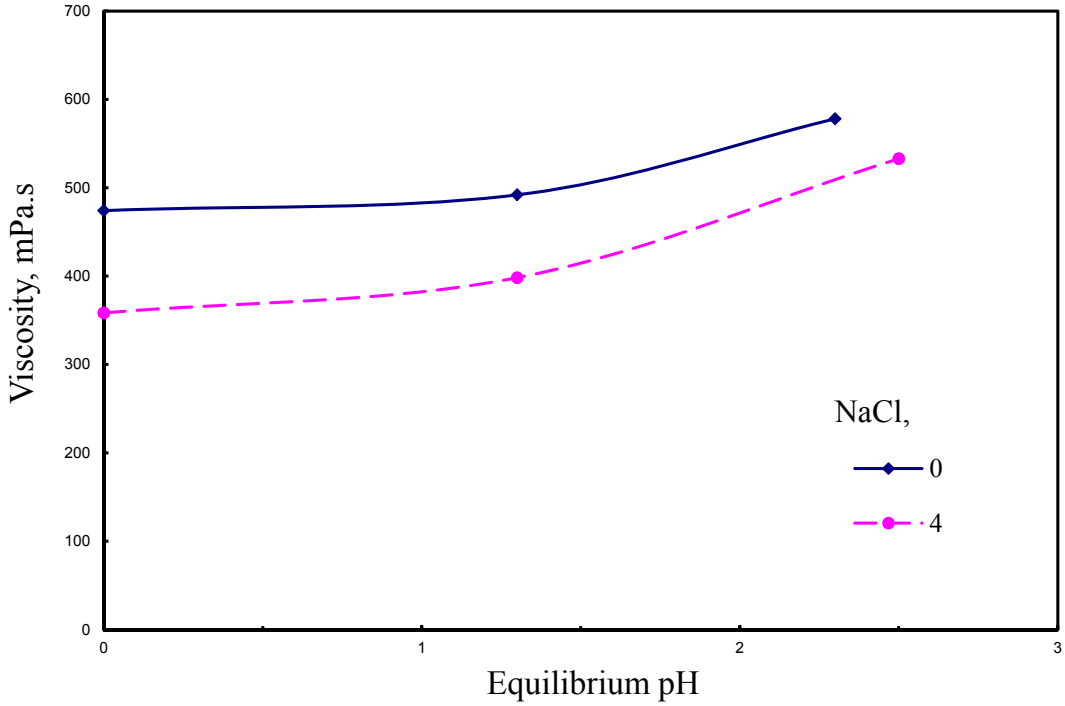

Fig. 2.6—Viscosity decrease of Acid C (shear rate = 1 s^{-1}, 5 wt% HCl, 28 ºC).

The crosslinker used in Acids A and C was $FeCl_3$, while zirconium was used to crosslink the polymer in Acid B. It is of interest to examine the effect of additional Fe (III) on the viscosity behavior of Acid B **(Table 2.7). Fig. 2.7** compares the viscosity obtained with Acid B prepared in deionized water, in 0.15 wt% $FeCl_3$, and in 4 wt% NaCl + 0.15 wt% $FeCl_3$. $FeCl_3$ reduced the maximum viscosity obtained. The viscosity further decreased for the acid system that contained both NaCl and $FeCl_3$. The latter, however, showed an increase in viscosity at much higher pH values, which will not be beneficial in diversion and breaking of the produced gel.

TABLE 2.6—EFFECT OF 4 WT% NACL ON THE POWER-LAW PARAMETERS OF ACIDS A, B, AND C (TABLE 2.1) AT DIFFERENT PH VALUES (28ºC)

Acid	NaCl, wt%	Equilibrium pH	K, mPa.s^n	n	R^2
A	0	Live acid	298.3	0.60	0.997
		1.7	456.3	0.59	0.999
		2.6	2,260.4	0.44	0.993
	4	Live acid	234.1	0.60	0.995
		2.5	457.6	0.62	0.996
		3.3	1,375.2	0.50	0.998
		4.7	1,463.9	0.50	0.998
B	0	Live acid	426.7	0.64	0.995
		2.5	873.5	0.56	0.997
		3.7	6,456.1	0.32	0.997
		5.5	3,367.3	0.40	0.993
	4	Live acid	581.5	0.59	0.992
		2.5	762.3	0.57	0.994
		3.5	3,136.6	0.42	0.997
		5.2	2,254.8	0.44	0.999
C	0	Live acid	439.2	0.62	0.994
		1.5	819.1	0.53	0.994
		3.5	4,158.4	0.35	0.994
		5.1	4,888.8	0.36	0.994
	4	Live acid	321.9	0.58	0.996
		1.3	355.1	0.60	0.993
		2.5	567.5	0.55	0.997

TABLE 2.7—EFFECT OF 4 WT% NACL, AND 0.15 WT% $FECL_3$ ON THE POWER-LAW PARAMETERS OF ACID B (TABLE 2.1) AT DIFFERENT PH VALUES (28 ºC)

Salt concentration	Equilibrium pH	K, mPa.s^n	n	R^2
0.15 wt% $FeCl_3$ which equivalent to (400-500) ppm of ferric	live acid	439.2	0.619	0.994
	1.5	819.1	0.532	0.994
	3.5	4,158.4	0.351	0.994
	5.1	4,888.8	0.356	0.994
4 wt% NaCl + 0.15 wt% $FeCl_3$	live acid	459.7	0.628	0.993
	1.4	440.8	0.619	0.990
	2.5	981.2	0.555	0.995
	3.5	2,469.3	0.466	0.994
	4.75	5,778.4	0.312	0.997
	5.8	4,133.2	0.342	0.996

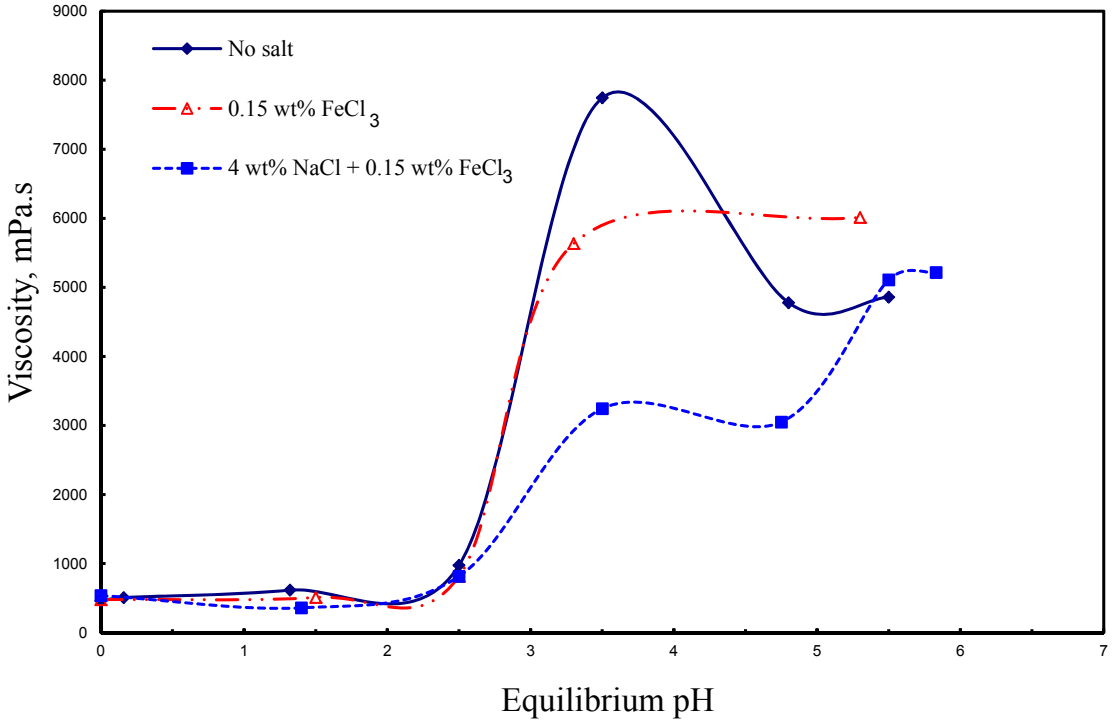

Fig. 2.7—Viscosity changes when Acid B (Table 2.1) was mixed with 4 wt% NaCl, and 0.15 wt% $FeCl_3$ (shear rate = 1 s^{-1}, 5 wt% HCl, 28 ºC).

2.3.3 Effect of the initial acid concentration

Taylor and Nasr-El-Din (2003) noted that there was no increase in viscosity when the in-situ-gelled acids were used at high HCl concentrations, but when these acids were tested at low HCl concentrations, the viscosity increased significantly when the pH reached a value higher than nearly 2. To investigate this observation further, Acid C was prepared (**Table 2.1**) at acid concentrations of 3, 5, and 10 wt% HCl. **Fig. 2.8** shows the viscosity at shear rate = 1 s^{-1} as a function of equilibrium pH. The viscosity at 3 wt% HCl was higher than those noted at higher HCl concentrations. It appears from these results that $CaCl_2$ that was produced from the acid reaction with calcium carbonate reduced the viscosity of in-situ-gelled acid (Fig. 2.8). Obviously, the concentration of calcium ions would increase when concentrated acids are used. The produced calcium reduced the viscosity of the in-situ-gelled acids, and the higher the initial acid concentration, the lower of the maximum viscosity that can be obtained. On the basis of these results, it is recommended to use this acid at an initial concentration of 3 to 5 wt%. Higher acid concentrations will not produce the high viscosity that is needed for proper diversion.

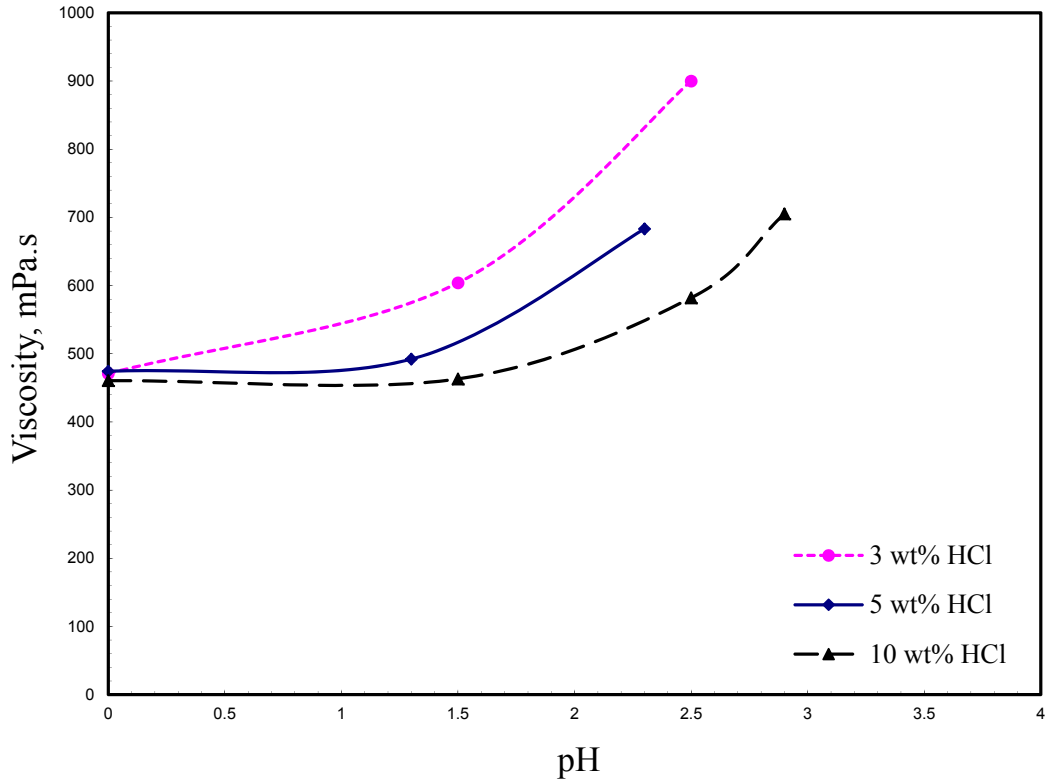

Fig. 2.8—Effect of initial acid concentration on Acid C (Table 2.1) neutralized by $CaCO_3$, (shear rate = 1 s^{-1}, 28 ºC).

2.3.4 Breaking mechanisms

Acids A and C were crosslinked by ferric ions; therefore an iron-reducing agent was used to break the gel formed by the acids. Acid B was crosslinked by zirconium ions; therefore, a resin-coated calcium fluoride was used to break the gel formed by this acid. Acids A and C were prepared with all additives (**Table 2.1**) and were neutralized by calcium carbonate powder. Theoretically, these systems are supposed to break at pH value 4 to 5, but actually pH reached 5.2 and sometimes 6 with no decrease in the viscosity for either acid. The breakers for these systems were carefully selected to break the gel at high pH values, when the acid is almost completely spent. However, at a pH

from 2 to 3, the concentration of acid is less than 0.04 wt% and the viscosity of the gel is very high. The high viscosity of the gel will reduce the diffusion coefficient of H^+ to transfer to the surface of the rock and react. In addition, the low acid concentration will reduce the driving force of H^+ to diffuse into the surface. Both factors will tend to delay the rate of gel breaking, at least under test conditions.

This observation raised a concern with the use of these acids. These gels will not be broken completely, and will cause damage inside the formation. This is in agreement with the results obtained by Lynn and Nasr-El-Din (2001), where a polymer-gel residue was found in cores after coreflood tests using Acids A or C. One of the disadvantages of these two acid systems is that they contain ferric salt, which precipitates ferric hydroxide even in the presence of the recommended iron-control agent.

3. RHEOLOGICAL PROPERTIES OF POLYMER-BASED IN-SITU GELLED ACIDS: EXPERIMENTAL AND THEORETICAL STUDIES

Polymer-based in-situ gelled acids have been used in the field for more than a decade. These acids are typically used for matrix applications at HCl concentrations of 3-5 wt%. Recent lab work and field data indicated that these acids are not fully understood, and that there is a need to better characterize and understand how these acid systems develop viscosity in-situ. This understanding will enhance the way these acids are used in the field. Therefore, the objective of this study is to determine the elastic and viscous properties of these acids as they react with the rock.

Experimental studies were conducted to measure the rheological properties for in-situ gelled acids using an oscillatory rheometer. To the best of our knowledge, this is the first time that the elastic properties were measured for these acid systems. Measuring the elastic modulus (G') and viscous modulus (G") were done using two techniques: Dynamic sweep and Creep tests.

Based on experimental results obtained, two regimes were identified: a pure viscous behavior and a semi-solid elastic behavior. A viscous regime was noted below pH 2 where G" was dominant. Yield stress, Young's modulus, G', and G" values were relatively small in the viscous regime. A semi-solid elastic behavior was observed at pH greater than 2. Yield stress, Young's modulus, G', and G" significantly increased at pH 2, and reached their maximum values at pH 3.2. G' increased by 3 orders of magnitude

while G" increased only by an order of magnitude during acid reaction with carbonate rock.

Maxwell and Kelvin-Voigt models were able to predict the experimental data for the viscous regime only. However, for the semi-solid elastic regime, these models didn't accurately predict experimental results. The three-parameter model was able to predict the semisolid elastic regime only. Therefore, a new model was developed to predict the rheological properties of these acids over a wide range of pH values. Model predictions were in good agreement with the experimental results.

3.1 Introduction

Yeager and Shuchart (1997), Conway et al. (1999), Taylor and Nasr-El-Din (2003), used a rotational viscometer to examine the behavior of in-situ gelled acid systems. To the best of our knowledge, the rheological properties of the in-situ gelled acids were not considered before, especially the impact of pH on the elastic and viscous modulii. Therefore, this objectives of this study are to: (1) measure the rheological properties (G" and G") of in-situ gelled acids, (2) determine the effect of pH value on these properties, (3) predict these properties using available models for viscoelastic fluids (mainly Maxwell; Kelvin and Voigt), and (4) develop new models to predict these properties if needed. Dynamic mechanical testing, and creep testing were used to in the present study.

3.2 Dynamic Measurements

A common method to assess the viscoelastic materials uses measurement of stresses during application of a sinusoidal oscillating shear strain. The applied strain, ε, is (Macosko 1994).

$$\varepsilon = \varepsilon_o \sin \omega t = \varepsilon_o e^{i\omega t} \quad \text{.....(3.1)}$$

while the stress is given by:

$$\tau = \tau_o \sin (\omega t + \delta) = \tau_o e^{i(\omega t + \delta)} \quad \text{.....(3.2)}$$

If the material is an elastic solid, then the phase angle, δ, in Eq. 3.2 is zero. In contrast, if the material is a Newtonian fluid, then the phase angle is 90˚. If the tested material is viscoelastic, the stress wave will be shifted by an intermediate phase angle (Liu and Seright, 2001)**.** For analysis, the stress wave is generally separated into two waves with the same frequency. One wave (τ' in **Fig. 3.1**) is in phase with the strain wave, while the second wave (τ" in **Fig. 3.1**) is 90˚ out of phase with the strain wave. In this way, the stress wave is separated into an elastic component and a viscous component. Using the terms in **Fig. 3.1**, the elastic modulus, G', is defined in Eq. 3.3 (Macosko 1994).

$$G' = \tau_o' / \varepsilon \quad \text{.....(3.3)}$$

The viscous modulus, G”, is defined as

$$G'' = \tau_o'' / \varepsilon \quad \text{.....(3.4)}$$

The complex viscosity, μ*, is defined as:

$$\left|\mu^*\right| = \sqrt{\left(\mu'\right)^2 + \left(\mu''\right)^2} = \sqrt{\left(G'/\omega\right)^2 + \left(G''/\omega\right)^2} = \tau_o/\varepsilon_0\omega \quad \text{.....(3.5)}$$

The complex modulus, G*, is defined as:

$$G^* = (G'^2 + G''^2)^{0.5} \quad \text{.....(3.6)}$$

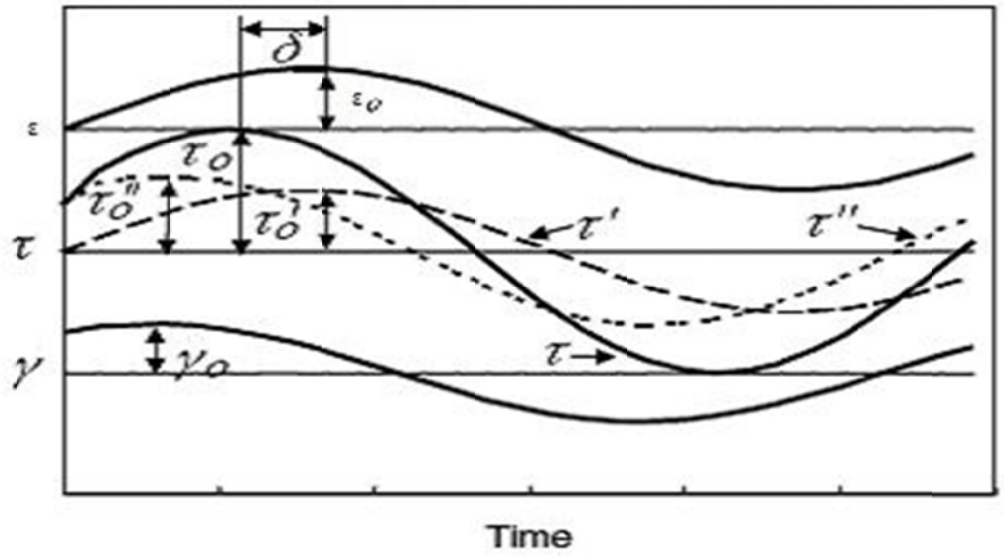

Fig. 3.1—Illustration of dynamic measurements (Macosko 1994).

3.3 Creep Test

The creep test is the most useful technique to characterize the material response as a function of time (Wineman and Rajagopal 2000). When a material is subjected to a step constant stress, the viscoelastic material experience a time-dependent increase in strain. This phenomenon is known as viscoelastic creep. Viscoelastic creep data presented by plotting the creep compliance (total strain at a particular time divided by the constant applied stress) as a function of time (Rosato et al. 2001). Below its critical stress, the viscoelastic creep compliance is independent of the applied stress. A family of curves describing strain versus time response to various applied stresses may be represented by single viscoelastic creep compliance versus time curve if the applied stresses are below the material's critical stress value. Many models were developed to describe the time dependence stress-strain relationships. A brief summary of theses models is given below:

Maxwell Model can be represented by a dashpot and a spring connected in series, **Fig. 3.2**. The rate of strain can be represented by Eq. 3.7 (Wineman and Rajagopal 2000).

$$\frac{d\varepsilon}{dt} = \frac{\sigma}{\mu} + \frac{1}{E}\frac{d\sigma}{dt} \quad \text{.....(3.7)}$$

Based on this model, if the material is subjected to a constant stress, the strain has two components. First, an elastic component occurs instantaneously, corresponding to the spring, and relaxes immediately upon the release of the stress. The second is a viscous

component that grows with time as long as the stress is applied. Maxwell model for the creep test (constant stress with time), Eq. 3.8 can be used to determine the compliance as a function of time, J(t):

$$J(t) = \frac{1}{E}\left(1 + \frac{Et}{\mu}\right) \quad \text{.....(3.8)}$$

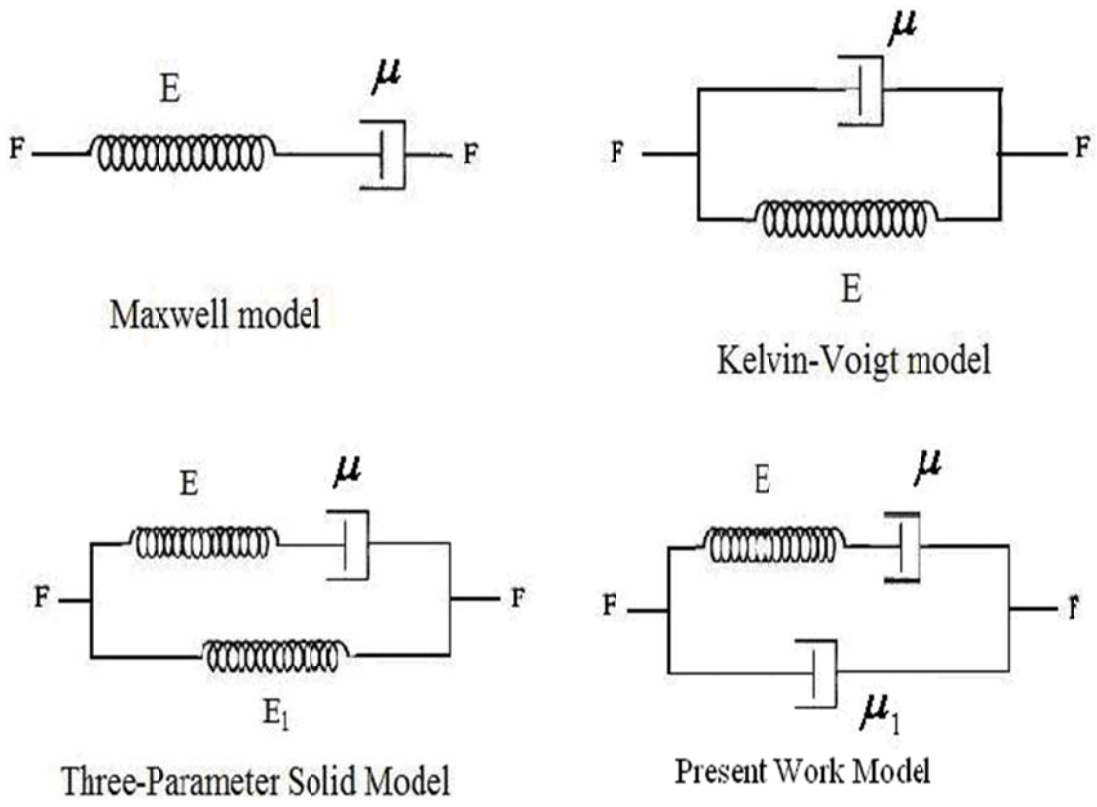

Fig. 3.2—Mechanical analogs: Maxwell Model, Kelvin-Voigt Model, and Three-Parameter Solid Model (Wineman and Rajagopal, 2000), and the present work model.

Kelvin-Voigt Model consists of a dashpot and a spring connected in parallel, **Fig. 3.2**. It is used to explain the creep behavior of polymers. The constitutive relationship is expressed as a linear first-order differential equation, Eq. 3.9 (Wineman and Rajagopal 2000).

$$\sigma = E\varepsilon + \mu \frac{d\varepsilon}{dt} \quad \text{.....(3.9)}$$

The constitutive equation for Maxwell model contains the first time derivative of both stress and strain, while the constitutive equation for the Kelvin-Voigt model contains the first time derivative of the strain only. The compliance as a function of time for Kelvin-Voigt model is:

$$J(t) = \frac{1}{E}\left(1 - e^{-(E/\mu E/)}\right), \text{ where } t > 0 \quad \text{.....(3.10)}$$

Three-Parameter Solid Model effectively combines the Maxwell Model and a spring in parallel. A viscous material is modeled as a spring and a dashpot in series, both of which are in parallel with a spring, **Fig. 3.2.** For this model, the governing constitutive relationship is defined in Eq. 3.11 (Wineman and Rajagopal 2000):

$$\frac{d\varepsilon}{dt} = \frac{\frac{E}{\mu}\left(\frac{\mu}{E}\frac{d\sigma}{dt} + \sigma - E_1\varepsilon\right)}{E_1 + E} \quad \text{.....(3.11)}$$

The compliance, J(t), for this model is:

$$J(t) = \frac{1}{E_1} + \left(\frac{1}{E + E_1} - \frac{1}{E_1}\right)e^{-\left(\frac{E_1 E}{\mu(E_1+E)}\right)t} \quad \text{.....(3.12)}$$

where, $J(0) = \frac{1}{E_1 + E}$ and $J(\infty) = \frac{1}{E_1}$ .....(3.13)

Under a constant stress, the modeled material will instantaneously deform to some strain, which is the elastic portion of the strain, and after that it will continue to deform and asymptotically approaching a steady-state strain. This last portion is the viscous part of the strain. Wineman and Rajagopal (2000) stated that the Standard Linear Solid Model is more accurate than the Maxwell and Kelvin-Voigt models in predicting material responses.

3.4 Experimental Studies

Materials: Hydrochloric acid (ACS reagent grade) titrated using a 1 N sodium hydroxide solution to determine the acid concentration, which was found to be 36.8 wt%. Calcium carbonate powder and sodium hydroxide (ACS grade) were used to partially neutralize live acids. Deionized water was used to prepare all acid solution. This water was obtained from a purification water system (BARNSTEAD EASYpure

PoDi-model D13321) and it had a resistivity of 18.2 MΩ.cm at room temperature. Polymer and other additives were all oilfield chemicals, and were used without further purification.

Measurements:Malvern-Bohlin Rheometer CS-10, which had a shear stress range from 1.2E-3 to 237.8 Pa, and a frequency range from 10^{-5} to 150 Hz, was used. Cone (4/40)/plate assembly with a gap 150 μm was used in all measurements. Two types of experiments were conducted to determine the viscoelastic properties of in-situ gelled acids: dynamic measurements (frequency, and amplitude sweep), and creep tests. pH values for the partially neutralized acids samples were measured using an Orion 370 PerpHecT Ross Electrode.

Procedure: The acid formula that was used in this work is listed in **Table 3.1**, which uses Fe^{+3} as a crosslinker. It is important to note that this is the formula that is typically used in the field. Acid solutions were prepared by mixing the corrosion inhibitor and HCl acid with water, then the polymer was added slowly to the acid. After that a crosslinker and a buffer were added to the solution, which was mixed for 30 minutes. A breaker was added to the system just before neutralizing the acid. Acid solutions were neutralized using calcium carbonate powder.

TABLE 3.1—FORMULA OF THE IN-SITU GELLED ACID	
Component	Concentration
Hydrochloric acid	5 wt% HCl
Acid gelling agent: a co-polymer of polyacrylamide emulsified in hydrotreated light petroleum distillates	20 gal/Mgal
Corrosion inhibitor: Methanol (30-60 wt%), Propargyl alcohol (5-10 wt%)	4 gal/Mgal
Cross-linker: Ferric chloride (37-45 wt%)	10 gal/Mgal
Breaker: sodium erythorbate (60 to 100 wt%)	20 lb/Mgal
Buffer: Hydroxyacetic acid (30-60 wt%)	2 gal/Mgal

Amplitude sweep, frequency sweep, and creep tests were done for acid samples. In the amplitude sweep test, stress ranged from 1.2E-3 to 237.8 Pa was applied at a constant frequency (0.1 Hz). The aim of this test was to define the linear viscoelastic region, where the elastic and viscous modulii are independent of stress. Also, the stress-strain relationship was established.

Frequency sweep test was applied by varying the frequency from 10^{-3} to 1 Hz at a constant stress (0.1 Pa). The applied stress was selected based on the amplitude sweep test to reflect the linear viscoelstic region. The objective of this test was to define the change of the viscoelastic properties with frequency or shear rate. Finally, the creep test was applied using different stress values from 0.1 to 50 Pa for 100 s, followed by a recovery creep test for another 100 s. The creep test was performed at different pH values.

3.5 Results and Discussion

3.5.1 Acid neutralization

In-situ gelled acid was prepared as described in **Table 3.1** with a crosslinker and a breaker. The prepared acid was neutralized by calcium carbonate powder to simulate the acid reaction inside the formation. During neutralization, samples from the acid were collected at different pH. The behavior of in-situ gelled acids can be divided into two regimes. The first regime was noted before crosslinking (at pH values less than 2) where in-situ gelled acids behaved as a pure viscous fluid while the second regime was observed after crosslinking (at pH values greater than 2) where the in-situ gelled acids behaved as a semi-solid elastic material.

3.5.2 Yield stress

Yield stress is defined as the stress at which a fluid begins to flow. A lower stress causes an elastic deformation that elastically disappears when the applied stress is released. The elastic deformation is linearly proportional to the applied stress. Above the yield point, the applied stress causes unlimited deformation, and the sample starts to flow. Under flow conditions, the applied stress is correlated to the rate of deformation with viscosity as the correlating factor. In the elastic region, the material behaves like Hooke's law with Young's modulus (E), Eq. 3.14 (Kreiba 2000).

$$\sigma = E\,\varepsilon \qquad (3.14)$$

The objective of in-situ gelled acids is to temporary plug high permeability zones at pH values from 2 to 4. Therefore, at that pH range, the yield stress should be high. This is because if the applied stress on the in-situ gelled exceed its yield stress, it will flow. **Fig. 3.3** shows the stress-strain curves of acid solutions at pH values from 0 (live acid) to 4.5. As the applied stress increased, the strain linearly increased. The yield stress is the point where the stress-strain curve starts to deviate from the straight line. As the applied stress further increased, the stress-strain relationship changed significantly in such a way that it became difficult to interpret the results (non-linear region).

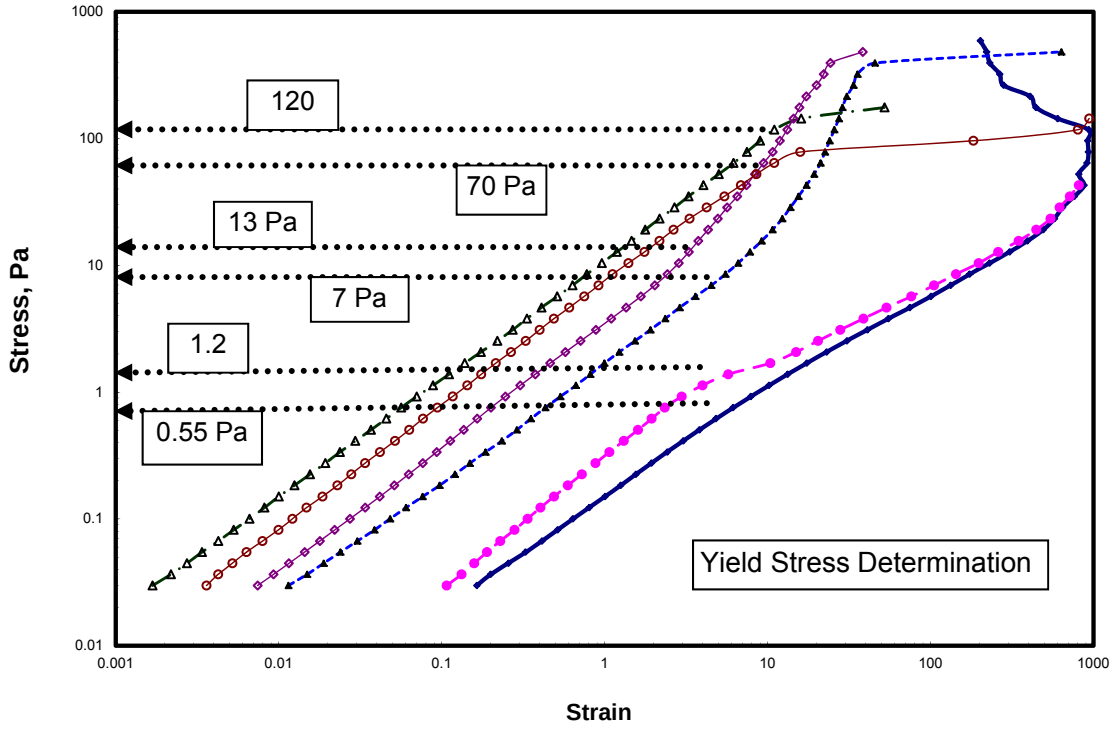

Fig. 3.3—Stress-strain curves of in-situ gelled acid at different pH values (25 ºC, frequency = 0.1 Hz). Yield stress is the point where the stress-strain curve starts to deviate from the straight line.

Fig. 3.4 shows the yield stress as a function of pH values. There was no significant change in the yield stress before the onset of the crosslinking reaction at pH 2. However at pH range from 2 to 3.2, a significant increase in the yield stress was observed due to the reaction of the polymer with the crosslinker. This was followed by a reduction in the yield stress at pH values greater than 4. This reduction occurred because of the activation of the breaker. From these results, only a shear stress of 0.55 Pa was needed to flow the live acid while a 120 Pa of stress was needed to flow the formed gel (pH 3.2). This means live acids can flow inside the formation until it reached pH 2. After neutralization above pH 2, the formed gel will remain inside the formation and will not be able to move causing plugging to the treated area. The plugged area will force the next acid stages to flow into untreated area.

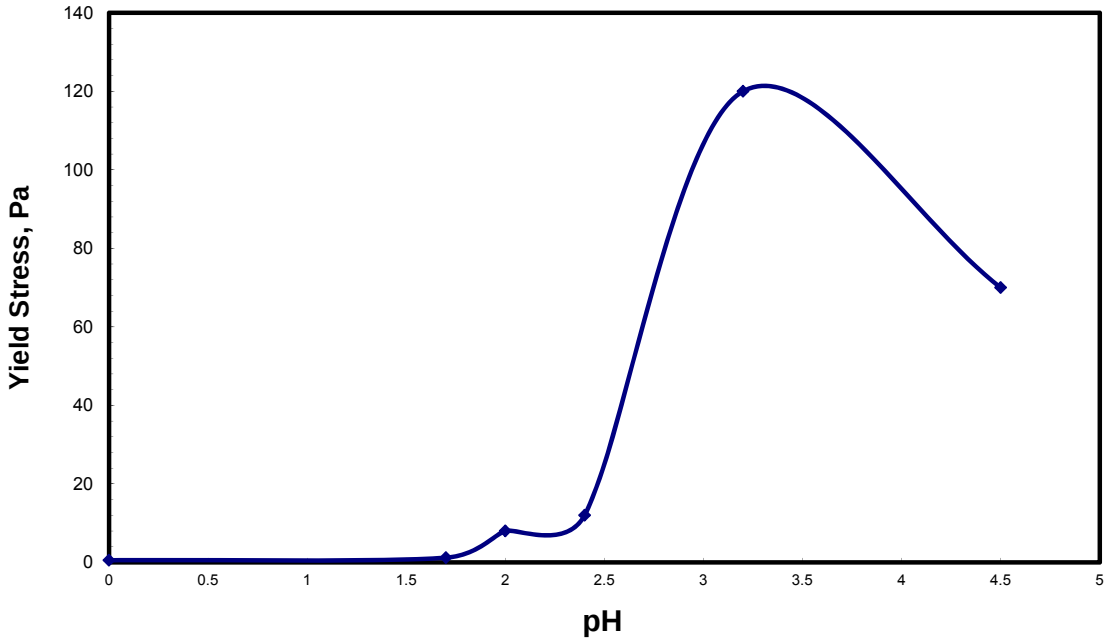

Fig. 3.4—Yield stress of in-situ gelled acid at different pH values (5 wt% HCl neutralized by $CaCO_3$, 25 ºC, frequency = 0.1 Hz).

Young modulus is another important parameter that defines the amount of strain achieved when applying a stress below the yield point, Eq. 3.14. **Table 3.2** gives Young modulus and the obtained strain before reaching the yield point as a function of pH. A significant increase in the maximum strain and Young modulus was noted at pH values from 2 to 3.2. At pH less than 2, the acid solution can stretch four times from its original dimension with 0.4 Pa Young's modulus, while at pH 3.2 it can stretch eleven times from its original dimension with 10.6 Pa Young modulus. The increase in Young modulus gives the gel more strength that is required to resist stresses from the next acid stages.

3.5.3 Complex viscosity and strain vs. shear rate

Another important point to consider when measuring strain is the shear rate at which the constant stress is applied. The shear rate was calculated from the applied frequency, ω, using Eq. 3.15 (Schramm 2000).

$$\dot{\gamma} = \frac{\omega}{\tan \alpha} \qquad \text{.....(3.15)}$$

Figs. 3.5 and 3.6 plot the complex viscosity and strain versus shear rate for live and partially neutralized (pH 3.2) in-situ gelled acids, respectively. Both measurements were conducted at a constant stress of 0.1 Pa. For live acids, **Fig. 3.5**, the complex viscosity didn't change with increasing the shear rate while the strain decreased with a

slope of 0.9615. The live acid had pure viscous properties where the strain increased to infinite with time when applying a constant stress. As the shear rate increases, the time that the fluid subjected to a constant stress decreased which reduced the strain.

For the spent acid (pH 3.2; **Fig. 3.6**), the complex viscosity decreased with a slop of 0.84 by increasing the shear rate, while the strain was almost constant. The partially spent acid represented pure elastic properties where the strain was constant with increasing the shear rate.

TABLE 3.2—YOUNG'S MODULUS AND MAXIMUM STRAIN VALUE AT DIFFERENT PH VALUES (FREQUENCY = 0.1 HZ)

pH	Young's Modulus, Pa	Maximum Strain
0	0.14	4
1.7	0.3	4
2	1.6	5.1
2.4	2.5	6.1
3.2	10.6	11.4
4.5	6.2	11.3

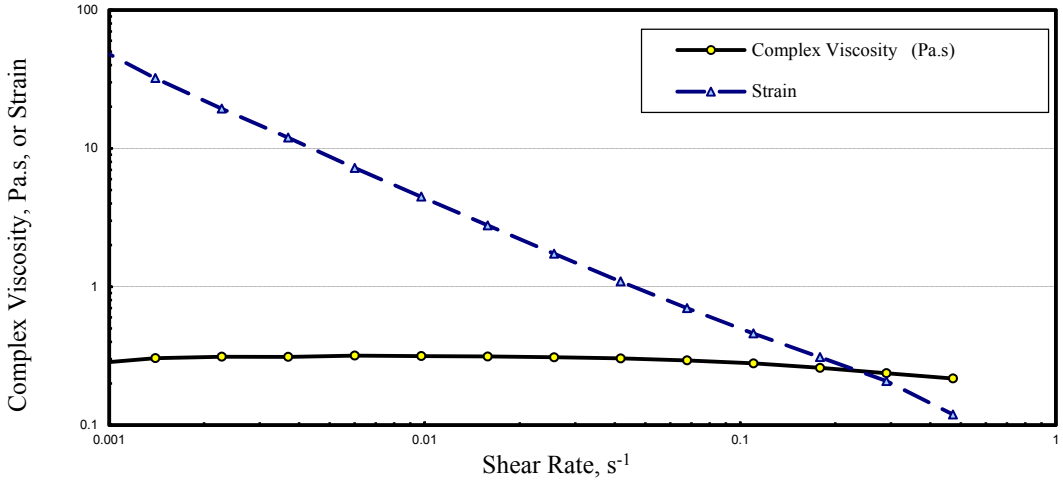

Fig. 3.5—Strain and complex viscosity vs. shear rate of live in-situ gelled acid (5 wt% HCl, 25 ºC).

3.5.4 G' and G" vs. frequency

Figs. 3.7 and 3.8 plot the complex, elastic, and viscous modulii versus frequency for live and partially spent acids (pH 3.2), respectively. **Fig. 3.7** shows the viscous modulus was dominant over the elastic modulus over the whole frequency range examined. The viscous modulus coincided with the complex modulus. As the frequency was increased from 10^{-3} to 1 Hz, the elastic modulus increased from 10^{-4} to 0.5 Pa, while the viscous modulus increased from 10^{-3} to 1 Pa. Applying a constant stress for pure viscous fluids will lead to a decrease in the strain as the frequency increases **Fig. 3.5.** Therefore, the elastic and viscous modulus increased, with frequency, Eqs. 3.3 and 3.4.

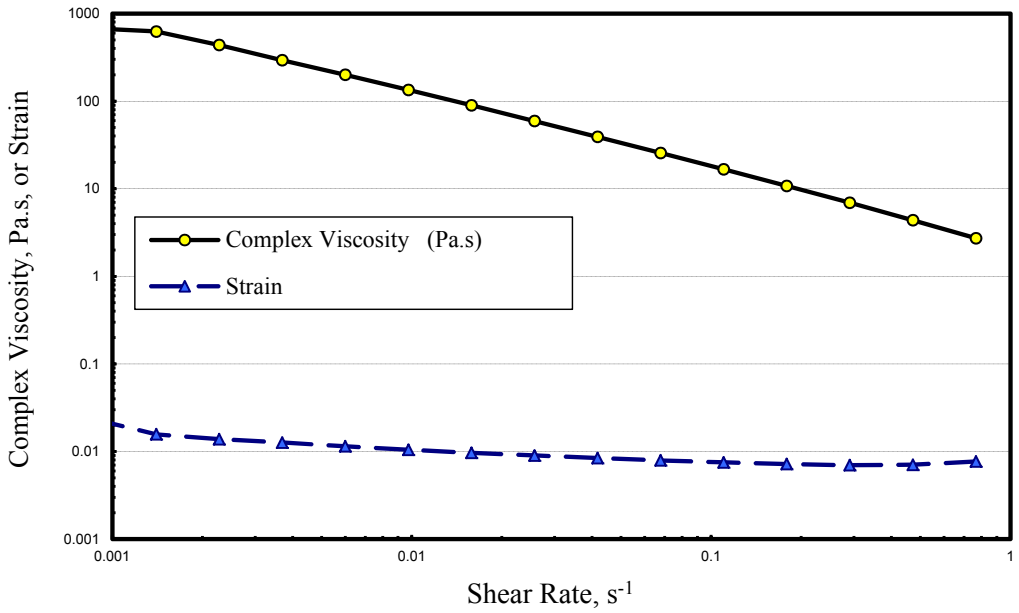

Fig. 3.6—Strain and complex viscosity vs. shear rate of 5 wt% HCl in-situ gelled acid partially neutralized to pH 3.2 (25 ºC).

For partially neutralized acid, **Fig. 3.8**, the elastic modulus was dominant over the viscous modulus. The strain was independent of the frequency at the partially neutralized acid. Therefore, G' and G" were constant with increasing the frequency. The elastic modulus data coincides with the complex modulus. Therefore, the viscous modulus can be neglected in the neutralized condition. It can be concluded that after acid crosslinking G' and G" were not affected by the shear rate while before acid crosslinking both of them increased with the shear rate. G' is the main characteristic after acid crosslinking while G" is the main characteristic before acid crosslinking, **Fig. 3.9.**

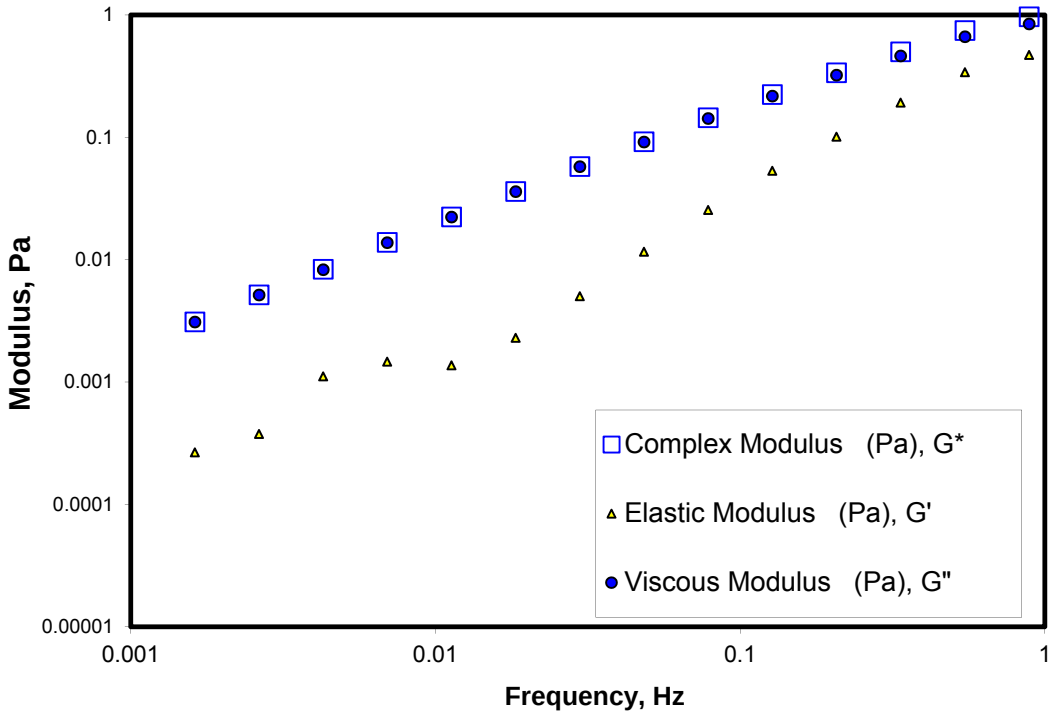

Fig. 3.7—G*, G', and G" versus frequency for live in-situ gelled acid (5 wt% HCl, 25 ºC).

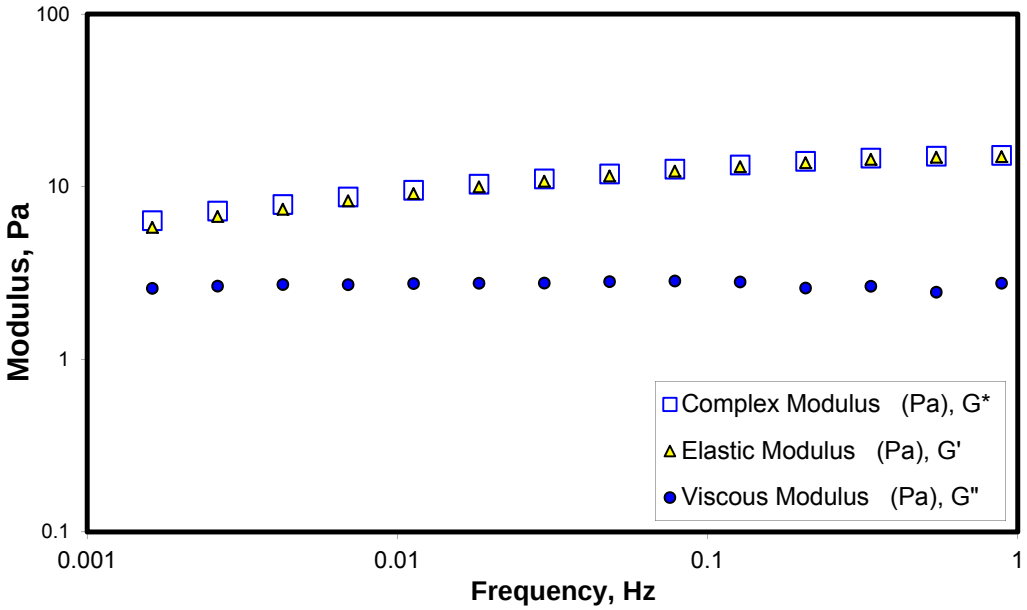

Fig. 3.8—G*, G', and G" versus frequency of 5 wt% HCl in-situ gelled acid partially neutralized to pH 3.2 (25 ºC).

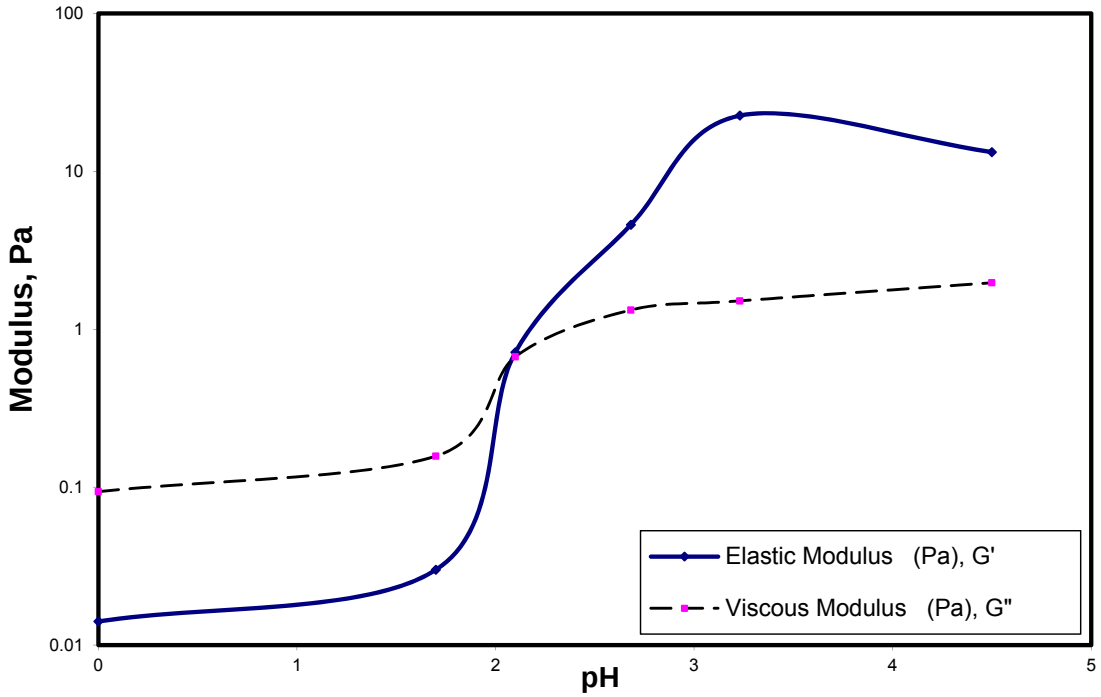

Fig. 3.9—G', and G" versus pH of in-situ gelled acid (5 wt% HCl neutralized by $CaCO_3$, 25 ºC).

3.5.5 Creep test

The creep compliance (J) is defined as the ratio between the strain to the applied stress. The value of the creep compliance doesn't depend on the applied stress, which is shown in Eqs. 3.8, 3.10, and 3.12. **Fig. 3.10** shows the results of creep test of live in-situ gelled acid at different stresses. Only at 0.1, and 0.5 Pa the creep compliance data overlapped. This means that the compliance was not depended on stress only at low applied stresses while it became dependent on stress at higher values. The yield stress of the live acid was 0.55 Pa. Therefore, any other stress above the yield point can't be applied for the creep test. The same performance was achieved for partially spent acid, **Fig. 3.11**. In partially neutralized acid, the acid had a yield stress of 120 Pa, therefore the compliance was impendent of applied stress.

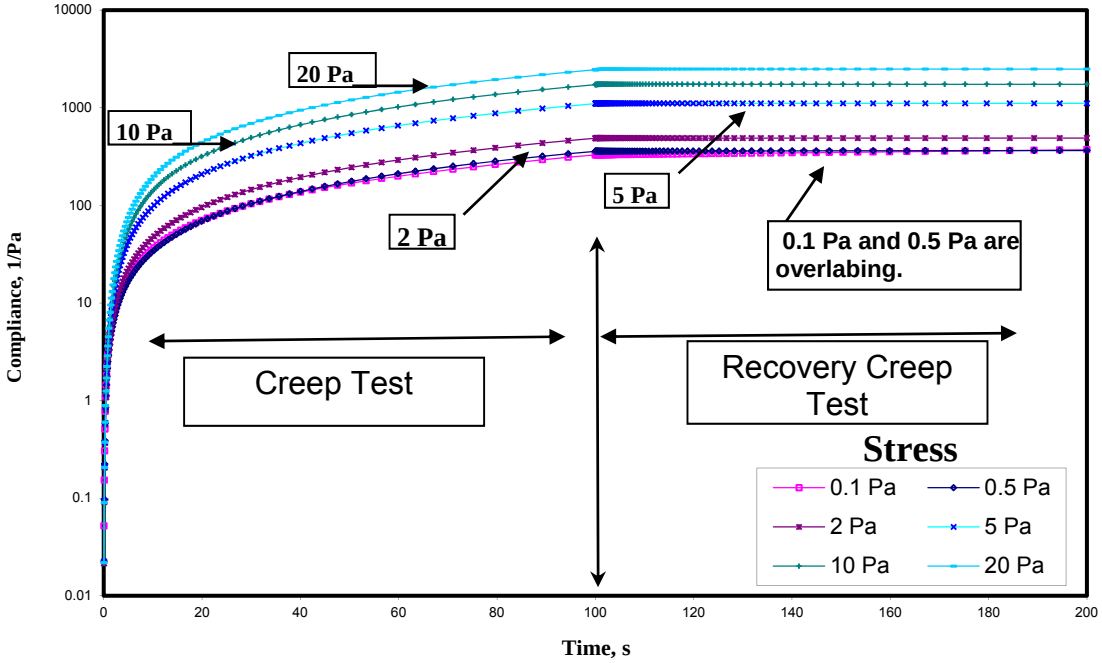

Fig. 3.10—Creep test of live in-situ gelled acid at different stresses (5 wt% HCl, 25 ºC).

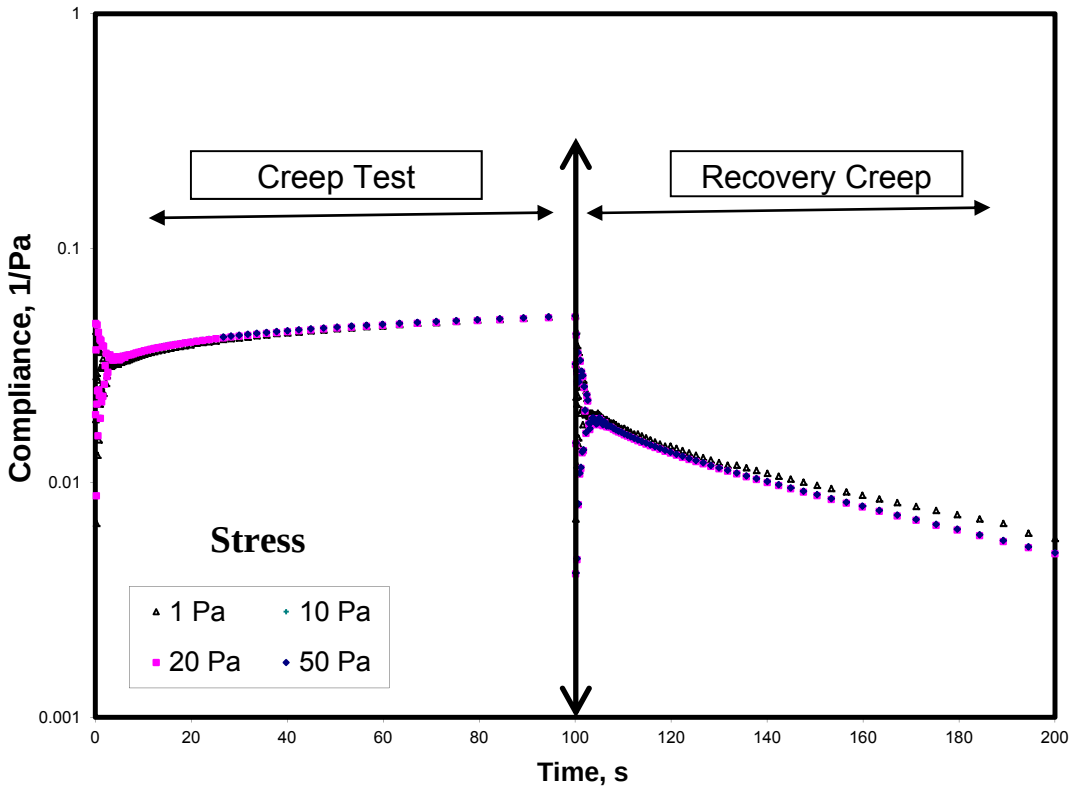

Fig. 3.11—Creep test of 5 wt% HCl in-situ gelled acid partially neutralized to pH 3.2 at different stresses (5 wt% HCl, 25 ºC).

The behavior of live acid is similar to that of pure viscous fluids, **Fig. 3.10**. When applying a constant stress, the compliance increased to infinity as the time increased, while it became constant above the time that the stress was released, i.e., the recovery creep test. The partially spent acid had a very strong viscoelstic behavior, **Fig. 3.11**. At time zero, a step increase in the compliance was noted, and then started to increase slightly with time. At the time that stress was released, 100 s, a sudden drop in the compliance was observed, and then it started to decrease with time.

3.5.6 Modeling of the rheological properties of in-situ gelled acids

Three models, Maxwell, Kelvin-Voigt, and Three-Parameter Solid have been widely used to mathematically describe the behavior of viscoelastic materials. Therefore, the three models were used to predict the rheological properties of in-situ gelled acid systems. **Figs. 3.12 and 3.13** show the results of applying the three models for the live and partially spent acids, respectively. The parameters of each model are given in **Table 3.3**. Maxwell and Kelvin-Voigt models described live acid reasonably well, while they did not predict those of the partially spent acid. Three-parameter solid model, which is more complex than Maxwell and Kelvin-Voigt models, can describe the behaviors of live and partially spent acids, **Figs. 3.12 and 3.13**. However, in live acid the values of one of the spring modulus became negative, which is not physically feasible, **Table 3.3**.

A modification was applied to the Three-Parameter Solid model to stress the viscous behavior of this acid system. This modification was to replace the attached parallel spring by dashpot which makes the systems behave more as viscous fluid. A new model was developed that has the same components of the three-parameter solid model. The new model effectively combines the Maxwell Model and a dashpot in parallel, **Fig 3.2.** For this model, the governing constitutive relationship is, Appendix A:

$$\frac{d\sigma/dt}{E}+\frac{\sigma}{\mu}=\frac{\mu_1}{E}\frac{d^2\varepsilon}{dt^2}+\left(\frac{\mu_1}{\mu}+1\right)d\varepsilon/dt \qquad \text{.....(3.16)}$$

Applying for creep test (constant stress with time), the compliance, J(t), is:

$$J(t) = \frac{1}{E}\left(1 - e^{-\left(\frac{(\mu_1 + \mu)E}{\mu\mu_1}\right)t}\right) \quad \text{.....(3.17)}$$

The constitutive equation for the Maxwell model contains the first time derivative of both stress and strain, while the constitutive equation for the Kelvin-Voigt model contains the first time derivative of strain only. According to this model and under a constant stress, the modeled material will not instantaneously deform because of the connected Newton dashpot, it will start from zero. After that it will continue to deform to approach a steady-state strain. This last portion is the elastic part of the strain. **Figs. 3.12 and 3.13** show that the new model predicts the experimental results better than the other models for both live and partially spent acids. Note that all parameters of the new model were positive, **Table 3.3.**

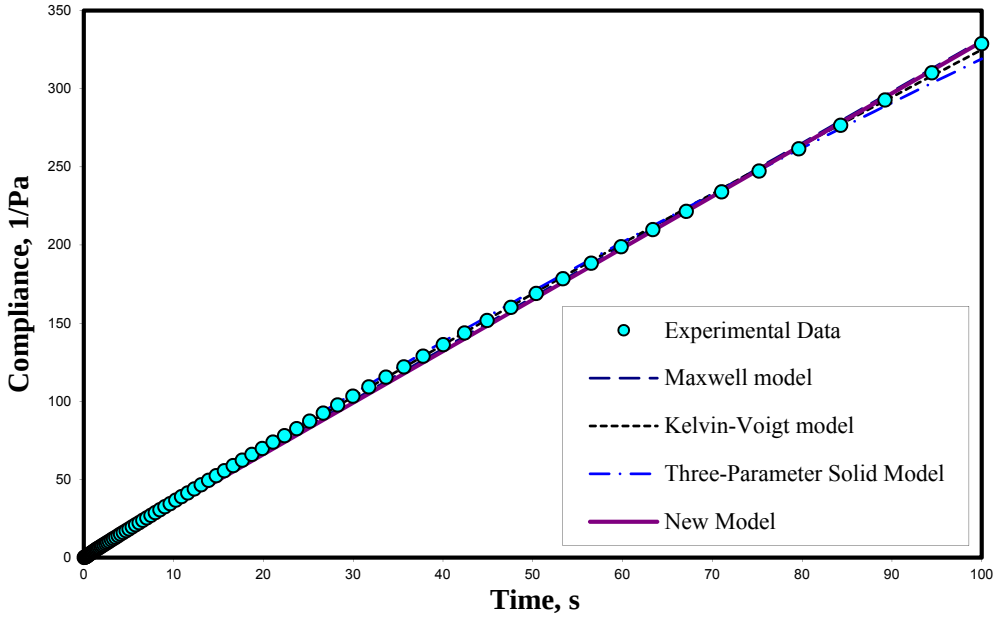

Fig. 3.12—Prediction of the creep test using various models for live 5 wt% HCl in-situ gelled acid (25 ºC).

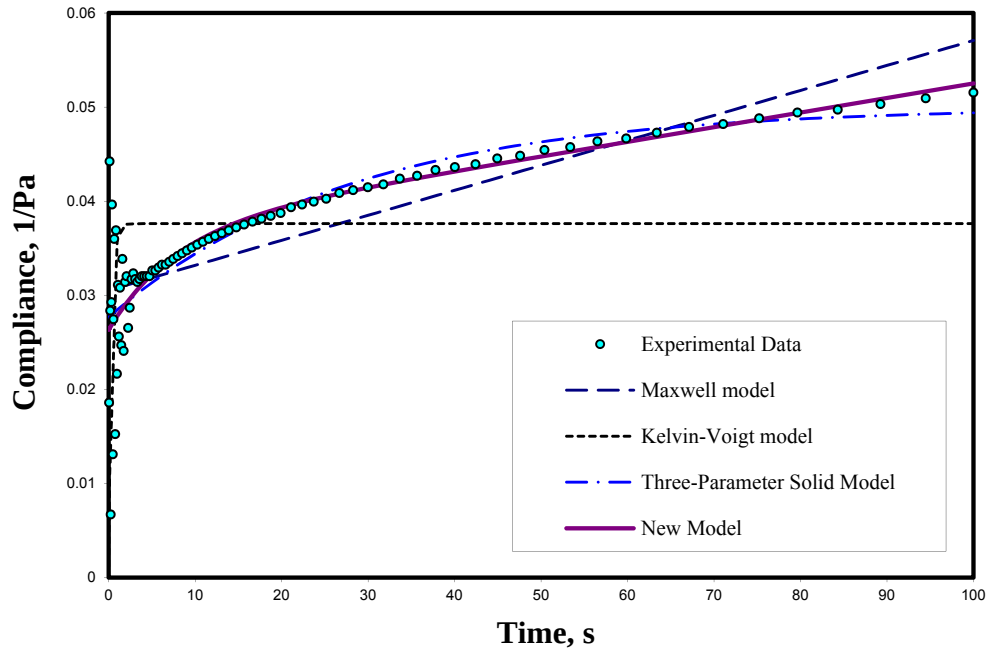

Fig. 3.13—Prediction of the creep test using various models for 5 wt% HCl in-situ gelled acid partially neutralized to pH 3.2 (25 ºC).

TABLE 3.3—RESULTS OF APPLYING THE THREE MODELS ON CREEP TEST

Model	Constant	Condition	
		Live acid	**Neutralized, pH 3.2**
Maxwell	E	0.522	32.752
	μ	0.304	3766.085
	R^2	1.000	0.802
Kelvin-Voigt	E	0.001	26.586
	μ	0.285	8.330
	R^2	1.000	0.221
Three-Parameter Solid	E_1	0.001	20.000
	E	*-1.476**	16.153
	μ	0.273	248.522
	R^2	1.000	0.950
Present Study	E	0.001	35.100
	μ	*0.321*	16.153
	$μ_1$	0.273	17.522
	R^2	1.000	0.988

* Three-Parameter Solid Model is not applicable for live acid because it gives a negative elastic value for the spring.

4. EFFECT OF VISCOEALSTIC PROPERTIES ON THE PROPAGATION OF GELLED AND IN-SITU GELLED ACIDS INSIDE CARBONATE FORMATION

Rheology of the polymer based acids exhibit to have some viscoelastic properties. Therefore, the objectives of this study are to determine the elastic and viscous properties of these acids, how these properties change as the acid reacts with carbonate formations, and what their effect on propagation of the acid inside 20-in. long cores.

Live gelled and in-situ gelled acids had weak viscoelastic properties while partially neutralized (pH 3.2) in-situ gelled acid had strong viscoelastic properties. Polymer filter-cake was observed only for the core that treated with gelled acid injection while the core that treated with in-situ gelled acids didn't form any polymer filter-cake. In-situ gelled acid formed a thin layer of gel that minimizes the leak-off which prevents the build of polymer filter-cake. For gelled acid, the polymer filter-cake reduced the core permeability to zero by plugged the core holder inlet during the water flow back. However after removing the plugging, a permeability enhancement was much higher than in-situ gelled acids. The wormhole obtained in case of gelled acid was nearly linear and thinner than the wormhole created by in-situ gelled acid. The strong viscoelastic properties give the ability to the gel to sustain around the wormhole and plug it. This will force the next acid stage to change its direction.

4.1 Introduction

Acids viscosified by polymers are probably applicable to all completion types. They are of particular benefit in horizontal, openhole, and gravel-packed wells, where many other diversion and selective placement techniques cannot be applied. The viscous fluid can be placed efficiently along the treatment interval because it can first limit fluid loss into the formation and then divert itself from regions of high to low injectivity as it was injected into the formation (Jones et al., 1996). Jones and Davies (1996) compared using a simulator between a gelled acid with a viscosity of 70 cp at a shear rate of 100 s^{-1} and conventional low-viscosity acids based on the coverage obtained over the wellbore interval. They showed that in many cases, viscosifying the fluid can dramatically improve the placement over the wellbore interval.

Two types of polymer-based acids had been used in the field: (1) gelled acid for acid retardation, and (2) in-situ gelled acids for acid diversion. Gelled acids were developed primarily for fracturing but have found some applications in matrix acidizing. They are used in acid fracturing to increase the viscosity and decrease the leak off rate. The same principle applies to matrix acidizing conditions in fissured or vugular formations with low primary porosity. Gelled acids can also be used as a carrier fluid for ball sealers or particulate diverters. Since gelled acid is a shear-thinning (non-Newtonian) fluid, its viscosity increases further away from the wellbore, thereby blocking the following acid and diverting it to other, less permeable zones (Economides, 2000).

In-situ gelled is another polymer-based acid systems that have been proposed and successfully used for viscous acid diversion in carbonate formations. In-situ gelled acid consists of HCl mixed with a gelling agent and a crosslinker (Conway et al., 1999).

Taylor and Nasr-El-Din (2003) examined three different in-situ gelled acids and found that the viscosity of some of these systems did not behave with the pH as claimed by some vendors. Therefore, testing of in-situ gelled acids in the lab before field application is recommended. Amro (2006) noted that viscosity of the polymer-based in-situ gelled acids depends on shear rate, salinity, temperature, acid, and polymer concentration. Abdel Fatah et al. (2008) found that in-situ gelled acids that are based on aluminum formed a gel at pH higher than that noted with iron-based cross-linkers. Also, corrosion inhibitor affected the pH at gelation: it reduced the pH at gelation for the iron cross-linker; whereas it increased the pH at gelation for the aluminum cross-liker. Polymer was separated out at high salt concentrations. Therefore, this acid should not be prepared using seawater.

Metzner (1961) stated that the most polymer solutions have rheological properties that are partly viscous and partly elastic. Whereas elasticity is usually the result of bond stretching along crystallographic planes in an ordered solid, viscoelasticity is the result of the diffusion of atoms or molecules inside of an amorphous material (Meyers and Chawla, 1999). Jones (1981) showed that viscoelasticity of polymer solutions is the main factor influencing sweep efficiency in polymer flooding. As the sweep efficiency increases, the fingering problems will decrease which leads to better diversion. Therefore, Elastic modulus will be the main parameter in acid diversion.

Gelled and in-situ gelled acids have been used extensively in the field. To the best of our knowledge, no pervious studies were done to examine the differences between the behavior of theses acids using oscillatory rheometer. Therefore, the objectives of this work are to: (1) study the viscoelastic properties of gelled acids and in-situ gelled acids and (2) examine the effect of these properties on the propagation of gelled and in-situ gelled acid inside 20-in. long cores.

4.2 Experimental Studies

Materials: Hydrochloric acid (ACS reagent grade) was titrated using a 1 N sodium hydroxide solution to determine the acid concentration, and which was found to be 36.8 wt%. Calcium carbonate powder (ACS grade) was used to neutralize the live acid. Pink desert limestone cores (1.5-in. diameter, and 20-in. length) had the properties given in **Table 4.1**. Deionized water obtained from a water purification system that had a resistivity of 18.2 MΩ.cm at room temperature. Polymer, cross-linker and other additives were all oilfield chemicals, and were used without further purification.

Measurements: The rheology of gelled and in-situ gelled acid was measured using Malvern-Bohlin Rheometer CS-10. Cone (4/40) - plate assembly with a gap of 150 μm was used in all measurements. Core flood setup was constructed to simulate matrix stimulation treatments. A back pressure of 1,000 psi was applied. Pressure transducers were connected to a computer to monitor and record the pressure drop across the core during the experiments. Teledyne ISCO D500 precision syringe pump, that had maximum allowable working pressure equal to 2,000 psi, was used to inject the acid

inside the core. pH values for the collected samples were measured using Orion 370 PerpHecT Ross Electrode, while calcium and iron concentrations were measured using atomic absorbance spectrometer (AAnalyst 700-flame type). X-ray Computed Tomography (CT) was used to scan the cores before and after acid injection.

Procedures: Gelled and in-situ gelled acids were prepared using the same polymer type and concentration. Also, both systems had the same HCl concentration (5 wt%) and additives. The only difference between the two systems was adding the crosslinker (Fe^{+3}) and breaker for in-situ gelled acid while gelled acid was prepared without adding the crosslinker (Fe^{+3}) and breaker. The acid formula that used in this work is listed in **Table 4.2**. It is important to highlight that these are the formulas that are typically used in the field.

TABLE 4.1: SUMMARY OF THE COREFLOOD EXPERIMENTS DATA

Core	Porosity, vol%	Acid type	Rate, cm^3/min	Volume of injected acid, PV	Permeability, md	
					Before	After
1	32.1	Gelled	10	3.5[a]	89	0[e]
2	31.1	Gelled	20	3.9[b]	80	0[f]
3	31.7	In-situ Gelled	10	4.1[c]	82	146
4	35.0	In-situ Gelled	20	3.7[d]	88	251

a. Acid propagated only 75% of the core
b. Acid breakthrough the whole core
c. Acid propagated only 45% of the core
d. Acid propagated only 60% of the core
e. During flow back, core holder inlet was plugged by polymer filter-cake. The permeability was measured after removing polymer filter-cake and was found to be 251 md.
f. During flow back, core holder inlet was plugged by polymer filter-cake. The permeability was measured after removing polymer filter-cake and was found to be 871 md.

TABLE 4.2—FORMULA OF GELLED AND IN-SITU GELLED ACIDS		
Component	**Gelled**	**In-situ**
Hydrochloric acid	5 wt% HCl	5 wt% HCl
Acid gelling agent: a co-polymer of polyacrylamide	20 ml/l	20 ml/l
Corrosion inhibitor: Methanol (30-60 wt%),	4 ml/l	4 ml/l
Cross-linker: Ferric chloride (37-45 wt%)	-	10 ml/l
Breaker: sodium erythorbate (60 to 100 wt%)	-	20 lb/Mgal
Buffer: Hydroxyacetic acid (30-60 wt%)	2 ml/l	2 ml/l

Calcium carbonate powder was used to neutralize the gelled and in-situ gelled acid solutions. During neutralization, different samples from both acids were collected, and tested at different equilibrium pH values. Each sample was adged at least 1.5 hr after neutralization to be sure that the equilibrium state was reached. Amplitude sweep, frequency sweep, and creep tests were done for partially spent acids samples. For amplitude sweep test, a stress range from 1.2E-3 to 237.8 Pa was applied at a constant frequency (0.1 Hz) to define the linear viscoelastic region. Also from this test, the stress-strain relationship was established.

Based on results from the amplitude sweep test, a 0.1 Pa stress value was selected to run the frequency sweep test. The selected stress value reflected the linear viscoelastic region at all pH values for both acids. The objective of frequency sweep test was to define the change in the viscoelastic properties with frequency. Finally, the creep test was applied using a shear stress of 0.1 Pa for 100 s, followed by a recovery creep test for another 100 s at different pH values. Results from creep test will show how gelled and in-situ gelled acid will behave with time.

Coreflood experiments were conducted for each system (gelled and in-situ gelled acid) at flow rates of 10 and 20 cm^3/min. A new core was used in each experiment. Core preparation was done by weighed the core dry and saturated with water to calculate the pore volume. The core was CT scanned before and after acid injection. The core permeability was measured by inject water at 10 cm^3/min, and monitor the pressure across the core. To heat up the core to 250°F, a heat jackets was placed around the coreholder and all accumulators. Water was injected at 2 cm^3/min during the heating period. Temperature was monitored at the outlet of the core. Pressure drop across the core was monitored during acid injection. After acid injection, water was injected in the opposite direction of acid injection (production direction). Effluent samples were collected throughout the experiment using an automatic fraction collector. pH value, density, and the concentrations of calcium and total iron for the collected samples were measured to conduct material balance on both calcium and total iron.

4.3 Results and Discussion

4.3.1 Creep test

The results of creep test of gelled acid at different equilibrium pH values shown in **Fig. 4.1.** The behavior of gelled acids was independent of pH. By applying a constant stress, the compliance increased to infinity as the time increases, while it became constant at and above the time that stress was released. Gelled acid behavior was typically the behavior of fluid that had weak viscoelastic properties (Wineman and Rajagopal, 2000).

The compliance of the in-situ gelled acids as a function of time at different pH values was plotted in **Fig. 4.2**. At pH values less than 2, compliance of in-situ gelled acid behaved as the compliance of gelled acid with nearly the same values. However, at pH values higher than 2, compliance of in-situ gelled acid increased instantaneously at time zero and became nearly constant until the time that the stress was released. Values of the compliance were significantly reduced when pH increased. Therefore, a log scale was used in the compliance to highlight its different at different pH values. The behavior of in-situ gelled acids was dependent on the pH values where before initiating the crosslinking reaction (at pH values less than 2) in-situ gelled acids behaved as weak viscoealstic fluid like gelled acids. While after initiating the crosslinking reaction (at pH values greater than 2), in-situ gelled acids behaved as a semi-solid elastic material.

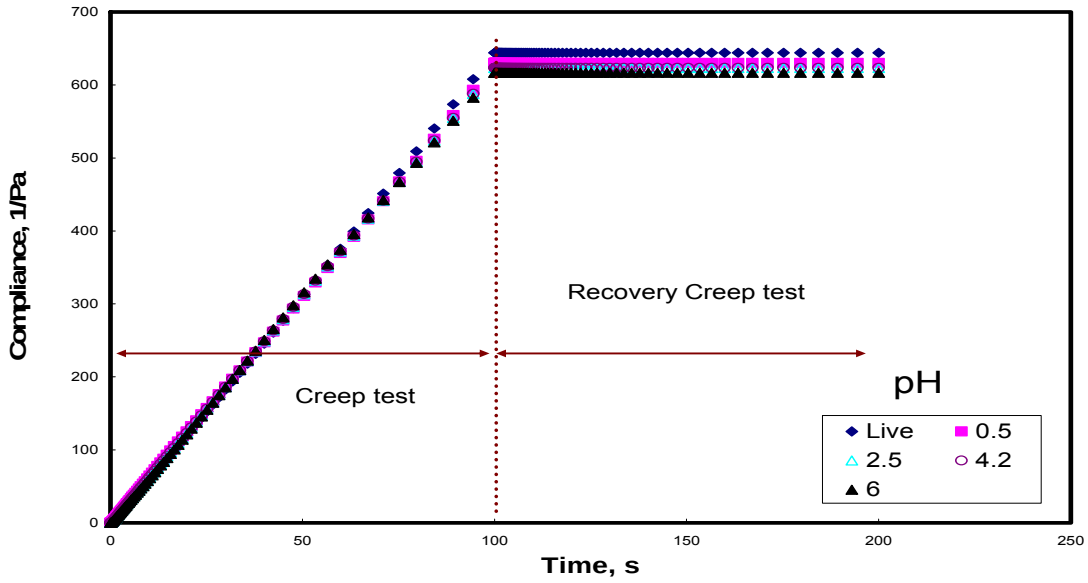

Fig. 4.1—Compliance as a function of pH values for gelled acids (5 wt% HCl, 25 ºC, shear stress = 0.1 Pa).

4.3.2 Yield stress

Yield stress is the stress needed to initiate fluid flow. Liu and Seright (2001) defined the yield stress as the point where the stress-strain curve started to deviate from its linear trend. The objective of polymer-based acids was to force the acids toward the less permeable or damaged zones. Therefore, a high yield stress value was needed. **Fig. 4.3** shows the yield stress of gelled and in-situ gelled acids as a function of equilibrium pH values. There was no change in the gelled acid's stress-strain relationship as the pH was increased due to neutralization. Therefore, the yield stress of gelled acid was nearly constant at a value of 0.56 Pa.

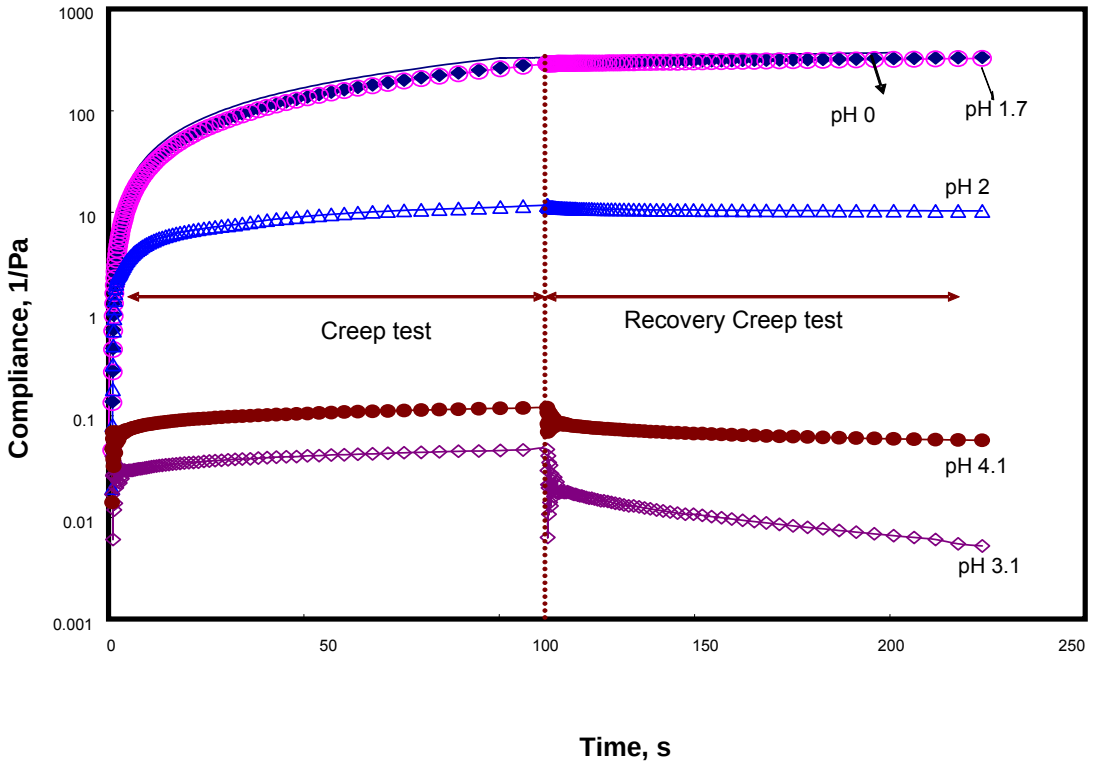

Fig. 4.2—Compliance as a function of pH values for in-situ gelled acids (5 wt% HCl, 25 ºC, shear stress = 0.1 Pa).

For in-situ gelled acid, there was no significant change in the yield stress before initiating the crosslinking reaction (pH less than 2). However, at pH >2, a significant increase in the yield stress was observed. Only a shear stress of 0.55 Pa was needed to flow the live acid while a 120 Pa of stress was needed to flow the formed gel (partially neutralized acid, pH 3.2). This means live in-situ gelled acids could flow inside the formation until it reached pH 2. After that, the formed gel would remain inside the formation and wouldn't be able to move. This would plug the treated area and force the next acid stages to flow into the untreated area.

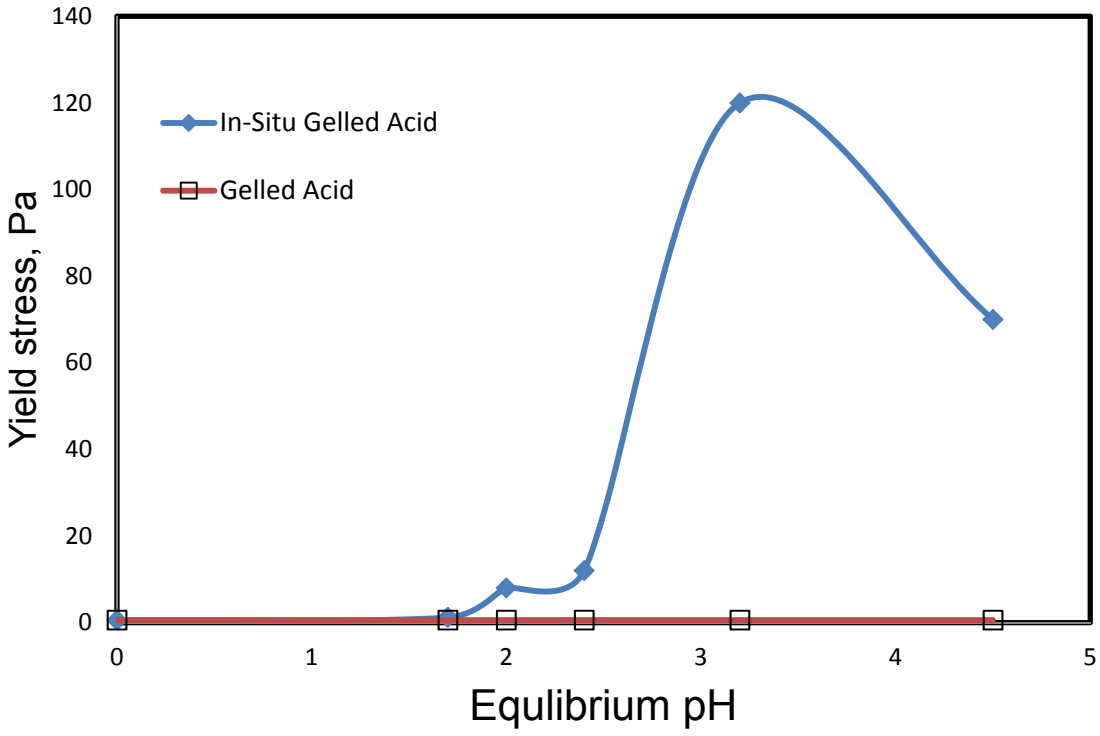

Fig. 4.3—Yield stress values of gelled and in-situ gelled acids as a function of equilibrium pH values (25 ºC, frequency = 0.1 Hz).

4.3.3 G’ and G” vs. frequency

Fig. 4.4 shows the elastic (G’), and viscous (G’’) modulii as a function of frequency for live and neutralized (pH = 6) gelled acids, respectively. Values of G’ and G” was independent of the values of pH where G’ and G” where identical at different pH values. As the frequency increased from 10^{-3} to 1 Hz, the elastic modulus increased from 10^{-4} to 0.5 Pa, while the viscous modulus increased from 10^{-3} to 1 Pa. The viscous modulus was higher than the elastic modulus for the whole applied frequency range. The elastic modulus could be ignored when it compared to viscous modulus. In addition, the values of G’ and G” were relatively small at all pH values. This is evidence on the weak viscoelastic properties of the gelled acid.

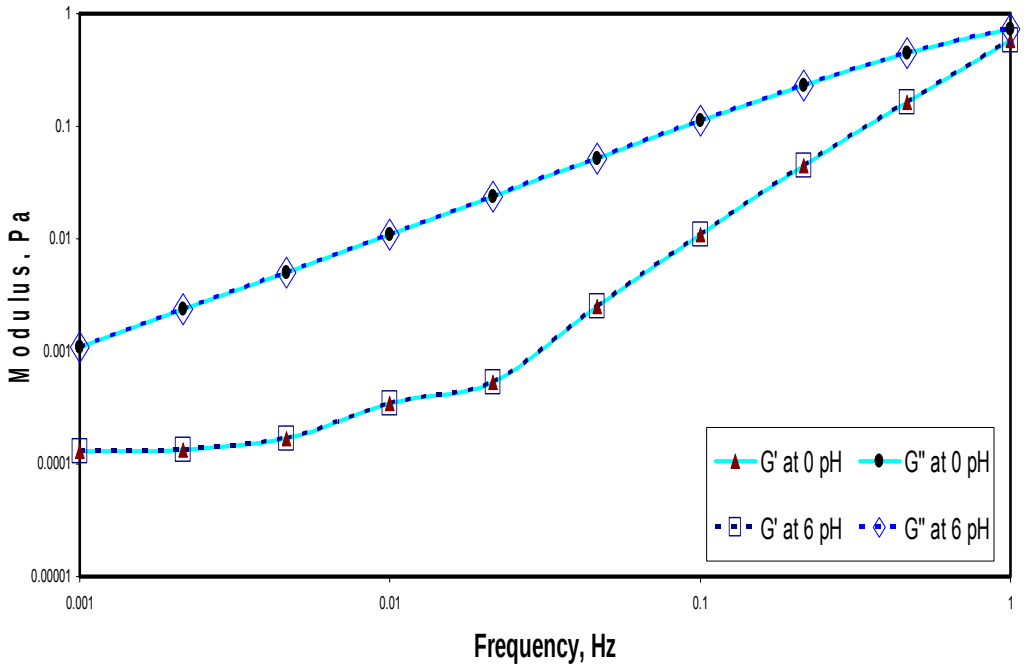

Fig. 4.4—G’, and G” versus frequency of 5 wt% HCl gelled acids neutralized at live and neutralized (pH 6) conditions, 25 ºC, shear stress = 0.1 Pa.

Fig. 4.5 shows the elastic, and viscous modulii of in-situ gelled acid versus frequency at live and spent (pH = 3.2) conditions, respectively. At live conditions, the viscous modulus was dominant over the elastic modulus for the whole applied range of frequency. This was the same behavior of gelled acids with nearly the same values. As the frequency increased from 10^{-3} to 1 Hz, the elastic modulus increased from 10^{-4} to 0.5 Pa, while the viscous modulus increased from 10^{-3} to 1 Pa. For partially neutralized acid (pH = 3.2), the elastic modulus was dominant over the viscous modulus, **Fig. 4.5**. G' and G" were nearly constant with increasing the frequency. Also, the viscous modulus could be neglected when it was compared to the elastic modulus. Therefore, it can be concluded that after acid crosslinking: G' and G" didn't affect by frequency while before acid crosslinking both of them increased with the frequency. G' was the main characteristic after acid crosslinking while G" was the main characteristic before acid crosslinking.

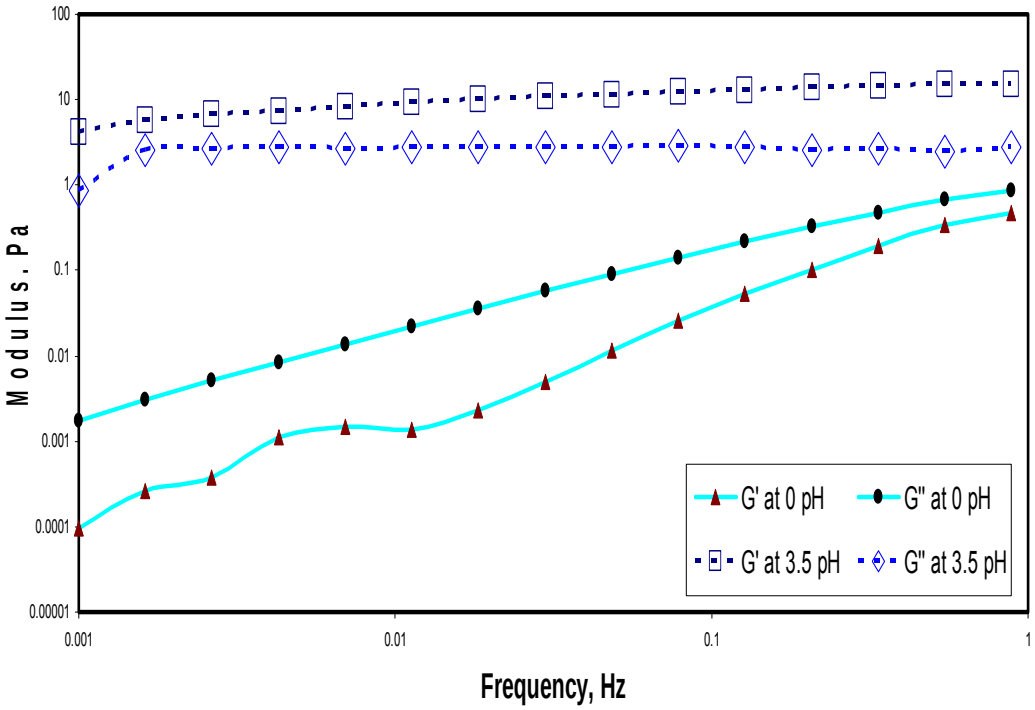

Fig. 4.5—G', and G" versus frequency of 5 wt% HCl in-situ gelled acid at live and neutralized (pH 3.5) conditions, 25 ºC, shear stress = 0.1 Pa.

4.3.4 Coreflood study

The first two core flood experiments were conducted at rate of 10 cm^3/min using gelled and in-situ gelled acids for cores 1 and 3, respectively. **Fig. 4.6** shows the change in the pressure drop a cross the cores 1 and 3 as a function of the cumulative volume injected for both acids. Pressure drop across Core 1 increased gradually until it reached to 500 psi after injection of 1.1 PV of gelled acid. After that pressure drop was nearly constant until injection of 2 PV when it stared to decrease to a value of 300 psi at the point that gelled acid injection was stopped, **Fig. 4.6**. As in-situ gelled acid entered the core (**Fig. 4.6**), pressure drop increased instantaneously by 84 psi and became a constant until 0.5 PV. After that pressure drop increased again by 70 psi at 0.6 PV then behave in

cycling performance until in-situ gelled acid injection was stopped. A 3.5 PV of gelled acids was injected while a 4.2 PV of in-situ gelled acid was injected. Both acid systems were not able to propagate through the whole core. There was no indication for acid breakthrough. Acid injection of both experiments was stopped because of reaching to the maximum capacity of the acid accumulator.

Two additional coreflood experiments were conducted at 20 cm^3/min for cores 2 and 4 using gelled and in-situ gelled acids, respectively. A 3.9 PV slug of gelled acid was injected through Core 2. **Fig. 4.7** shows the change in the pressure drop a cross the Core 2 as a function of the cumulative volume injected. As the gelled acid entered the core, the pressure drop increased gradually (as it noted for Core 1) until reached 0.75 PV. However, the pressure drop kept to increase in steps performance. The step level was around 10 psi until reaching 1.5 PV which instantaneously increased to 75 psi. From 1.5 to 1.9 PV, pressure drop slowly increased with the acid injection from 435 psi to 450 psi, then another step was achieved at 1.9 PV with a 117 psi increasing. The same performance was repeated until acid breakthrough from the core after reaching a maximum pressure drop value of 695 psi.

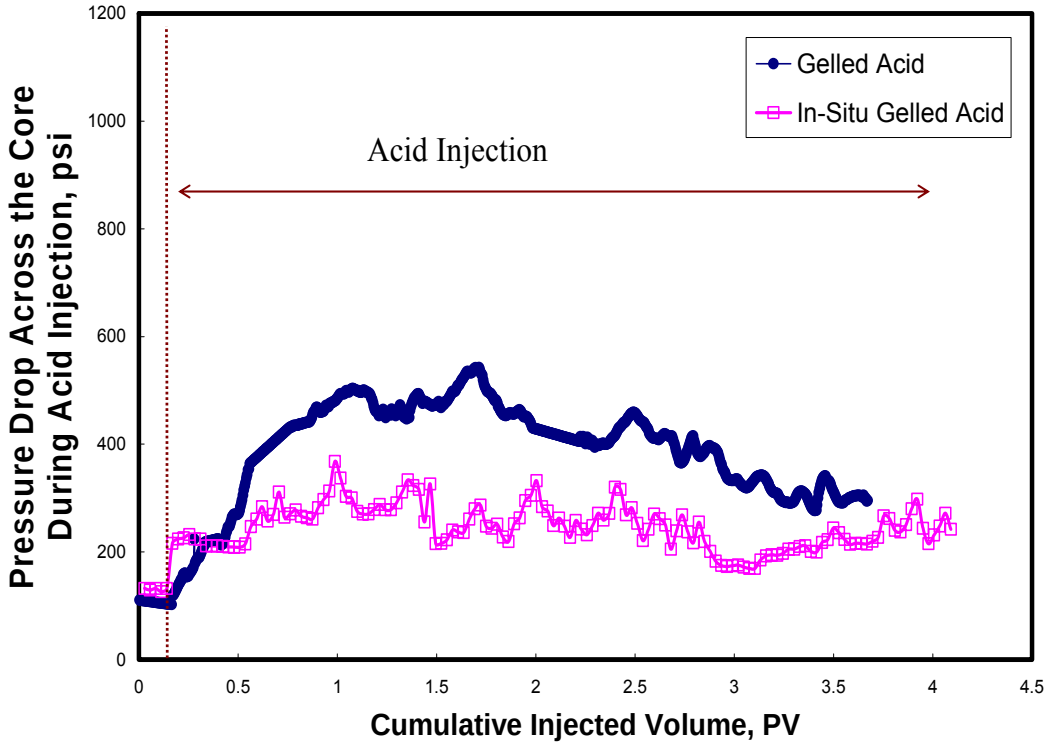

Fig. 4.6—Pressure drop across cores 1 and 3 during injected gelled and in-situ gelled acid at 10 cm^3/min and T = 250 ˚F.

Fig. 4.7 shows the pressure drop across core 4 during the injection of in-situ gelled acid at 20 cm^3/min. A 3.7 PV acid slug was injected, which was the maximum capacity of the acid accumulator. The pressure drop increased instantaneously (as it noted for Core 3) to 370 psi. After that the pressure drop increased slowly in a cycling behavior.

The pressure drop across the core increased gradually with gelled acid injection while for in-situ gelled acid, the pressure drop across the core increased incautiously as the in-situ gelled acid entered the core, **Figs. 4.6 and 4.7**. Also, the values of the pressure drop across the core in the case of gelled acid injection were higher than in the case of in-situ gelled acid injection, **Figs. 4.6 and 4.7**. Rheological study confirmed that

when in-situ gelled acid reacted with the carbonate, it formed a gel that wouldn't flow inside the formation. Therefore, it should be expected a high pressure drop across the core that injected by in-situ gelled acid. However, the two experiments confirmed that the core that injected with the gelled acid has a higher pressure drop. This is because a significant filter-cake was formed on the inlet face of the cores that were treated with gelled acid. This agrees with Bazin et al. (1999) where they noted a potential problem with polymer gelling agents was filter-cake formation near the core surface which hinders the wormhole formation.

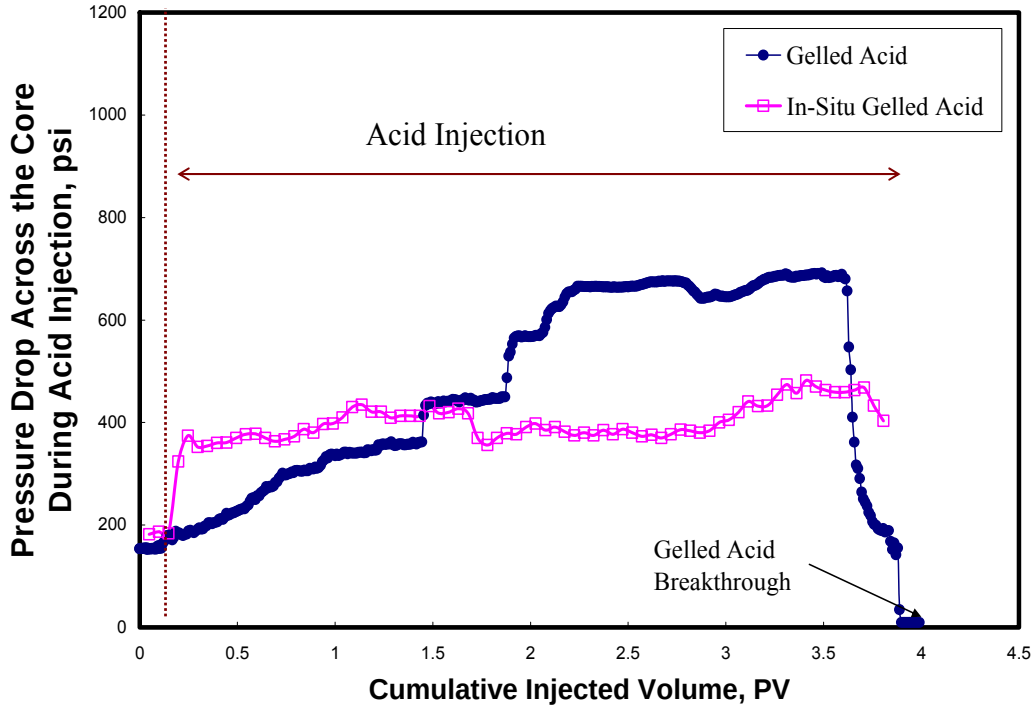

Fig. 4.7—Pressure drop across cores 2 and 4 during injected gelled and in-situ gelled acid at 20 cm^3/min and T = 250 ˚F.

Fig. 4.8-A shows a photo of the inlet of Core 2, which was covered by a polymer filter-cake that formed during gelled acid injection. While **Fig. 4.8-B** shows the core-holder inlet face of the same core, which was totally plugged by the filter-cake during the flow back of the gelled acid by the water. All cores that injected by gelled acid suffered from a polymer filter-cake that reduced the return permeability to a value of zero.

However, after cutting the damaged zone from the core inlet using electrical saw, and re-flow back the core again with water. The permeability was increased significantly from 89 to 251 md for Core 1 and from 80 to 871 md for core 2, **Table 4.1**. The outlet of Core 2 was not damaged as seen in **Fig. 4.8C**.

For the in-situ gelled acid, the problem of the polymer filter-cake wasn't significantly achieved. There was a thin layer of gel material found on the core inlet, **Fig. 4.8D.** Also, the flow back of the core was done without plugging of the core-holder inlet. The permeability was increased from 82 to 146 md for core 3 and from 88 to 251 md for core 4, **Table 4.1**.

Based on the above observations, an important question was raised: why only a significant polymer filter-cake was observed in the case of gelled acid only? To answer this question, it needed to highlight that a polymer filter-cake wouldn't form except when a leak-off in the core inlet occurred.

A. Core 2: Inlet Face (Gelled Acid)

B. Core 2: Core-Holder Inlet Face (Gelled Acid)

C. Core 2: Outlet Face (Gelled Acid)

D. Core 4: Inlet Face (In-Situ Gelled Acid)

Fig. 4.8—Photos of the cores inlet and outlet after acidizing.

Therefore, the above question could be rephrased as why there was a leak-off in the core inlet for gelled acid system while there was no leak-off in the core inlet of the in-situ gelled acid? When in-situ gelled acid entered the core, it reacted with the core inlet face leading to form a gel layer on the core inlet. As it discussed before, this formed gel (at pH higher than 2) had a high yield point and high elastic modulus (strong viscoelastic properties). This gel layer plugged the inlet phase, and forced polymer to flow only through the open path (wormhole). The formed gel layer by in-situ gelled acid could not sustain the polymer because there was no leak-off that required building the polymer filter-cake.

However, in case of gelled acid, the formed polymer layer had low yield point and weak elastic properties that cannot prevent the leak-off. This conclusion was supported by the monitored pressure drop across the cores, **Figs. 4.6 and 4.7**. For gelled acid, pressure drop increased gradually due to the build of the filter-cake while for in-situ gelled acid the pressure increased instantaneously because of the plugging effect of the formed gel layer. It is important to highlight that: in the field, the formed polymer filter-cake can plug the perforation and cause saver damage during the flow back of the well.

4.3.5 Effluent sample analysis

Fig. 4.9 shows the pH values and density of the effluent samples of core 3 (in-situ gelled acid) as a function of the cumulative volume injected. Initial pH value was nearly 7 and the initial density was nearly 1 gm/cm^3. After injection 0.85 PV of acid solution, pH started to decrease with the acid injection to value of 5 just before stopping the acid injection. This decrease of the pH values combined with increasing of density of effluent samples. The decrease of pH value and the increase in the density was the evidence of the breakthrough of calcium and iron as it shown in **Fig. 4.10**. Calcium and iron concentration increased at the same time that the pH decreased. Using titration technique, there was no indication of acid breakthrough from the core at that time that the pH started to decrease.

During the water flow back, pH instantaneously decreased due to the flow back of un-reacted acid. However, pH increased again until a value of nearly 7 due to water

flow back, **Fig. 4.9**. Calcium and iron concentrations decreased as water flow beak increased, **Fig. 4.10**. Same pH, density, calcium and Iron performance were achieved for all other cores (Cores 1, 2 and 4).

Table 4.3 shows a summary of material balances conducted on total calcium and iron for the four experiments. Using the concentration of each sample and its volume, the amount of Calcium and iron were calculated in grams. The amount of dissolved $CaCO_3$ was calculated by multiplying the amount of dissolved calcium by 2.5 (MW_{CaCO3} / MW_{Ca}), **Table 4.3**. The calculated amount of $CaCO_3$ was agreed with amount of $CaCo_3$ that calculated based on the dissolved acid during each experiment. Material balance on iron concentration indicated that there was iron loss inside the core for cores 3 and 4 where 35 and 29 wt% of iron present in the injected acid was left inside the core. Iron, which remained inside the core, might be in one of the following forms: hydrated ferric hydroxide precipitated in the core and/or as a gel residue that didn't break at the test conditions as noted by lynn and Nasr-El-Din (2001).

TABLE 4.3—MATERIAL BALANCE CALCULATION FOR IRON AND CALCIUM

Core	Collected calcium, g	Dissolved $CaCO_3$, g	Total iron, g	Collected iron, g	Remaining iron, %
1	18.9	47.5	-	-	-
2	18.8	47.1	-	-	-
3	20.6	51.4	0.69	0.45	34.7
4	20.4	50.9	0.68	0.48	29.4

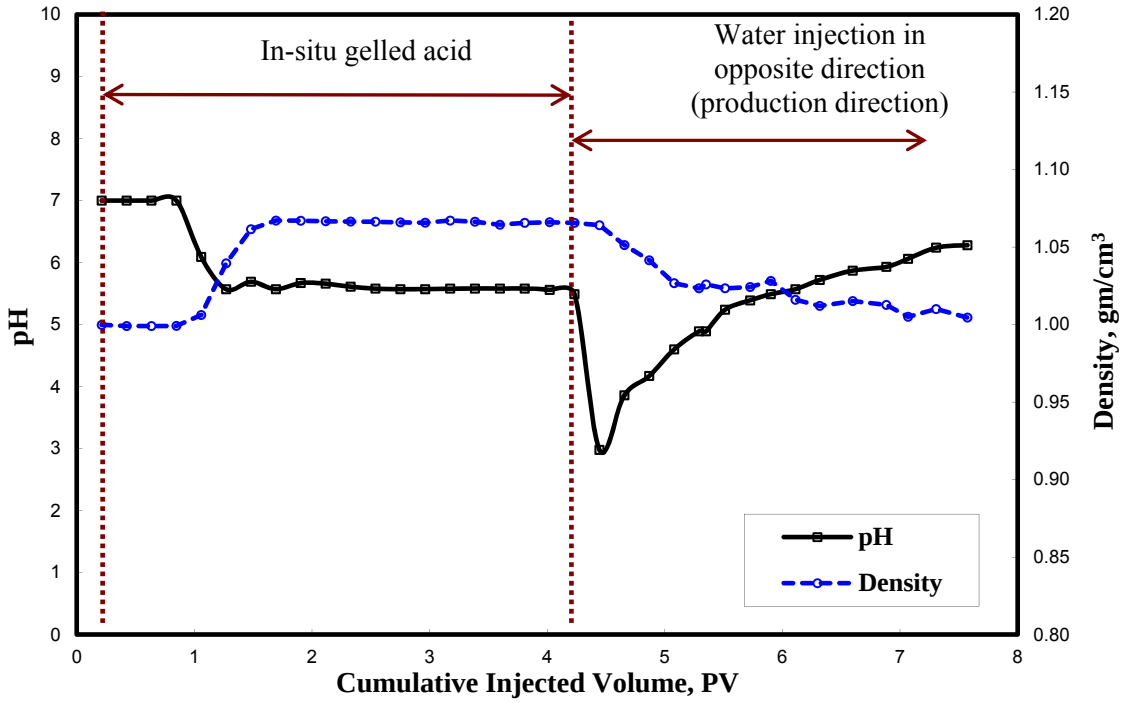

Fig. 4.9—pH value and density of the core effluent samples, T = 250 ˚F, Core 3, in-situ gelled acid.

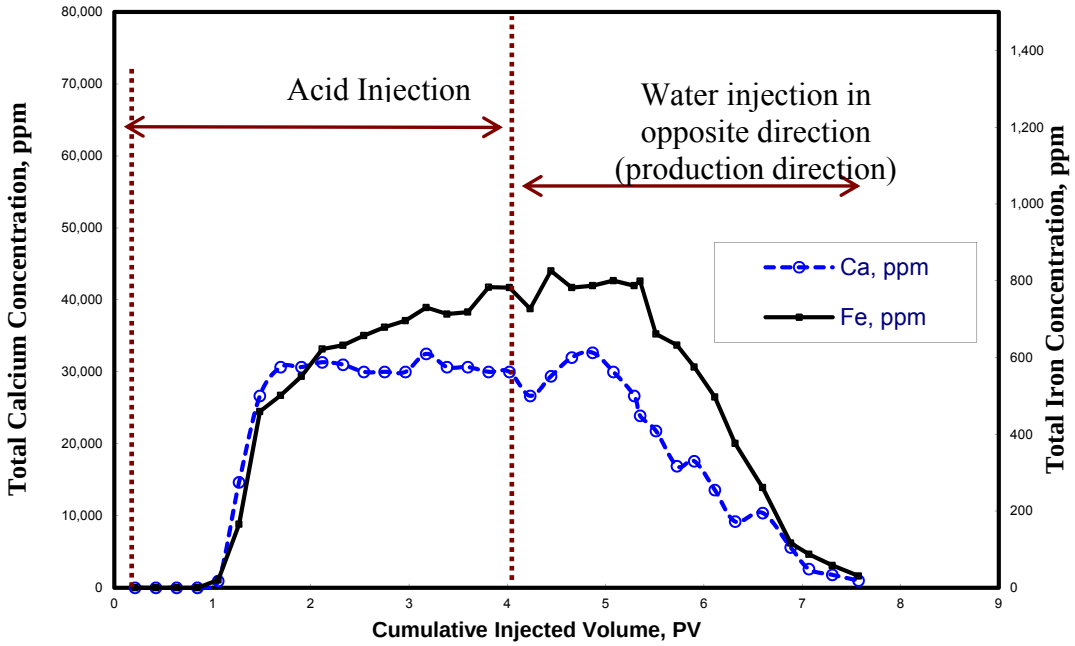

Fig. 4.10—Total calcium and Iron concentration in the core effluent samples, T = 250 ˚F, Core 3, in-situ gelled acid.

4.3.6 CT scan

Figs. 4.11 and 4.12 show the 3D visualization image of wormholes that created by gelled and in-situ gelled acid for cores 1- 4. The shape of the wormhole for gelled acid was much linear and thinner than wormhole created by in-situ gelled acid. The average radius of wormhole created by in-situ gelled acid was 5.4 and 6.8 mm for cores 3 and 4 while the average wormhole radius was 3.1 and 3.4 mm for cores 1 and 2 (gelled acid). Also, propagation of in-situ gelled acid inside the core was less than the propagation of gelled acid. At injection rate of 10 cm^3/min, in-situ gelled acid penetrated only 45% of the core length while gelled acid penetrated 75% of the core length. Also, at an injection rate of 20 cm^3/min, in-situ gelled acid penetrated only 60% of the core length while gelled acid penetrated the whole core length.

Adding only polymer (gelled acid) reduced acid consumption because of a lower diffusion coefficient and a lower leak off rate through the wormhole walls. The net result of these two effects was expected to be a higher wormhole propagation velocity with a small wormhole diameter. However, adding the crosslinker and polymer (in-situ gelled acid) allowed acid penetrated wormholes until initiated the crosslinking. This significant increase in viscosity forced the next fresh acid to change its direction inside the cores. Therefore, in-situ gelled acid had a slower propagation with higher diameters.

In-situ gelled acid changed its direction in a tortuous way as it propagated inside the core as it shown in **Figs. 4.11 and 4.12**. The strong viscoelastic properties that exist in the partially neutralized in-situ gelled acid leaded to sustain the formed gel in its formed location and plug the wormhole completely. Therefore, next acid stage was

pressurized inside the wormhole until the fresh acid break the highest permeability point in the formed gel and changed its direction. This performance shown in the cycling behavior of the pressure drop, **Figs. 4.6 and 4.7**.

Gelled acid which have a weak viscoelastic properties didn't sustain the polymer inside the formation. Polymer had low yield point. There was no any plug effect inside the wormhole by the polymer. Actually gelled acid wormhole was much linear than wormhole formed by in-situ gelled acid. **Figs. 4.11 and 4.12** confirm that there wasn't any indication that the gelled acid was able to change it direction inside the core.

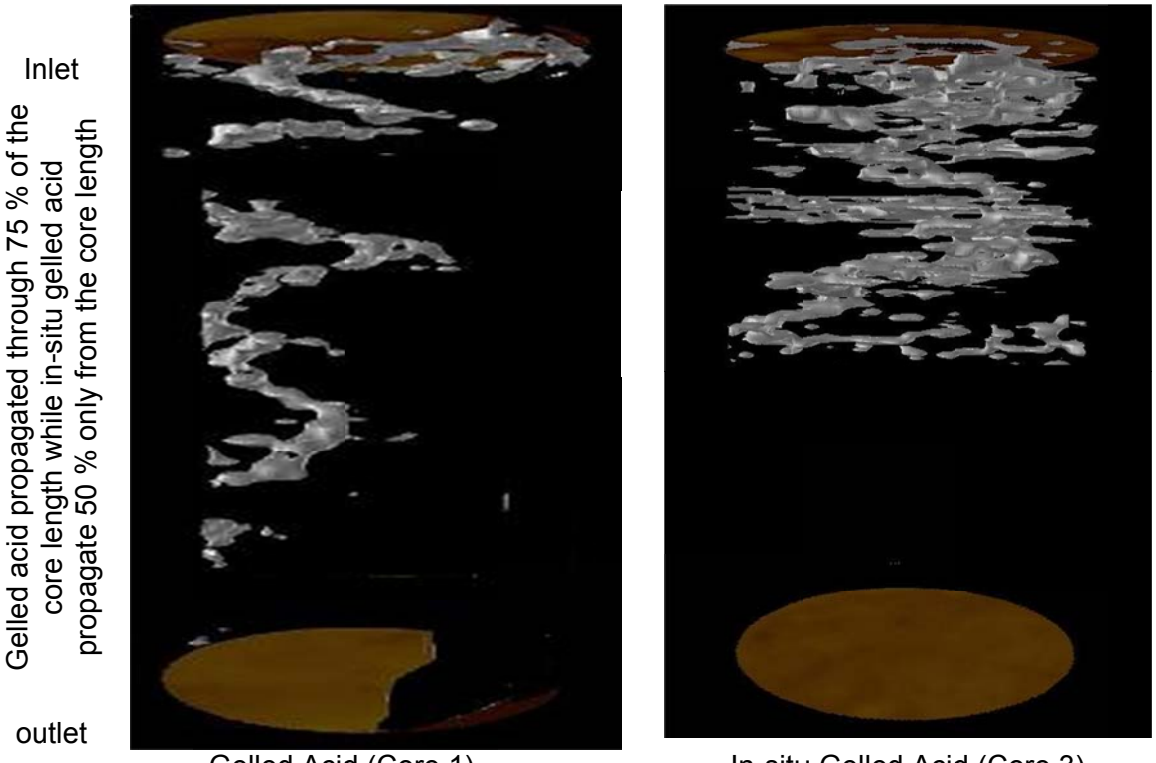

Fig. 4.11—CT scan for the cores that acidized by 10 cm^3/min as injection rate.

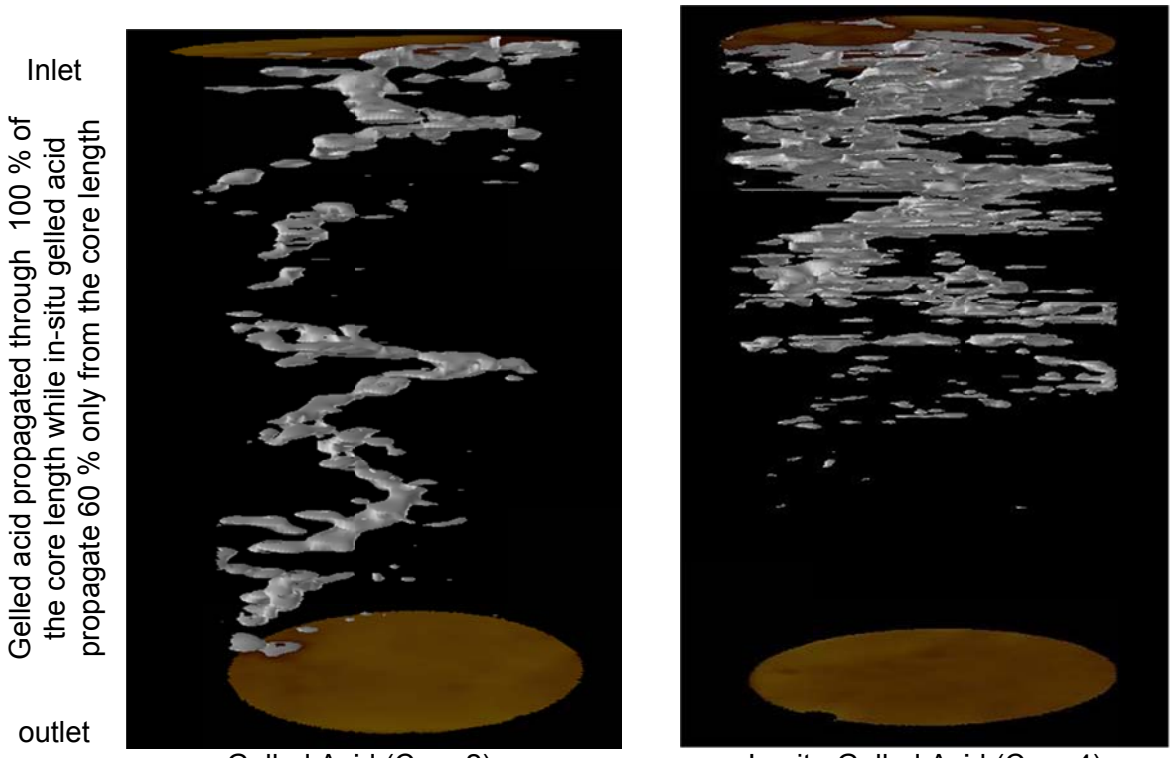

Fig. 4.12—CT scan for the cores that acidized by 20 cm^3/min as injection rate.

5. EFFECT OF THE SHEAR RATE ON THE PROPAGATION OF IN-SITU GELLED ACIDS INSIDE CARBONATE CORES*

In-situ gelled acids that are based on polymers have been used in the field for several years, and were the subject of many lab studies. An extensive literature survey reveals that there are conflicting opinions about using these acids. On one hand, these acids were used in the field, with mixed results. Recent lab work indicated that these acids can cause damage under certain conditions. There is no agreement on when this system can be successfully applied in the field.

A core flood study was conducted using Indiana limestone cores (1.5 in. diameter & 20 in. long) at high temperatures and pressures. Propagation of the acid, polymer, and cross-linker inside the long cores was examined in detail. Samples of the core effluent were collected and the concentrations of calcium, cross-linker, and acid were measured. Permeability enhancement and location of any precipitation was detected using CT scanner to the core after, and before the acid injection. Different sections were cut from the core to investigate the propagation, and precipitation of polymer and cross-linker. Material balance was conducted to determine the amounts of cross-liker that retained in the core.

At high shear rates, a smaller amount of gel was formed inside the core and the acid ability to change its direction inside the core was less than that noted at low shear rate. A significant permeability enhancement was achieved. Wormhole length increased as the shear rate was increased, while the diameter of wormhole increased as the cumulative injected volume of acid was increased. CT scan indicated the presence of gel residue inside the and around the wormhole. Gel residue increased at low shear rates. Material balance on the cross-linker indicated that a significant amount of the cross-linker was retained in the core. This amount increased at low shear rates.

5.1 Introduction

Literature review indicated that there is conflicting opinions regarding this system. Therefore, the aim of this study is to further examine this acid system and determine when it can be used in the field. Our study was conducted using 20.in long Dessert Pink limestone cores.

5.2 Experimental Studies

Materials: Hydrochloric acid (ACS reagent grade) was titrated using a 1 N sodium hydroxide solution to determine the acid concentration, and which was found to be 36.8 wt%. Calcium carbonate powder (ACS grade) was used to neutralize the live acid. Indiana limestone cores (1.5 in. diameter, and 20 in. length) had the properties given in **Table 5.1**. Deionized water obtained from a water purification system (BARNSTEAD EASYpure PoDi-model D13321) that had a resistivity of 18.2 MΩ.cm at

room temperature. All the acid prepared using Deionized water. Polymer, cross-linker and other additives were all oilfield chemicals, and were used without further purification. In-situ gelled acids system includes polymer (the gelling material that used to increase the viscosity of the acid)), crosslinker (Ferric chloride used to connect the polymer chain with each other at pH 2, this produces the viscosity increasing), breaker (sodium erythorbate used to reduce the ferric to ferrous, this will reduce the viscosity gain by ferric), corrosion inhibitor (used to reduce HCl corrosion rate by developing a thin layer on the tubular), and buffer (Hydroxyacetic acid initiates degradation of the polymer chain and the active ligand removes the metal ion from the polymer to allow further degradation of the polymer, which in turn reduces the viscosity).

TABLE 5.1—PROPERTIES OF INDIANA LIMESTONE CORES

Core	Porosity, vol%	Permeability, md	Pore volume, cm^3
1	27.0	53.0	159.9
2	31.0	55.7	177.2
3	29.0	49.0	168.8
4	35.0	88	202.7

Measurements: Viscosity measurements were made using M5600 viscometer at 300 psi and various temperatures. All acids were mixed using a magnetic stirrer. Core flood setup, **Fig. 5.1**, was constructed to simulate matrix stimulation treatments. A back pressure of 1,000 psi was applied to keep CO_2 in solution. Pressure transducers were connected to a computer to monitor and record the pressure drop across the core during the experiments. Teledyne ISCO D500 precision syringe pump, that has maximum allowable working pressure equal to 2,000 psi, was used to inject the acid inside the core.

Based on the maximum pump pressure and the back pressure, the maximum pressure drop across the core was 1,000 psi. pH values for the collected samples were measured using Orion 370 PerpHecT Ross Electrode, while calcium and iron concentrations were measured using atomic absorbance spectrometer (AAnalyst 700-flame type). X-ray Computed Tomography (CT) was used to scan the cores before and after acid injection.

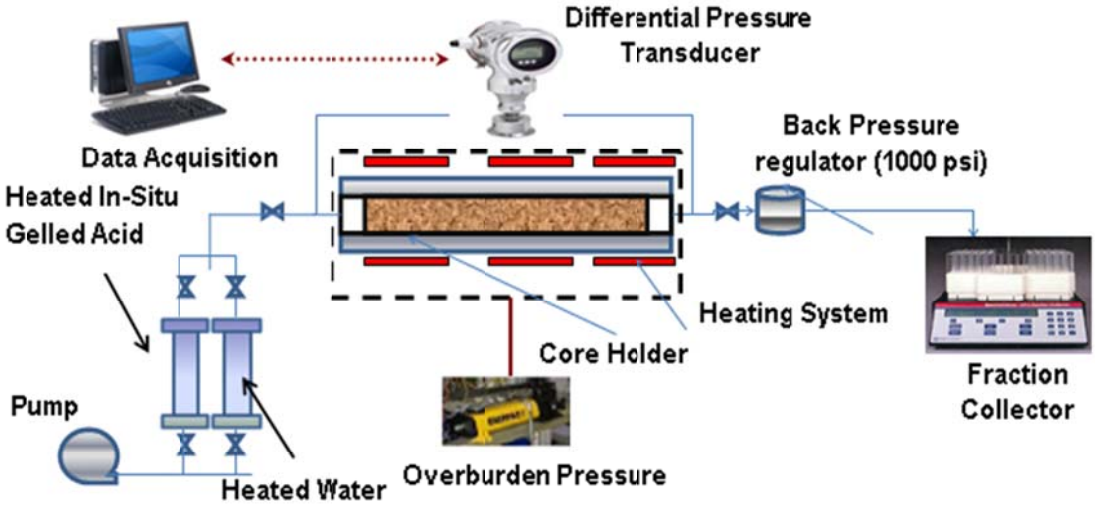

Fig. 5.1—Core flood setup.

Procedure: The acid formula used in this work is given in **Table 5.2.** $FeCl_3$ was used as a source of Fe^{+3} (crosslinker). It is important to note that this is the formula that was typically used in the field. In section 2, we studied three different acid system: two based on Fe and one based of Zr. They found that all of then are non-Newtonian shear thinning behavior. The viscosity at live and neutralized conditions was nearly the same

for the three sytems. Therefore, in this study one system was used in this study, and all the results can be applicable for the other systems.

TABLE 5.2—FORMULA OF THE IN-SITU GELLED ACID EXAMINED IN THE PRESENT STUDY

Component	Concentration
Hydrochloric acid	5 wt% HCl
Acid gelling agent: a co-polymer of polyacrylamide emulsified in hydrotreated light petroleum distillates	20 gal/Mgal
Corrosion inhibitor: Methanol (30-60 wt%), Propargyl alcohol (5-10 wt%)	4 gal/Mgal
Cross-linker: Ferric chloride (37-45 wt%)	4.5 gal/Mgal
Breaker: sodium erythorbate (60 to 100 wt%)	20 lb/Mgal
Buffer: Hydroxyacetic acid (30-60 wt%)	2 gal/Mgal

The Acid solutions were prepared by mixing the corrosion inhibitor and HCl acid with water, then the polymer was added slowly to the acid. After that a crosslinker and a buffer were added to the solution, which was mixed for 30 minutes. The breaker was the last chemical added to the acid. Core preparation was done through the following steps:

1. An Indiana limestone core was weighed dry, and was saturated with water under vacuum. The core porosity was calculated from these measurements.
2. The water saturated core was CT scanned before acid injection.
3. The core was placed inside the core holder, and water was injected at different flow rates (5, 10, and 20 cm^3/min) to calculate the core permeability.
4. The core was heated up to 250°F using heat jackets surrounding the core holder, and all accumulators. Water was injected at 2 cm^3/min during the heating period and until the core reached the required temperature. Temperature was monitored at the outlet of the core.

5. In-situ gelled acid was injected at a constant flow rate while the pressure drop across the core was monitored.
6. Water was injected in the opposite direction of acid injection (production direction).
7. Effluent samples were collected throughout the experiment using an automatic fraction collector. Volume of each sample was 7.5 cm^3.
8. The core was examined using CT scan to characterize the wormholes generated by the acid. Core was water saturated during the scanning.
9. The collected samples were analyzed to determine pH value, density, and the concentrations of calcium and total iron.

5.3 Results and Discussion

5.3.1 Viscosity measurements

The viscosity behavior of live in-situ gelled acids was measured at HCl concentration of 5 wt%**.** The viscosity behavior of the in-situ gelled acid behaves as non-Newton fluids (shear-thinning). Viscosity and shear rate relationship for polymer based in-situ gelled acids was described by the power-law model, Eq. 2.1:

The effect of temperature on the acid viscosity was investigated at different shear rates, where acid solution was examined at different temperatures: 75, 100, and 150°F, respectively. **Fig. 5.2** shows that as temperature was increased, the viscosity decreased. The viscosity of the most used polymers decreases with temperature.

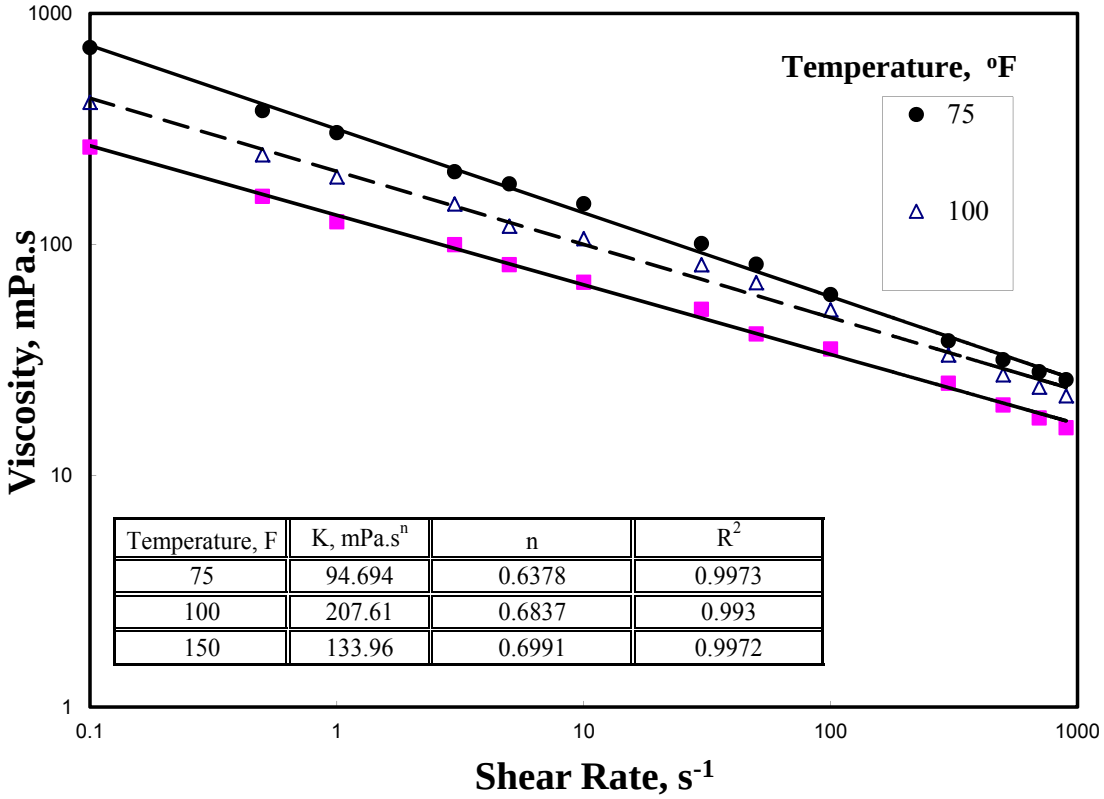

Temperature, F	K, mPa.s^n	n	R^2
75	94.694	0.6378	0.9973
100	207.61	0.6837	0.993
150	133.96	0.6991	0.9972

Fig. 5.2—Effect of temperature on the apparent viscosity of live in-situ gelled acid (5 wt% HCl, 300 psi, polymer concentration 2 vol %).

5.3.2 Coreflood study

Four experiments were conducted with in-situ gelled acid at 5, 10, 15 and 20 cm^3/min using 5 wt% in-situ gelled acid, **Table 5.2**. All experiments were conducted at 250°F while the pressure drop across the core was monitored. A new core was used in each experiment. Analysis of density, calcium, and total iron concentrations in the effluent samples was used to conduct material balance on both calcium and total iron.

The in-situ gelled acid was injected at a flow rate of 5 cm^3/min in Core1, **Table 5.1**. During the experiment, the pressure drop across the core was monitored. A 2.85 PV slug of acid was injected through the core followed by a 3.27 PV slug of water injected

in the opposite direction (production direction). **Fig. 5.3** shows the change in the pressure drop as a function of the cumulative volume injected. As the acid entered the core, the pressure drop increased due to the higher acid viscosity (**Fig. 5.2**) than water. However, the pressure drop changed in a cycling manner where the crest and trough of each cycle increased with time. The cycle amplitude was 10-25 psi, and then the amplitude increased at 1 PV to 250-300 psi. Acid injection was stopped because of reaching the maximum allowable pressure drop across the core.

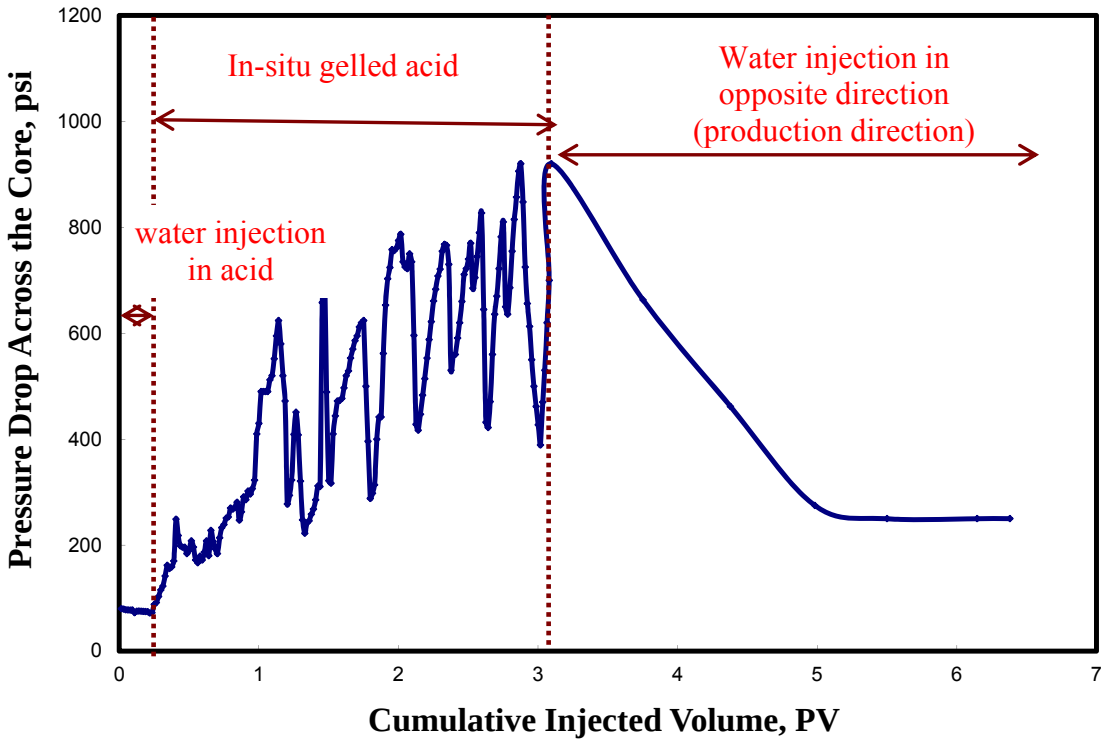

Fig. 5.3—Pressure drop across Core1, In-situ gelled acid was injected at 5 cm^3/min and T = 250°F.

As the acid entered the core, the pH of the acid increased due to acid reaction with carbonate. At pH 2, polymer was crosslinked, and a gel was formed. Gel located

around the wormhole due to acid leak-off, and at the tip of the wormhole due to reaction at this point. Wormhole was plugged by gel, and the fresh acid was pressurized due to constant injection rate leading to increase the pressure drop. Pressure drop increased until acid was able to penetrate the weakest point and change its direction inside the core. Weakest point is the point that had the highest permeability. This point was the crest of each cycle. The same acid behavior was repeated during each cycle. Cycling of the pressure drop indicates that the acid was able to change its direction inside the core.

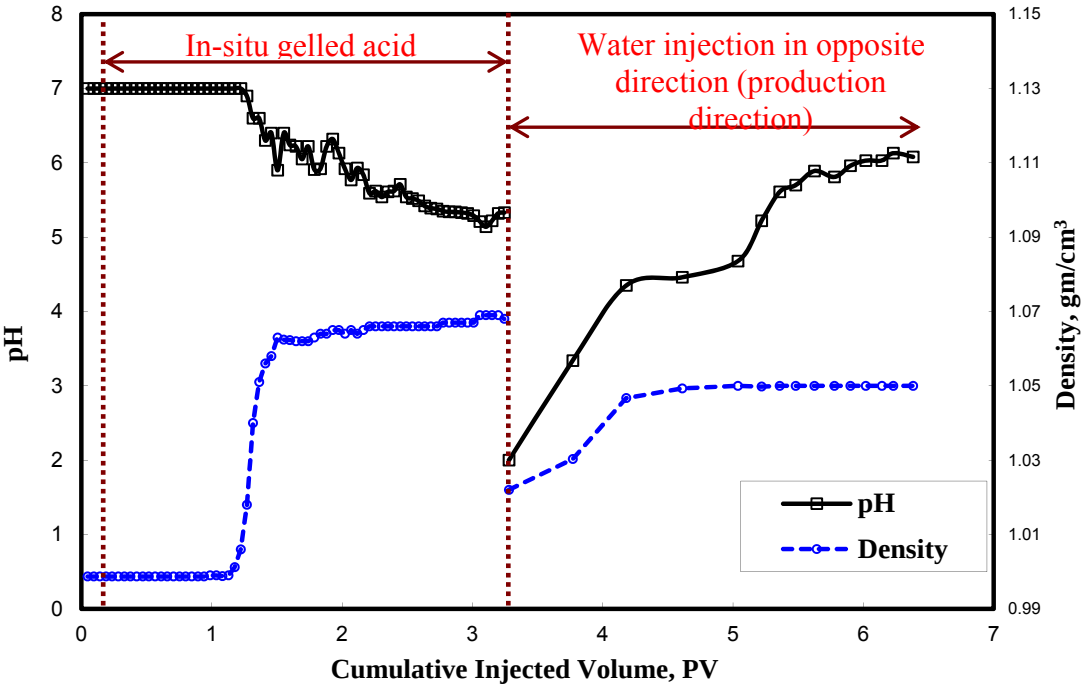

Fig. 5.4—pH value and density of the core effluent samples, T = 250˚F, Experiment 1.

Fig. 5.4 shows the pH values and density of the core effluent samples as a function of the cumulative volume injected. Initial pH value was nearly 7. After injection 0.9 PV of acid solution, pH started to decrease reaching 5 at the point that acid injection was stopped and water flow back was started (this called the end point of the acid injection). pH decreased to 2 at the point that water was injected in the opposite direction of the acid injection. This is because the flow back of partially reacted acid. However, pH increased as injected water increased. Ca and Fe were detected in the core effluent at the same time that the pH values started to decrease, **Fig. 5.5.** However, from pH and acid concentration measurements, there was no indication that the acid breakthrough the core. That means there was a breakthrough of Ca and Fe from the core while acid was still propagating inside the core. Ca reached an average value of 30,000 ppm while Fe increased slightly to a maximum value about 175 ppm at the end point of acid injection. Sample from live acid was taken and diluted 100 times using Deionized water. The iron concentration was found to read 9.25 ppm. Therefore, it is important to note that total iron in the injected acid was 925 ppm.

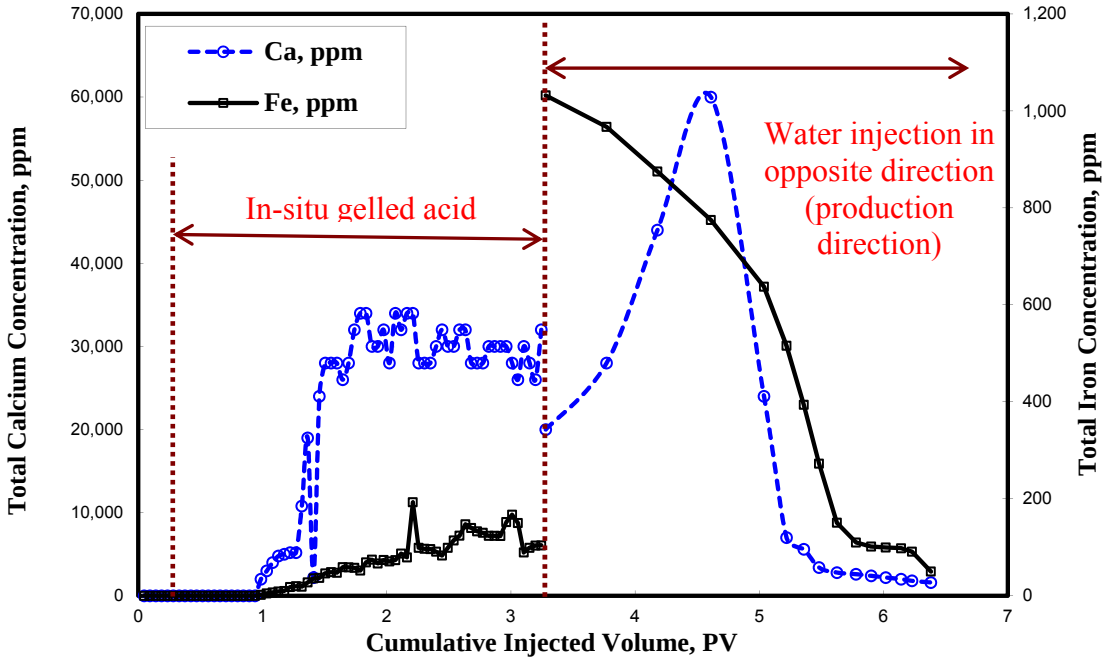

Fig. 5.5—Ca and Fe concentrations in the core effluent samples, T = 250˚F, Experiment 1.

Taylor et al. (1999) showed that ferric cations precipitated at pH 1-2. In the present study, the presence of iron in the core effluent indicates Fe was present in ferrous form not in a ferric form. It can be concluded that ferric cations (cross linker) was reduced by the reducing agents (breaker), and exited from the core in a ferrous form. Ferrous cations can't crosslink the polymer and form a gel (Hill, 2005). The effluent samples were clear for several days; however, a brown precipitate of ferric hydroxide was noted in the test tubes. Ferrous was oxidized by air to ferric, which precipitated in the glass test tubes.

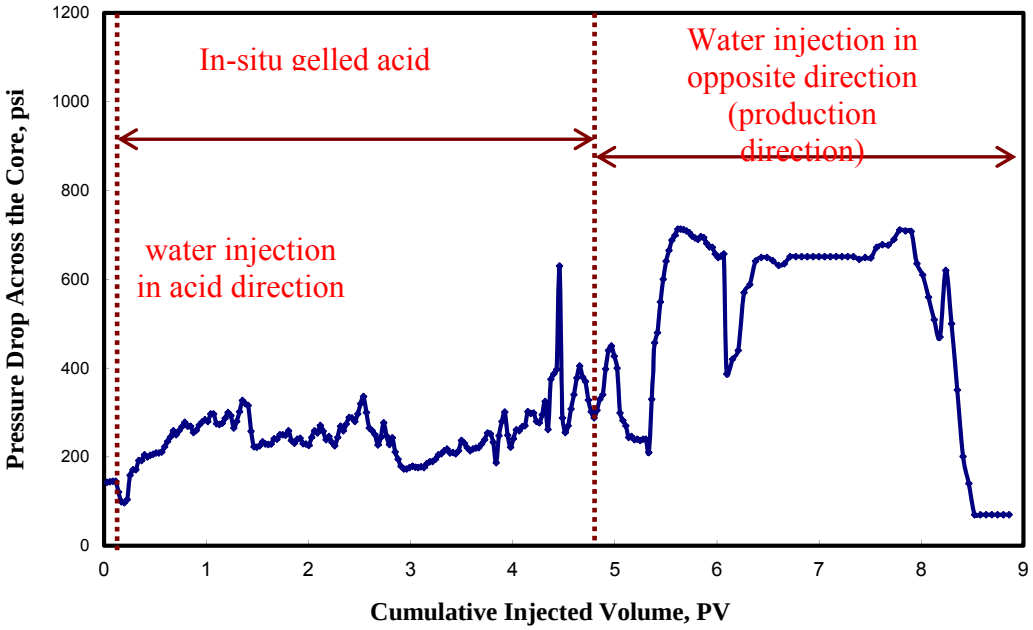

Fig. 5.6—Pressure drop across Core2, in-situ gelled acid was injected at 10 cm^3/min and T= 250°F.

Fig. 5.6 shows the pressure drop across Core2 during the injection of in-situ gelled acid at 10 cm^3/min. A larger acid volume was injected this time (4.68 PV), which was the maximum capacity of the accumulator. The pressure drop increased to 300 psi at 0.85 PV. After that the pressure drop was almost constant. Cycling of the pressure drop in experiment 2 was less than that noted in experiment 1, which means less gel was formed at this flow rate. pH started to decrease after 0.74 PV of acid injection from 7 to 5.5 at the end point of acid injection, **Fig. 5.7**. At the same point of starting decreasing pH, Ca and Fe concentrations (**Fig. 5.8**) increased. Ca became constant at 1.7 PV with an average value 27,000 ppm while Fe increased rapidly until 2.1 PV to reach to 625 ppm, then increased slowly to 825 ppm at the stop point of acid injection.

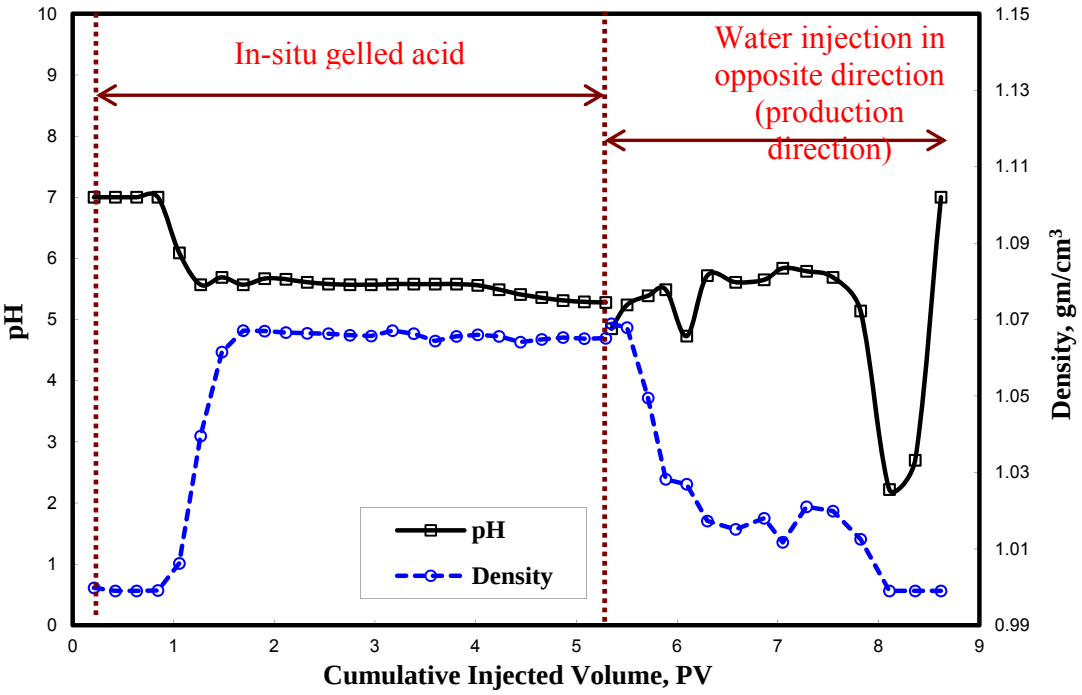

Fig. 5.7—pH value and density of the core effluent samples, T = 250˚F, Experiment 2.

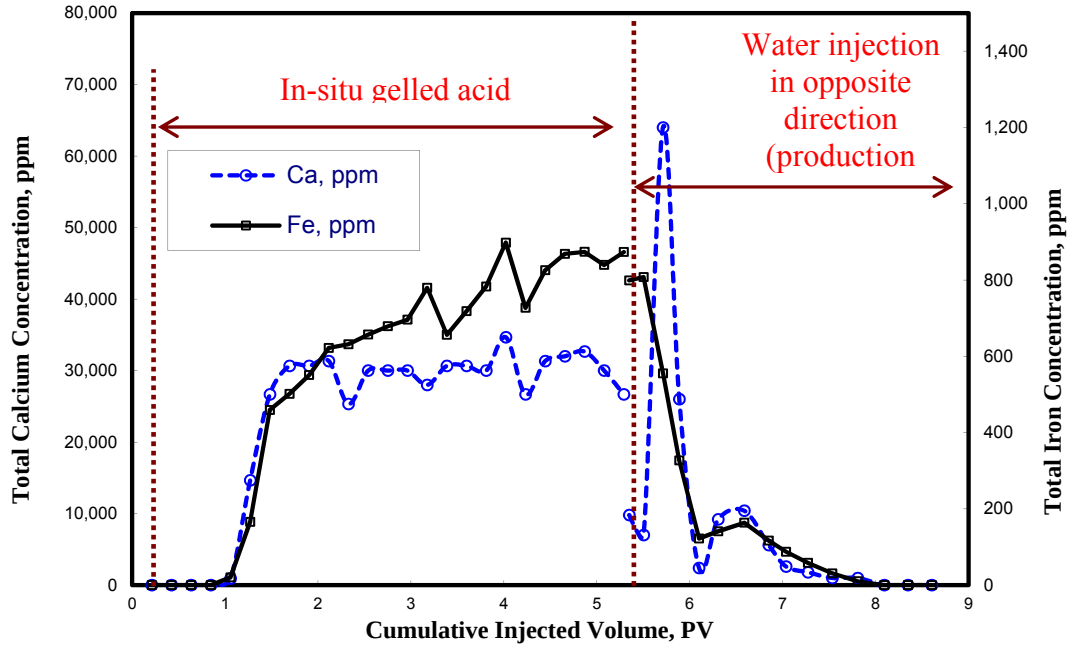

Fig. 5.8—Ca and Fe concentrations in the core effluent samples, T = 250˚F, Experiment 2.

The third core flood was conducted at an injection rate of 15 cm^3/min. The pressure drop across Core3 (**Fig. 5.9**) increased due to acid viscosity as the acid entering the core, and then became constant around 450 psi until 1.75 PV. After that the pressure drop decreased until acid breakthrough where only 3.3 PV was the injected acid slug. After only injection 0.6 PV of acid, pH started to decrease, **Fig. 5.10**. Ca and Fe concentrations (**Fig. 5.11**) increased with the same performance of the previous two experiments. The final experiment was conducted at 20 cm^3/min. Pressure drop started increasing due to acid viscosity then became constant till the end of the point of acid injection. A 3.66 PV of acid was injected for this experiment.

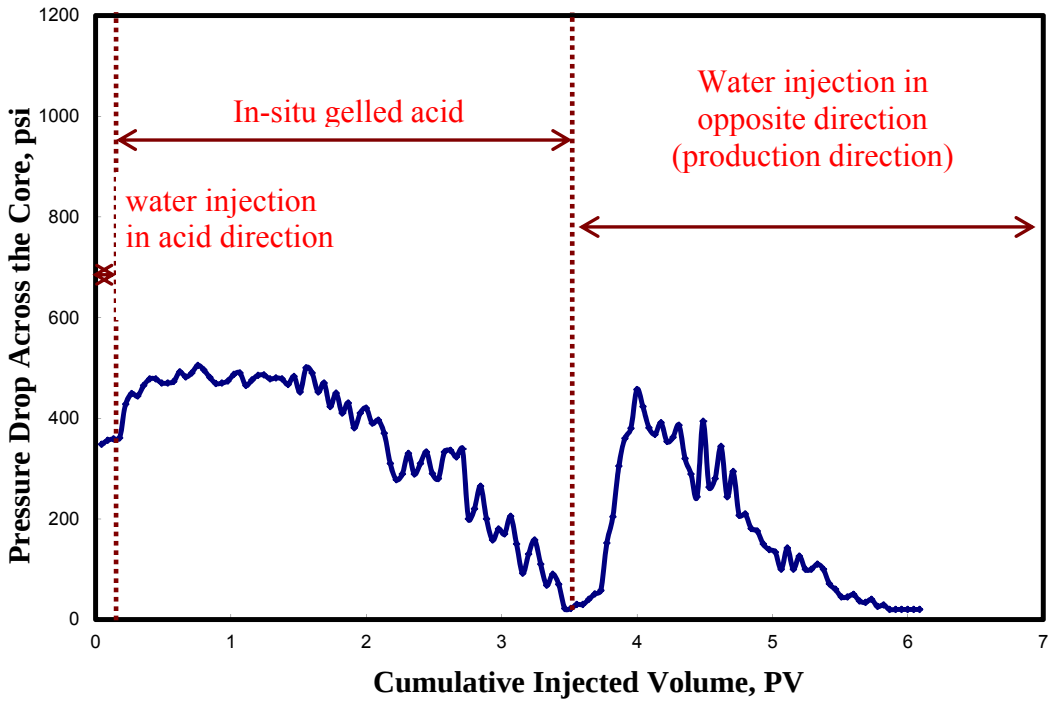

Fig. 5.9—Pressure drop across the Core 3, in-situ gelled acid injected at 15 cm^3/min, T = 250˚F.

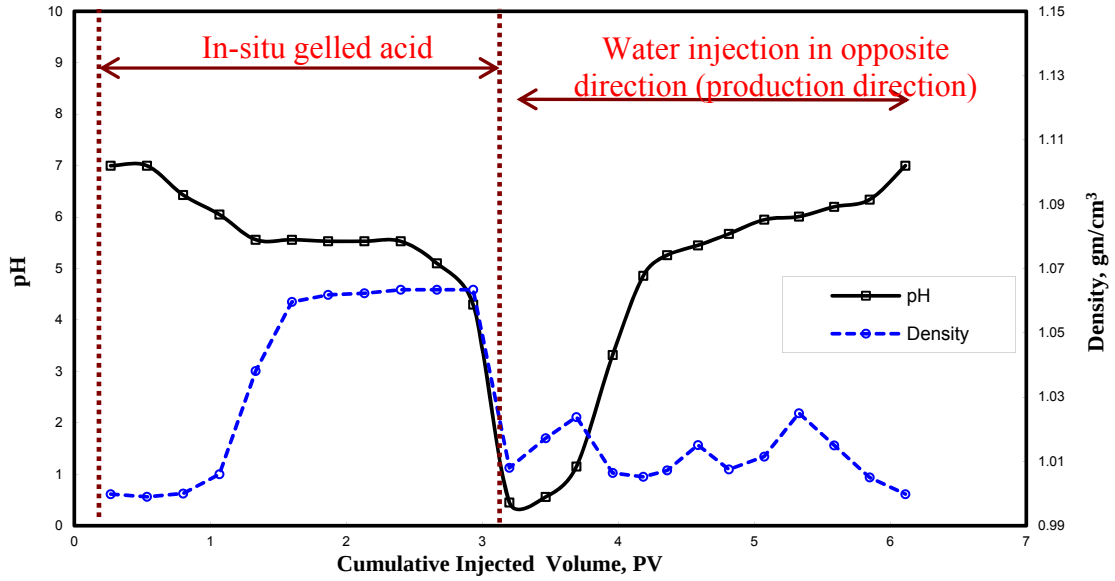

Fig. 5.10—pH value and density of the core effluent samples, T = 250˚F, Experiment 3.

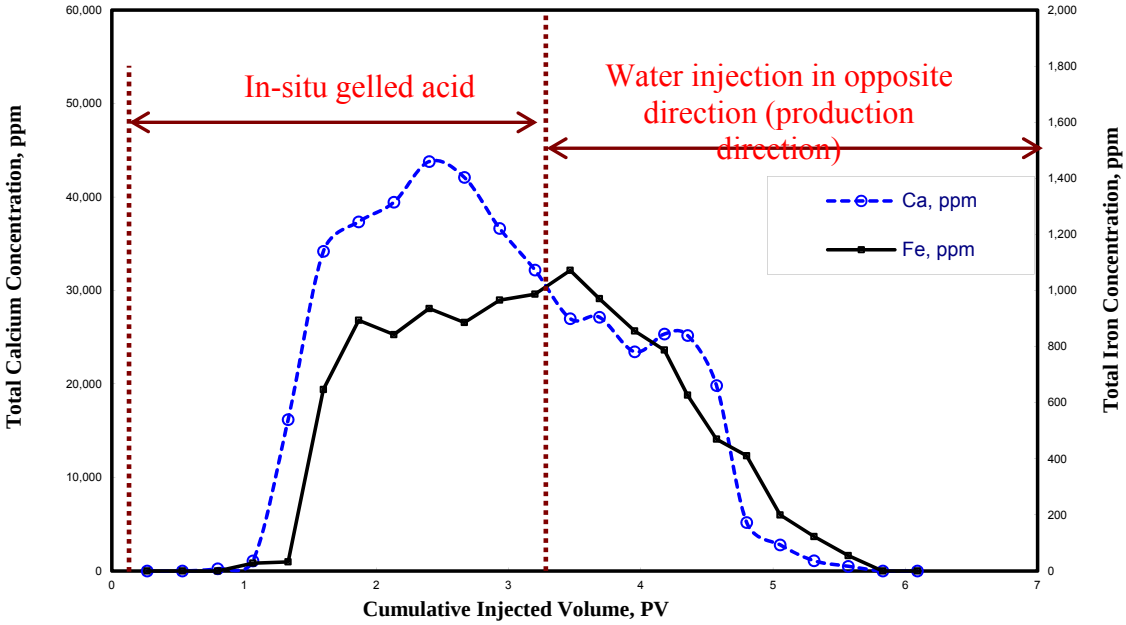

Fig. 5.11—Ca and Fe concentrations in the core effluent samples, T = 250˚F, Experiment 3.

Table 5.3 summaries the injection volumes of acid for the four experiments. The minimum slug volume of in-situ gelled acid was injected in Core1. However, this core was damaged by the acid where permeability decreased from 53 to 22 md. Permeability enhancement was achieved on experiments 2, 3, and 4 where larger volumes of acid were injected. That means damage does not depend on the amount of polymer that was injected in the core, but there were other factors like injection rate and shear rate could affect on the damage mechanisms. HCl concentration for the effluent samples was measured and was found to be zero in all cases.

TABLE 5.3—SUMMARY OF THE CORE FLOOD EXPERIMENTS

Experiment	Volume of injected acid, PV	Cumulative volume of acid at Ca, Fe breakthrough, PV[1]	Permeability, md	
			Before acidizing	After acidizing
1	2.85	0.90	53.0	22.0
2	4.68	0.74	55.7	156.0
3	3.30	0.60	49.0	744.0
4	3.66	0.88	88	251

1: Cumulative volume of the injected acid at the point where Ca and Fe exit from the core.

5.3.3 Effluent analysis and material balance

For each effluent sample tube collected from the four experiments, the weight of the collected sample was measured, and the collected volume of the samples was calculated from the sample density. Using the concentration of each sample and its volume, the amount of Ca and Fe in grams were calculated. Finally, summation of all samples in each experiment was calculated to define the amount of calcium and iron.

Summary of material balances conducted on Ca and total iron for the four experiments are shown in **Tables 5.4 and 5.5,** respectively. The amount of dissolved $CaCO_3$ was calculated using two methods: the first method by multiplying the amount of dissolved calcium by 2.5 (MW_{CaCO3} / MW_{Ca}). The second method by multiplying the injected moles of HCl by 2 to calculate the number of moles of dissolved $CaCO_3$.

TABLE 5.4—MATERIAL BALANCE CALCULATION FOR CALCIUM

Experiment	Amount of collected Ca, g	Amount of dissolved $CaCO_3$, g (based on Ca)[1]	No. of injected moles of HCl	Amount of dissolved $CaCO_3$, g (based on HCl)[2]
1	13.42	33.55	0.624	31.22
2	22.85	57.11	1.136	56.81
3	14.86	37.15	0.764	38.20
4	20.35	50.87	1.016	50.8

1: Amount of dissolved $CaCO_3$ calculated based on Ca analysis.
2: Amount of dissolved $CaCO_3$ calculated based on HCl analysis.

TABLE 5.5—MATERIAL BALANCE CALCULATION FOR TOTAL IRON[1]

Experiment	Amount of Fe in the injected acid, g	Amount of Fe in all effluent samples, g	Amount of Fe inside the core, g	Amount of Fe in the core to total iron injected, %
1	0.42	0.24	0.18	42.9
2	0.77	0.52	0.25	32.5
3	0.52	0.42	0.10	19.2
4	0.68	0.48	0.20	0.29

1: Initial iron concentration live acid was 925 ppm, and Ca concentration was null.

There was an acceptable match between the dissolved $CaCO_3$ that calculated based on Ca effluent analysis, and that calculated based on amount of HCl that injected

inside the core, **Table 5.4**. For iron there was a loss inside the core for the four experiments where 42.9, 32.5, 19.2 and 29 wt% of iron present in the injected acid was left inside the core for the four experiments, respectively. The higher iron loss was inside the core1, the core that its permeability was reduced after the acid, while the minimum iron loss was found in core 3, the core that its permeability was significantly increased after the acid. Therefore, as injection rate increases, the amount of iron that remains inside the core reduces leading to better stimulation treatment.

5.3.4 CT scan

To cover the whole core, 102 slices with 2 mm thickness and 5 mm separation between each slice, were selected. During processing, some slices at the core inlet and outlet were removed because of unclear imaging that resulted from phase dissolution and core placement. In the processing step, the binary image data collected by the CT-scanner were processed on a SUN workstation using the petrophysical CT-scanning software VoxelCalc. Analysis of VoxelCalc show a cross-sectional area for each slice along the core length combined with a 3-D visualization image for the wormhole. This enabled us to show the difference in the shape of the wormhole when in-situ gelled acid was injected at various flow rates.

A slice from CT scan for a core that acidized with in-situ gelled acid is shown in **Fig 5.12**. In this section the wormhole, that developed by acid, had a portion filled with the gel, and other parts had no gel residue (empty wormholes). **Parts a and b** are CT distribution across two axes: the first one passes through the empty wormholes, and the

second axis passes through the filled wormhole. **Fig 5.12-a** shows the CT number distribution through the matrix was greater than 2000 while for the empty wormhole was less than zero. **Fig 5.12-b** confirms that the CT number distribution through the matrix was greater than 2000 but the gel residue CT number reached 1500. This was repeated in other sections and it was confirmed that gel residue that adhered to matrix had a CT number that ranged from 0 to 1500 depending on the volume of the residual gel, **Fig 5.12**.

To confirm that, four test tubes filled with air, water, live acid, and neutralized acid (pH 2.87) were scanned. CT numbers of air, water, and live acid were found to be homogenous and have values of -1118, zero, and 219, respectively. Also, CT number of the carbonate core was homogenous and have arrange from 2000 to 2500. However, neutralized acid (gel) was found to be not-homogenous as shown as in **Fig. 5.13**. To form this gel acid was neutralized using $CaCO_3$. An excess remaining of $CaCO_3$ was still with the gel, which was concentrated on part of tubing; it was not distributed in all gel. This allowed to scan only the part that has only gel (right part of **Fig. 5.13**), and the part that had both gel and $CaCO_3$ (left part of **Fig. 5.13**). Gel was found to have a CT number of 400 while gel and $CaCO_3$ were found to have a CT number of 1000 to 2000 (average value taken was 1500).

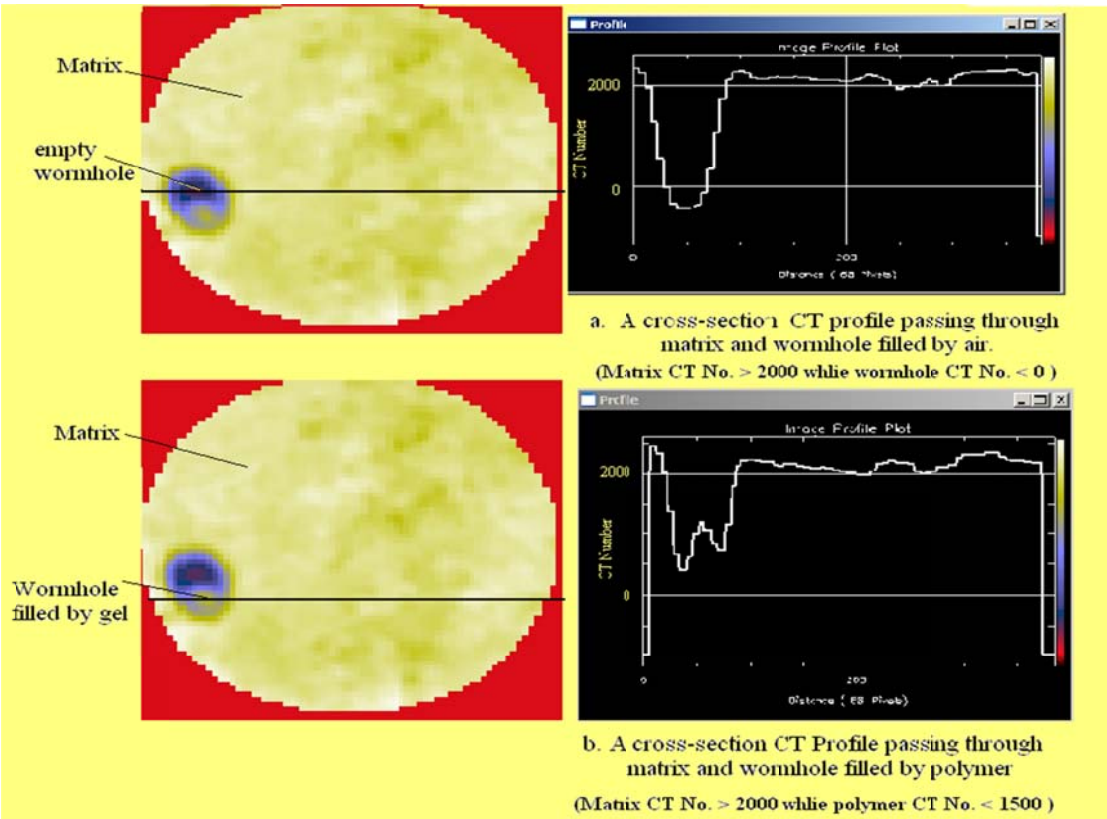

Fig. 5.12—Determination of CT number for gel residue.

Based on the above data, wormhole will have a CT number less than zero because it was filled by air or water, while the wormhole that was filled with the gel had CT above zero, and less than 400 (gel CT number). Gel inside the formation had a CT number from 400 to 1,500. Finally the untreated formation had a CT number higher than 2000. This technique was used to define the gel location inside the core after acid injection.

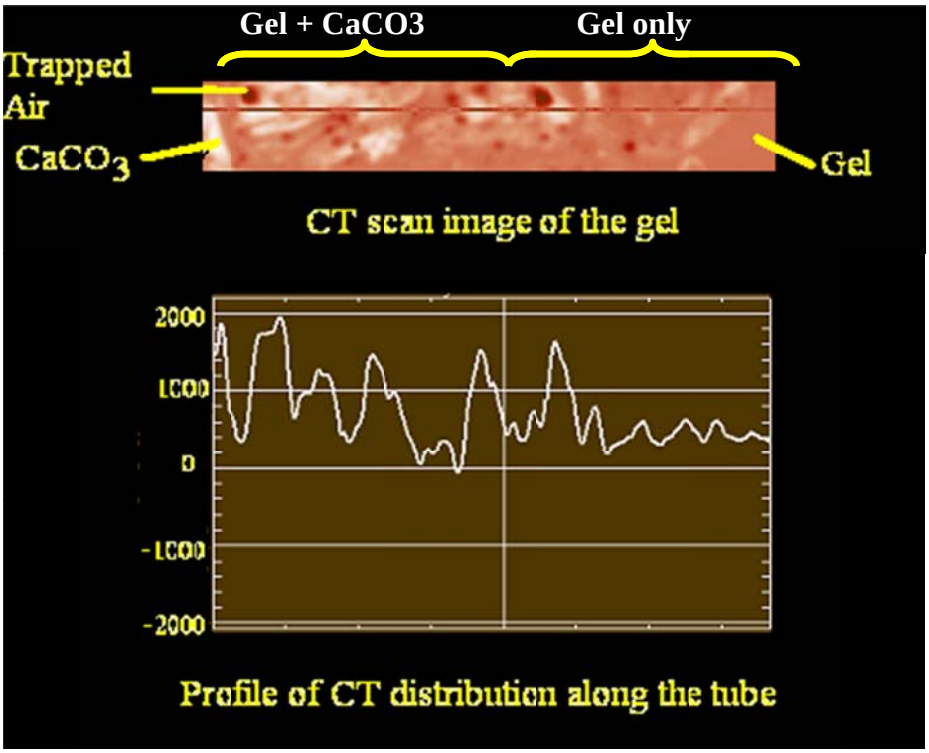

Fig. 5.13—CT profile for a gel (in-situ gelled acid neutralized by $CaCO_3$).

Fig. 5.14 shows the shape of wormholes that created by in-situ gelled acid for experiment 1. The 3D visualization image of the wormhole shows how the acid changed its direction in a tortuous way as it propagated inside the core. The acid propagated only through the first one third of the core, but distributed in every location. In other words, acid filled the first portion of the core completely. The 2D slices image shows the location of gel residue inside the cores. Gel residue was formed on the wormhole wall, and inside the surrounding pores. The amount of the residual gel was higher in the larger wormholes than the smaller ones. The average radius of wormhole was 3.4 mm.

Unlike experiment 1, the acid was able to deeply penetrate the core in experiment 2, **Fig. 5.15.** Acid propagated 68% of the core length. The 3D visualization image of the wormhole shows the shape of wormhole that created by the acid inside the core. The created wormholes inside the cores still have the tortuous shape but with less intensity than experiment 1. Acid changed its direction in core 2. Wormhole diameter and length were much larger than those noted in experiment 1. The average radius of wormhole was 5.8 mm. Gel residue was much higher, especially at the entrance, and in the larger wormholes.

Fig. 5.16 shows the results of CT scan for experiment 3. The 3D visualization image of the wormhole shows that the acid created wormholes through the whole core in a linear behavior. Wormhole tortuosity was the minimum in this experiment. Actually, there was no indication that acid changed its direction. In this case acid behave most likely as regular acid. From the 2D slices image, the residual gel was minimized. Wormhole diameter was smaller than what achieved in experiment 2. The average radius of wormhole was 3.2 mm.

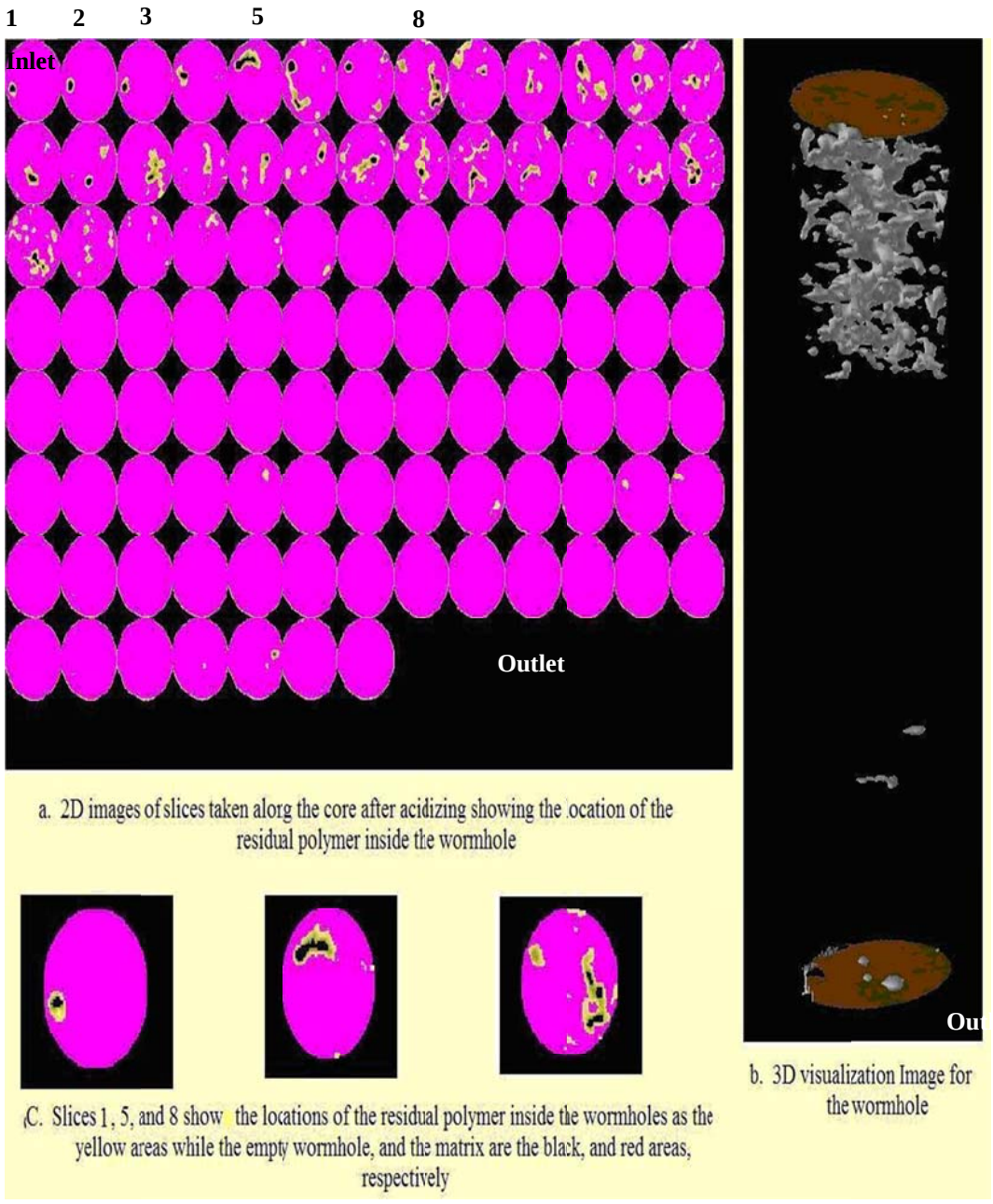

a. 2D images of slices taken alorg the core after acidizing showing the location of the residual polymer inside the wormhole

b. 3D visualization Image for the wormhole

C. Slices 1, 5, and 8 show the locations of the residual polymer inside the wormholes as the yellow areas while the empty wormhole, and the matrix are the black, and red areas, respectively

Fig. 5.14—CT scan for the core1 after acidizing.

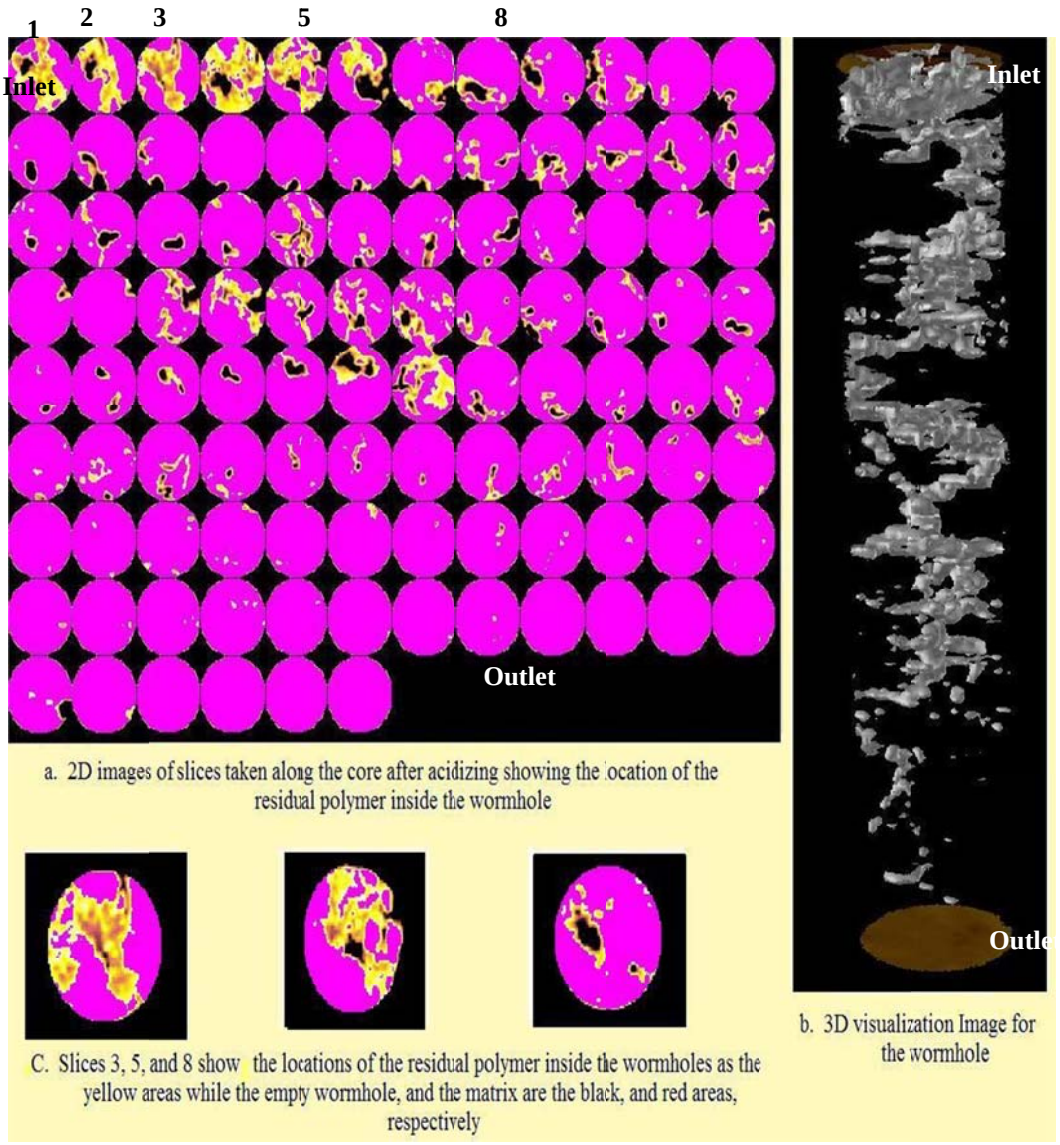

Fig. 5.15—CT scan for the core 2 after acidizing.

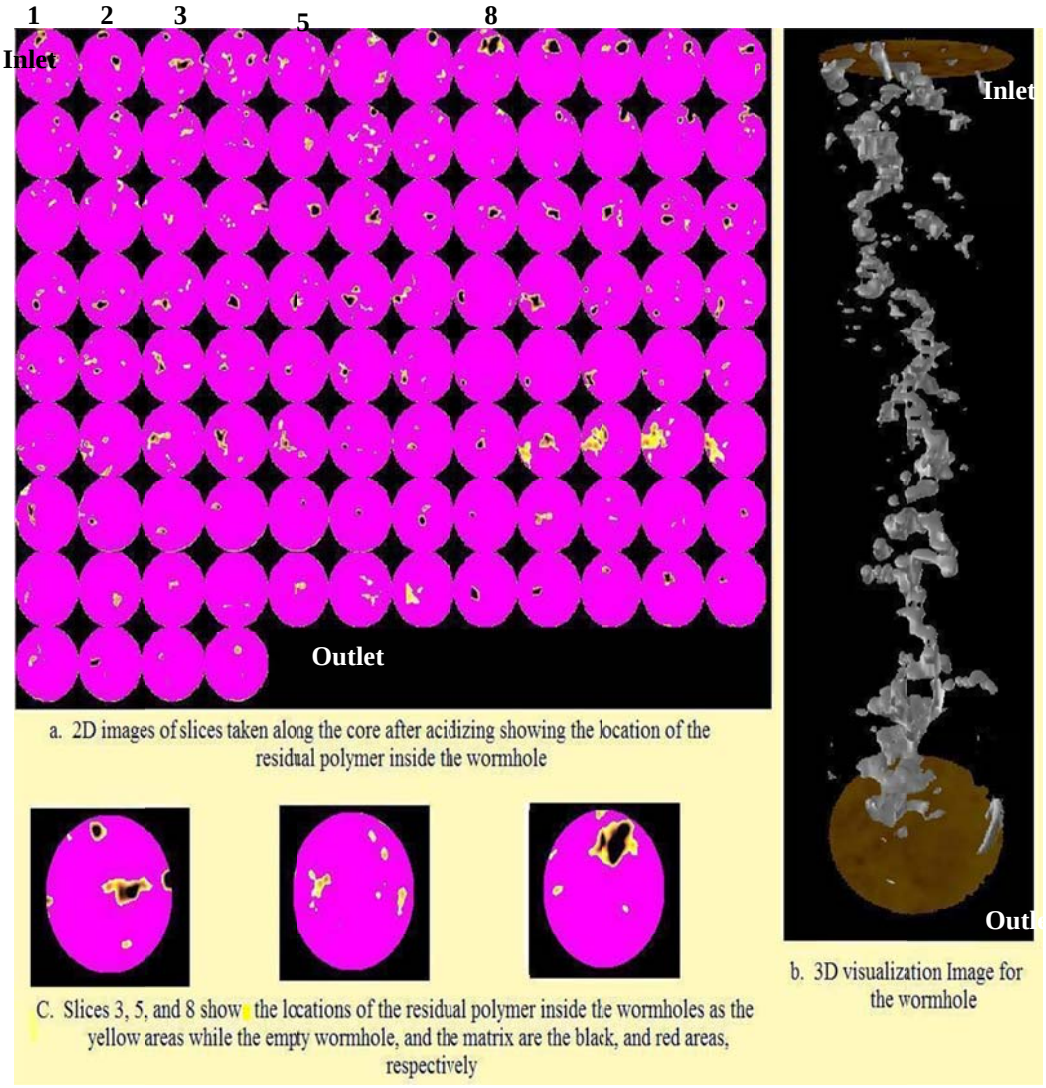

Fig. 5.16—CT scan for the core 3 after acidizing.

5.3.6 Effect of shear rate on flow of in-situ gelled acids in porous media

Based on the injection rate and initial core permeability, the shear rate that the acid will subject was calculated using Eq. 5.1, (Rojas et al. 2008).

$$\dot{\gamma} = \frac{u}{\varphi L} \quad \text{.....(5.1)}$$

where u is the Darcy velocity, m/s; Φ is porosity, fraction; L is a characteristic length representative of the pore-scale velocity gradients, L= 0.05D, D is the average pore throat diameter. Dick et al. (2000) stated that pore size (microns) can be estimated from permeability by taking the square root of the permeability (md).

The shear rates that the acid was subjected in each experiment were 743, 1,288, 2,161, and 1780 s^{-1}, respectively, **Table 5.6**. **Fig. 5.17** shows the ratio between the pressure drop during acidizing to the initial pressure drop during water injection as a function of the cumulative volume injected. The pressure drop ratio in case of low shear rate was much higher than that noted in the case of high shear rate. Even for experiment 4, where a higher injection rate was used, it gives a performance same as experiment 2. It can be concluded that Shear rate is the critical parameter in all experiments.

As mentioned earlier, the viscosity of the in-situ gelled acid decreased, as the shear rate was increased. Therefore, the viscosity behavior in each experiment was different. At low shear rates, the viscosity was higher, the amount of injected acid per unit time was less (because of injection rate), reaching to pH 2 was faster (crosslinking point). Therefore, the pressure drop was high in experiment 1. At high shear rates, viscosity was less, amount of injected acid per unit time was high, and reaching to pH 2 was slower. Therefore, the pressure drop was less in experiment 3.

In experiment 1, acid was strongly able to change its direction, but there was a significant damage in core permeability. In experment 3, a significant permeability enhancement was achieved, but acid was not able to change its direction. Therefore, only experiments 2 and 4 can considered a successful treatment where acid was able to

change its direction, and achieve permeability enhancement. Therefore, it is recommended to use this acid in the range of shear rate used in experiment 2 and 4.

TABLE 5.6—CALCULATED SHEAR RATE FOR EACH EXPERIMENT[1]				
Experiment	**1**	**2**	**3**	**4**
Initial core permeability, md	53	55	49	88
Porosity, vol%	27	31	29	35
Average pore throat diameter, μm	7.3	7.4	7.0	9.4
Flow rate, cm^3/min	5	10	15	20
Darcy velocity, cm/s	7.31E-03	14.60E-03	21.90E-03	29.2E-03
Shear rate, s^{-1}	743	1288	2161	1780

1: Shear rate was calculated using Eq. 5.1

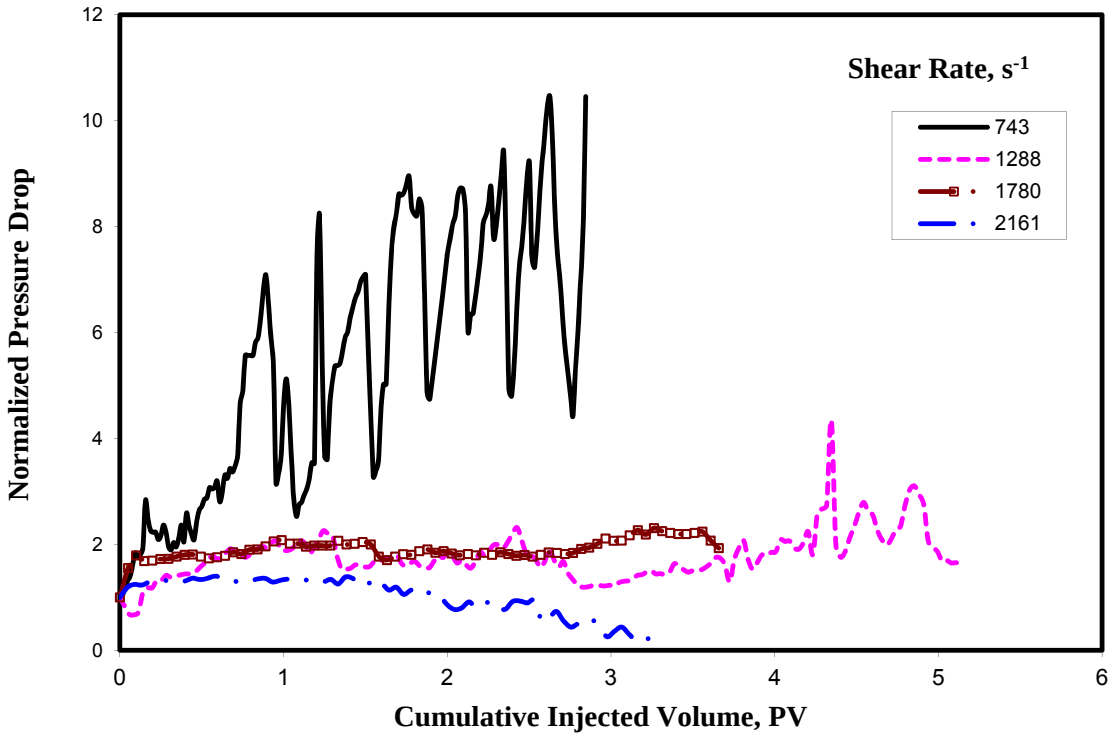

Fig. 5.17—Pressure drop to initial pressure drop performance for the four experiments, T = 250°F.

6. PROPAGATION OF REGULAR HCL ACIDS IN CARBONATE ROCKS: THE IMPACT OF AN IN-SITU GELLED ACID STAGE

In-situ gelled acids based on polymer have been used in the field for several years, and were used in the field in stages between the regular acids. Literature survey reveals that certain plugging effects within highly permeable layers may occur and result in the diversion of the injected acid into less permeable zones. Recent studies indicated that sometimes diversion was not achieved with a severe damage that can lead to loss the whole well. There is no agreement on when this system can be successfully applied in the field.

Single-stage and multi stage-stages acid test of well performance were conducted using Indiana limestone cores (1.5 in. diameter & 20 in. long) at 250^{o}F. 15 wt% regular HCl and 5 wt% in-situ gelled acid based on Fe(III) as a crosslinker were the acid that used in this study. Propagation of the acid, polymer, and cross-linker inside the long cores was examined for the first time in detail. Stage volume and injection rate, that were the parameters that affect on the propagating of various chemical species, were examined in details. Samples of the core effluent were collected and the concentrations of calcium, cross-linker, and acid were measured. Material balance was conducted to determine the amounts of polymer, and cross-liker that retained in the core.

Experimental results show that Unlike in-situ gelled acid behavior at high shear rate conditions, in-situ gelled acid at low shear rate conditions instantaneously plugged the tip of the wormhole and didn't create additional wormhole inside the core. Therefore,

when the final regular acid stage bypassed the gel, it started to propagate from nearly the last point that the first stage ended. Increasing the in-situ gelled acid stage volume from 0.5 to 1 PV leaded to decrease the acid ability to change its direction at high shear rate conditions. However, at low shear rate conditions, the acid ability to change its direction didn't changed. In multi-stage treatments, calcium and iron propagated faster than the acid because they breakthrough earlier than the acid. This is an indication that the acid had been slowed inside the core by the effect of the gel. In multi-stage treatments, final regular acid stage created its own wormhole away from the gel that formed by in-situ gelled stage. Therefore, the percentage of the remaining iron was very high.

6.1 Introduction

Increasing the acid viscosity overcame the problems associated with acid diversion in the formation (Coulter and Jennings 1999). A disadvantage associated with increasing the acid viscosity was formation damage due to polymer entrapment or precipitation of crosslinker (Bazin et al. 1999). Bazin (2001) concluded that viscosifying the acid reduced water filtration by a factor ranging from 3 to 10. Lynn and Nasr-El-Din (2001) showed that adding polymer to the regular acid changed its physical and chemical properties where it behave as a shear thinning fluid and its reaction rate with calcite decreased. They noted that a residue of a polymeric material inside the wormholes and the permeability enhancement depended somehow on the injection rate.

Welton and Van Domelen (2008) experimentally showed that viscosity yield of some synthetic polymer-acid gelling agents provided not only high initial viscosity in

HCl/formic acid blends, but the gelled HCl/Formic acid blends were more robust and maintain higher viscosities for longer periods at 270^{o}F.

In Section 2, we evaluated the in-situ gelled acid at different flow rates using 20 in. long cores. They found that at low flow rates, in-situ gelled acids significantly reduced the core permeability while at high flow rates a significant permeability enhancement was achieved. However, they used only a single stage of in-situ gelled acids while in the field these acids used in stages to block the treated zone and forcing the next regular acid stages to the untreated zones. Therefore, the objective of the present study is to evaluate the impact of an in-situ gelled acid stage volume on the propagation of regular HCl acid in carbonate cores. Two different injection rats and two different in-situ gelled acid stages volume were selected based on our earlier work (Section 2) to represent high and low shear rate conditions

6.2 Experimental Studies

Materials: Hydrochloric acid (ACS reagent grade) titrated using a 1N sodium hydroxide solution to determine its concentration, and was found to be 36.8 wt%. Limestone cores (1.5 in. diameter, and 20 in. length) had properties listed in **Table 6.1**. This type of limestone was found to be homogenous where it contains only one pore-level heterogeneity. All acid solutions were prepared using deionized water with a resistively of 18.2 MΩ.cm at room temperature. Polymer and other additives were all oilfield chemicals, and were used without further purification.

Measurements: All acids were mixed using a magnetic stirrer. Core flood setup was constructed to simulate the matrix stimulation treatment. 1,000 psi back pressure on the core outlet was conducted to keep CO_2 in solution. Pressure transducers were connected to computer to monitor, and record the pressure drop during the experiments. Acid concentration and pH values for the collected samples were measured using Orion 370 PerpHecT Ross Electrode, while calcium, and iron, concentrations for the collected samples were measured using atomic absorbance spectrometer (AAnalyst 700-flame type).

TABLE 6.1—SUMMARY OF CORES DATA BASED ON EXPERIMENTS SETUP

Core	Porosity, vol%	Permeability, md	Pore volume, cm^3	Acid type	Rate, cm3/min	Subjected shear rate, s^{-1}
1	31.6	75	164.3	Regular	5	534
2	29.3	82	152.3	Regular	20	2203
3	32.3	73	168	In-situ gelled	5	530
4	31.2	75	162	In-situ gelled	20	2163
5	29.5	79	153.2	Multi-stage	5	558
6	29	85	150.6	Multi-stage	5	547
7	29.7	84	154	Multi-stage	20	2148
8	29.3	82	152	Multi-stage	20	2203

Acid Preparation: Two acid formulas were used in this work: 15 wt% regular acid and 5 wt% in-situ gelled, **Table 6.2.** $FeCl_3$ was used as a source of Fe^{+3} (crosslinker). Regular acid solutions were prepared by mixing the corrosion inhibitor and HCl acid with water. For the in-situ gelled acid, water, HCl, and corrosion inhibitor

were mixed then the polymer was added slowly to the acid. After that the crosslinker and a buffer were added to the solution, which was mixed for 30 min. The breaker was the last chemical added to the acid.

Core Preparation: Eight cylindrical cores were cut from an Indiana limestone block. The cores were 20 in. length by 1.5 in. diameter. Cores were placed inside an oven set at 257 ^{o}F for 5 hours, and then their weight was measured. Core was saturated with deionized water under vacuum. The porosity was calculated from these measurements. After that, the core was placed inside the core holder, and water was injected at different flow rates (5, 10, and 20 cm^3/min) to calculate core initial permeability. The core was heated up to 250°F using heat jackets surrounding the core holder. Water was injected at 2 cm^3/min during the heating period and until the core reached the required temperature. Temperature was monitored at the outlet of the core. A new core was used in each experiment.

TABLE 6.2—FORMULA OF REGULAR AND IN-SITU GELLED ACIDS

Component	Regular acid	In-situ
Hydrochloric acid	15 wt% HCl	5 wt% HCl
Acid gelling agent: a co-polymer of polyacrylamide	-	20 ml/l
Corrosion inhibitor:	4 ml/l	4 ml/l
Cross-linker: Ferric chloride (37-45 wt%)	-	4.5 ml/l
Breaker: sodium erythorbate (60 to 100 wt%)	-	20 lb/Mgal
Buffer: Hydroxyacetic acid (30-60 wt%)	-	2 ml/l

Injection Rate Selection Based on Subjected Shear Rate: In-situ gelled acids are non-Newtonian shear thinning fluids. Changing the shear rate will affect significantly on

these acids performance because it's effect on the in-situ gelled acid viscosity. In Section 5, we recommended that in-situ gelled acid treatment's design should be determined based on the expected shear rate inside the formation, not based on the injection rate. The porous medium shear rate that the acid will subject was calculated using Eq. 5.1.

Table 6.1 shows the subjected shear rate for each core based on core data. Two injection rates were selected to simulate the low and high shear rate inside the core. For low shear rate conditions, an injection rate of 5 cm^3/min gives a shear rate range from 430 to 558 s^{-1} while for high shear rate conditions an injection rate of 20 cm^3/min gives a shear rate range from 2148 to 2203 s^{-1}.

Single-Stage Acidizing: Regular and in-situ gelled acids were injected as a single acid stage using cores 1-4. Two cores for each acid system were used at two injection rates of 5 and 20 cm^3/min. Regular and in-situ gelled acid were injected at a constant flow rate while the pressure drop across the core was monitored. Water was injected in the same direction of acid injection. Effluent samples were collected throughout the experiment using an automatic fraction collector. The collected samples were analyzed to determine pH value, density, and the concentrations of calcium and total iron.

Multi-Stage Acidizing: Four experiments using cores 5-8 were conducted using different stages of both acids. Acid injection sequence was first stage of regular acid followed by a second stage of in-situ gelled acid, which was followed by a final stage of regular acid until the breakthrough. The volume of the first stage was 0.5 PV and was constant in all experiments, while volume of the in-situ gelled acid was 0.5 PV in two experiments (flow rates were 5 and 20 cm^3/min) and 1 PV in the other experiments (flow

rate was also 5 and 20 cm^3/min). The selected volumes of the in-situ gelled acids represented 33 and 50% of the total acid injection, respectively. Effluent samples were collected and analyzed as described in the case of single acid treatments.

6.3 Results and Discussion

6.3.1 Single stage acidizing: regular acid

Regular acid, that had a concentration of 15 wt% HCl, was injected into core 1 with an injection rate of 5 cm^3/min. During the experiment, the pressure drop across the core was monitored. The normalized pressure drop was plotted in **Fig. 6.1** as a function of the cumulative volume injected. The normalized pressure drop is defined as the ratio between the pressure drop during acidizing to the initial pressure drop. The normalized pressure drop decreased sharply upon acid injection, then started to decrease almost linearly with time, until acid breakthrough**.** Acid breakthrough is defined as the amount of acid needed to propagate the wormhole through the whole core. At injection rate of 5 cm^3/min, acid volume to breakthrough from the 20 in. length core was 1.73 PV, **Table 6.3.**

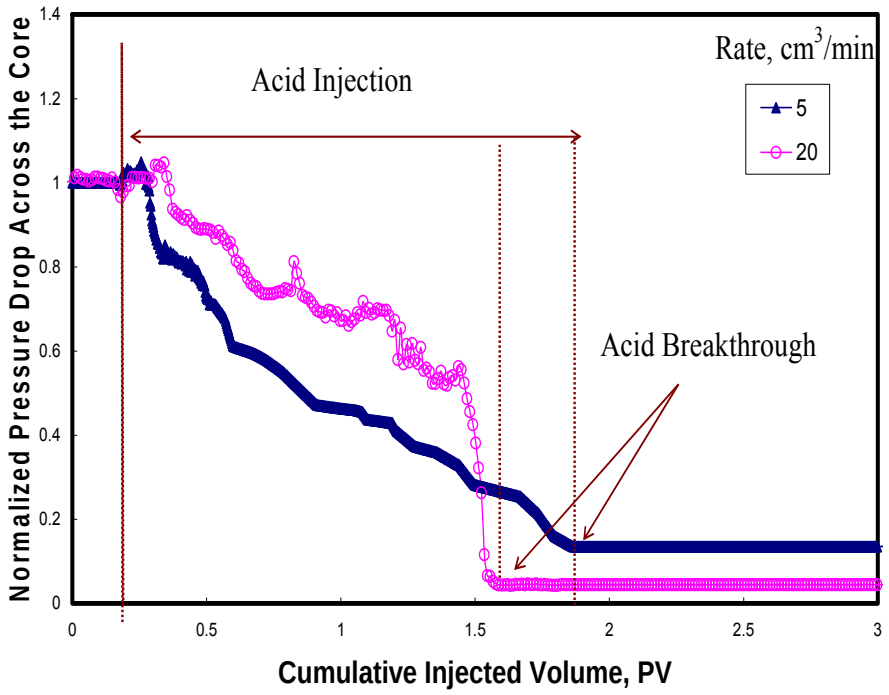

Fig. 6.1—Normalized pressure drop across cores 1 and 2 during injection of 15 wt% regular HCl at 5 and 20 cm^3/min, T = 250˚F.

For Core 2, the acid injection rate was 20 cm^3/min. The normalized pressure drop across the core declined linearly with time, **Fig. 6.1**. However, only 1.47 PV was needed for 15 wt% regular acid to breakthrough from the 20 in. long core. Permeability enhancement was achieved in both experiments, **Table 6.3**. Increasing acid injection rate affected the regular acid propagation inside the core in two ways. The first one was that the normalized pressure drop of core 2 was higher than in core 1. For Newtonian fluids like regular acid, the pressure drop increases as injection rate increases. Therefore, for regular acid pressure drop across the core at injection rate of 20 cm^3/min is higher than at injection rate of 5 cm^3/min. Also at the acid breakthrough, a sharp decline in the

normalized pressure was observed for core 2, **Fig. 6.1**. This agree with Hill et al. 1995 where they noted a linear decrease in pressure drop through most of the injection time with a sharper decrease in pressure drop occurring when the wormhole neared the exist end of the core.

TABLE 6.3—SUMMARY OF THE CORE FLOOD EXPERIMENTS

Core	Volume of injected acid, PV			Permeability, md	
				Before acidizing	After acidizing
Single-Stage Acids					
1		1.73		75	590
2		1.47		82	2025
3		3.6		73	21
4		4.1		75	225
Multi-Stage Acidizing					
	Regular	In-situ gelled	Regular		
5	0.5	0.5	0.83	79	450
6	0.5	1	0.6	85	682
7	0.5	0.5	0.5	84	2200
8	0.5	1	0.45	82	2150

A summary of material balance conducted on the total calcium in the effluent samples was conducted. The amount of calcium carbonate dissolved in core 2 was less than that dissolved at core 1. This was predictable because core 2 required less acid volume to breakthrough which was confirmed by Al-Ghamdi et al. (2009). Therefore, increasing the injection rate for regular acid provide retardation to the acid to penetrate the same core length with less amount of acid.

For core 1, the HCl concentration was measured in the effluent samples and was found to be not significant before the acid breakthrough. However, after breakthrough, the HCl concentration increased to be 9 and 0.5 wt% HCl, for only two samples after

acid breakthrough, respectively. After that HCl concentration became not significant because of starting the water injection. It is important to highlight that before acid breakthrough HCl was totally consumed inside the core, while after acid breakthrough a part of the HCl was consumed. There was a reaction inside the wormhole after acid breakthrough. The pH profile reflected the HCl concentrations in the effluent samples. In the acidic samples, pH values were nearly zero while at the end of the experiment the pH value was nearly 5.8. A similar trend for pH and calcium was noted in core 2.

6.3.2 Single-stage acidizing: in-situ gelled acid

In-situ gelled acid, that had a concentration of 5 wt% HCl, was injected at a flow rate of 5 cm^3/min in core 3, **Table 6.1**. A 3.6 PV of acid was injected through the core followed by water injection in the same acid injection direction. **Fig. 6.2** shows the normalized pressure drop as a function of the cumulative volume injected. As the acid entered the core, the pressure drop increased instantaneously. Then pressure drop became constant for around 0.5 PV, after that pressure keep increasing with acid injection. However, the pressure drop changed in a cycling manner during acid propagation inside the core. Acid injection was stopped because the maximum allowable pressure drop across the core was reached.

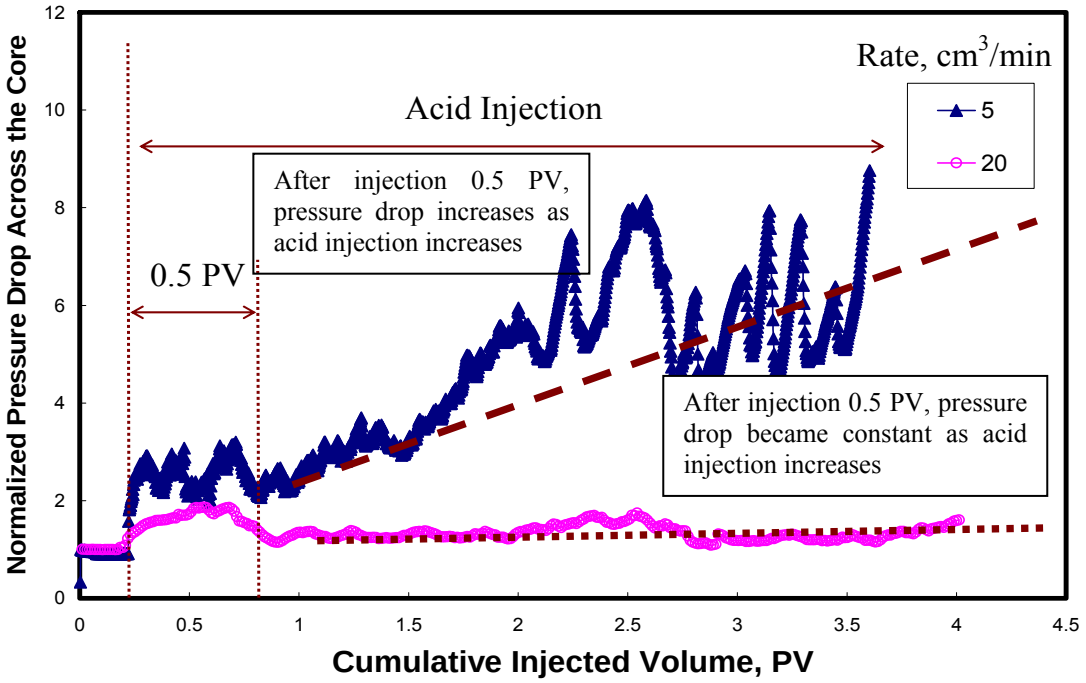

Fig. 6.2—Normalized pressure drop across cores 3 and 4 during the injection of 5 wt% in-situ gelled at 5 and 20 cm^3/min, T = 250 ˚F.

Fig. 6.2 shows the normalized pressure drop across core 4 during the injection of in-situ gelled acid at 20 cm^3/min. For core 4, pressure drop increased during the injection of first 0.5 PV of in-situ gelled acid. After that, pressure decreased to a value near its initial value and became constant till the end of acid injection. A larger acid volume was injected this time (4.1 PV), which was the maximum capacity of the accumulator.

Unlike the behavior of regular acid, the normalized pressure drop of in-situ gelled acid at injection rate of 5 cm^3/min (rate represent low shear rate conditions) was higher than at injection rate of 20 cm^3/min (rate represent high shear rate conditions), **Figs. 6.1 and 6.2**. Viscosity and gelling mechanisms were the main two factors affecting the pressure performance inside the core. In-situ gelled acids are non-Newtonian shear

thinning fluids (Taylor and Nasr-El-Din 2003). Therefore, increasing the shear rate by increasing the injection rate will decrease the viscosity of the acid that leads to decrease in the pressure drop. Also, increasing the injection rate decreases the opportunity of the acid to reach to a pH value of 2. Therefore at high injection rate, gel will not form as fast as at low injection rate. It can be concluded that, the acid ability to change its direction is higher at low shear rate conditions. This agrees with the experimental results for cores 3 and 4, during the injection of first 0.5 PV of in-situ gelled acid, the normalized pressure drop increased by three times at 5 cm^3/min rate while it increased twice at 20 cm^3/min, **Fig. 6.2**.

At acid injection rate of 5 cm^3/min, permeability was reduced from 73 to 21 md while at 20 cm^3/min, permeability was increased from 75 to 225 md, **Table 6.3.** This agreed with data obtained from Section 5 where the core was damaged at the low shear rate conditions, while a permeability enhancement was achieved at the high shear rate shear rate conditions. This is because the ability of gel to form faster and stronger at low shear rate conditions as it discussed earlier.

Based on the material balance calculations, **Table 6.4**, 59% of the injected Fe(III) was retained inside core 3 whereas only 23% of the injected iron was retained inside core 4. The remaining iron might be in one of the following forms: hydrated ferric hydroxide precipitated in the core as it noted by Lynn and Nasr-El-Din (2001), and/or as a gel residue that did not break at the test conditions as it observed in Section 2. Both of theses forms represent damage inside the core. However, the remaining gel inside the core, that has the much damaging mechanism, has the highest possibility to occur. This

is because the breakers for these systems were supposed to work at pH 4-5 values (Hill 2005), when the acid is almost completely spent. However, the high viscosity of the gel and the low HCl concentration will after pH 2 will reduce the driving force of H^+ to diffuse into the surface, that will effect of reaching to pH values of 4-5. Both factors will tend to delay the rate of gel breaking, at least under test conditions. Therefore, the gel will remain inside the core and create a lot of damage.

TABLE 6.4—MATERIAL BALANCE CALCULATION FOR CALCIUM AND TOTAL IRON[1]

Core	**1**	**2**	**3**	**4**	**5**	**6**	**7**	**8**
Amount of Calcium carbonate, g	50.49	41.06	37.28	57.47	47.9	45.92	37.26	42.15
Amount of Calcium carbonate, g	50.85	42.04	38.42	55.26	49.7	47.13	38.54	43.82
total iron in the injected	-	-	0.51	0.73	0.07	0.14	0.07	0.14
Amount of total iron in effluent samples, g	-	-	0.21	0.56	0.01	0.02	0.03	0.06
Amount of total iron inside the core, g	-	-	0.3	0.17	0.06	0.12	0.04	0.08
Amount of total iron in the core to total iron injected, %	-	-	59	23	86	86	57	57

1: Initial iron concentration in the live in-situ gelled acid was 925 ppm, and Ca concentration was zero.

6.3.3 Multi-stage acidizing at low shear rates

Two experiments were conducted using Cores 5 and 6 at an injection rate of 5 cm^3/min. The injection sequence for core 5 was 0.5 PV of 15 wt% regular acid followed

by 0.5 PV of 5 wt% in-situ gelled acid and finally 15 wt% regular acid until breakthrough. The volume of the last acid stage was a 0.83 PV.

For Core 6, the same sequence was used, but the volume of in-situ gelled acid was increased to 1 PV. The volume of the final regular acid stage decreased to 0.6 PV, **Table 6.3**. The volume of the in-situ gelled acid that injected in Cores 5 and 6 represented 27.3 and 47.6% of the total acid volume injected to each core, respectively.

To the best of our knowledge, this is the first time to examine the behavior of multi-stages of regular acid and in-situ gelled acid inside 20 in. long cores at 250^{o}F. **Fig. 6.3** shows the pressure drop across core 5. At the point that regular acid reached to the core inlet, the pressure drop decreased linearly with regular acid injection. After injection of the first stage of regular acid the pressure drop was 38 psi. The pressure drop started to increase with injection of the in-situ gelled acid stage to a maximum value of 140 psi. However, when the final regular acid stage was injected, the pressure drop instantaneously decreased to 38 psi and then decreased linearly until acid breakthrough.

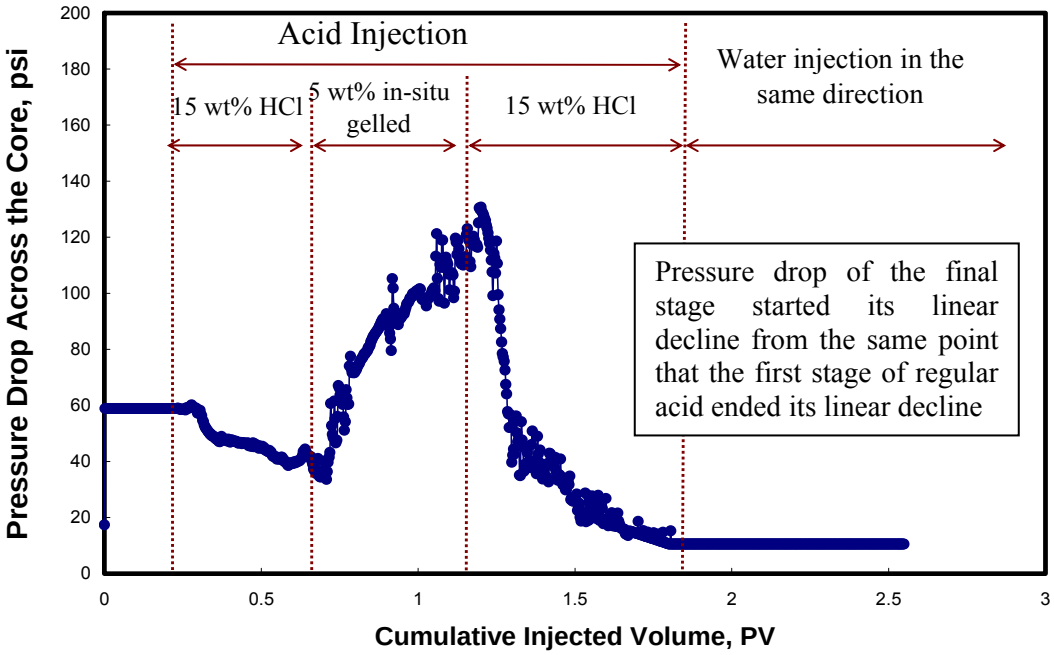

Fig. 6.3—Pressure drop across core 5 during the injection of three acid stages at 5 cm^3/min and T = 250°F.

The performance of regular and in-situ gelled acid inside the core is illustrated in **Fig. 6.4.** During the first stage injection of regular acid, the pressure drop decreased linearly because of the wormhole propagation through the core as it shown in **Fig. 6.4-A**. As the second stage of in-situ gelled acid injected through the core, the gel was formed around the wormhole and inside the wormhole tips as was discussed in Section 5. This leaded to plug the wormhole and increasing in the pressure drop to the value of 140 psi just before the final stage of regular acid (**Fig. 6.4-B**). As the final stage of regular acid entered the core, it penetrated the weakest point and created a channel away from the plugged zone. Therefore, pressure drop decreased instantaneously to value of 38 psi, which is the same pressure drop value that achieved before injection of the in-situ gelled

acid stage. After that regular acid penetrated the core and created wormhole until acid breakthrough (**Fig. 6.4-C**).

As it known, during injection of regular acid, the pressure drop across the core depend of the wormhole propagation length inside the core. The pressure drop across the core decreases as the wormhole propagates inside the core. It is important to highlight that the pressure drop of the final stage started its linear decline from the same point that the first stage of regular acid ended its linear decline. This means that in-situ gelled acid plugged the tip of the wormhole and didn't create additional wormhole inside the core. Therefore, when the final regular acid stage bypassed the gel, it started to propagate from nearly the last point that the first stage ended.

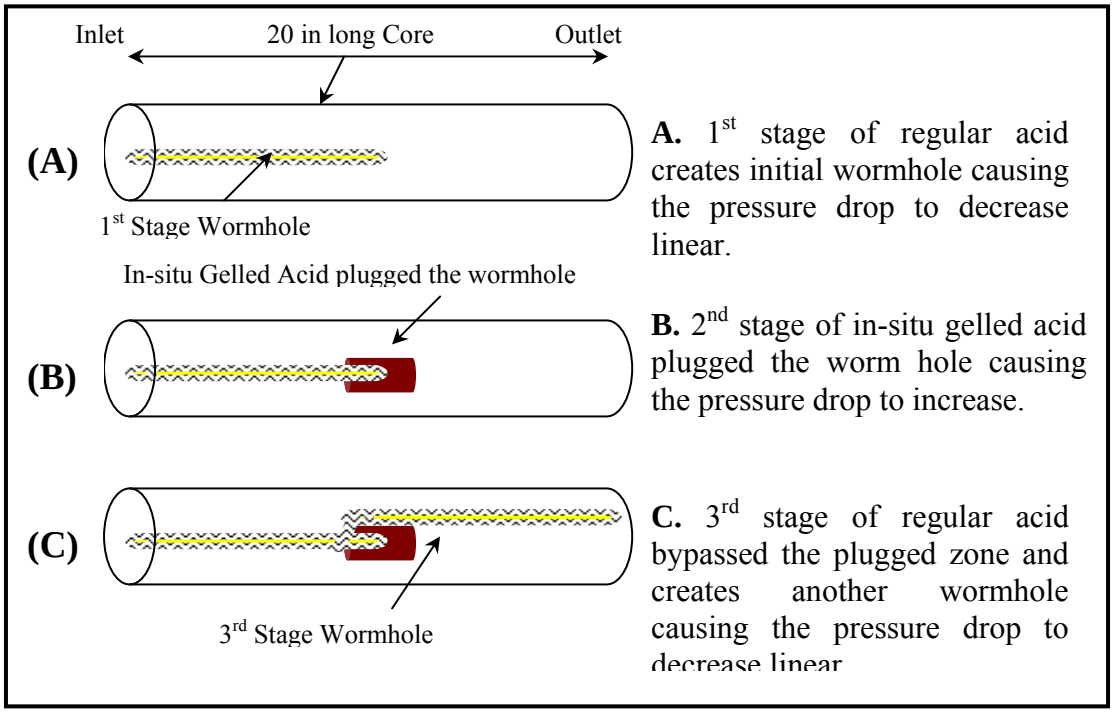

Fig. 6.4—A schematic diagram describes the performance of the regular and in-situ gelled acids inside the cores.

The pressure drop across core 6 was similar to the pressure behavior across core 5, **Fig. 6.5**. The difference was that in-situ gelled acid stage became wider in pore volume injection axis, **Fig. 6.5**, due to increasing in the in-situ gelled acid injection volume. Also, during the injection of the first 0.5 PV of in-situ gelled acid, the pressure drop increased to a value around 200 psi. However, the pressure drop became constant for the next 0.5 PV of in-situ gelled acid injection. There were no much increases in pressure drop by increasing the injected volume of in-situ gelled acid from 0.5 to 1, **Fig. 6.5**. Therefore, the acid ability to change its direction does not change by increasing the in-situ gelled acid stage volume at low shear rate conditions. Also, as it observed in core 5, when final stage of regular acid was injected, the pressure drop across core 6 instantaneously decreased to the same pressure value before the injection of the in-situ gelled acid.

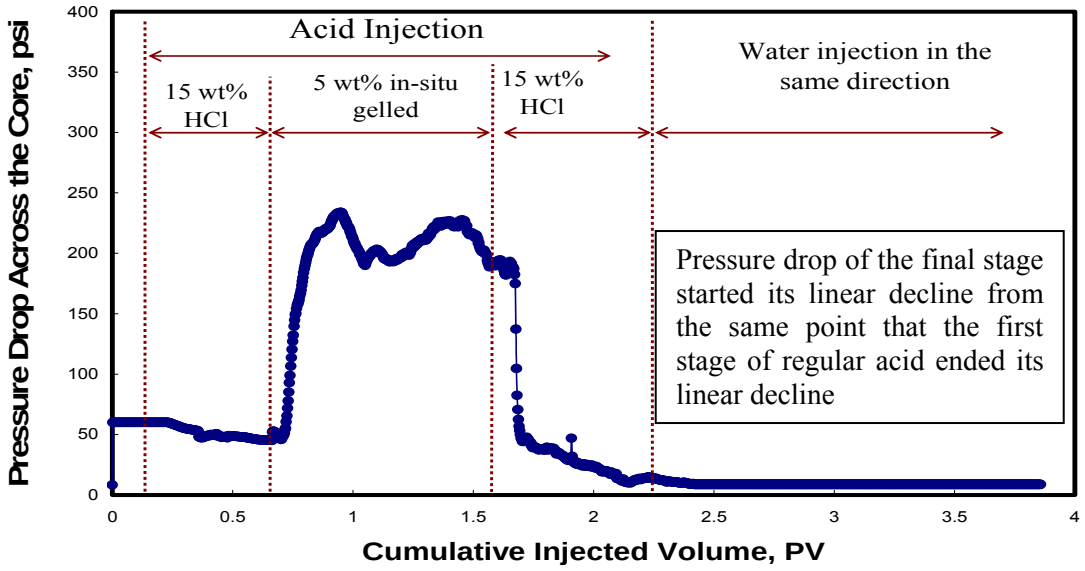

Fig. 6.5—Pressure drop across Core 6 during the injection of three acid stages at 5 cm^3/min and T = 250˚F.

The density and pH values of the effluent samples of cores 5 and 6 are plotted in **Figs. 6.6 and 6.7** while the total calcium and iron are plotted in **Figs. 6.8 and 6.9**, respectively. For core 5, the initial pH value was nearly 7. After injection 0.75 PV of acid solution, pH started to decrease reaching 5.5 before acid breakthrough. At acid breakthrough pH value was zero. However, pH increased again with water injection until it reached to a maximum value of 6. The pH value is the refection of HCl concentration behavior. Before acid breakthrough, all the acid was totally consumed inside the core.

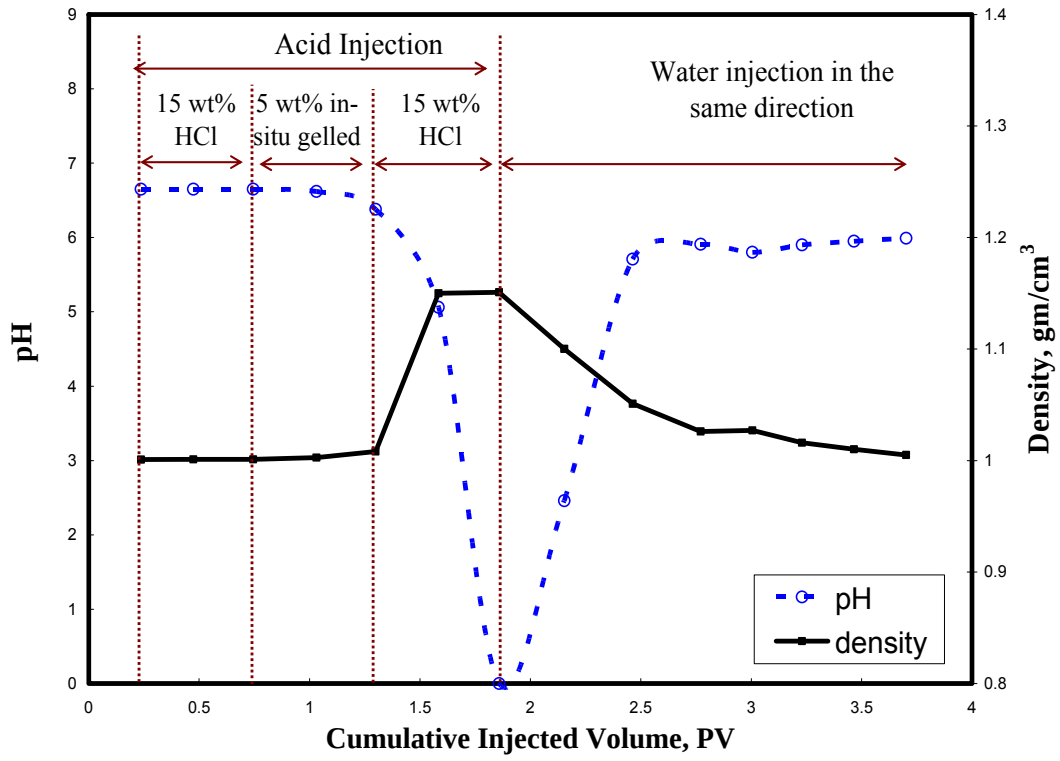

Fig. 6.6—Density and pH value of the core effluent samples, T = 250°F, Core 5.

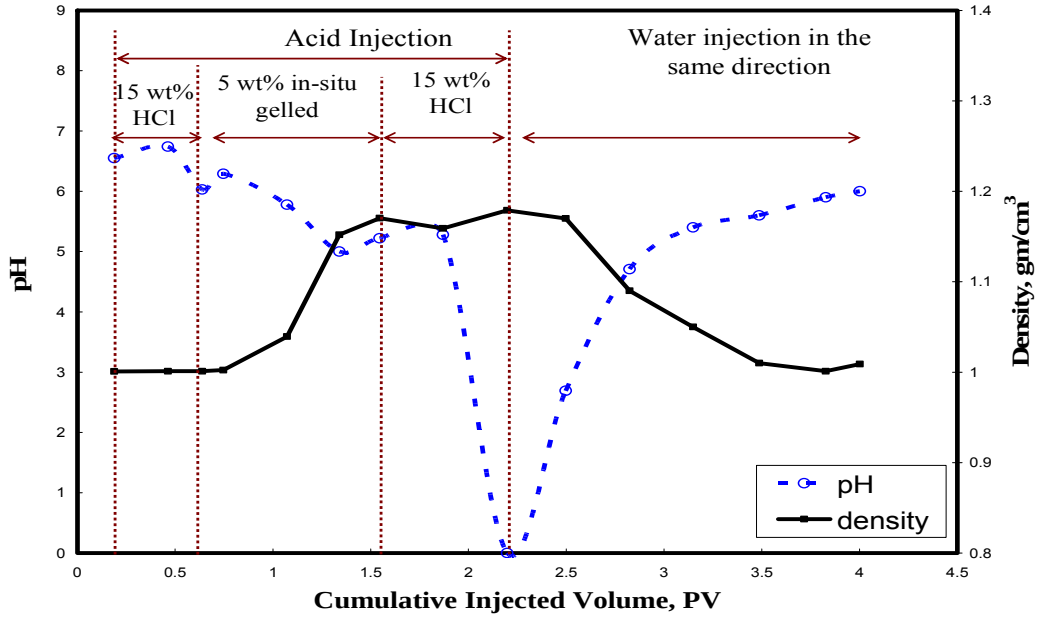

Fig. 6.7—Density and pH value of the core effluent samples, T = 250˚F, Core 6.

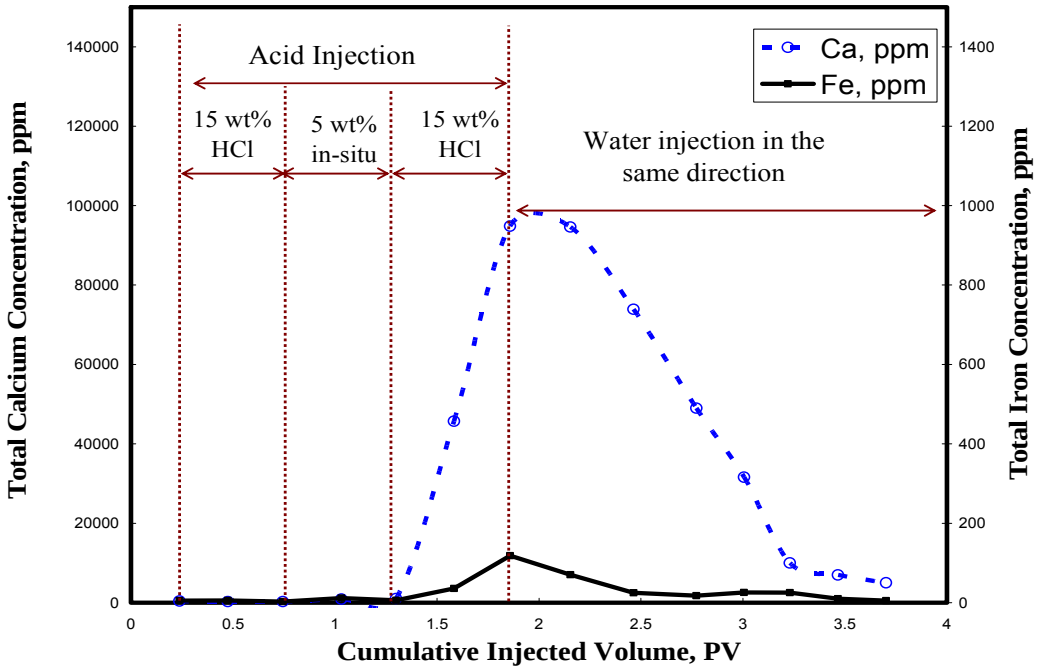

Fig. 6.8—Total calcium and iron concentrations in the core effluent samples, T = 250˚F, Core 5.

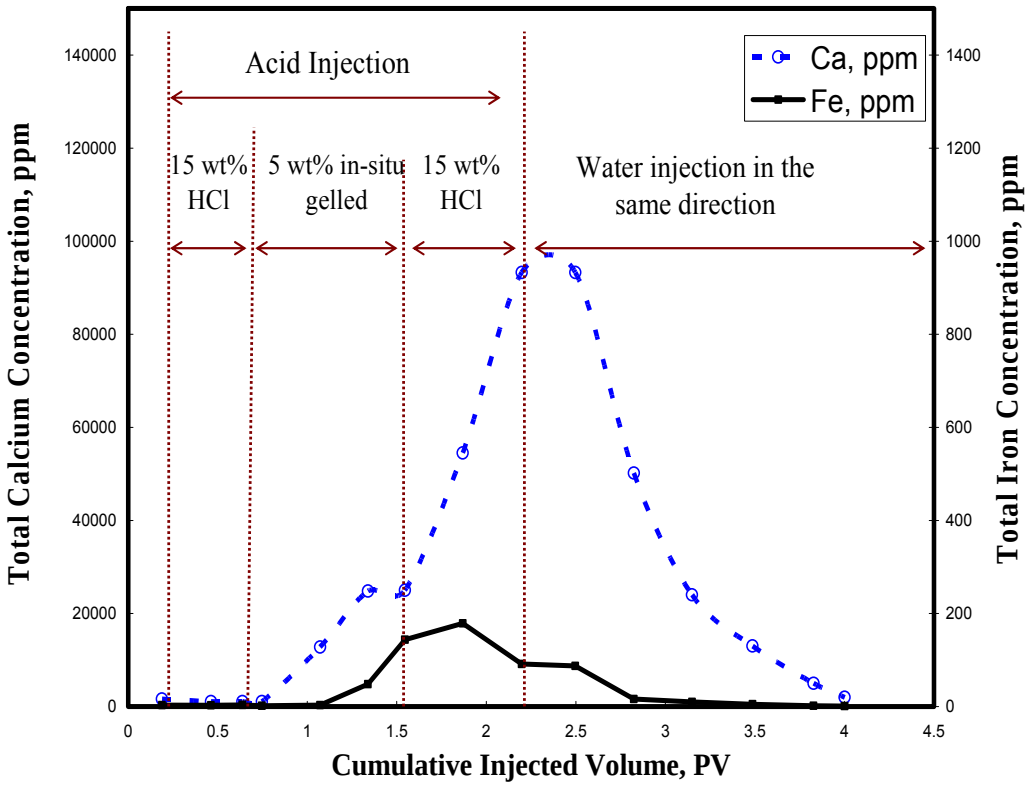

Fig. 6.9—Total calcium and iron concentrations in the core effluent samples, T = 250˚F, Core 6.

For Core 5, calcium and iron were not detected during the first 1 PV. However, after that calcium started to increase and reached an average value of 95,000 ppm while iron increased slightly to a maximum value about 175 ppm at the end point of acid injection. Both of calcium and iron decreased as the water injection volume increased. Calcium measurements were used to determine the amount of calcium carbonate that was dissolved by the acids. Also, it is important to show how the reaction product propagates inside the core. From these results, calcium and iron propagated faster than the acid because they breakthrough earlier than the acid. This is another indication that the acid had been slowed inside the core by the effect of the gel.

Permeability enhancement was achieved in both cores. However, from the material balance on the total iron concentration, 86% of the injected iron was retained inside the core in core 5 and 6. As mentioned earlier, the remaining iron is a potential source of damage because it remaining inside the core in a form of a residual gel.

6.3.4 Multi-stage acidizing at high shear rates

To investigate the effect of the volume of the in-situ gelled acid stage at high shear rate conditions, two other experiments were conducted using cores 7 and 8 at 20 cm^3/min. For core 7, the injection sequence was 0.5 PV of 15 wt% regular acid followed by 0.5 PV of 5 wt% in-situ gelled acid and finally 15 wt% regular acid until breakthrough. Whereas for Core 8, the same sequence was used, but the volume of in-situ gelled acid was increased to 1 PV. As a result, the volume of the final regular acid stage decreased to 0.45 PV, **Table 6.3**. The volume of the in-situ gelled acid that injected in cores 7 and 8 represented 33.3 and 51.3% of the total acid volume injected to each core, respectively.

The pressure drop across core 7 is shown in **Fig. 6.10**. As regular acid entered the core, the pressure drop decreased linearly until the injection of in-situ gelled acid where it increased to 250 psi. However, when the final regular acid stage was injected, the pressure drop instantaneously decreased to a value less than that noted before in-situ gelled acid stage. This means that in-situ gelled acid partially plugged the tip of the wormhole and create additional wormhole inside the core. Therefore, when the final regular acid stage bypassed the gel, it started to propagate from deep distance than the

last point that the first stage ended. This observation was confirmed in core 8, **Fig. 6.11**. Pressure drop of the final stage started its linear decline from the less pressure value than the first stage of regular acid ended its linear decline.

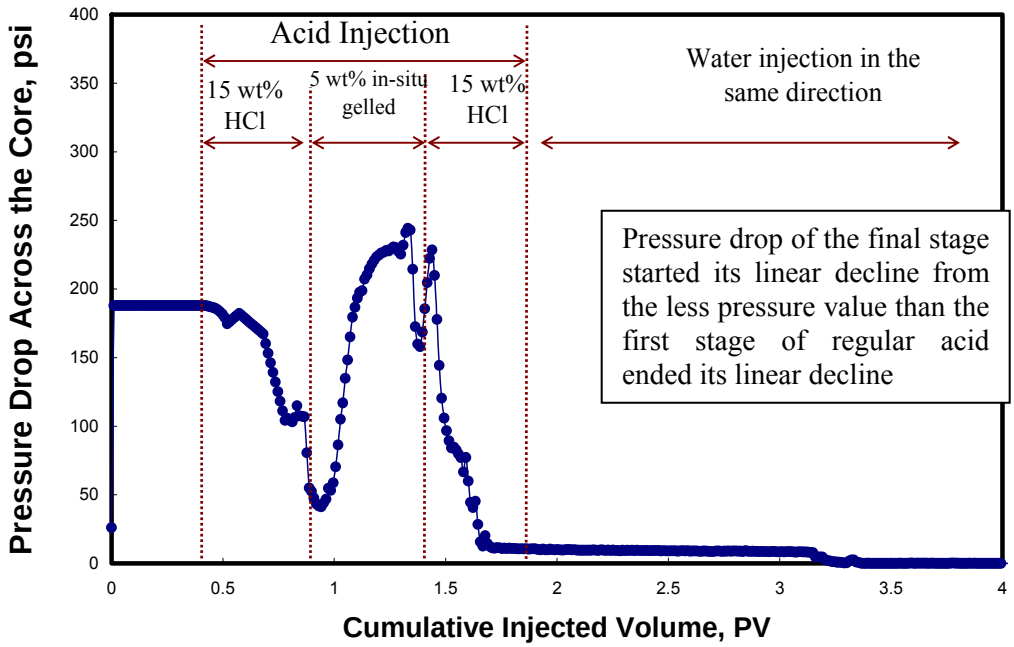

Fig. 6.10—Pressure drop across Core 7 during the injection of three acid stages at 20 cm^3/min and T = 250°F.

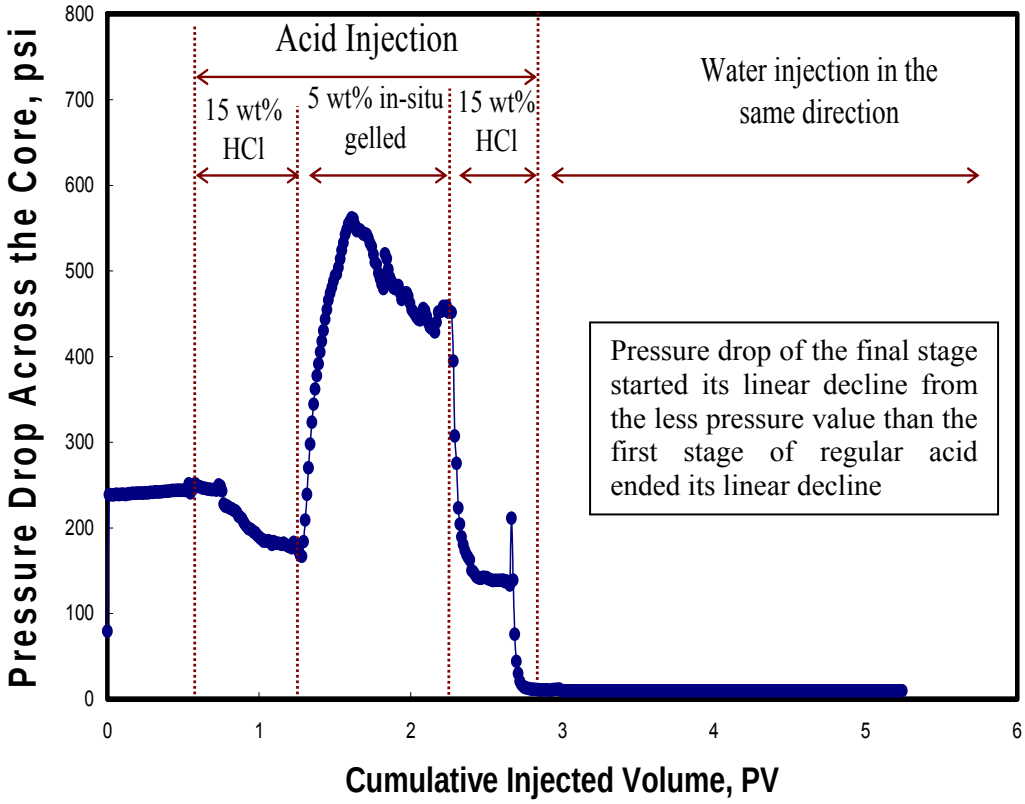

Fig. 6.11—Pressure drop across Core 8 during the injection of three acid stages at 20 cm^3/min and T = 250˚F.

Fig. 6.2 shows the normalized pressure drop across the cores 3 and 4 during the injection of in-situ gelled acids as a single stage treatment. It can be observed that the pressure drop instantaneously increased to a certain value during the injection of the first 0.5 PV. After that the pressure drop took one of the two trends: kept increasing at low shear rate conditions, or kept constant or decreasing; at high shear rate conditions. Based on that observation, at high shear rate, injection of in-situ gelled acid for more than 0.5 PV will not add any benefits because the pressure drop will decrease. This is confirmed by the results from cores 7 and 8 where the shear rate is high. Pressure drop for core 7

was constant when only 0.5 PV of in-situ gelled acid was injected (**Fig. 6.10**). While by increasing the in-situ gelled acid volume to 1 PV as in core 8, a decrease in pressure drop after 0.5 PV of in-situ gelled acid stage (**Fig. 6.11**). Therefore, the acid ability to change its direction at high shear rate conditions decreased with increasing the in-situ gelled acid volume. This agrees with Mohamed et al. (1999) where they examined matrix acid treatments of a large number of seawater injectors. Field data indicated that this acid system can cause loss of well injectivity when large volumes of in-situ gelled acid was used. They indicated that the volume of in-situ gelled acid should not exceed nearly 30 vol% in of the total volume of acids used in typical matrix acid treatments. This 30% is about 0.5 PV injection of ion-situ gelled acid.

6.3.5 Material balance

At low shear rate conditions, only 1.73 PV of regular acid was needed to break through the core in a single stage treatment (core 1). While it took 1.33 PV of regular acid plus 0.5 PV of in-situ gelled acid (Core 5) or 1.1 PV of regular acid plus 1 PV of in-situ gelled acid (core 6). As the volume of the in-situ gelled acid was increased, the amount of the regular acid needed to breakthrough decreased. Also, this observation was confirmed for the high shear rate experiments, **Table 6.4**. This means increasing the volume of in-situ gelled acid stage will enhance the regular acid to breakthrough from the core with less volume.

A summary of the material balance indicated that the amount of iron decreased with increasing the subjected shear rate. In a single stage treatment, the remaining iron in

the core decreased from 59 to 23% with increasing the injection rate from 5 to 20 cm^3/min. Also, in multi-stage treatments, the remaining iron decreased from 86 to 57% by increasing the injection rate with the same amount. In multi-stage treatments the percentage of the remaining iron was higher than single-stage. This can be explained by the final regular acid stage when created its own wormhole away from the gel that formed by in-situ gelled stage. Therefore, it became the difficult to break using water injection. **Table 6.4** confirmed that doubling the volume of in-situ gelled acid pore gives the same percentage of iron that remaining inside the core. This means that the amount of the iron inside the core was doubled by doubling the injection volume. This amount of iron represents a potential source of damage.

7. NEW INSIGHTS INTO WORMHOLE PROPAGATION IN CARBONATE ROCKS USING REGULAR, GELLED AND IN-SITU GELLED ACIDS

It is well known that the efficiency of regular acid treatments goes through a maximum at an optimum acid injection rate where it gives the maximum wormhole propagation rate (ratio between wormhole length to pore volume of acid required to breakthrough). This rate is a strong function of the acid-rock reaction: diffusion of the acid to the rock, surface reaction, and mass-transport of the reaction products. Adding a polymer and other additives to the acid may affect the wormhole propagation rate. However, literature survey didn't highlighted in details how the wormhole propagation rate will change when polymer and crosslinker will be existing with the regular acid. Therefore, the objective of this study is to determine the wormhole propagation rate of gelled and in-situ gelled acids as a function of the injection rate. The effects of temperature, lithology, and initial permeability on the wormhole propagation rate were considered in this work.

A coreflood study was conducted using calcite cores at temperature range 100 to 250 ºF. Injection rate was varied from 1 to 20 cm^3/min using 5 wt% HCl regular, polymer gelled, and in-situ gelled acids. Calcium, cross-linker, and acid concentrations were measured for the core effluent samples.

The wormhole propagation rate of gelled acid required was higher than regular acid where gelled acid required less acid volume to breakthrough. However, the wormhole propagation rate of in-situ gelled acid required was lower than regular acid

where in-situ gelled acid required a higher pore volume to breakthrough. Three regions were obtained for the wormhole propagation rate of in-situ gelled acid as a function of the injection rate: Region I, where acid injection rate is low, and in-situ gelled acid wasn't able to breakthrough from the cores at injection rate less than 5 cm^3/min. Region II, where the acid volume required to breakthrough decreased as injection rate increased in the range between 5 and 10 cm^3/min. Region III, where the acid volume injected increased with the injection rate at injection rate higher than 10 cm^3/min. The optimum injection rate wasn't affected by temperature, or initial core permeability. The volume required to breakthrough decreased as the temperature was increased, and as the initial core permeability increased.

7.1 Introduction

Several investigators have studied the phenomenon of wormhole formation in a variety of fluid-mineral systems and reported the existence of an optimum injection rate for regular acids (Hoefner and Fogler, 1988; Daccord et al., 1989, 1993; Wang et al., 1993; Frick et al., 1994; Mostofizadeh and Economides, 1994; Bazin et al., 1995; Huang et al., 1997; Fredd and Fogler, 1998a, 1998b). The optimum injection rate represents the conditions at which a minimum volume of stimulating fluid is required to breakthrough the whole core. The optimum injection rate corresponds to the formation of dominant wormhole channels. All the acid types exhibit an optimum injection rate at which the number of pore volumes to breakthrough is minimized and dominant wormhole channels are formed (Economides 2000). Daccord et al. (1993) showed that dissolution patterns in

limestone are classified as compact, wormholes, or uniform, depending on the relative influence of flow rate with respect to the overall reaction rate. At low flow rates, the convection-limited regime leads to compact pattern. At intermediate flow rates, mass-transport-limited kinetics produces wormhole patterns. At high flow rates, the surface-reaction-limited regime yields a uniform dissolution pattern.

Buijse (2000) and Huang et al. (1997) showed that two mechanisms at the origin of wormhole growth termination have been proposed: high consumption at wormhole walls, which limits acid concentration at the wormhole tip for extension and filtration losses through the wormhole. In the first case, extinction is linked to a transition from mass-transport-limited kinetics to the convection-limited regime occurring at the wormhole tip; in the second case, it is the transition from mass-transport-limited kinetics to the surface-reaction-limited regime.

Taylor and Nasr-El-Din (2003) tested three different in-situ gelled acid systems based on polymer at different temperatures. They found the reaction of all three of the in-situ gelled acids was significantly retarded compared to the corresponding regular HCl acid. The primary cause of this trend was the polymer present in each of the acid formulae. Core flood studies showed that the polymer and cross-linker component of in-situ gelled acids irreversibly reduced the permeability of carbonate reservoir rock. The objective of this study is to determine the wormhole propagation rate of gelled and in-situ gelled acids. Effects of temperature, initial permeability, and acid type on the wormhole propagation rate were considered in this work.

7.2 Experimental Studies

Materials: Hydrochloric acid (ACS reagent grade) titrated using a 1N sodium hydroxide solution to determine its concentration, and was found to be 36.8 wt%. All acid solutions were prepared using deionized water with a resistively of 18.2 MΩ.cm at room temperature. Polymer and other additives were all oilfield chemicals, and were used without further purification.

Measurements: Single core flood setup was constructed to simulate the matrix stimulation treatment. Back pressure of 1,000 psi on the outlet of the two cores was conducted to keep CO_2 in solution. Pressure transducers were connected to computer to monitor, and record the pressure drop during the experiments every five seconds. Viscosity measurements were made using M5600 viscometer at 300 psi and various temperatures. Viscosity was measured as a function of shear rate from 0.1 to 1020 s^{-1}. Measurements were conducted at 300 psi and temperature range from (75-150^{o}F). All acids were mixed using a magnetic stirrer.

Acid Preparation: Three acid formulas were used in this work: 5 wt% regular acid, 5 wt% gelled acid, and 5 wt% in-situ gelled, **Table 7.1.** Gelled and in-situ gelled acids were prepared with the same polymer concentration, but with different polymer from two different company. Gelled acid was prepared without adding the crosslinker (Fe^{+3}) and breaker. $FeCl_3$ was used as a source of Fe^{+3} (crosslinker) for in-situ gelled acid. Regular acid solutions were prepared by mixing the corrosion inhibitor and HCl acid with water. All systems had the same and HCl concentration (5 wt %). The acid

formula that used in this work is listed in **Table 7.1**. It is important to highlight that this is the formula that is typically used in the field.

TABLE 7.1—FORMULAE OF REGULAR, GELLED, AND IN-SITU GELLED ACIDS

Component	Regular	Gelled	In-situ
Hydrochloric acid	5 wt% HCl	5 wt% HCl	5 wt% HCl
Acid gelling agent (polymer)	-	20 ml/l	20 ml/l
Corrosion inhibitor:	4 ml/l	4 ml/l	4 ml/l
Cross-linker: Ferric chloride	-	-	4.5 ml/l
Breaker: sodium erythorbate	-	-	20 lb/Mgal
Buffer: Hydroxyacetic acid	-	2 ml/l	2 ml/l

Core Preparation: A 6-in. length cylindrical cores with a 1.5-in. diameter were cut from two blocks: Pink dessert limestone block and Austin chalk block, **Table 7.2**. Twenty three cores were cut from the pink dessert limestone block while four cores were cut from Austin chalk block. Cores were placed inside an oven set at 257 ^{o}F for 5 hours to be completely dry, and then their weight was measured. Core was saturated with deionized water under vacuum for 24 hr. The porosity was calculated from these measurements. After that, the core was placed inside the core holder, and water was injected at different flow rates (5, 10, and 20 cm^3/min) to calculate core initial permeability.

TABLE 7.2—SUMMARY OF THE CORE DATA

Rock Type	Porosity, vol%	Permeability, md
Pink Dessert	27-30	81-95
Austin Chalk	18-20	9-11

7.3 Results and Discussion

7.3.1 Viscosity measurements: gelled acids

Gelled acid was prepared and reacted with increasing amounts of calcium carbonate to simulate spending of the acid with carbonate rocks. The apparent viscosity of this acid was measured as a function of shear rate at each equilibrium pH and the data were fitted using the power-law model. **Table 7.3** gives the power-law parameters at each pH value. The viscosity increased and reached to a maximum value of 860 mPa.s at pH of 1.8. The viscosity remained constant as the pH value was further increased. In Section 2, we noted that the carboxylate groups will be protonated at pH values greater than nearly 2. It appears from these results that the calcium ions with two positive charges interacted with the negatively charged carboxylate groups, and increased the viscosity of the acid.

TABLE 7.3—POWER-LAW PARAMETERS FOR 5 WT% HCL, GELLED ACID AT DIFFERENT PH VALUES NEUTRALIZED BY $CACO_3$ (28ºC)

Equilibrium pH	K, mPa.s^n	n	R^2
Live acid (pH= 0)	748.1	0.42	0.981
1.8	860.3	0.47	0.975
3.5	910.2	0.50	0.992
5.0	915.5	0.49	0.992

7.3.2 Viscosity measurements: in-situ gelled acids

The viscosity behavior of in-situ gelled acids was examined at an initial HCl concentration of 5 wt%, temperature of 28°C, and atmospheric pressure. It is desirable to have live gelled acids with low viscosity to allow pumping of the acid into the

formation. This is an important issue when stimulating deep vertical wells or horizontal wells with extended reach. Live acids were gradually neutralized by adding calcium carbonate powder while the pH was monitored. **Fig. 7.1** shows the apparent viscosity of in-situ gelled acid at different pH values and shear rate of 1 s^{-1} while **Table 7.4** shows the Power-law parameters for in-situ gelled acid at different pH values. The maximum value of viscosity was 7,750 mPa.s at pH 3.3, and then the viscosity was decreased 4650 mPa.s at pH 5.5. The change in viscosity of in-situ gelled acid increased at nearly pH 2, which was similar to the results obtained by Taylor and Nasr-El-Din (2003).

TABLE 7.4—POWER-LAW PARAMETERS FOR 5 WT% HCL, IN-SITU GELLED ACID AT DIFFERENT PH VALUES NEUTRALIZED BY $CaCO_3$ (28°C).

Equilibrium pH	K, mPa.s^n	n	R^2
Live acid (pH= 0)	361.7	0.60	0.993
1.5	819.1	0.53	0.992
3.5	4,158.4	0.35	0.993
5.1	4,888.8	0.36	0.998

The vendor companies, that produce these acids, were recommended to use these acids with polymer concentration equal to 20 GPT. However, to investigate the effect of polymer concentration, in-situ gelled acid was prepared three times with different polymer concentrations: 1, 2, and 4 vol.% GPT. **Fig. 7.2** shows that the viscosity increased with polymer concentration at all shear rates examined and 150 °F. Also, it was noted that at polymer concentration 4 vol.%, the viscosity drop with shear rate was higher than the viscosity drop with at 1 and 2 vol.%. This mean at high polymer concentration, acid become more sensitive to the shear rate. Also, high polymer

concentration will need also high pumping energy to overcome the viscosity which can cause many operation problems.

The viscosity difference between polymer concentration of 1 and 2 vol.% was much smaller than the differences between 2 and 4 vol.%. Actually, the difference in viscosity between 1, and 2 vol.% was small, that will encourage us to do more study using 1 vol.% polymer concentrations, especially for low permeability formations.

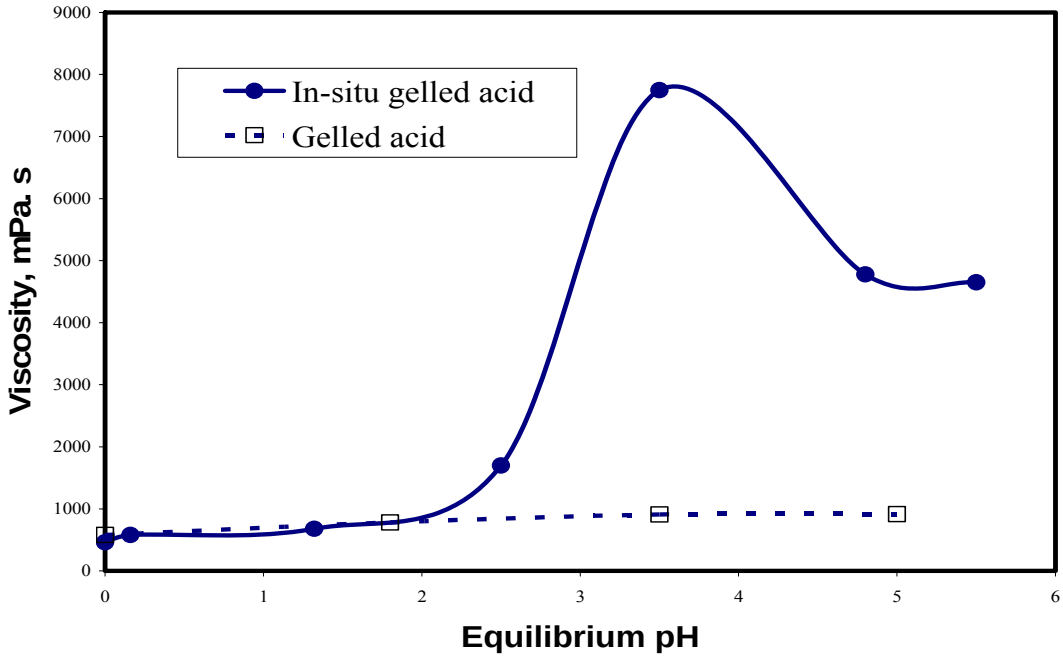

Fig. 7.1—Apparent viscosity of gelled and in-situ gelled acid at different pH values neutralized by $CaCO_3$ powder (5 wt% HCl, shear rate = 1 s^{-1}, 28 ºC).

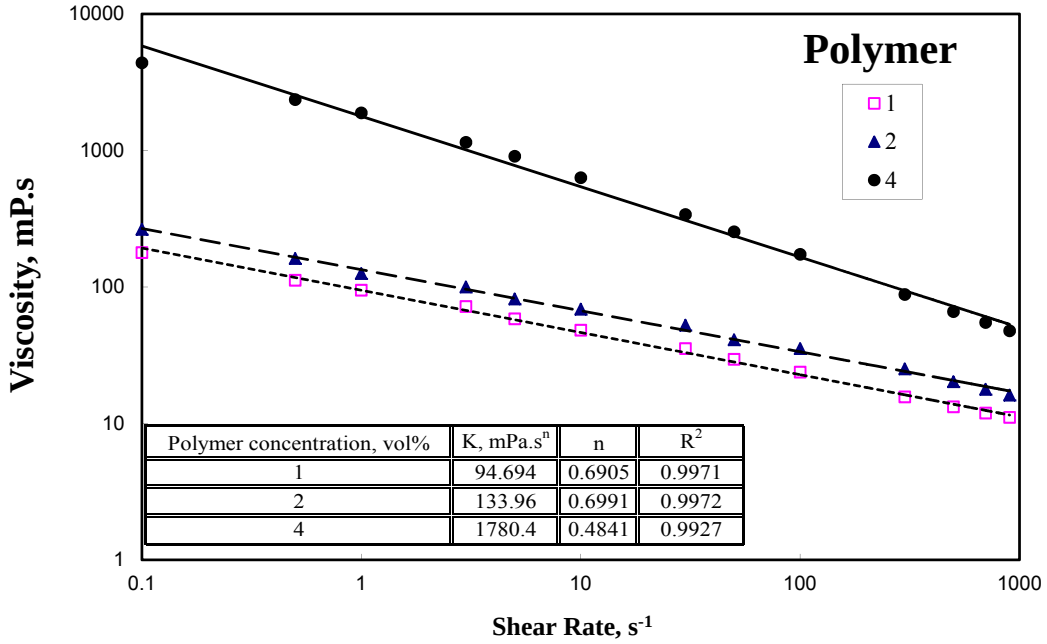

Fig. 7.2—Effect of polymer concentration on the viscosity of live in-situ gelled (5 wt % HCl, 300 psi, 150°F).

7.3.3 Pressure drop across the core: gelled acid

The change in the pressure drop across the core mainly depends on acid viscosity and injection rate. Increasing the injection rate or acid viscosity, or both will lead to increase in the pressure drop across the core. **Fig. 7.3** shows the normalized pressure drop for 5 wt% gelled acid as a function of cumulated acid injection volume at 250°F. The normalized pressure drop is defined as the ratio between the pressure drop during acidizing to the initial pressure drop. For all injection rates, as the gelled acid entered the core, the pressure drop increased. The normalized pressure drop at rate 5 cm^3/min was less than the normalized pressure drop at 20 cm^3/min. However, the highest normalized pressure was achieved at injection rate of 10 cm^3/min. Based on the gelled acid viscosity, increasing gelled acid injection rate will decrease its viscosity because it will increase

the shear rate. Therefore, the viscosity of gelled acid at rate 5 cm^3/min is higher than at rate 10 cm^3/min, which is higher than 20 cm^3/min.

For injection rates 5, 10, and 20 cm^3/min, the shear rates, that the acid was subjected in each experiment, were 750, 1,500, and 3,000 s^{-1}, respectively. Based on the power-law model, the viscosity and shear rate relationship are linear on a log-log scale. Therefore, the viscosity drop due to increase the shear rate from 750 to 1,500 s^{-1} was higher than the viscosity drop due to increase the shear rate from 1,500 to 3,000 s^{-1}. Based on the viscosity in **Fig. 7.2**, it can assume the decreased in viscosity wasn't significant between 750 to 3,000 s^{-1}. Therefore, the effect of injection rate on the normalized pressure can't explain by the viscosity change due to the shear rate change.

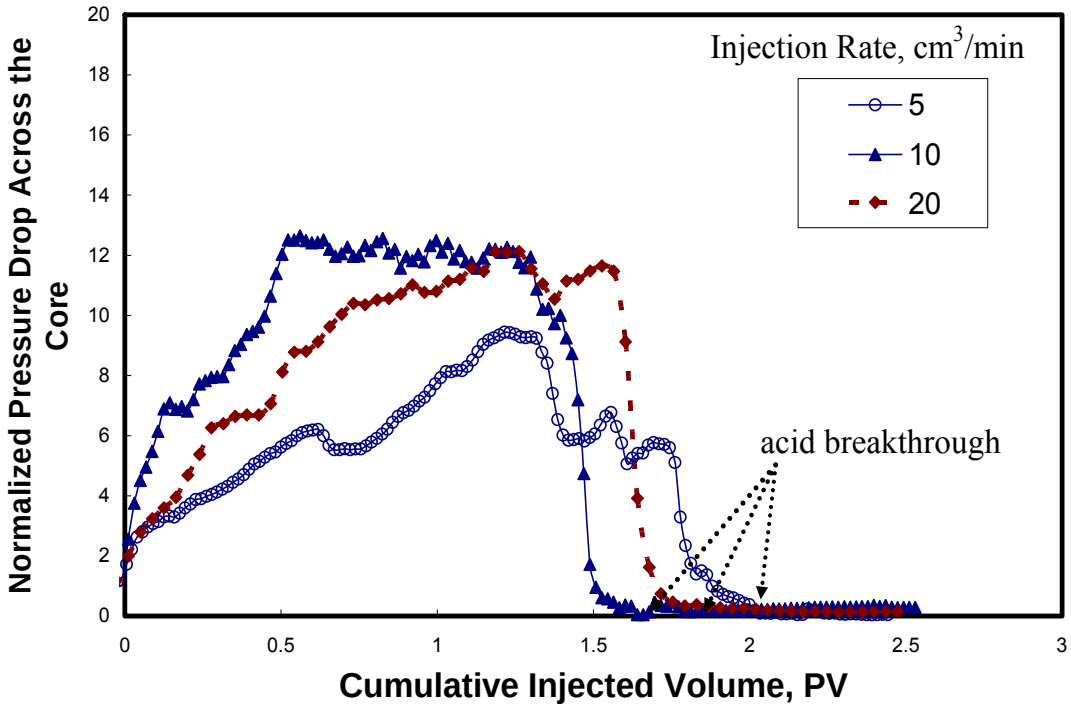

Fig. 7.3—Normalized pressure drop during the injection of gelled acid with 5 wt% HCl at 5, 10, and 20 cm^3/min, = 250˚F.

7.3.4 Pressure drop across the core: in-situ gelled acids

The normalized pressure drop during the injection of 5 wt% in-situ gelled acid at injection rate of 5, 10, and 20 cm^3/min using Pink dessert cores is shown in **Fig. 7.4.** The three experiments were conducted at 250 ^oF. The normalized pressure drop of in-situ gelled acid at injection rate of 5 cm^3/min was higher than at injection rate of 10 cm^3/min which was higher than the injection at 20 cm^3/min. Viscosity and gelling mechanisms were the main two factors affecting the pressure drop across the core. In-situ gelled acids are non-Newtonian shear thinning fluids (Taylor and Nasr-El-Din 2003). Therefore, increasing the shear rate by increasing the injection rate decreased the viscosity of the acid that led to decrease in the pressure drop. Also, increasing the injection rate decreased the opportunity of the acid to reach to a pH value of 2 (crosslinking point). Therefore at high injection rate, gel will not form as fast as at low injection rate. The required volume to breakthrough from the 6-in cores at rates 5, 10, and 20 cm^3/min were 14.7, 3.9, and 5.4 PV, respectively. For the low injection rate, in-situ gelled acid required more acid volume to breakthrough than at the rates 10 and 20 cm^3/min.

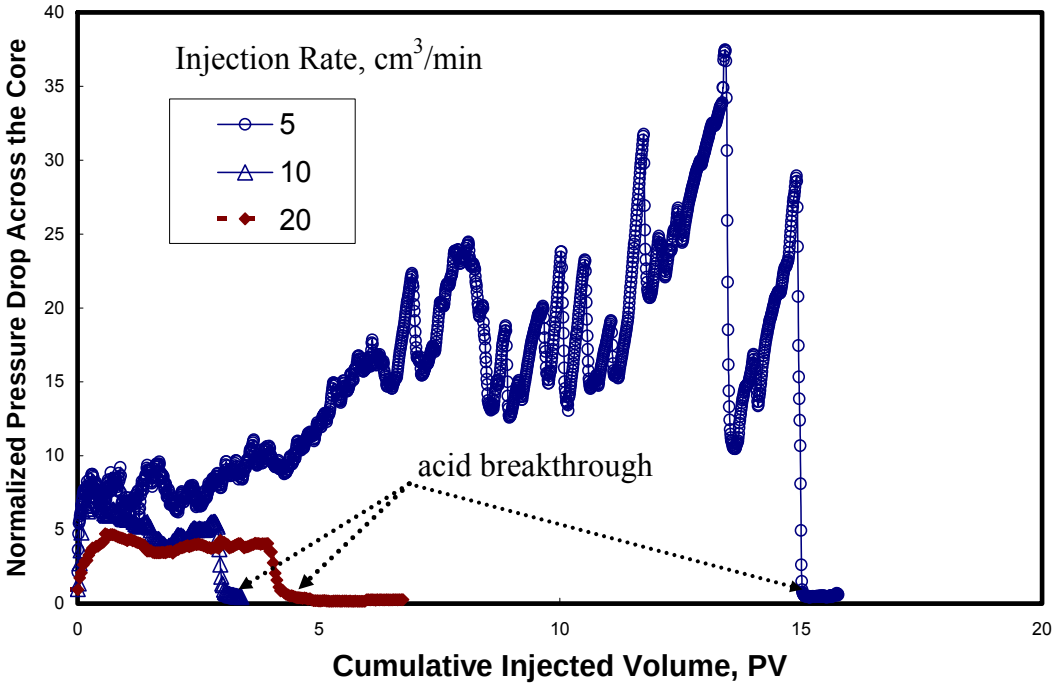

Fig. 7.4—Normalized pressure drop during the injection of in-situ gelled acid with 5 t% HCl, and 20 cm^3/min, T = 250˚F.

7.3.5 Wormhole propagation rate of regular acids

Wormhole Propagation rate defined by the ratio between the created wormhole length to the acid volume required to create this wormhole. For certain core length, the wormhole propagation rate can be evaluated by the volume of acid required to breakthrough. The wormhole propagation rate decreased as the acid volume to breakthrough increased. Bazin (2001) divided the wormhole propagation rate as a function of the injection rate into three regions: Region I, where acid injection rate was low, and the wormhole might form but didn't breakthrough from the core. Region II, where the acid volume required to breakthrough decreased as injection rate increased. Region III, where the acid volume injected increased with the injection rate. Bizan

(1996) highlighted how the mechanisms of wormhole propagation in Regions II and III using CT scan. Region II, at the beginning of acid injection, a fast growth of the wormhole tip. Then, as acid injection continued, the wormhole extension in length occurred slowly with a severe-branching occurred at the wormhole tip with an increase of wormhole diameter. Region III, a fast forming for the wormhole and continued in propagates. Very fine branches were formed around the main wormhole channel.

An increase in temperature shifted the optimum flow rate to higher values with increasing in the volume of acid required to breakthrough at the optimum rate (Bazin 2001). The increasing in the optimum injection rate and the volume of acid at optimum conditions could be explained: as temperature increased, the acid reaction rate became higher. Acid consumed at shallower penetration depth led to decrease the acid concentration at the wormhole tip. Therefore, a larger acid volume needed to achieve breakthrough. Also, at higher permeabilities, a higher injection rates and larger volumes at the optimum condition were found (Bazin 2001). Increasing the permeability will increase the pores volume inside the rock. Therefore, each core needed larger acid volume to fill these pores.

7.3.6 Wormhole propagation rate of in-situ gelled acids

The effect of the in-situ gelled acid injection rate on the volume required to breakthrough from 6-in length cores is shown in **Fig. 7.5**. Three regions were obtained: Region I, where acid injection rate was low, and in-situ gelled acid wasn't able to breakthrough from the cores at injection rate less than 5 cm^3/min. Region II, where the in-situ gelled acid volume required to breakthrough decreased as injection rate increased in the range between 5 and 10 cm^3/min. Region III, where the in-situ gelled acid volume injected increased with the injection rate at injection rate higher than 10 cm^3/min.

At low injection rates, in-situ gelled acid was able to reach to the pH of 2 (crosslinking point) faster than at high injection rate which produced a gel material. This gel material kept to plug the way that the acid was moving. Therefore, acid forced to change it direction several times inside the core leading to decrease the wormhole propagation rate. Therefore for Region I, the gel material was formed quickly in the way that acid wasn't able to breakthrough from the core. However, increasing the injection rate reduced the gel ability to form faster. This allowed to the acid to breakthrough from the core (starting of Region II). At an injection rate of 5 cm^3/min, a 15 PV of in-situ gelled acid was required to breakthrough. However, it decreased to 4.8 PV by increasing the injection rate to 7.5 cm^3/min. A larger volume of the acid needed to breakthrough at low rates confirmed the acid changed its direction several times until acid breakthrough. The injection rates gave the lowest in-situ gelled acid volume was found to be 10 cm^3/min.

Effluent samples were collected throughout the experiment using an automatic fraction collector. Effluent samples for all experiments were weighted, and the collected volume of the samples was calculated from the sample density. Using the concentration of each sample, and its volume the amounts of Ca and Fe were calculated for all collected samples. The iron concentration in live acid was found to read 918 ppm.

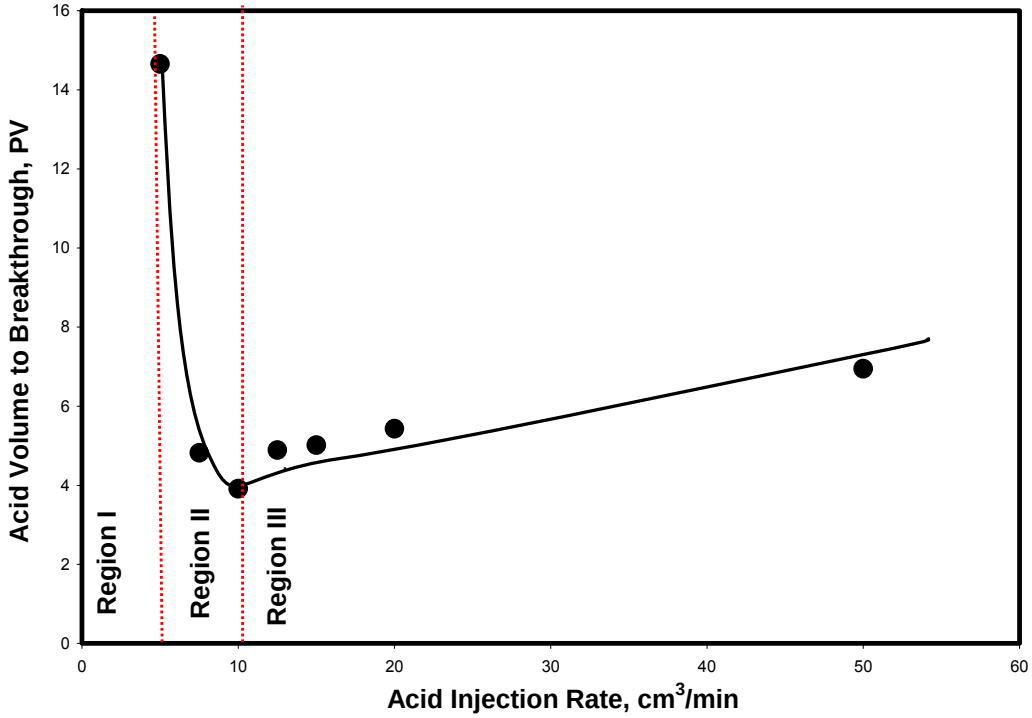

Fig. 7.5—Effect of acid injection rate on the acid volume to breakthrough of in-situ gelled acid with 5wt% HCl, 150°F.

Summary of the material balance indicated that the amount of iron that remained inside the core decreased with increasing the in-situ gelled acid injection rate, **Fig. 7.6**. The remaining iron inside the core decreased from 40 to 10% with increasing the injection rate from 5 to 50 cm^3/min. Iron, which remained inside the core, might be in

one of the following forms: hydrated ferric hydroxide precipitated in the core and/or as a gel residue that didn't break at the test conditions. Both of theses forms represent damage inside the core.

7.3.7 Effect of temperature

Bazin (2001) highlighted that for regular acid, as temperature increased, the volume required to breakthrough increased led to decrease the wormhole propagation rate. This is because increasing the temperature will increase the reaction rate. Therefore, regular acid will be consumed faster at shallow penetration distance. A high volume of acid is required to achieve acid breakthrough. However, this theory can't apply to in-situ gelled acid systems. Because viscosity of in-situ gelled acid decreased with temperature increasing. This decrease in the viscosity will allow to the acid to propagate easier inside the core. Therefore, it will required less volume to breakthrough at higher temperatures. **Fig. 7.7** shows how the volume required to breakthrough was decreased by increasing the temperature. Also from **Fig. 7.7**, the optimum injection rate didn't change by changing the temperature.

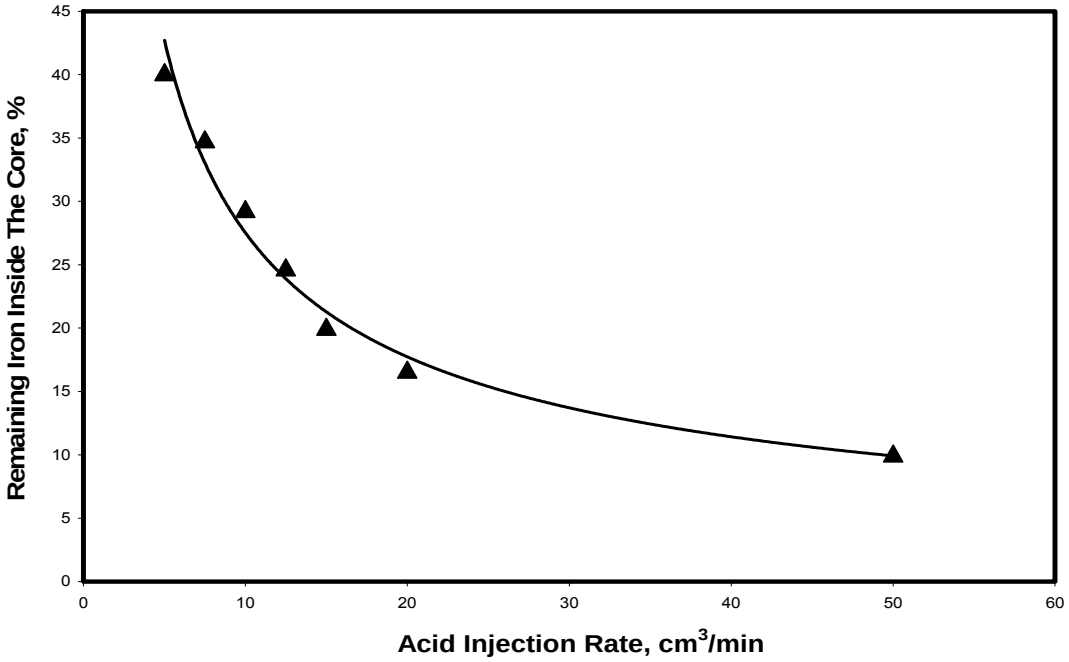

Fig. 7.6—Remaining iron inside the core as a function of acid injection rate, in-situ gelled acid, 5 wt% HCl, 250°F.

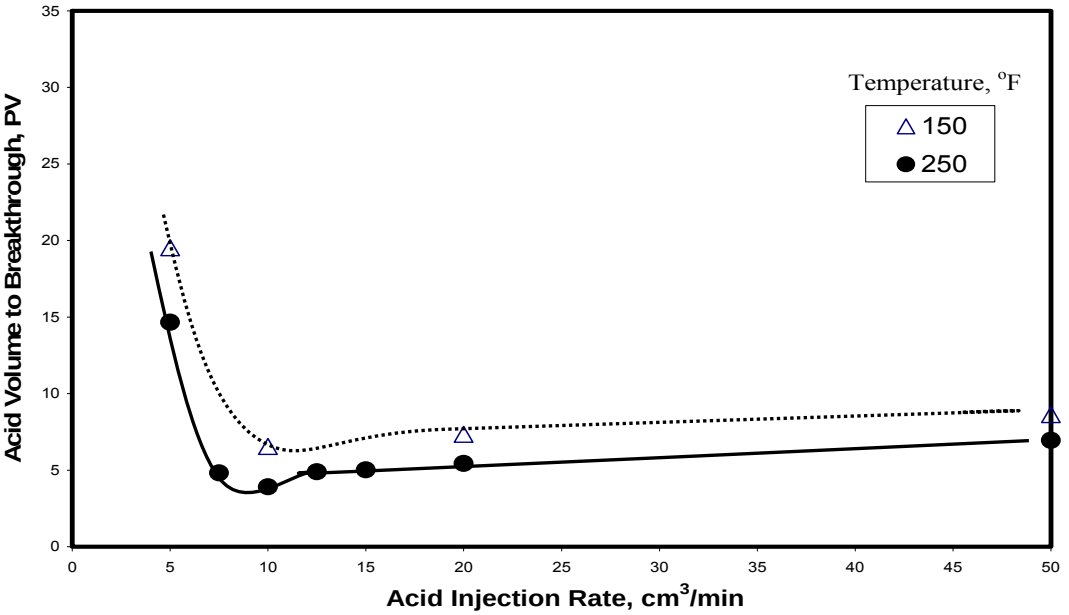

Fig. 7.7—Effect of temperature on the acid volume to breakthrough at different acid injection rate of in-situ gelled acid, 5 wt% HCl.

7.3.8 Effect of initial core permeability

The effect of initial core permeability mainly can be shown in the pore thought diameter. Therefore, decreasing the permeability means decreasing in the pores volume. The volume of acid can be found in the small pores (lower permeability formation) is less than the volume of acid that can be found large pores (high permeability formations). The smaller volume of in-situ gelled acid in small pores will reach to pH 2 faster than the large volume at larger pores. Therefore, the gel material will form faster at lower permeability formation that lead to increase the volume of in-situ gelled acid required to breakthrough. **Fig. 7.8** shows increase in the volume required to breakthrough by decreasing initial permeability. Also from **Fig. 7.8**, the optimum injection rate didn't change by changing the permeability from 81 to 9 md.

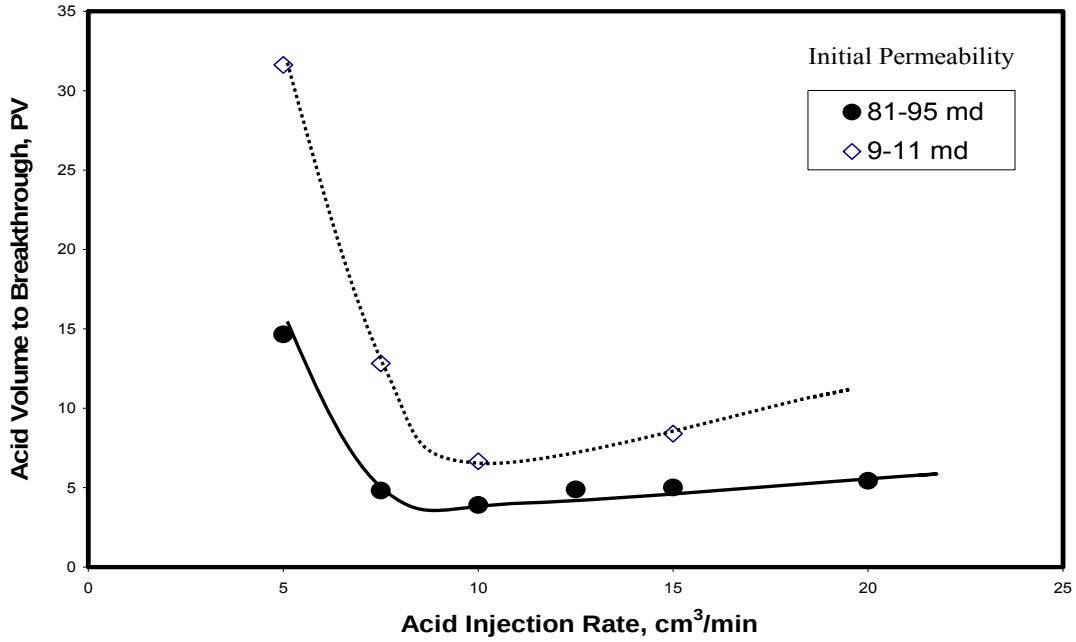

Fig. 7.8—Effect of initial core permeability on the acid volume to breakthrough at different injection rate of in-situ gelled acid, 5 wt% HCl, 250°F.

7.3.9 Effect of acid type

Gelled acid is regular acid with adding polymer while in-situ gelled acid is regular acid with adding polymer, crosslinker and breaker. Regular acid, gelled acid, and in-situ gelled (all at 5 wt% HCl) were the three acid formulas examined, **Table 7.1**. **Fig. 7.9** shows that the wormhole propagation rate as a function of the injection rate for the three acid formulas. The optimum injection rate wasn't affected by changing the acid type. However, the required volume to breakthrough was significantly changed.

Gelled acid required less volume of acid to breakthrough than the regular acid. Adding only polymer (gelling agent) reduced acid consumption because of a lower diffusion coefficient and a lower leak off rate through the wormhole walls. The net result of these two effects is expected to be a higher wormhole propagation velocity. However, a potential problem with polymer gelling agents is filter-cake formation near the core surface which hinders the wormhole formation.

In-situ gelled acid required the highest volume of acid to breakthrough from the cores. Adding polymer, crosslinker, and breaker changed the performance of the acid significantly. The lower fresh acid viscosity allows penetration in wormholes until acid reaction increases the pH and causes crosslinking. This significant increase in viscosity forced the next fresh to change it direction inside the cores. Because of the acid ability to change it direction, in-situ gelled acid path inside the core was longer than the path of regular acid. Therefore, in-situ gelled acid needed more volume to breakthrough from the core.

Fig. 7.10 shows the 3D visualization image of the wormhole created by regular, gelled and in-situ gelled acids at injection rate of 5 cm^3/min. The 3D visualization image of in-situ gelled acid shows how the acid changed its direction in a tortuous way as it propagated inside the core. In-situ gelled acid distributed in every location as shown in **Fig. 7.10**. The created wormholes of gelled and regular acids inside didn't have the tortuous shape as shown with in-situ gelled acid. However, the Wormhole diameter of gelled acid were smaller than this noted for regular acid.

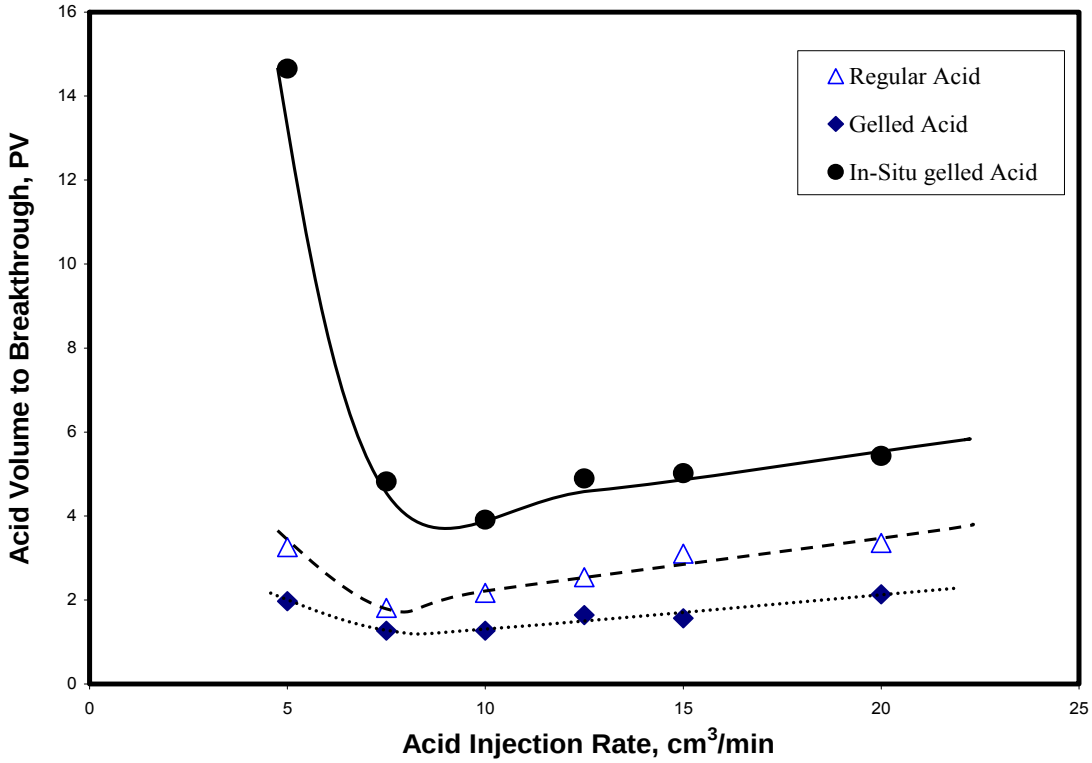

Fig. 7.9—Effect of acid type (regular, in-situ gelled, and gelled acids) on acid volume to breakthrough at different injection rate, 5 wt% HCl, 250°F.

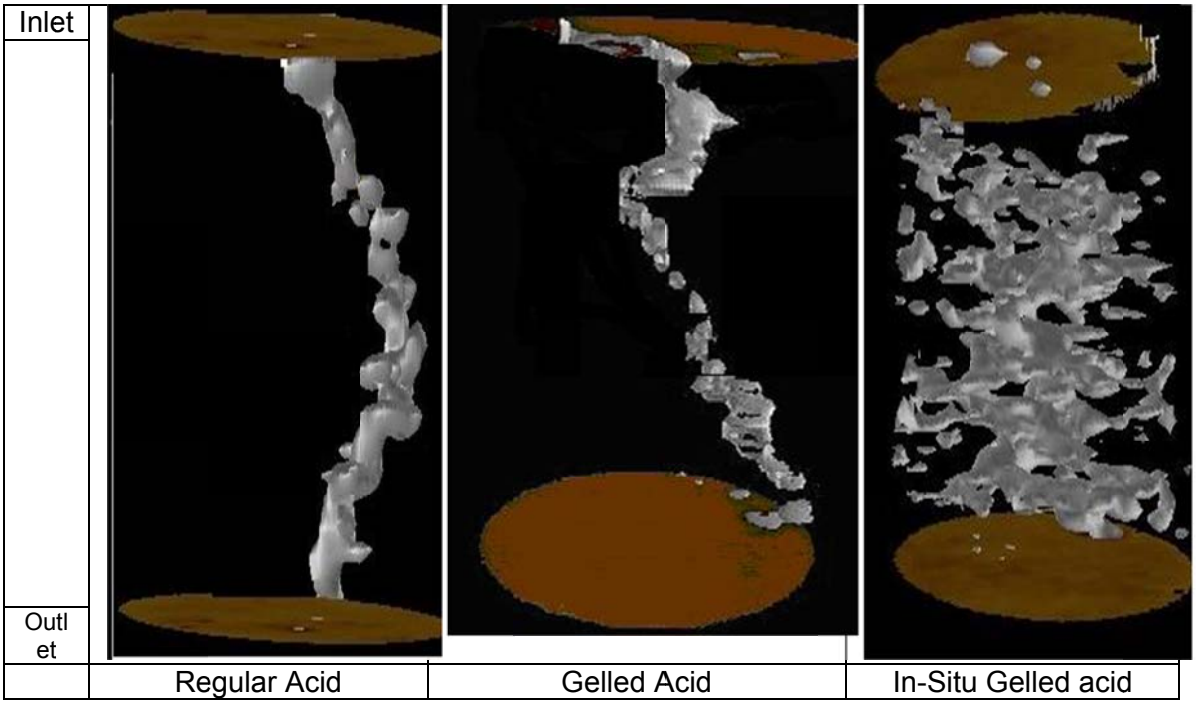

Fig. 7.10—3D visualization of wormholes created by regular, gelled, and in-situ gelled acids at acid injection rate of 5 cm^3/min, all at 5 wt% HCl, 250°F.

8. A STUDY OF DIVERSION USING POLYMER-BASED IN-SITU GELLED ACIDS SYSTEMS

In-situ gelled acids that are based on polymers have been used in the field for several years, and were the subject of many lab studies. These acids used in stages to block the treated zone and forcing the next regular acid stages to the untreated zones. An extensive literature survey reveals that there are conflicting opinions about using these acids. On one hand, these acids were used in the field, with mixed results. On the other hand, recent lab work indicated that these acids can cause damage under certain conditions.

The ability of polymer-based in-situ gelled acids to divert regular acids was studied using parallel core flood setup. The sequence of the injection involved In-situ gelled acid at 5 wt% HCl stage followed by regular acid at 15 wt% HCl until acid breakthrough. Experimental results show that even for nearly the same permeability formation (1:1.1), regular acid preferred to flow only through the high permeability zones. Therefore, diversion was needed for all acid treatments. At an injection rate of 1 cm^3/min, in-situ gelled acid plugged the two cores. For low permeability contrast (1:2), polymer was able to divert the acid with permeability enhancement in both cores.

For high permeability contrast (1: 20 up to 25), in-situ gelled acid was able to divert the acid only at injection rate less than 10 cm^3/min. However, at higher injection rates, in-situ gelled acid was not able to build enough pressure that could force the regular acid into the low permeability core. Increasing the injection rate reduced the

viscosity of the in-situ gelled acid. Therefore, acid injection rate should be determined based on the expected fluid viscosity in the formation. The results obtained can be used to better design acid treatments in carbonate reservoirs.

8.1 Introduction

Previous studies that examined diversion of in-situ gelled acid are limited used. Therefore, the objective of the present study is to study the ability of in-situ gelled acid to divert regular acid into low permeability cores using parallel core flood setup. A second objective is to determine the impact of initial permeability contrast on the effectiveness of in-situ gelled acid to divert regular acids into low permeability cores.

8.2 Experimental Studies

Materials: Hydrochloric acid (ACS reagent grade) titrated using a 1N sodium hydroxide solution to determine its concentration, and was found to be 36.8 wt%. All acid solutions were prepared using deionized water with a resistively of 18.2 MΩ.cm at room temperature. Polymer and other additives were all oilfield chemicals, and were used without further purification.

Measurements: Parallel core flood setup was constructed to simulate the matrix stimulation treatments, **Fig. 8.1**. A back pressure of 1,000 psi on the outlet of the two cores was applied. Pressure transducers were connected to a computer to monitor and record the pressure drop across the cores during the experiments.

The density of 15 wt% regular and 5 wt% in-situ gelled acid was measured using DMA 35N portable density meter and were found to be 1.075 and 1.021 g/cm^3, respectively. X-ray Computed Tomography (CT) was used to scan the cores after acid injection. Viscosity measurements of live in-situ gelled acid were made using M3600 viscometer. To resistant corrosion by acids, both the rotor (R1) and the bob (B1) of the viscometer were made of Hastelloy C. The viscosity was measured as a function of shear rate (from 0.1 to 1020 s^{-1}).

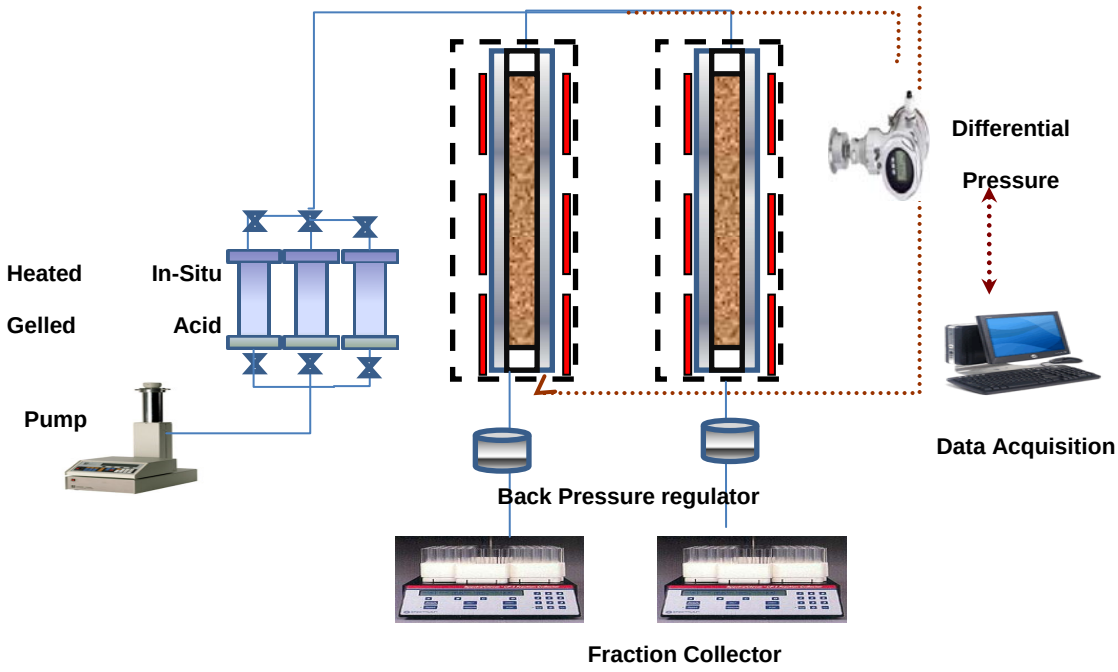

Fig. 8.1—Parallel core flood setup.

Acid Preparation: Two acid formulae were used in this work: 15 wt% regular acid and 5 wt% in-situ gelled, **Table 8.1.** $FeCl_3$ was used as a source of Fe^{+3} (crosslinker). Regular acid solutions were prepared by mixing the corrosion inhibitor and HCl acid with water. For the in-situ gelled acid, water, HCl, and corrosion inhibitor were

mixed then the polymer was added slowly to the acid. After that the crosslinker and a buffer were added to the solution, which was mixed for 30 min. The breaker was the last chemical added to the acid.

TABLE 8.1—FORMULAE OF REGULAR AND IN-SITU GELLED ACIDS

Component	Regular	In-situ
Hydrochloric acid	15 wt% HCl	5 wt% HCl
Acid gelling agent: a co-polymer of polyacrylamide emulsified in	-	20 ml/l
Corrosion inhibitor:	4 ml/l	4 ml/l
Cross-linker: Ferric chloride (37 - 45 wt%)	-	4.5 ml/l
Breaker: sodium erythorbate (60 to 100 wt%)	-	20 lb/Mgal
Buffer: Hydroxyacetic acid (30 - 60 wt%)	-	2 ml/l

Core Preparation: Cylindrical core plugs were cut from two blocks: Pink dessert limestone block and Austin chalk block. Pink dessert limestone that had a permeability of 55 to 136 md was used to represent the high permeability formation, while Austin chalk with a permeability of 3 to 10 md was used to represent the low permeability formation. Sixteen cores were cut with a length of 6-in. while four cores were cut with a length of 20-in. all cores had 1.5-in. diameter. Cores were placed inside an oven set at 257^{o}F for 5 hours and then their weight was measured. The cores were saturated with deionized water under vacuum for 24 hr. Core porosity was calculated from these measurements. After that, the core was placed inside the core holder, and water was injected at different flow rates (5, 10, and 20 cm^3/min) to calculate core initial permeability. Summary of cores permeability are given in **Table 8.2**.

Injection Sequence: Before starting injection of the acid, water was injected separately in each core with the selected rate. This ensured that the core was fully saturated with water. Also, the pressure drop required to flow the water in each core was measured. For the lower permeability core, this pressure drop was important because in-situ gelled acid should build that pressure in the high permeability core to allow regular acid to flow into the lower permeability core. After measuring the pressure drop for each core, water was pumped through the two cores.

TABLE 8.2—SUMMARY OF EXPERIMENTAL RESULTS

No.	Injection rate, cm^3/min	Core	Length, in	Permeability, md		In-situ gelled
				Initial	final	
1	5	1	6	62	acid breakthrough	Not achieved
		2	6	58	83	
2	5	3	6	102	acid breakthrough	achieved
		4	6	52	250	
3	1	5	6	88	40	Not achieved
		6	6	3.5	0	
4	1.5	7	6	109	25	Achieved
		8	6	5	acid breakthrough	
5	2.5	9	6	96	28	Achieved
		10	6	4.5	acid breakthrough	
6	5	11	6	84	41	Achieved
		12	6	4	acid breakthrough	
7	10	13	6	136	98	Achieved
		14	6	7	acid breakthrough	
8	15	15	6	97	acid breakthrough	Not achieved
		16	6	5	6	
9	5	17	20	106	acid breakthrough	Not achieved
		18	20	5	5	
10	2.5	19	20	105	acid breakthrough	Achieved
		20	20	5	10	

After reaching a stable pressure drop across the cores, a stage of in-situ gelled acid was injected until the pressure drop increased to a value that allowed the regular acid to flow into the low permeability core. This pressure drop was the monitored pressure drop during pumping water into the low permeability core. Finally, regular acid was injected until the acid breakthrough from one of the two cores. The permeability was measured for the core that did not have a breakthrough. The flow rate inside each core was determined by collecting certain effluent volume over a specific period of time.

8.3 Results and Discussion

8.3.1 Rheological studies

The apparent viscosity of live in-situ gelled acids was measured at an HCl concentration of 5 wt% and room temperature. **Fig. 8.2** shows that the viscosity of the in-situ gelled acid decreased from 1,080 to 26 mPa.s, as the shear rate was increased from 0.1 to 1,000 s^{-1}. As the acid injection rate increases, the shear rate inside the cores will increase leading to a decrease in the in-situ gelled acid viscosity.

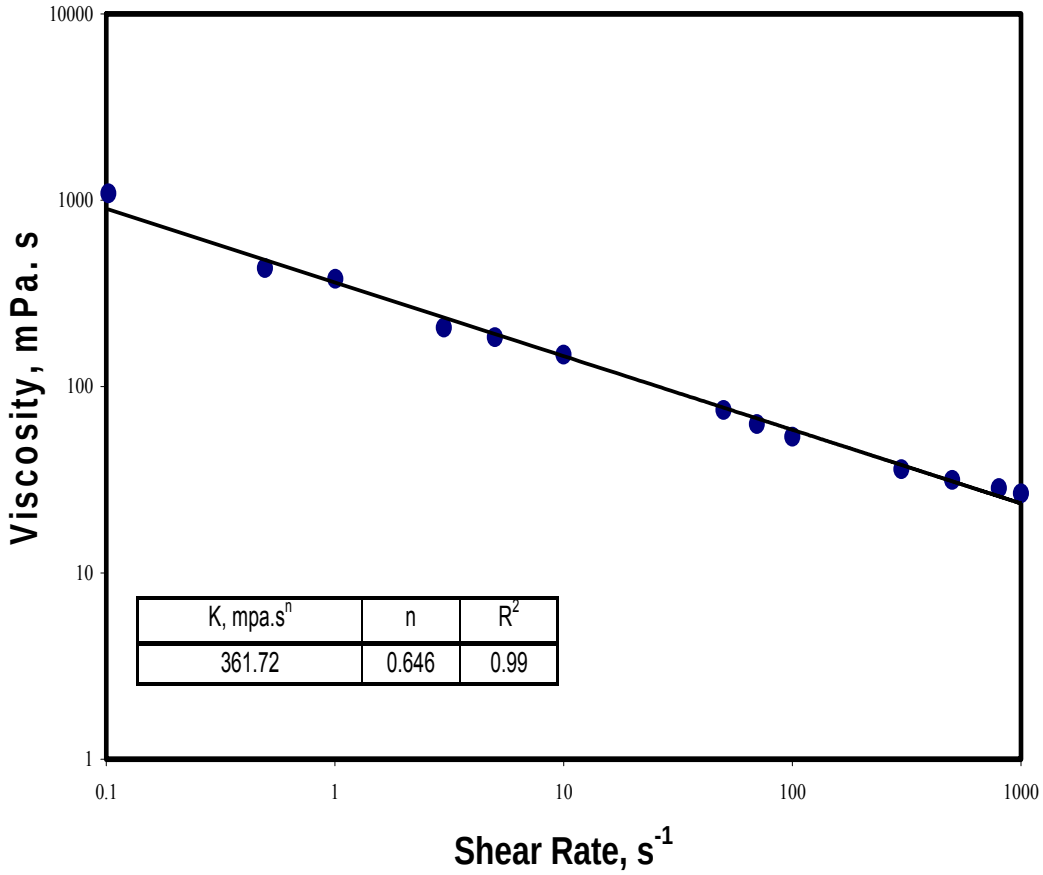

Fig. 8.2—Viscosity of live in-situ gelled acid at 5 wt% HCl, room temperature.

8.3.2 Single-stage regular acid treatment in permeability cores

Experiment 1 was conducted using cores 1 and 2. The two cores had nearly the same initial permeability. Therefore, water injection (before the acid injection) at rate of 5 cm^3/min was divided nearly evenly between the two cores. Regular acid, that had 15 wt% HCl, was injected at a rate of 5 cm^3/min. **Fig. 8.3** shows the pressure drop and injection rate of the two cores as a function of the cumulative injected volume into both cores. The pressure drop decreased linearly as the volume of regular acid increased. The decline in the pressure drop had two linear parts with different slopes. The first one had a pressure drop decline slope equal to 11.4 psi/PV where the regular acid was able to flow

in the both cores. The second part where the acid flow only into one core (the higher permeability core) where the slope became steeper with average value of 23 psi/PV. This change indicated that the acid flow rates in the two cores were different. As the rate increased in one core, the volume of acid increased in this core leading to faster acid breakthrough.

From the rate behavior during acidizing, it was clear that even when there was no significant permeability contrast between the cores, regular acid preferred to flow in one of the cores. Acid breakthrough was achieved in Core1 while the permeability of Core2 increased from 58 to 83 md instead of completely breakthrough. Therefore, to achieve a good stimulation treatment for the entire production zone, diverting agents should be used.

Fig. 8.4 shows the 3D visualization of the created wormhole for cores 1 and 2 after acid injection. Based on **Fig. 8.4**, the wormhole length of Core1 was 6-in. while the wormhole length of Core 2 was 2.16 in. Also, the average wormhole diameter of cores 1 and 2 were 3.3 and 1.6 mm, respectively. The 3D image of the wormhole of both cores confirmed that even if there was no significant permeability contrast, regular acid will flow through the high permeability core.

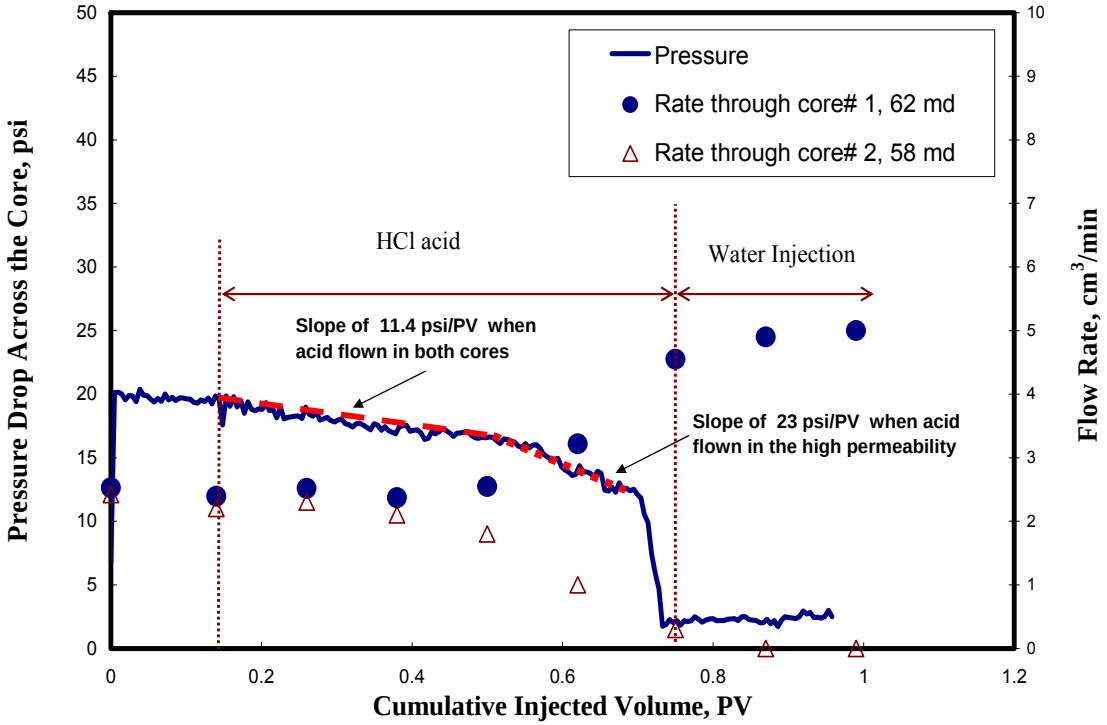

Fig. 8.3—Pressure drop and flow rate distribution across cores 1 and 2, 15 wt% HCl, total flow rate 5 cm^3/min, room temperature.

8.3.3 Multi–stage acidizing using low permeability contrast cores

In experiment 2, cores 3 and 4 that had initial permeability of 102 and 52 md, respectively, were used to evaluate the in-situ gelled acid diversion at rate of 5 cm^3/min. **Fig. 8.5** shows the pressure drop and injection rate for both cores as a function of the total injected pore volume. Before acid injection rate, water injection rate was distributed by 3.65 and 1.35 cm^3/min for cores 3 and 4, respectively. As the in-situ gelled acid entered to the cores, the pressure drop increased significantly to a value of 365 psi with a decrease in the rate inside Core3 to value of 2.7 cm^3/min and an increase in the rate in Core4 to a value of 2.4 cm^3/min. The increase in the flow rate for Core4 was good

evidence that in-situ gelled acid started to divert the acid to the lower permeability core. When regular acid was injected, the pressure drop increased for 0.2 PV, then decreased significantly to value of 240 psi. At this time, rates inside the cores were kept constant until acid breakthrough from Core3 (the higher permeability core). Permeability enhancement was achieved in both cores where acid breakthrough in Core3 and the permeability of Core4 was increased from 50 to 250 md. Only 0.52 PV of in-situ gelled acid was injected followed by 0.78 PV of 15 wt% HCl regular acid until acid breakthrough from the Core3.

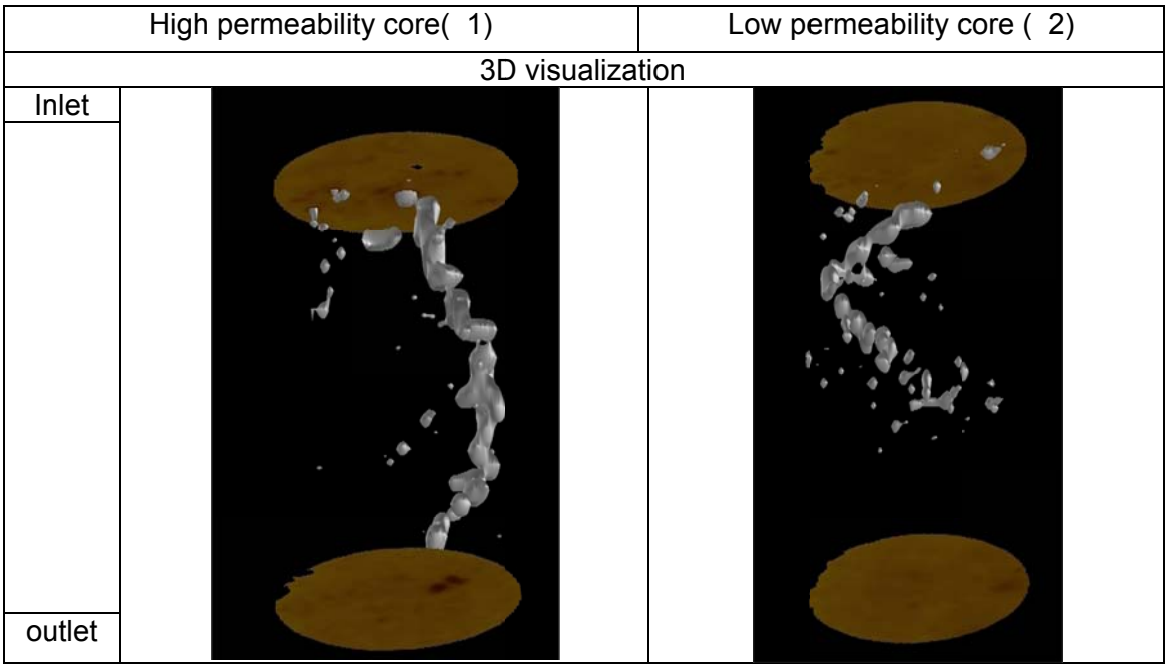

Fig. 8.4—CT scan for experiment 1.

The 3D visualization of the wormhole for cores 3 and 4 after acid injection is shown in **Fig. 8.6**. Wormhole length of Core3 was 6-in., while the wormhole length of Core 4 was 5.04-in. Also, the average wormhole diameter of cores 3 and 4 were 4.5 and

1.5 mm, respectively. 3D image confirmed that a wormhole was created in the both core nearly with the same length. Therefore, it can be concluded that in-situ gelled acid was able to divert the regular acid from the high permeability core (Core 3) to the low permeability core (Core 4).

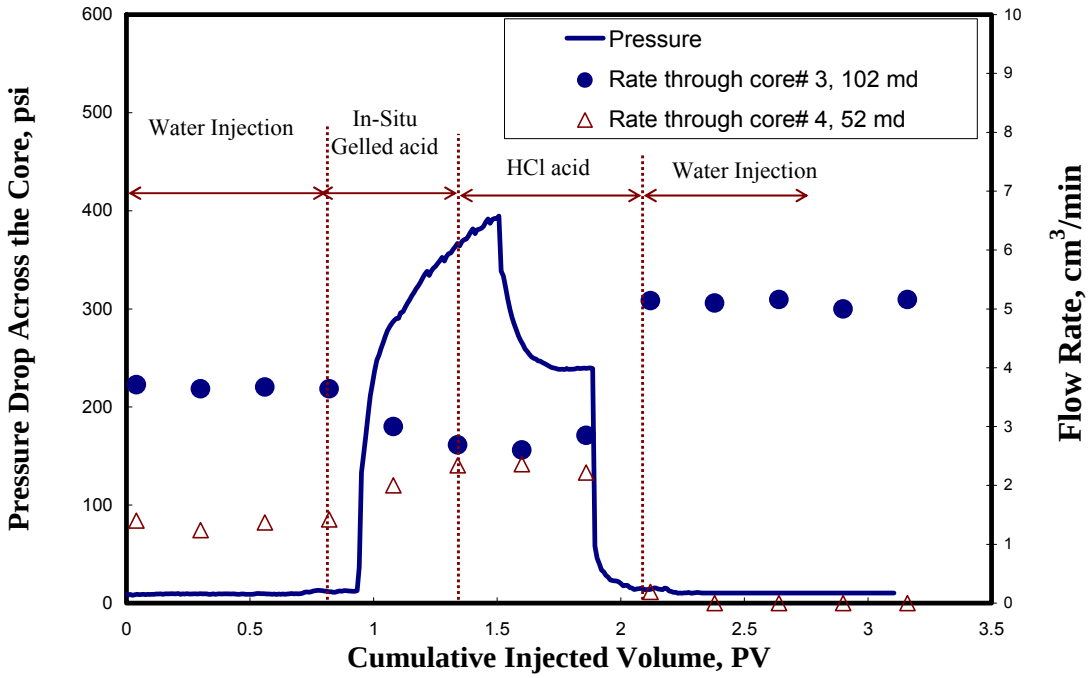

Fig. 8.5—Pressure drop and flow rate distribution across cores 3 and 4, multi-stage acid, total flow rate 5 cm^3/min, room temperature.

8.3.4 Multi–stage acidizing using high permeability contrast cores

In the following set of experiments (3-8), two parallel cores that had nearly 1 to 20 permeability contrast were used. The injection rate was the key parameter that was studied. The selected rates were 1, 1.5, 2.5, 5, 10, and 15 cm^3/min**. A s**ummary of all experimental results is given in **Table 8.2**. Experiments at rates 1, 2.5, and 15 cm^3/min

will be discussed in detail. This is because they highlight three major trends noted: no diversion at low rates, diversion at intermediate rates, and no diversion at high rates.

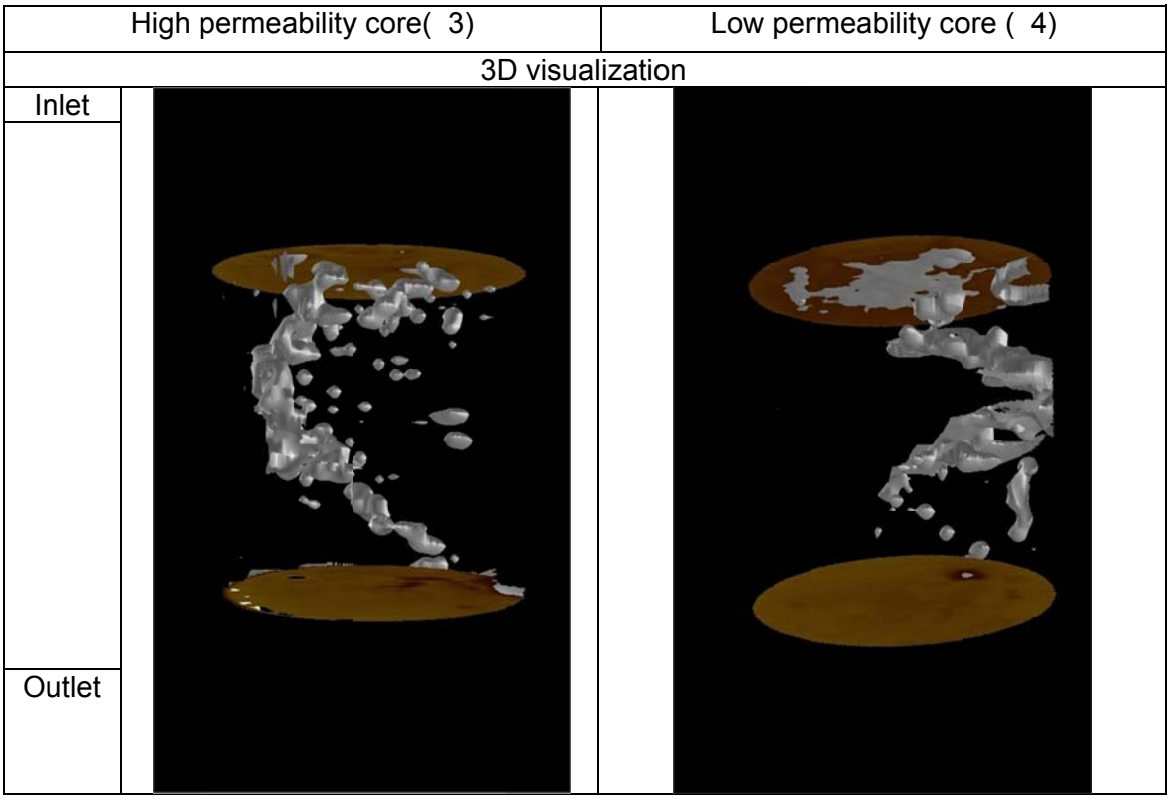

Fig. 8.6—CT scan for experiment 2.

Experiment 3 was conducted using an injection rate of 1 cm^3/min through cores 5 and 6. **Fig. 8.7** shows the pressure drop and injection rates for cores 5 and 6 as a function of the total injected pore volume. As the in-situ gelled acid entered the inlet of the core, the pressure drop increased instantaneously until reached to a value of 400 psi during the injection of 0.3 PV of in-situ gelled acid. The linear increase in the pressure drop during in-situ gelled acid injection was an evidence of face plugging. By starting

the injection of regular acid, the pressure drop continued its increase to 540, after that it decreased to 270 psi.

From the rate distribution in both cores, the flow rate inside Core 6 was zero during the experiment while the rate in Core 5 decreased to nearly zero during the period of injection of in-situ gelled acid stage. The rate inside Core 5 increased again to nearly 1 cm^3/min during the injection of regular acid. In-situ gelled acid was not able to divert the regular acid at injection rate of 1 cm^3/min. therefore; the test was terminated before the acid breakthrough Core 5. The final permeability of Core 5 was reduced from 88 to 40 md, and the permeability of Core 6 decreased from 3.5 to zero md.

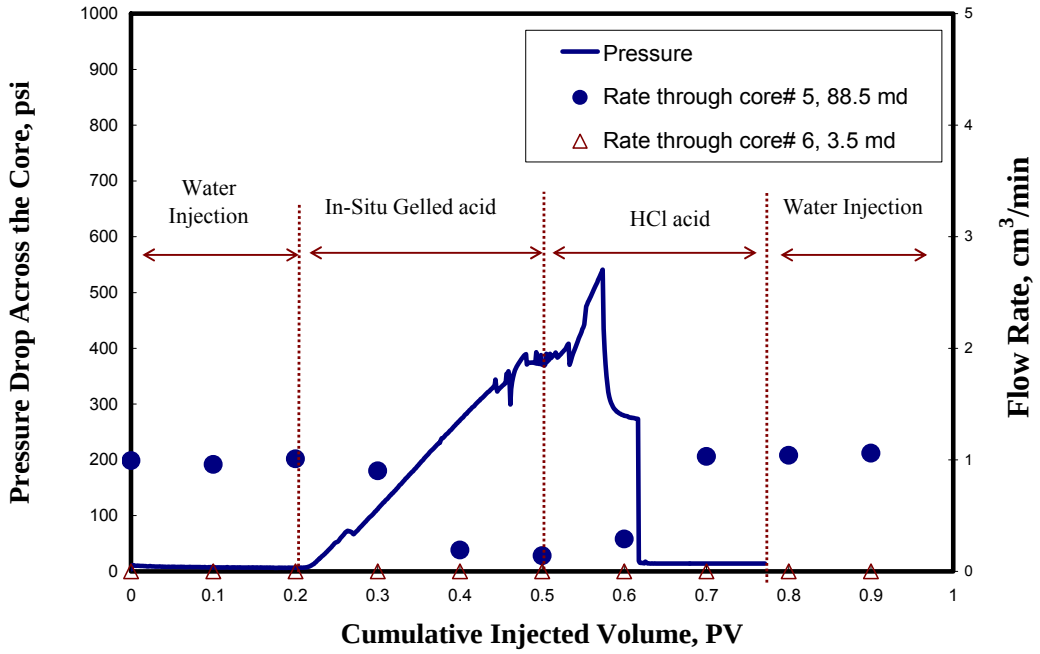

Fig. 8.7—Pressure drop and flow rate distribution across cores 5 and 6, multi-stage acid, total flow rate 1 cm^3/min, room temperature, (no diversion achieved).

When in-situ gelled acid entered the core, it started to react immediately and produced a gel material that plugged the inlet face of the core. Therefore, the pressure drop increased with the acid injection, **Fig. 8.7**. At this low injection rate (1 cm^3/min), the gel had enough time to form. This was because as the injection rate decreased the volume of live acid that entered the core decreased and as a result, the pH increased to 2 in a shorted period of time than at higher injection rates. This gel was strong enough to eliminate any reaction or penetration of the next fresh acid to produce wormholes, especially at the inlet of Core 6. Therefore, there was no flow inside cores 5 and 6 during the injection of the in-situ gelled acid. Also, the next stage of regular acid was not able to penetrate this gel until the pressure drop increased to 540 psi. At this pressure drop, regular acid penetrated Core 5 without significant flow into Core 6. **Fig. 8.8** shows a thin layer of gel material that formed in the both cores inlet face and it also shows how regular acid penetrated Core 5 only.

Core 5
Gel covered the inlet face of the high permeability core(88.5 md). However, regular acid penetrated the core face in many locations

Core 6
Gel covered the inlet face of the low permeability core (3.5 md)

Fig. 8.8—Inlet faces of cores 5 and 6, injection rate 1 cm^3/min.

It is important to highlight that the formed gel in the low permeability formation was stronger than the formed gel in the high permeability formation. There were two observations to support this statement. The first one shown from the rate distribution of cores 5 and 6 where the rate inside Core 6 was zero and the rate inside Core 5 was nearly 0.2 cm^3/min. This means there was a minor flow in Core 5. The second observation was the regular acid penetrated only Core 5 (the high permeability core) leaving core 6 with a zero permeability.

The 3D images of the slices, that taken along cores 5 and 6, show that wormhole was produced only in Core 5 where there was no evidence for wormhole creation in Core 6, **Fig. 8.9**. Based on the volume of regular acid that was injected, the wormhole length inside Core 5 was 1.68-in. with a diameter less than 1.5 mm. The 3D visualization of the created wormhole for the two cores shows that wormhole was propagated only

through Core 5, **Fig. 8.9.** CT results confirmed that at acid injection rate of 1 cm^3/min, in-situ gelled acid was not able to divert regular acid to the low permeability core.

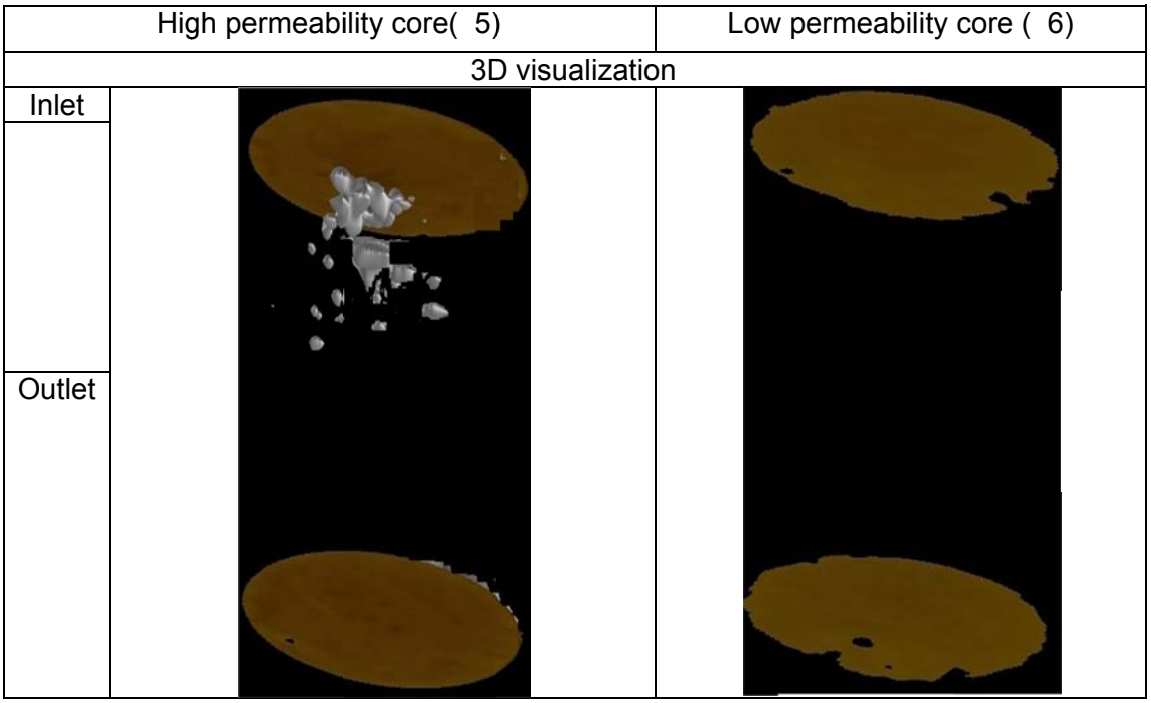

Fig. 8.9—CT scan for experiment 3.

In the next experiment (5), the injection rate was increased to 2.5 cm^3/min using cores 9 and 10. **Fig. 8.10** shows the pressure drop and injection rate performance for cores 9 and 10 as a function of the total injected pore volume. As the in-situ gelled acid entered the core, the pressure drop increased to value of 100 psi then it kept increasing with in-situ gelled acid injection until it reached to 200 psi before regular acid injection. As regular acid entered the core, the pressure drop decreased slowly until acid breakthrough from Core 10 (the low permeability core). A volume of 1.53 PV of in-situ gelled acid was needed to build the required pressure to divert the regular acid into the

small permeability core. Permeability enhancement was achieved only in Core 10 because of the acid breakthrough. However, damage was noted in Core 9 where permeability was reduced from 96 to 28 md. **Fig. 8.11** shows the inlet and outlet of cores 9 and 10. A then layer of gel material was found only on Core 9 where there was a minor gel on the inlet of Core 10.

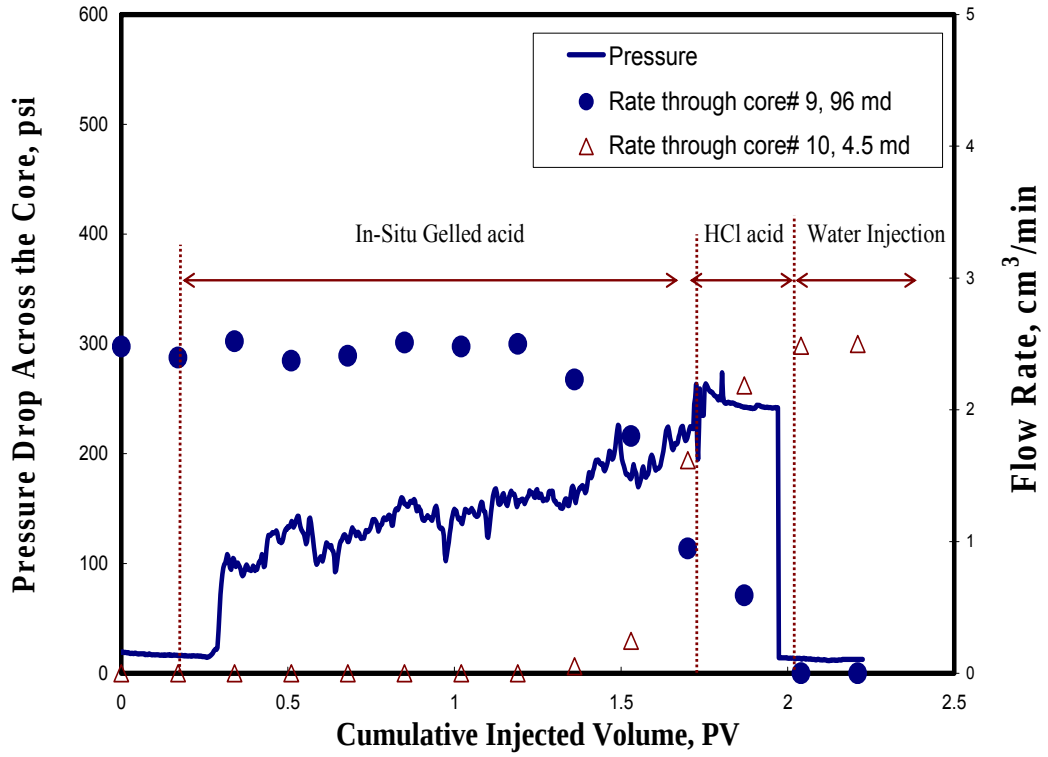

Fig. 8.10—Pressure drop and flow rate distribution across cores 9 and 10, multi-stage acid, total flow rate 2.5 cm^3/min, room temperature, (diversion achieved).

Inlet of Core 9
Gel covered the inlet face of the high permeability core(96 md). Regular acid penetrated the core face in many locations. However, there was no breakthrough

Outlet of Core 10
Gel covered the inlet face of the low permeability core(4.5 md). However, regular acid penetrated the core

Outlet of Core 9
No acid breakthrough in the high permeability core(96 md)

Outlet of Core 10
Acid breakthrough in the low permeability core (4.5 md)

Fig. 8.11—Inlet and outlet faces of cores 9 and 10, injection rate 2.5 cm^3/min.

Fig. 8.12 shows that the wormhole length was 3.12-in. for Core 9, while the wormhole length of Core 10 was 6-in. (the whole core length). Also, the average wormhole diameter of cores 9 and 10 were 4.5 and 1.5 mm, respectively. Results from

the CT scan confirmed that in-situ gelled acid was able to divert the regular acid from the high permeability core (Core 9) to the low permeability core (Core 10).

High permeability core(9)	Low permeability core (10)
3D visualization	
Inlet Outlet	 

Fig. 8.12: CT scan for experiment 5.

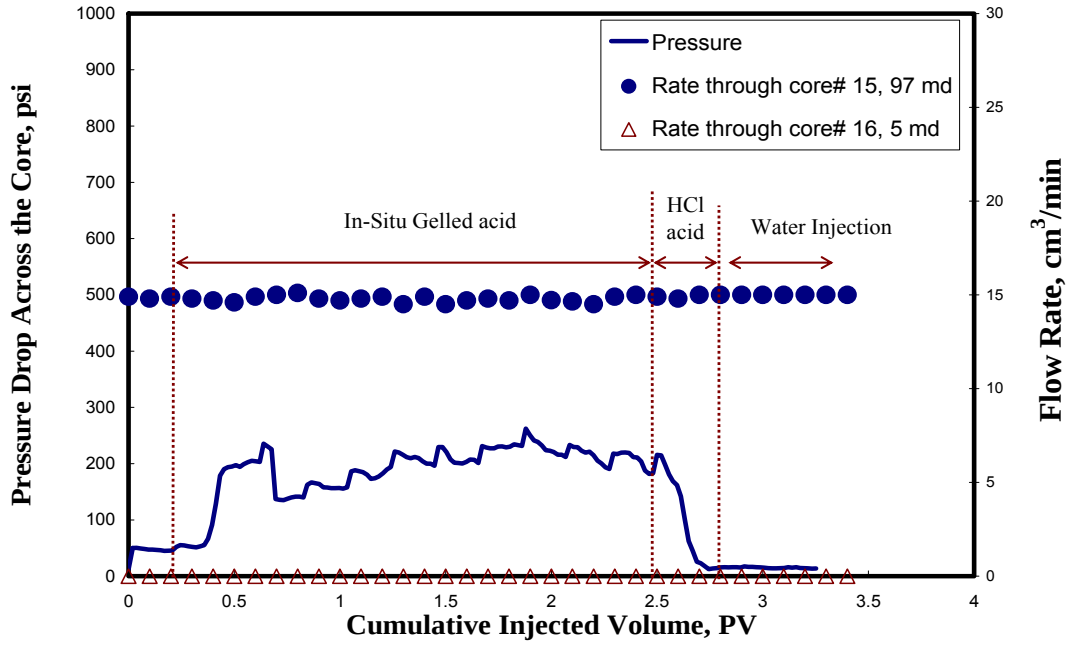

Fig. 8.13—Pressure drop and flow rate distribution across cores 15 and 16, multi-stage acid, total flow rate 15 cm^3/min, room temperature, (no diversion achieved).

By increasing the acid injection rate to 15 cm^3/min using cores 15 and 16 (Experiment 8), in-situ gelled acid still was not able to divert the regular acid into the lower permeability core, **Fig. 8.13.** A volume of 2.2 of in-situ gelled acid was injected to divert the regular acid. However, the pressure drop did not increase to the needed value that will be able to divert the regular acid. Acid breakthrough was achieved in Core 15 (the high permeability core).

The 3D images of the slices taken along cores 15 and 16 after acid injection shows that there was no evidence for wormhole creation in Core 16 while wormhole length in Core 15 was 6-in. (the whole core length). Regular acid propagates only through the high permeability core creating wormhole with 4.8 mm diameter. The 3D

visualization of the created wormhole for the two cores confirmed that at 15 cm^3/min, in-situ gelled acid was not able to divert the regular acid from the high permeability core (Core 15) to the low permeability core (Core 16), **Fig. 8.14**.

8.3.5 Summary of core flood experiments

Table 8.3 show the effect of acid injection rate on the permeability reduction (Eq. 8.1) in the high permeability core and the required in-situ gelled acid volume needed to achieve diversion.

$$\text{Permeability reduction},\% = \left(1 - \frac{K_f}{K_i}\right) x100 \quad \text{.....(8.1)}$$

where, K_i is the initial permeability in md and K_f is the final permeability in md. As the injection rate was increased, three regions were identified as follows, **Fig. 8.15**:

1. Region 1 at injection rate less than 1 cm^3/min where no diversion was achieved. In-situ gelled acid produced gel very fast on the cores inlet that plugged the both core inlet. Regular acid was able to penetrate the high permeability core only where the low permeability cores became totally plugged (zero permeability).
2. Region 2 at injection rates between 1 to 10 cm^3/min, where diversion was achieved. In-situ gelled acid was able to produce enough pressure to divert regular acid into the low permeability core. In this region, as the injection rate increased, the permeability reduction decreased but the volume of the polymer needed to achieve diversion increased.

3. Region 3 at injection rates higher than 10 cm^3/min, no diversion was achieved. In-situ gelled acid was not able to build enough pressure that could force the regular acid into the low permeability core.

Acid injection rate had a significant effect on the performance of in-situ gelled acid inside the core. The viscosity of the in-situ gelled acid decreased, as the injection rate increased. Therefore, the viscosity behavior at each rate was different. At low injection rate as in Region 1 (**Fig. 8.15**), the viscosity was higher and the volume of injected acid per unit time was less (because of injection rate) leading to reaching pH 2 in a short period of time. Therefore, there was plugging at the inlet face of the core by the gel.

Increasing the injection rate decreased the viscosity of the in-situ gelled acid, and delayed the crosslinking reaction. Therefore, at high injection rates as in Region 3 (**Fig. 8.15**), viscosity was less, the volume of injected acid per unit time was high, and reaching pH 2 was slower. Therefore, in-situ gelled acid was not able to create enough pressure for diversion.

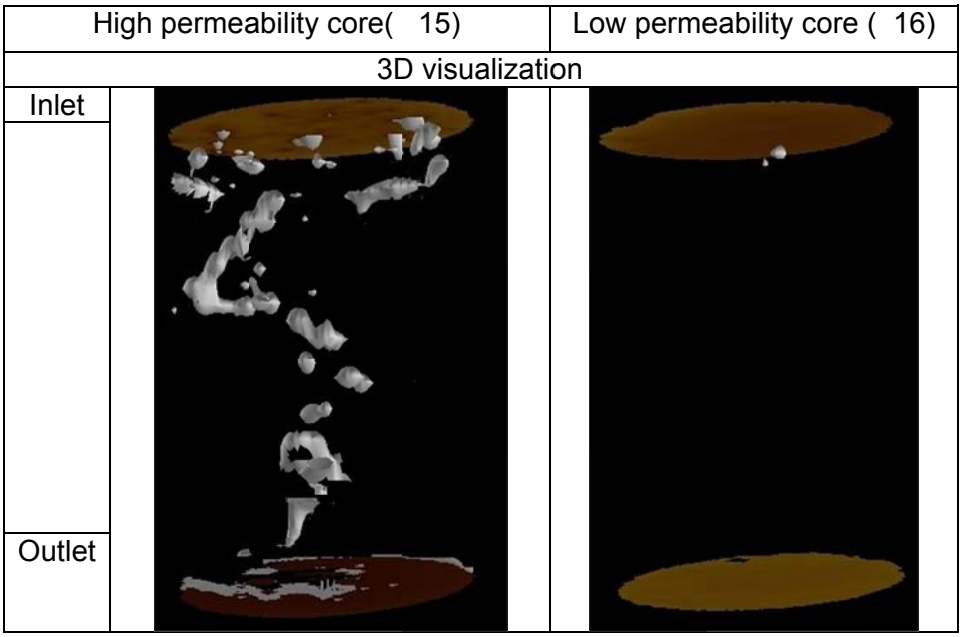

Fig. 8.14—CT scan for experiment 8.

TABLE 8.3—EFFECT OF ACID INJECTION RATE ON THE PERMEABILITY REDUCTION IN THE HIGH PERMEABILITY CORE AND ON THE REQUIRED IN-SITU GELLED ACID VOLUME NEED TO ACHIEVE DIVERSION, CORE LENGTH 6-IN., ROOM TEMP

Injection rate, cm^3/min	Permeability reduction percent in high permeability core, %	Injected in-situ gelled acid volume, PV
1	No diversion was achieved	
1.5	77	0.54
2.5	71	1.53
5	51	1.7
10	28	1.8
15	No diversion was achieved	

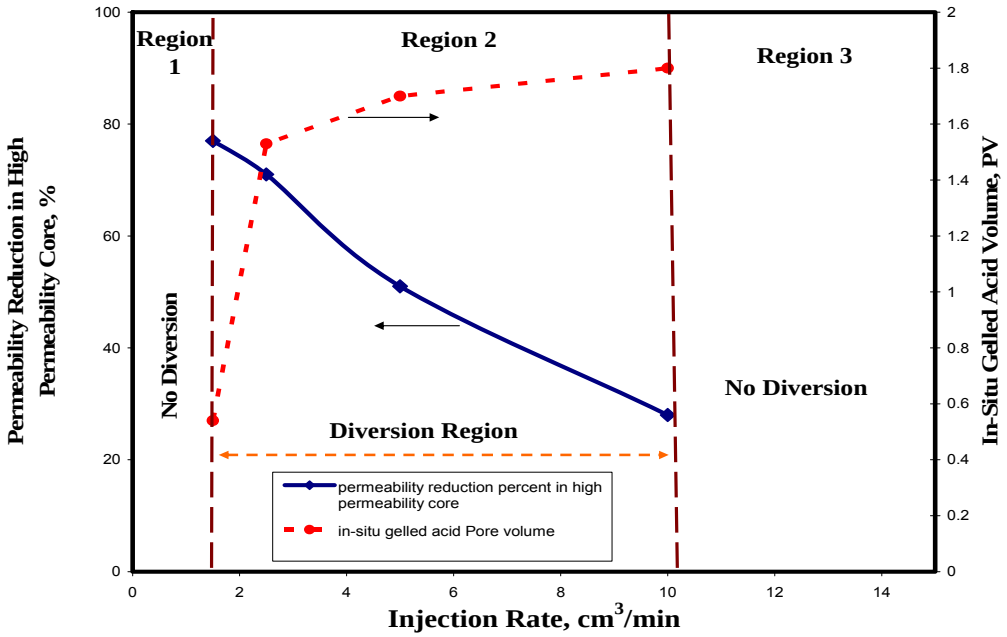

Fig. 8.15—Regions of diversion developed by changing the injection rate, core length 6-in., room temp.

At Region 2 (**Fig. 8.15**), the region that gave good diversion results, a variation of the acid volume and the reduction in the high permeability core were noted. Permeability reduction decreased as the injection rate increased while a larger volume of in-situ gelled acid was needed to achieve diversion. This performance depended on the in-situ gelled acid viscosity as it discussed earlier. Acid injection rate should be determined based on the expected fluid viscosity in the formation. An optimization in acid injection rate should be achieved based on the economic (defined the volume of in-situ gelled acid) and the reduction in the high permeability zones.

Table 8.4 gives a summary of CT results for the scanned cores. Wormhole length and average diameter are the two parameters that were used to characterize the

wormholes. As the injection rate of in-situ gelled acid was increased, the length of the wormhole increased.

8.3.6 Effect of core length

In the next two experiments (9 and 10) a 20-in. cores were used to investigate the effect of increasing the core length. Based on Darcy law, increasing the length and keep all the other parameters constant will affect the pressure drop across the core. The first experiment was done at rate of 5 cm^3/min using cores 17 and 18 (experiment 9). **Fig. 8.16** shows the pressure drop and flow rate distribution of this experiment. Based on the rate distribution in both cores, In-situ gelled acid was not able to divert the acid to the low permeability core. However in experiment 20, the injection rate was decreased to 2.5 cm^3/min. **Fig. 8.17** shows the pressure drop and flow rate distribution across cores 19 and 20. Based on the rate distribution, part of the regular acid entered the low permeability core. In these two experiments, the acid breakthrough was achieved in the high permeability core. However, there was no permeability enhancement at rate 5 cm^3/min while there was permeability enhancement at rate 2.5 cm^3/min.

TABLE 8.4—SUMMARY OF CT RESULTS					
No.	Injection rate, cm^3/min	Core	PV	Wormhole length, in.	Diameter, mm
1	5	1	41.88	6	3.3
		2	40.89	2.16	1.6
2	5	3	48.70	6	4.5
		4	40.77	5.04	1.5
3	1	5	46.04	1.68	1.5
		6	37.20	0	0
5	2.5	9	44.74	3.12	4.5
		10	36.50	6	1.5
8	15	15	38.28	6	4.8
		16	34.10	0	0
9	5	17	156.96	20	3.4
		18	110.10	0	0
10	2.5	19	155.89	20	3.3
		20	124.20	7.3	3.5

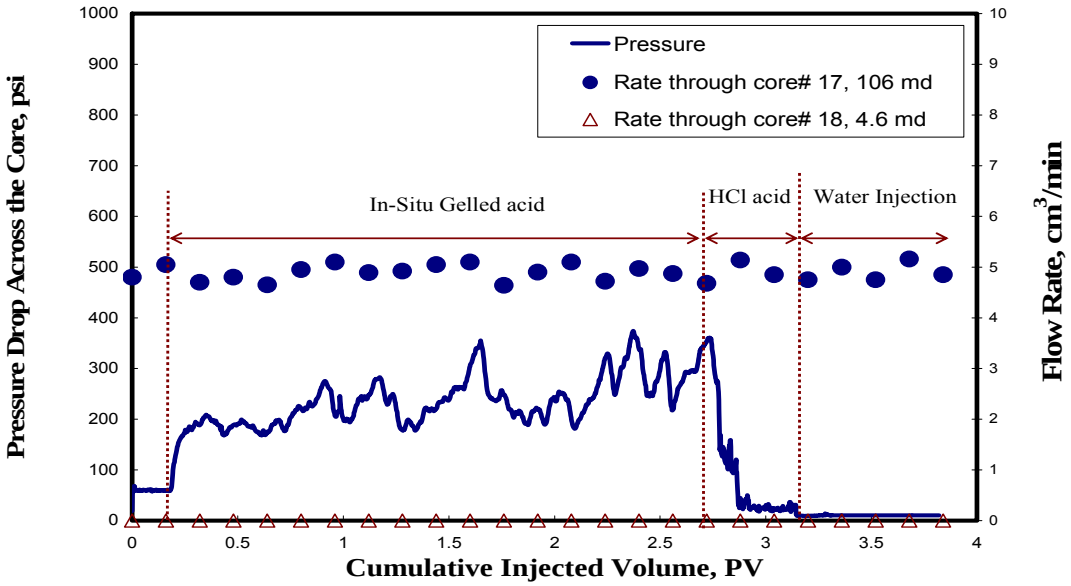

Fig. 8.16—Pressure drop and flow rate distribution across cores 17 and 18, multi-stage acid, core length 20-in, total flow rate 5 cm^3/min, room temperature, (no diversion achieved).

An 85 slices of a CT scan were selected to investigate the in-situ gelled acid inside 20-in. long cores (19 and 20), **Fig. 8.18.** The 3D images show that the wormhole length of Core 19 is 20-in. while the wormhole length of Core 20 is 7.3-in. (wormhole covered 31 of 85 slices). Also, the average wormhole diameter of cores 19 and 20 were 0.15 and 0.45 mm, respectively. The results from the CT scan confirmed that in-situ gelled acid was able to divert the regular acid from the high permeability core (Core 19) to the low permeability core (Core 20).

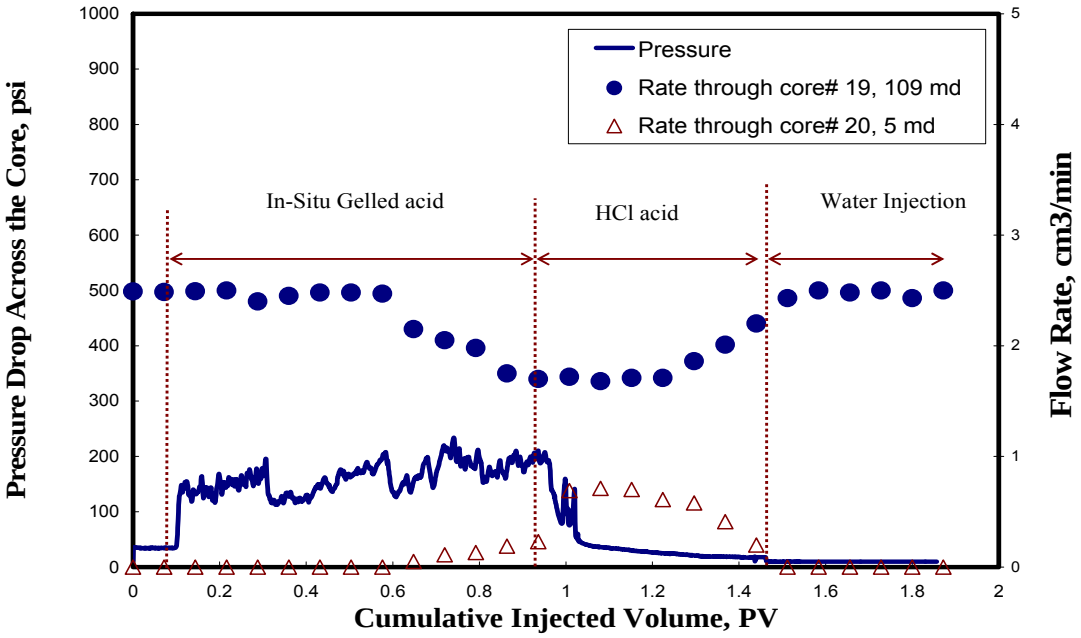

Fig. 8.17—Pressure drop and flow rate distribution across cores 19 and 20, multi-stage acid, core length 20 in., total flow rate 2.5 cm^3/min, room temperature, (partial diversion achieved).

High permeability core(19)	Low permeability core (20)
3D visualization	
Inlet 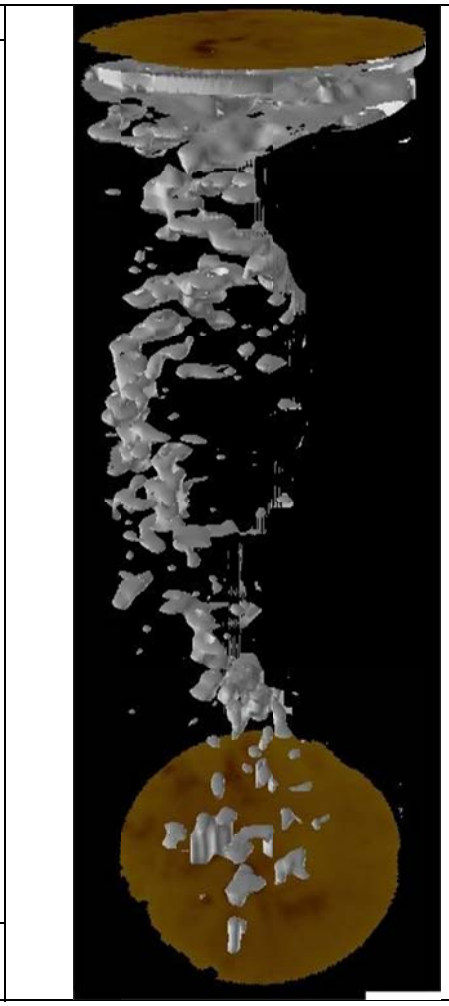 Outlet	

Fig. 8.18—CT scan for experiment 10.

9. DETERMINATION OF REACTION RATE OF IN-SITU GELLED ACIDS USING ROTATION DISK APPARATUS

In-situ gelled acids have been used extensively in matrix acidizing and acid fracturing for acid diversion, reducing the leak-off rate, and retarding the acid reaction to enhance deep acid penetration. Literature review shows few previous studies that have investigated the rate of dissolution of calcite in polymer- based acid, yet none has addressed in details the cross-linked polymer systems. Therefore, the aim of this work was to study the mass transport and the reaction rate kinetics of the reaction of 5 wt% HCl in-situ gelled acid with carbonate rocks and to investigate the effect of Fe-crosslinker on the rate of calcite dissolution.

The rate of reaction of 5 wt% HCl in-situ gelled acid was measured using the rotating disk apparatus. Rock samples of 1.5 in. diameter and 1 in. length were used. The effect of temperature (100-250^{o}F), and disk rotational speed (100-1800rpm) was investigated using Pink Dessert limestone rock samples. Calcium concentration was measured in the collected samples and was used to determine the acid reaction rate.

Experimental results showed that the rate of calcite dissolution at 150^{o}F is controlled mainly by the rate of mass transfer of the acid to the surface up to a rotational speed of 1000 rpm and by the rate of the surface reaction above this value. Based on the results obtained, the diffusion coefficient of 5 wt% HCl in in-situ gelled acid at 150^{o}F, the reaction activation energy, and the reaction rate constant at 150, 200, and 250^{o}F were determined and reported for such system for the first time. A power law kinetic model

was used to determine the kinetics parameters. The presence of Fe^{3+} crosslinker had a reduction effect on the rate of dissolution in comparison to reactions with gelled acid (no crosslinker) at the same condition. The reaction rate was reduced by a factor of 1.75 and by a factor of 1.4 when the reaction occurred at 100 and 1500 rpm, respectively. A gel layer, formed on the surface, is believed to act as a barrier between the acid and the rock and reduces the acid diffusivity.

9.1 Introduction

In carbonate formations, acidizing treatment provides not only a mean to remove the damage from the wellbore area, but also an opportunity to improve the near-wellbore permeability. The latter effect results from the acid ability to dissolve the rock matrix that leads to increase the pore space and the creation of wormholes. Successful design of these treatments requires understanding the acid-rock interaction. This interaction is best determined by quantifying the rate of reaction between the acid and the rock. The reaction rate is then used to determine the distance that acid can penetrate from the wellbore at a given pump rate before it is completely spent.

The reaction rate is a combined effect of three processes: the diffusion of acid from the bulk of the solution to the rock surface, the acid/rock reaction at the rock surface, and the diffusion of reaction products from the rock surface to the bulk of the solution. The slowest of these processes is called the rate-limiting step and determines the overall acid dissolution rate (Schechter 1992).

Woo et al. (1999), Chang et al. (2001), and Kalfayan and Martin (2009) stated the need for proper fluid diversion to enhance the outcome of matrix acid treatments. One way to enhance diversion is to increase the treating fluid viscosity by mixing the acid with a polymer. In-situ gelled acid is an example of such based system, which is prepared by gelling the HCl acid with a polyacrylamide polymer in the presence of crosslinker. As the reaction progresses, the acid is consumed and the pH of the reaction medium rises. At nearly pH 2, the polymer undergoes deprotonation and the positively charged crosslinker reacts with the polymer and forms highly interconnected network of a very viscous gel. This gel temporarily blocks the wormholes being created and forces the acid into the untreated zones. At pH values around 4 and in the presence of a breaker, Fe^{+3} is reduced to Fe^{+2} and the gel breaks. As a result, the fluid becomes less viscous and easier to flow back to the surface (Yeager and Shuchart 1997; MaGee et al. 1997; Taylor and Nasr-El-Din 2002; Hill 2005).

However, the viscosity of the in-situ gelled acid should be carefully designed and monitored during the acidizing treatment. The high viscosity of the in-situ gelled acid reduces the diffusion of the hydrogen ion (H^+) to the rock surface and as a result, reduces the rate of reaction which if not proceeds to a pH value around 4, the presence of the breaker is useless and the gel will never break down (Lynn and Nasr-El-Din 2001).

Conway et al. (1999) measured the HCl diffusion of regular, gelled, and emulsified acid at different temperatures and for different Ca^{2+} and Mg^{2+} concentrations. Based on the results, a correlation was introduced to predict the acid diffusivity. In the correlation, the acid diffusivity is proportional to the temperature and H^+ concentration

and inversely proportional to the Ca^{2+} and Mg^{2+} concentrations and predicts lower acid diffusivity in case of gelled and emulsified acids. Lakatos and Lakatos- Szab´o (2004) investigated the H^{+} diffusion in a double network of cross-linked, high molecular weight, partially hydrolyzed polyacrylamide and polysilicate gel. They found that the effective diffusion coefficient of H^{+} ions decreased with the silicate content, and increased with increasing HCl content. A correlation based on the modified Fick's I law was introduced to determine the transport properties knowing the gel properties such as the formation factor, effective porosity, and tortuosity of gels. The authors showed that the diffusion transport of H+ ions in polymer/silicate gels could be described accurately by this formula that provides an appropriate method for prediction of the effective diffusion coefficient in gels if the properties of gels and the absolute diffusion coefficient in bulk aqueous phase are known and vice- versa.

Taylor and Nasr-El-Din (2003) examined three different in-situ gelled acids: two were based on Fe-crosslinker, while the third one was based on Zr-crosslinker. The authors measured the relative reaction rate in a continuous stirred-tank reactor (CSTR) at atmospheric pressure and they found that increasing the polymer concentration reduces the acid reaction rate at $100^{o}F$ and the presence of Zr-crosslinker does not affect the reaction of in-situ gelled acid with carbonate rock. The reduction in the rate of reaction, in case of Fe-crosslinker, was possibly attributed to polymer adsorption on the rock surface (Taylor et al. 2004). Continuous stirred-tank reactor can be used qualitatively for comparison purposes, however the rate of dissolution cannot be correctly measured until the reactor is pressurized enough to keep CO_2 in solution.

Nasr-El-Din et al. (2008) used the rotating disk to measure the dissolution rate of calcite with gelled acids (no crosslinker). Measurements were conducted over a temperature range of 25 to 65°C at a pressure of 1,000 psi, and rotational speeds of 100 to 1,000 rpm. There was a significant increase in the apparent viscosity of gelled acids and a major decrease in the dissolution rate when the polymer concentration increased from 0.5 to 1.5 wt%. The reaction of gelled acids with calcite was controlled by a surface reaction at 25°C, and by mass transfer at 65°C. Increasing the temperature increased the dissolution rate of calcite and reduced the viscosity of the gelled acid.

The objectives of this work are to: (1) study in detail the mass transport and the reaction rate kinetics of the reaction of 5 wt% HCl in-situ gelled acid with limestone, (2) investigate the effect of temperature, disk rotational speed, and the presence of Fe^{3+} crosslinker on the rate of calcite dissolution.

9.2 Rotating Disk Theory

In heterogeneous reactions such as solid-liquid reactions, transport process of the reactant fluid to the solid surface and transport of products away from the surface affect greatly the rate of reaction. The overall reaction is a resultant of three steps: (1) transfer of the reactant from the bulk of solution to the solid surface, (2) the reaction at the surface, and (3) transfer of the products from the surface back to the bulk of the solution. The speed of the overall reaction is controlled by the rate of the slowest step. The latter is often called the rate-limiting step or the controlling step. In order to study the effect of one step on the overall reaction, it is important to eliminate the effect of the other steps.

Therefore, kinetics of the surface reaction can be determined when the mass transport process is faster than reaction at the surface. This case is then known as surface reaction limited. On the other hand if the diffusion to the surface is slower than the rate of surface reaction, the main resistance lies in the mass transfer boundary layer and the reaction is called mass transfer limited. Levich (1962) introduced the mathematical description of the situation in which a molecule diffuses from the bulk solution of a fluid to the surface of a solid, Eq. 9.1:

$$\frac{\partial C}{\partial t} + u\nabla C = D \quad \nabla^2 C \qquad \text{.....(9.1)}$$

where C is the solute concentration, u is the velocity, and D is the solute diffusivity. The problem was solved analytically for different geometries such as parallel plates, tubular reactor, and disk rotating in semi-infinite volume (Barron et al. 1962; Nierode and Williams, 1971; Roberts and Guin 1974; Levich 1962; Newman 1966; Ellision 1969). Under laminar flow condition ($Re < 3*10^5$), Navier-Stokes equations for the three-dimensional flow system were solved. The mass transfer flux of a solute to the solid surface can then be determined as follows, Eq. 9.2:

$$J = k_m \left(C_b - C_s\right) \qquad \text{.....(9.2)}$$

where J is the mass flux, k_m is the reactant mass transfer coefficient, and C_b, and C_s are the concentration in the bulk solution and at the solid-liquid interface, respectively. For non-Newtonian fluids, Hansford and Litt (1968) solved the convective diffusion equation and introduced modified Reynolds and Schmidt numbers to take into account the shear dependence of the viscosity power-law, Eq. 9.2. The modified Reynolds and Schmidt numbers become:

$$\mathrm{Re} = \frac{r_s^{\,2}\,\omega^{\,2-n}}{N} \qquad \text{.....(9.3)}$$

$$\mathrm{Sc} = \frac{N\,\omega^{\,n-1}}{D} \qquad \text{.....(9.4)}$$

where N is equal to (K/ρ), ρ is the fluid density, r is the radius of the disk, and D is the diffusivity. The final solution was introduced in the form of three dimensional groups Re, Sc, and Sherwood number, Sh as depicted in Eq. 9.5. The average mass flux to the solid surface can then be determined using Eq. 9.6:

$$\mathrm{Sh} = \varphi'(n)\,\mathrm{Sc}^{1/3}\,\mathrm{Re}^{1/3[(n+2)/(n+1)]} \qquad \text{.....(9.5)}$$

$$J = \frac{\mathrm{Sh}\,D}{r}(C_b - C_s) \qquad \text{.....(9.6)}$$

Values of Φ (n) as a function of n is given in **Table 9.1**. By substituting Eq. 9.5 in Eq. 9.6 and replacing Re and Sc numbers by their definitions from Eqs. 9.3 and 9.4, the average mass flux of a solute diffuses from the bulk of solution to the solid surface as a function of the disk rotating disk speed ω, bulk concentration C_b, diffusivity D, and the power-law parameters n and K can be obtained as follows:.

$$J = \left[\varphi'(n) \left(\frac{K}{\rho}\right)^{\frac{-1}{3(1+n)}} (r_s)^{\frac{(1-n)}{3(1+n)}} (\omega\omega^{\frac{1}{1+n}} D^{2/3} \right] (C_b - C_s) = k_m (C_b - C_s) \quad \text{.....(9.7)}$$

TABLE 9.1—VALUES OF Φ'(N) AS A FUNCTION OF N, (HANSFORD AND LITT, 1968)							
n	0.2	0.4	0.5	0.6	0.8	1	1.3
Φ'(n)	0.695	0.662	0.655	0.647	0.633	0.620	0.618

The term k_m is the mass transfer coefficient for non-Newtonian fluids rotating at the surface of semi-infinite disk. However, if the reactor vessel is at least twice the disk radius, the observed rate is independent of the vessel diameter. It is important to note that according to Eq. 9.7, mass flux for non-Newtonian fluids is proportional to the disk rotational speed raised to the power l/(l + n). In case of Newtonian fluid, n is equal to 1 and the rotational speed is raised to the power 0.5.

At low rotational speeds, the mass transfer of the reactant to the surface is remarkably slower than the surface reaction. The rate of reaction then can be determined directly from the mass flux equation, Eq. 9.7. In that case the reaction rate is

proportional to the rotating speed raised to the power 1/ (1+n). It is then acceptable to assume that the surface concentration will be much less than the bulk concentration and for rapid surface reactions it would be practically zero. Therefore, the rate of reaction R can be determined from Eq. 9.8:

$$R = \left[\varphi'(n) \left(\frac{K}{\rho}\right)^{\frac{-1}{3(1+n)}} (r_s)^{\frac{(1-n)}{3(1+n)}} (\omega\omega^{\frac{1}{1+n}} D^{2/3} \right] C_b = A(w)^{\frac{1}{1+n}} \quad \text{.....(9.8)}$$

For a certain initial bulk concentration, plotting the initial rate of reaction versus the disk rotational speed to the power 1/(1+n) should yield a straight line with a slope “A” that is proportional to the diffusivity raised to the power 2/3. Hansford and Litt (1968) stated that the results they obtained suggest that the mass transfer is reflecting the presence of three different flow regimes: reverse, toroidal, and centrifugal flow in which Eq. 9.7 is only valid for the centrifugal regime.

At high rotational speeds, the mass transfer boundary layer decreases and as a result, the mass transfer resistance decreases. The rate of reaction becomes controlled by the rate of reaction at the surface of the solid. In such case the rate of reaction is no longer proportional to the disk rotational speed and it should be obtained from the rate expression that describes the rate of reaction as a function of the reactant and product concentrations at the surface and the temperature of reaction. For solid-liquid reactions at the interface of the solid surface, progression of reaction does not change the amount of solid per unite volume of the solid. Therefore, the solid concentration becomes

constant and is usually lumped into the reaction rate constant as in the case of the carbonate reaction with in-situ gelled acid. In case that the surface reaction is the rate limiting step, the mass transfer resistance is considered very small especially at high rotational speeds. Therefore, the acid concentration on the rock surface is assumed to be equal to the acid concentration in the bulk concentration. The rate expression can then be written as a function of the acid bulk concentration assuming simple power law expression that was reported for HCl with calcite (Nieride and Williams, 1971; Lund et al., 1973; 1975; Taylor et al., 2004; 2006). The general expression can be formulated as follows, Eq. 9.9:

$$R = k_r [H_b^+]^m \quad \text{.....(9.9)}$$

where k_r is the reaction rate constant, $[H_b^+]$ is the acid concentration in the bulk solution, and m is the reaction rate order. The dependence of the reaction rate constant on temperature is described by Arrhenius equation, Eq. 9.10:

$$k_r = k_o \, e^{\frac{-E_a}{RT}} \quad \text{.....(9.10)}$$

where k_o is the pre-exponential factor, and E_a is the reaction activation energy. Plotting of Log k_r (the reaction rate constant) versus the reciprocal of the absolute temperature yields a straight line that has a slope of $(-E_a/R)$.

9.3 Experimental Studies

Materials: The HCl solutions were prepared from concentrated hydrochloric acid (ACS reagent grade) and deionized water with resistivity of 18.2 MΩ.cm at room temperature. The concentration of the acid stock was measured by titration using a 1N sodium hydroxide solution and was found to be 36.8 wt% (± 0.01). Polymer and other additives were all oilfield chemicals, and were used without further purification.

Acid Preparation: Three acid systems were used in this study: 5 wt% regular HCl acid, 5 wt% gelled acid, and 5 wt% in-situ gelled, **Table 9.2**. The main acid formula used in all reaction rate experiments was the 5 wt% HCl in-situ gelled**.** In two sets of experiments, the rate of reaction was measured at 100 and 1500 rpm rotational speed for 5 wt% gelled and in-situ gelled acids at 150 ^{o}F. In another static experiment, three disk samples were soaked in 5 wt% regular acid, 5 wt% gelled acid, and 5 wt% in-situ gelled for 2 hr. The purpose from these experiments was to study the effect of the presence of the polymer and crosslinker on the reaction rate.

TABLE 9.2—FORMULAS OF REGULAR, GELLED, AND IN-SITU GELLED ACIDS USED IN THIS STUDY

Component	Regular Acid	Gelled Acid	In-situ
Hydrochloric Acid	5 wt% HCl	5 wt% HCl	5 wt% HCl
Acid Gelling Agent	-	20 ml/l	20 ml/l
Corrosion Inhibitor:	4 ml/l	4 ml/l	4 ml/l
Cross-linker: Ferric Chloride (37-45 wt%)	-	-	4.5 ml/l
Breaker: Sodium Erythorbate (60 to 100 wt%)	-	-	20 lb/Mgal
Buffer: Hydroxyacetic acid (30-60 wt%)	-	-	2 ml/l

Regular acid solutions were prepared by mixing the corrosion inhibitor and HCl acid with water. Gelled and in-situ gelled acids were prepared using the same polymer type and concentration, but the former was prepared without adding the crosslinker agent or the breaker. Ferric chloride ($FeCl_3$) was used as a source of Fe^{3+}-crosslinker for the in-situ gelled acid. Sodium erythorbate was used as the breaking agent that reduced the ferric to ferrous ions at pH higher than 4. Viscosity Measurements: Viscosity measurements of live and spent in-situ gelled acids were made using a HP/HT rotational viscometer. The rotor and the bob of the viscometer were made of Hastelloy C, a corrosion resistant alloy. The viscosity was measured as a function of shear rate (from 0.1 to 1020 s^{-1}). Disk Preparation: Rock samples were cut from blocks of Pink Dessert limestone (> 99 wt% calcite) into disks with a diameter of 3.81 cm (1.5 in.) and a thickness of 2.54 cm (1 in.). **Table 9.3** shows the basic properties of these rocks. Disk samples were saturated with deionized water for 24 hours under vacuum and the initial porosity and permeability were measured. All samples were soaked in 0.1N HCl for 30 to 40 minutes then rinsed thoroughly with deionized water before reaction. According to Fredd and Fogler (1998c), this procedure ensures good reproducibility and eliminates problems associated with preparing the disk surfaces.

TABLE 9.3—BASIC PROPERTIES OF THE CORE SAMPLES

Rock Type	Pink Dessert Limestone
Porosity, vol.%	27-30
Permeability, md	50-150

The Rotating Disk Apparatus: Reaction rate experiments were performed using the rotating disk apparatus RDR-100 shown in **Fig. 9.1**. The calcite disks were fixed in the disk holder assembly in the reactor vessel using heat-shrinkable Teflon tubing, **Fig. 9.1**. Reaction fluid was poured in the reservoir vessel and both were heated up to the desired temperatures. Compressed N_2 gas was used to pressurize the reservoir vessel to a pre-determined pressure that is sufficient to transfer the acid to the reactor vessel and results in a reactor pressure of 1500 psig. A pressure greater than 1000 psig is necessary in the reaction vessel to ensure that the evolved CO_2 is kept in solution and does not affect the system hydrodynamic and the dissolution rate (Lund et al. 1973; Fredd and Fogler 1998c). The rotational speed was then set up to the selected value and the time is started by the moment at which the valve between the reservoir and the reactor vessels is opened.

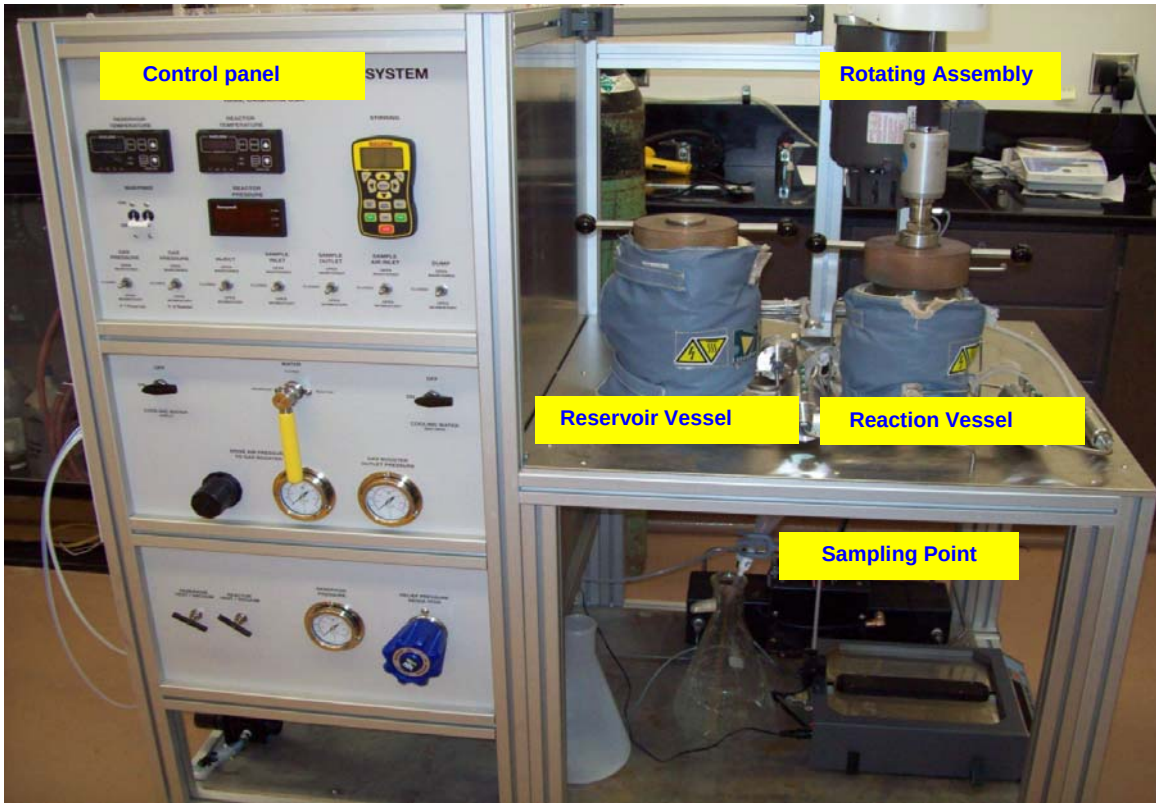

Fig. 9.1—Rotating disk apparatus RDA-100 used for reaction rate measurements.

Samples, each of 2 ml, were withdrawn at equal interval of 2 minutes up to 20 minutes. Calcium concentration in the samples was measured using Perkin-Elmer atomic absorption spectrophotometer. Corrections were made to account for the change in the volume of the reaction medium (500 ml) due to sample withdrawing. A new disk sample was used for each experiment. The rate of calcium production along with the initial area of the sample was used to determine the dissolution rate. The experiments aimed to study the effect of temperature (150, 200, and 250^{o}F), disk rotational speed (100-1800 rpm), the presence of cross linker Fe^{3+} in the form of $FeCl_3$ on the reaction rate, and to

determine the reaction rate and mass transfer parameters in both mass-transfer and surface-reaction limited regimes.

9.4 Results and Discussion

9.4.1 Viscosity measurement of live and spent in-situ gelled acids

The viscosity behavior of live 5 wt% in-situ gelled acid was measured at a temperature range from 75 to 250^{o}F, and a shear rate from 0.1 to 100 s^{-1} and was found to follow the behavior of (shear-thinning) non-Newton fluids. The viscosity and shear rate relationship can be described by the power-law model, Eq. 9.2 and the power-law parameters (K, and n) are listed in **Fig. 9.2**.

Fig. 9.2 shows decreasing in the viscosity of the in-situ gelled acid with increasing the temperature at specific shear rate. However, the difference in viscosity becomes less significant at higher shear rate. It is important to highlight that the viscosity measurements were performed in both ascending and descending directions. There was no significant change in the viscosity in both directions.

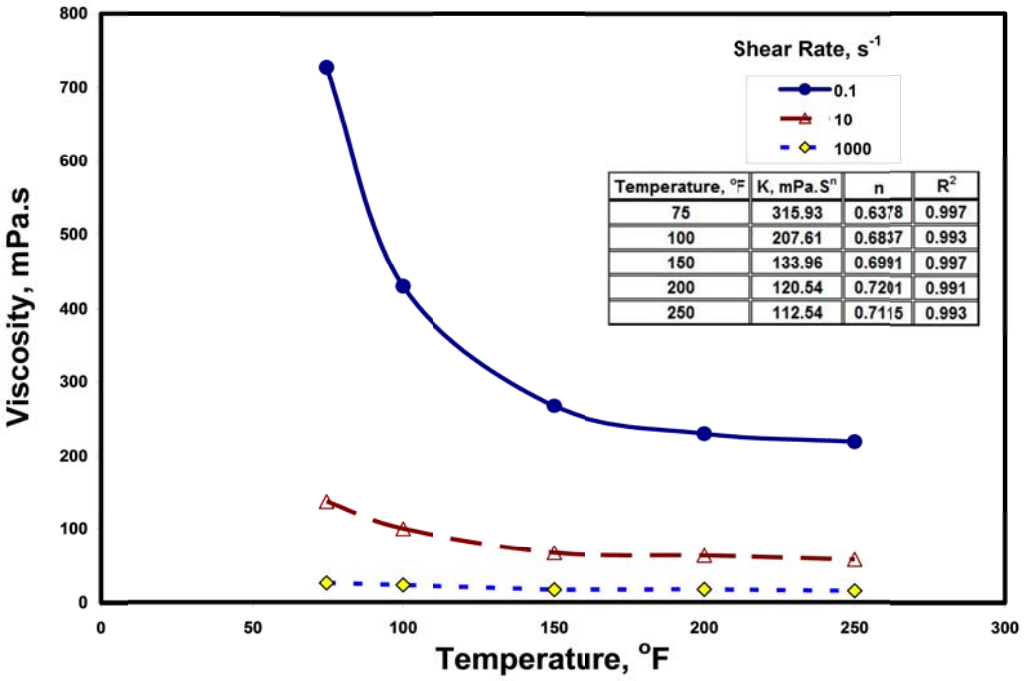

Fig. 9.2—Effect of temperature on the viscosity of live in-situ gelled acid (5 wt% HCl, 300 psi, polymer concentration 2 vol%).

9.4.2 Static test for the reaction of regular, gelled, and in-situ gelled acid

Simple static reaction test was conducted to investigate the differences between the gelled and the in-situ gelled acids. Three rock samples were soaked in regular, gelled (no cross linker), and in-situ gelled 5 wt% HCl for 2 hours. Although the static procedure can not be used to determine the reaction rate, the objective was to highlight the differences between the three cases visually before conducting the rotating disk experiments. **Fig. 9.3** shows the three disk samples after reaction in reference to a blank sample. The reaction with regular 5 wt% HCl was very vigorous and most of the rock sample was consumed as shown in the percentage reduction in the sample weight after reaction, The presence of the polymer in the other two acids retarded the reaction rate,

however the sample that was soaked in the crosslinked gelled acid with ferric chloride showed a darker reddish coating and was associated with lesser percentage of weight reduction. In another experiment, two samples of the same diameter (1.5 in.) where coated with heat-shrinkable Teflon tubing in which the volume above one sample was filled with 5 wt% gelled acid and the volume above the second sample was filled with in-situ gelled acid with the same acid concentration. After 3 minutes, the two samples were photographed as shown in **Fig. 9.4** that shows higher leak-off rate of the gelled acid in comparison with the in-situ gelled acid. The results of these two experiments show that gelled and in-situ gelled acid react differently with the same rock at the same acid concentration. Rotating disk experiments are then needed for better understanding of these two systems and to quantify the rate of dissolution of each one of them at different conditions.

(a) (b) (c) (d)

	(a) blank	(b) in situ gelled acid	(c) gelled acid	(d) regular acid
Diameter	3.6	3.4	3.4	2.8
% weight reduction	---	9.31	14.82	54.44

Fig. 9.3—Comparison between three rock samples after 2-hr of static reaction with a) no acid, b) in-situ gelled acid, c) gelled acid, and d) regular acid at room temperature.

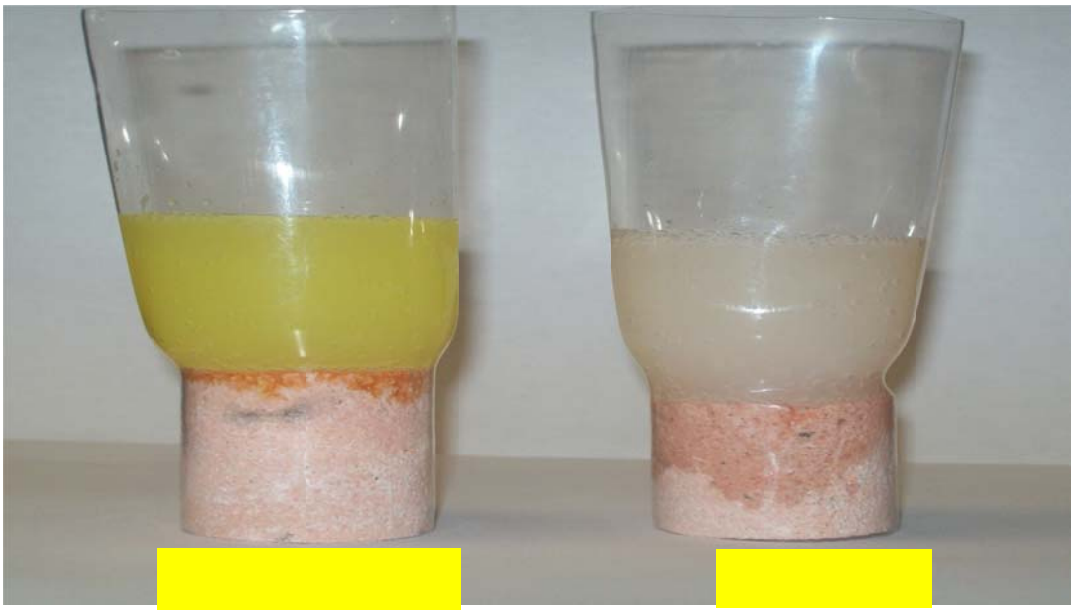

Fig. 9.4—Gelled and in-situ gelled acid in the space above two samples of Pink Dessert limestone.

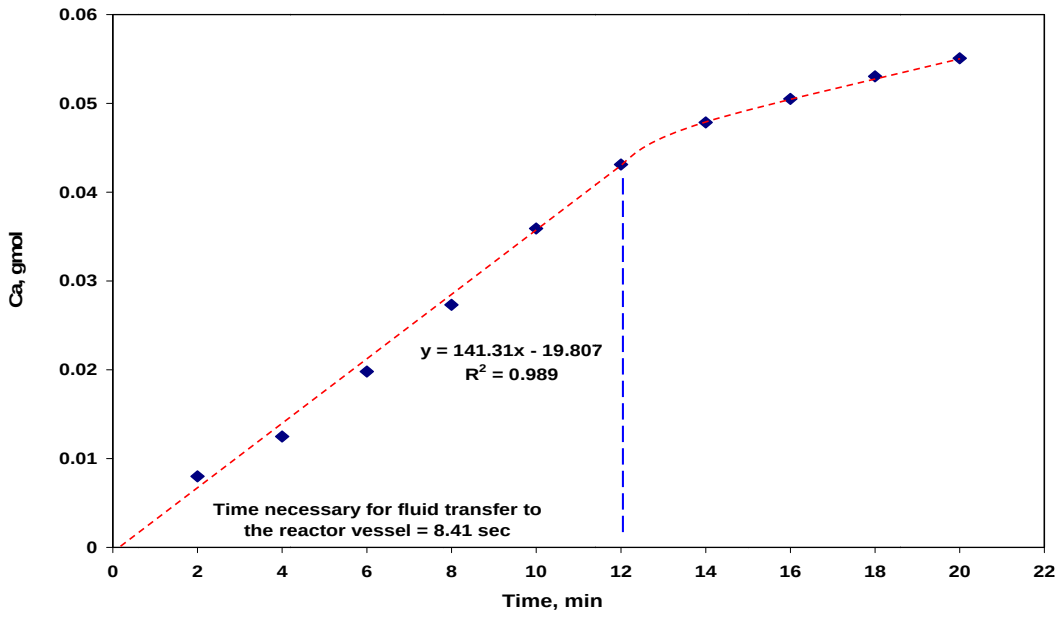

Fig. 9.5—Calcium concentration versus time for the reaction between 5 wt% in-situ gelled acid and Pink Dessert limestone at 100 rpm and 150°F. (Experimental data points were best fitted with straight line that accounts for the fluid transfer time.)

9.4.3 Determination of the dissolution rate using the rotating disk reactor

Periodical samples were withdrawn from the reactor every two minutes and 10 samples were collected in each experiment. Calcium concentration in each sample was measured using Perkin-Elmer atomic absorption. The amount of calcium in the reaction vessel was then calculated and plotted versus time. The slop of this figure gives the rate of change in calcium concentration with time (d[Ca]/dt) and because of the change of the area of the disk, the initial sold surface area was used to determine the initial calcium dissolution rate as follows:

$$R_d = \frac{1}{A_0}\frac{d[Ca]}{dt} \quad \text{.....(9.11)}$$

where R_d is the rate of dissolution, A_o is the initial sold surface area of the disk. Calcium concentration as a function of time is shown in **Fig. 9.5** for a reaction of 5 wt% HCl in-situ gelled acid and Pink Dessert limestone at 100 rpm and 150^{o}F. It was interesting to notice that after certain time, the rate of calcium production decreases and in some cases reaches a plateau. Residual acid concentration after each experiment was measured by titration with 1N sodium hydroxide solution in the presence of phenolphthalein as an end-point indicator. Results showed that the acid was never depleted totally which indicates that this plateau is not because the absence of the acid from the reaction medium. The decrease in calcium production is because the change in the surface area and as a result of the gelled layer that was formed on the surface of the disk and lowered the acid diffusion through the boundary layer. Therefore, the first few points that

represent the linear portion were fitted to the best straight line and was used to determine the rate of dissolution. Because the time in each experiment was started by the moment at which the valve between the reactor and the reservoir vessels is opened, fitting the data points to the best straight line was allowed not to pass through the origin as it should be theoretically expected. The reason for that is to consider the time necessary for the reaction fluid to transfer from the reservoir vessel to the reactor vessel and to eliminate the effect of the transition period on the formation and stabilization of the mass transfer film. Improving in the least square fitting parameter is noticed when this procedure was followed.

The pH of the final bulk solution was measured and was found to be practically zero in all experiments. However, a pH of 2 can be reached within the mass transfer film that is the necessary condition for gel formation and on the surface.

9.4.4 Mass transport of in-situ gelled acid for mass transfer limited reaction

The rate of reaction can be directly measured from the mass flux when mass transfer limited regime predominates. Plotting the reaction rate versus the disk rotational speed raised to the power 1/(1+n) has three main advantages; one is to determine the effect of changing the rotational speed on the reaction rate of in-situ gelled acid. The second is to determine the boundary in which the reaction is mass transfer or surface reaction limited and finally is to estimate the diffusion coefficient of the hydrochloric acid in in-situ gelled acid, such information is very useful in matrix acidizing and acid fracturing modeling purposes. Determination of the controlling step is important in

saving effort, cost, and time that might be spent trying to obtain higher or lower acid reaction rate by controlling the wrong parameter. For instance, increasing the pumping rate of the acid system beyond the mass transfer period has no more effect on the overall dissolution rate.

The effect of the rotational speed on the reaction rate is shown in **Fig. 9.6** which shows the rate of dissolution of Pink Dessert limestone in 5 wt% in-situ gelled HCl at 150^{o}F at different rotational speeds. The figure shows increasing in the rate of dissolution with the increase in the disk rotational speed up to 1000 rpm which can be confirmed also by the percentage of reduction in the weight of each sample after each reaction, **Table 9.4**. Therefore, the rate of dissolution is controlled by the mass transport of the acid up to 1000 rpm. In this regime, the dissolution rate increases in a linear fashion with increasing the rotational speed, raised to power 1/(1+n). Above this value (1000 rpm), the reaction is no longer dependant on the rotational speed and it is said to be surface reaction limited.

For accurate determination of the diffusion coefficient of HCl in in-situ gelled acid at 150^{o}F, the region of the rotational speed in which centrifugal flow has to be determined. In this regime, Eq. 9.8 can be used to determine the acid diffusivity. A log-log plot of the rate of dissolution versus the rotational speed should yield a straight line with a slope of 1/(1+n). **Fig. 9.7** shows that two distinguished slopes can be noted, 0.368 (100-500) rpm and 0.649 (500-1000) rpm. Measuring the viscosity of the 5 wt% of the in-situ gelled HCl at 150^{o}F gave a value of n equals to 0.699 as listed in **Fig. 9.2** which gives a value of 0.589 for 1/1+n. Therefore, the data points from 500 to 1000 rpm are

believed to represent the centrifugal regime and the corresponding slope was used to calculate the acid diffusivity. Recalling **Fig. 9.2 and Table 9.1,** values of n, K□ □and Φ(n), were determined to be 0.699, 134, and 0.64, respectively. Substituting these values in the Eq. 9.8 determines the acid diffusivity to be equal to $2.1632*10^{-5}$ cm/s^2. This value is in good agreement with what was reported by Lakatos and Lakatos-Szabo (2004) who measured the H^+ diffusivity in silicate/polyacrylamide gels. The authors measured the H^+ diffusivity in crosslinked gel for different silicate contents and for different initial acid concentration. The H^+ diffusivity in the gelled acid was found to be up to 50 % less than the diffusivity of H^+ in aqueous solution, $9.32*10^{-5}$ cm^2/s. Based on measured data, Conway et al. (1999) introduced a correlation to predict the diffusivity of H^+ for regular, gelled, and emulsified acids at different temperature and for different acid concentrations. This correlation predicts $5.81*10^{-5}$, and $3.63*10^{-5}$ for the diffusivity of H^+ in regular, and gelled acid, respectively, at 150^oF for 5 wt% HCl. These estimated values indicate a reduction of 63% and 40% in comparison to measured diffusivity of the in-situ gelled acid at the same condition.

TABLE 9.4—INITIAL, FINAL, AND PERCENTAGE OF REDUCTION IN THE WEIGHT OF SAMPLES AFTER REACTION OF 5 WT% IN-SITU GELLED ACID WITH PINK DESSERT LIMESTONE AT 150^oF AND DIFFERENT ROTATIONAL SPEEDS

Disk Rotational Speed, rpm	Sample Weight Before Reaction, gm	Sample Weight After Reaction, gm	Reduction, %
100	51.58	46.93	9.01
500	50.96	39.97	21.57
800	50.33	37.36	25.77
1000	48.56	31.25	35.65
1500	46.44	26.30	43.37
1800	51.44	32.00	37.79

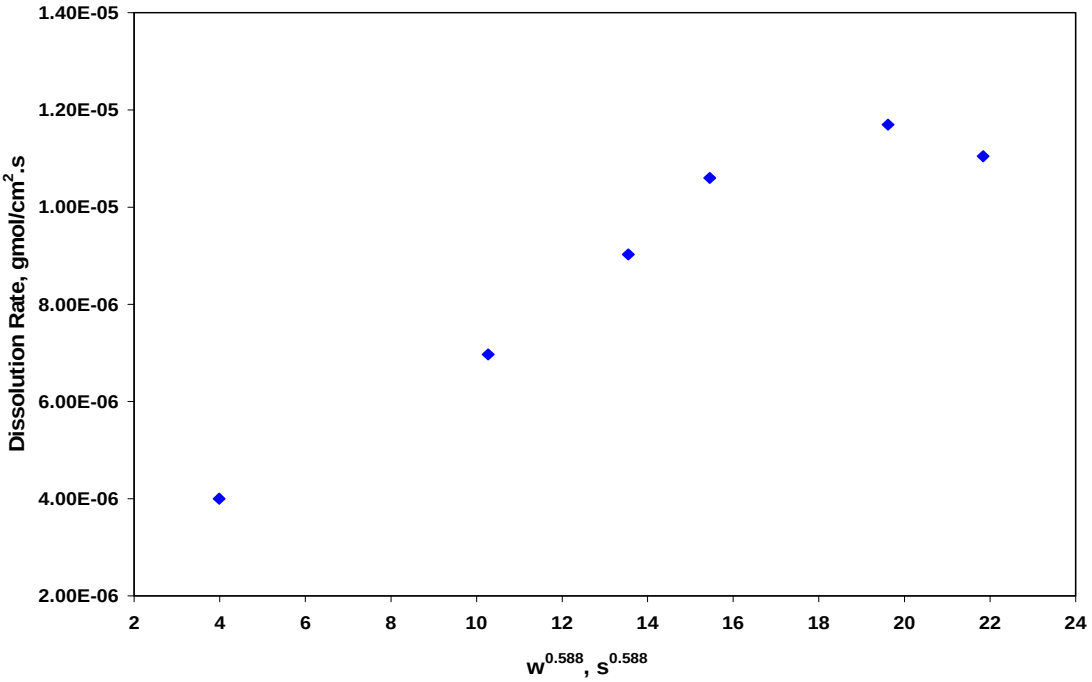

Fig. 9.6—Effect of disk rotational speed on the dissolution rate of Pink Dessert limestone in 5 wt% in-situ gelled acid at 150°F.

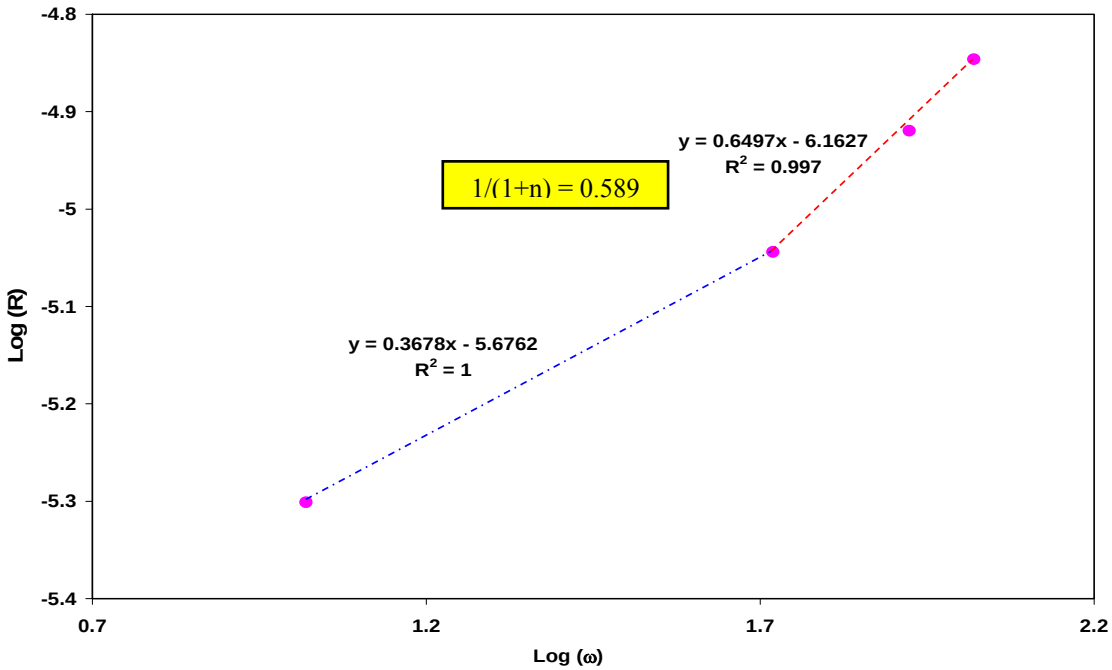

Fig. 9.7—Log-Log plot of the rate of dissolution rate of Pink Dessert limestone in 5 wt% in-situ gelled acid at 150°F indicating a centrifugal region between (500-1000) rpm.

9.4.5 Kinetic study of in-situ gelled acid with calcite

The effect of temperature on the reaction rate of in-situ gelled acid with calcite was investigated by measuring the reaction rate over a range of temperature (100-250^{o}F) at 1500 rpm. This rotational speed was selected to ensure a surface reaction limited regime. Three disk samples at 100, 200, and 250^{o}F were photographed after reaction and are shown in **Fig. 9.8**. It is obvious that severe reaction has occurred at higher temperatures of 200 and 250^{o}F. The acid has consumed large parts of the rock samples and a centrifugal pattern of flow is assumed to be dominant. Although the shape of the rock samples at 200 and 250^{o}F might be similar from the top view, reaction at 250^{o}F was higher and that was assessed by measuring the weight loss in each rock sample which gave 40.5 wt% and 44 wt% for 200 and 250^{o}F, respectively. The reaction rate was measured over the whole range of temperatures as shown in **Fig. 9.9**. It is clear that increasing the temperature increases the reaction rate and this is noted from the dependency of the rate reaction constant on the temperature as shown in the Arrhenius relation, Eq. 9.10. Using the rates of reactions and applying the simple reaction expression that was mentioned Eq. 9.9, reaction rate constants k_r was determined at each temperature. The reaction rate order was taken as 0.319 as reported for gelled acid with Khuff limestone (Nasr El-Din et al. 2002a). Results are summarized in **Table 9.5**. Arrhenius equation was then used to determine the reaction activation energy E_a and the pre-exponential factor k_o by plotting Ln(k_r) versus the reciprocal of the temperature as shown in **Fig. 9.10**. The results determine the activation energy to be 3.25 kcal/gmol, and a pre-exponential factor of $1.341*10^{-2}$. The activation energy value is comparable to

that obtained by Nasr El-Din et al. (2002b) who reported a value of 3.51 kcal/gmol for the reaction of 15 wt% gelled acid and Khuff limestone.

a) 100°F **b) 200°F** **c) 250°F**

Fig. 9.8—Three rock samples after 30 minutes reaction at 1500 rpm with 5 wt% in-situ gelled acid at various temperatures.

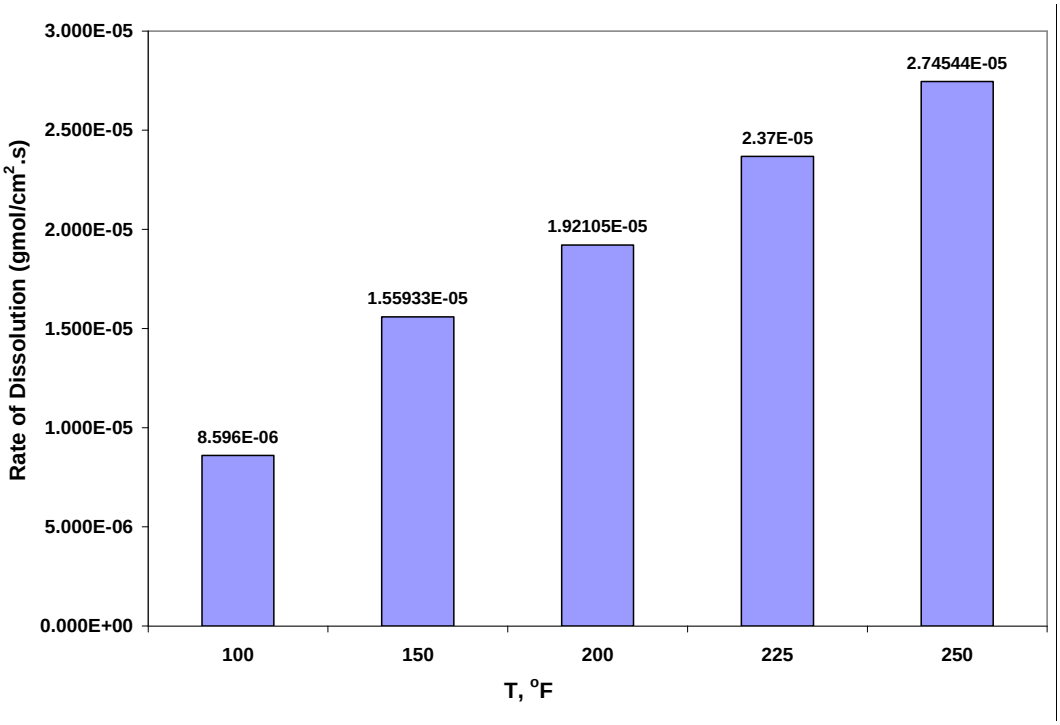

Fig. 9.9—Effect of temperature on the dissolution rate of 5 wt% in-situ gelled acid with Pink Dessert limestone at disk rotational speed of 1500 rpm.

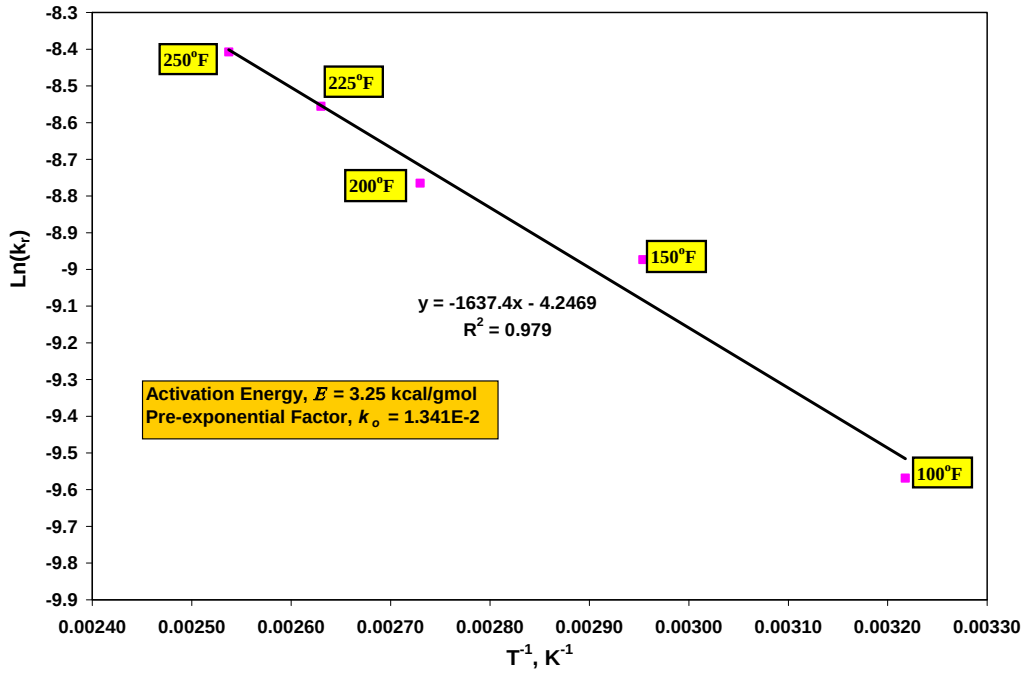

Fig. 9.10—Determination of the kinetics parameters for the reaction between 5 wt% in-situ gelled acid and Pink Dessert limestone at disk rotational of 1500 rpm.

TABLE 9.5—DETERMINATION OF REACTION RATE AND REACTION RATE CONSTANT OF 5 WT% IN-SITU GELLED ACID WITH PINK DESSERT LIMESTONE AT 150, 200, AND 250°F AND 1500 RPM

Temperature, °F	Reaction Rate, ($gmol.cm^{-2}.s^{-1}$)	Reaction Rate Constant, kr, ($gmol^{0.681}cm^{-1.043}.s^{-1}$)
100	8.5959E-06	6.98685E-05
150	1.5593E-05	12.6744 E-05
200	1.9211E-05	15.6145 E-05
225	2.3680E-05	19.2473 E-05
250	2.7454E-05	22.3152 E-05

9.5.6 Effect of the cross-linker

The main difference between the gelled acid and the in-situ gelled acid systems is that the latter has a cross-linking ion with multi valence in the bulk solution such as Fe^{3+}, Al^{3+}, and Zr^{4+}. At certain pH (2 for in-situ gelled acid), the carboxyl group is deprotonated resulting in negative charge on the COO^- group. Cross linking ion fills each vacancy with one polymer molecule and builds up a polymer network of significantly higher viscosity and gel-like structure. Without cross linker ions, no polymer network can be formed and there is no gel structure. To investigate the effect of the presence of crosslinker, in the form of ferric chloride, on the dissolution rate, the reaction rate of the gelled and the in-situ gelled acid was measured at two different rotational speeds of 100 and 1500 rpm at 150^{o}F. **Fig. 9.11** shows the change in the amount of calcium produced in the reactor with time for X-linked and Non-X-linked acid at 100 rpm, while **Fig. 9.12** depicts the change in this amount of calcium produced with time at the same temperature at 1500 rpm. The reason for choosing these two rotational speeds is to investigate the effect of cross linking in both mass transfer and surface reaction controlling regions. It is clear that less amount of calcium was produced when the acid was X-lined using ferric chloride and that resulted in lower reaction rate at both low and high rotational speed. The dissolution rate was determined a comparison between these different cases is shown in **Fig. 9.13.** The reaction rate was reduced by a factor of 2.22 at 100 rpm and by a factor of about 1.4 at 1500 rpm. These results confirm that in-situ gelled acid is an efficient method for retardation the acid reaction in both mass transport and surface reaction limited cases. It is believed that the gel layer that is

formed when using the in-situ gelled acid will reduce the acid diffusivity in the mass transport limited reactions. In the surface reaction limited, the gel layer adsorbed on the surface reduces the area for reaction and therefore reduces the rate of reaction.

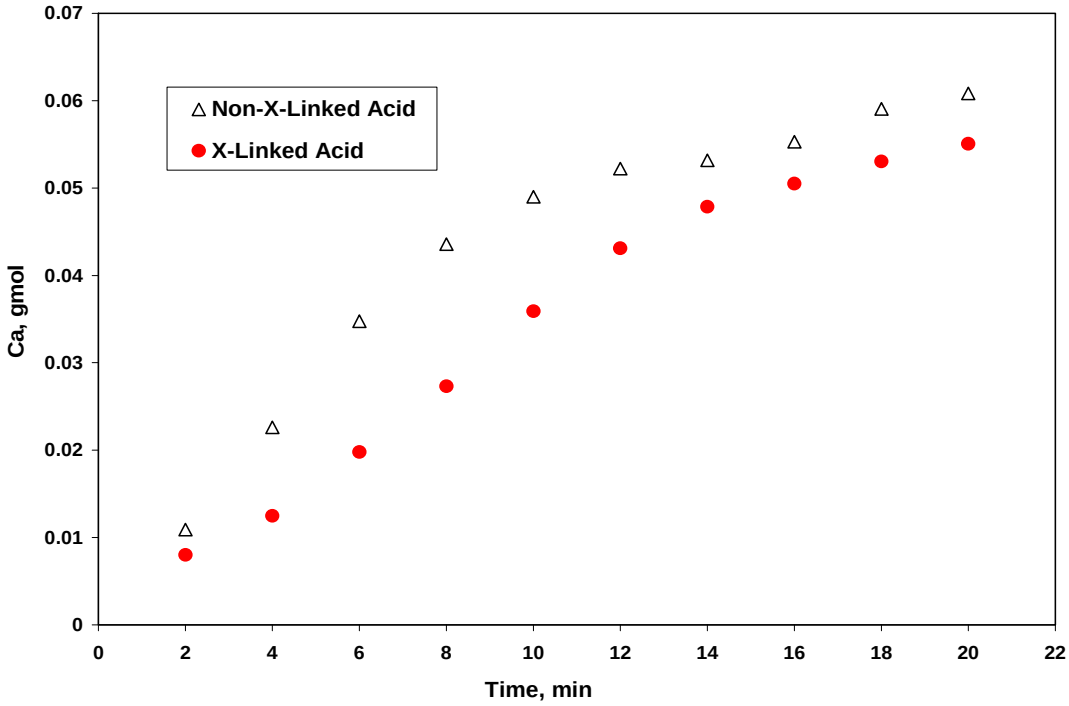

Fig. 9.11—Calcium concentration as a function of reaction time with and without cross-linker ($FeCl_3$) at 150°F and a disk rotational speed of 100 rpm.

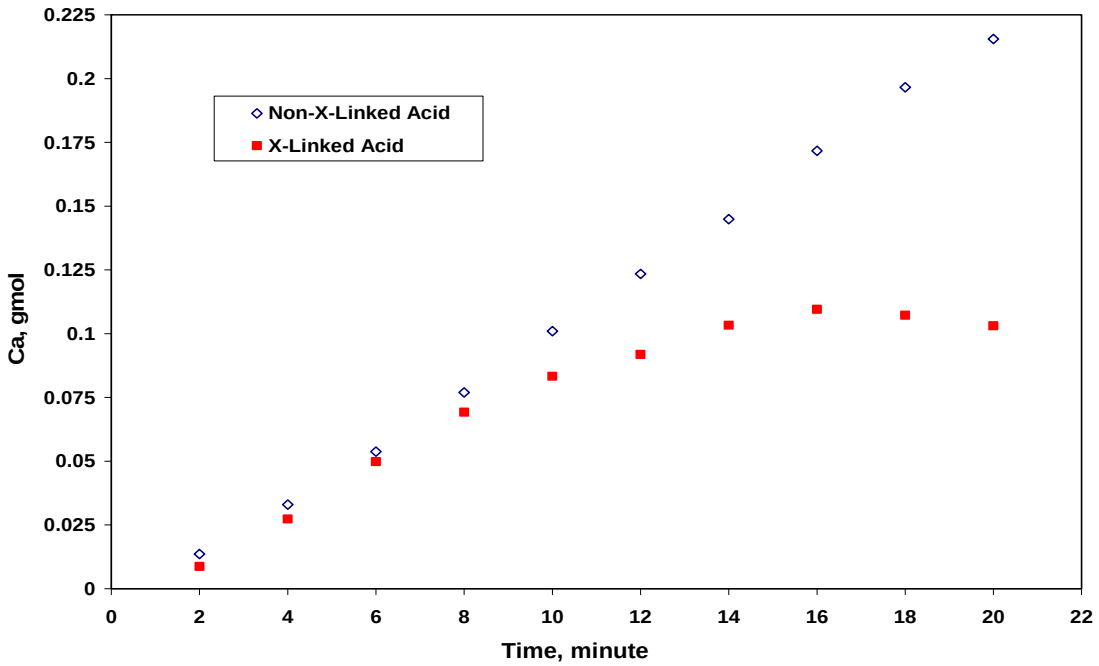

Fig. 9.12—Calcium concentration as a function of reaction time with and without cross-linker ($FeCl_3$) at 150°F and a disk rotational speed of 1500 rpm.

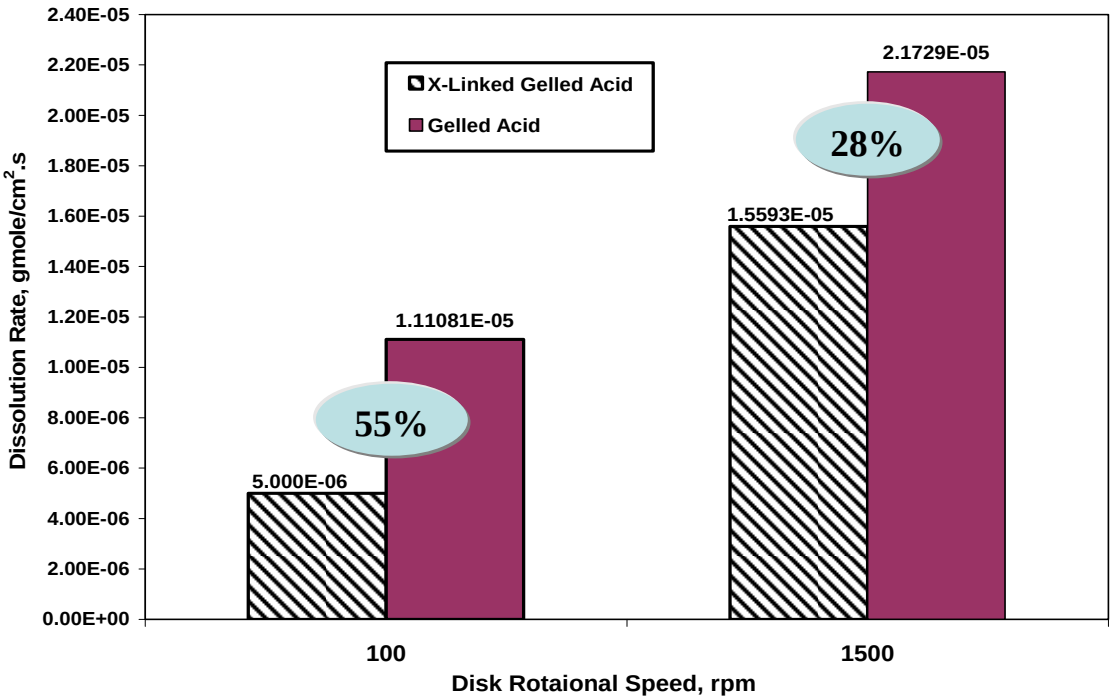

Fig. 9.13—Effect of the cross-linker on the rate of calcite dissolution for Pink Dessert limestone at 150°F and at disk rotational speed of 100 and 1500 rpm.

10. CONCLUSIONS AND RECOMMENDATIONS

Gelled and in-situ-gelled acids are used to reduce the leakoff rate during acid fracturing and to divert the acids during matrix acidizing. The effect of salts and iron contamination on the apparent viscosity of these acids was examined. On the basis of the results obtained, the following conclusions can be shown:

- Polymer and other additives were separated out when these acids were prepared in high-salinity water.
- $NaCl_3$, $CaCl_2$, or $FeCl_3$ reduced the apparent viscosity of live gelled acids.
- Preparing the in-situ-gelled acid with saline water decreased the viscosity of live and partially neutralized acids.
- High HCl concentrations produced significant amounts of calcium that decreased the viscosity of in-situ-gelled acid systems. Therefore, in-situ-gelled acids that are based on polymers should be used at low HCl concentrations (3 to 5 wt% HCl).
- A brown precipitate was noted during the neutralization of systems that contained Fe (III)**,** even in the presence of the recommended concentration of iron-control agents.

In-situ gelled acids were examined using an oscillatory rheometer to measure their viscoelastic properties. Based on the results obtained, the following conclusions can be drown:

- Two regimes were identified: a pure viscous behavior and a semisolid elastic behavior. The viscous regime was noted below pH 2 where G" was dominant. The semisolid elastic behavior was observed pH greater than 2 where G' was dominant.
- Yield stress, Young modulus, G', and G" significantly increased at pH 2, and reached their maximum values at pH 3.2. G' increased by 3 orders of magnitude while G" increased by one order of magnitude only.
- G' and G" are independent of shear rate at pH values greater than 2.
- Maxwell and Kelvin-Voigt models were able to predict the experimental data in the viscous regime. However, for semisolid elastic regime, these models didn't predict the experimental results.
- A mathematical model was developed to predict the rheological properties of in-situ gelled acids over a wide range of pH values. Model predictions were in good agreement with experimental results.

Differences between gelled and In-situ gelled acids were examined using rheological and coreflood study. The obtained results showed that:

- Live gelled and in-situ gelled acids had weak viscoelastic properties while partially neutralized (pH 3.2) in-situ gelled acid had strong viscoelastic properties.

- Polymer filter-cake was observed only for the core that treated with gelled acid injection while the core that treated with in-situ gelled acids didn't form any polymer filter-cake.
- In-situ gelled acid formed a thin layer of gel that minimizes the leak-off which prevents the build of polymer filter-cake.
- For gelled acid, the polymer filter-cake reduced the core permeability to zero by plugged the core holder inlet during the water flow back. However after removing the plugging, a permeability enhancement was much higher than in-situ gelled acids.
- The wormhole obtained in case of gelled acid was nearly linear and thinner than the wormhole created by in-situ gelled acid.
- The strong viscoelastic properties give the ability to the gel to sustain around the wormhole and plug it. This will force the next acid stage to change its direction.

In-situ gelled acids were examined under different shear rates inside limestone cores. The obtained results showed that:

- At low shear rates, in-situ gelled acid formed a gel inside the core, as indicated by the cyclic behavior noted in the pressure drop across the core, and the acid changed its direction inside the core several times. However, this gel significantly reduced the core permeability.

- At high shear rates, a smaller amount of gel was formed inside the core and the acid ability to change its direction inside the core was less than at low shear rate.
- A significant permeability enhancement was achieved.
- Wormhole length increased as the shear rate was increased, while the diameter of wormhole increased as the cumulative injected volume of acid was increased.
- CT scan indicated the presence of gel residue in the core surrounding the wormhole. Gel residue increased at low shear rates.
- Material balance on the cross-linker indicated that a significant amount of the cross-linker was retained inside the core. This amount was significant at low shear rates.

The effects of shear rate and an in-situ gelled acid stage on the propagation of 15 wt% HCl were examined. Based on the results obtained, the following conclusions can be drawn:

- Unlike in-situ gelled acid behavior at high shear rate conditions, in-situ gelled acid at low shear rate conditions instantaneously plugged the tip of the wormhole and didn't create additional wormhole inside the core. Therefore, when the final regular acid stage bypassed the gel, it started to propagate from nearly the last point that the first stage ended.
- Increasing the in-situ gelled acid stage volume from 0.5 to 1 PV leaded to

decrease the acid ability to change its direction at high shear rate conditions. However, at low shear rate conditions, the acid ability to change its direction didn't changed.

- In multi-stage treatments, calcium and iron propagated faster than the acid because they breakthrough earlier than the acid. This is an indication that the acid had been slowed inside the core by the effect of the gel.
- In multi-stage treatments, final regular acid stage created its own wormhole away from the gel that formed by in-situ gelled stage. Therefore, the percentage of the remaining iron was very high.

The effect of injection rate of polymer-based acids (gelled and in-situ gelled) on the acid volume required to breakthrough from 6-in. length cores was studied. Based on the results obtained the following conclusions were drawn:

- The wormhole propagation rate of gelled acid was higher than regular acid. On the other hand, the wormhole propagation rate of in-situ gelled acid was lower than regular acid.
- Gelled acid required the lowest acid volume to breakthrough. However, in-situ gelled acid required the highest acid volume to breakthrough.
- Three regions were obtained for the wormhole propagation rate of gelled acid as a function of the injection rate:

a. Region I, where acid injection rate is low, and in-situ gelled acid wasn't able to breakthrough from the cores at injection rate less than 5 cm^3/min.
b. Region II, where the acid volume required to breakthrough decreased as injection rate increased in the range between 5 and 10 cm^3/min.
c. Region III, where the acid volume injected increases with the injection rate at injection rate higher than 10 cm^3/min.

- The optimum injection rate wasn't affected by temperature, or initial core permeability.
- The acid volume required to breakthrough decreased as the temperature, or initial core permeability was increased.

The ability of polymer-based in-situ gelled acids to divert regular acids was studied using parallel cores. The sequence of the injection involved a stage of in-situ gelled acid at 5 wt% HCl followed by a regular acid at 15 wt% HCl until acid breakthrough. Based on the results obtained the following conclusions were drawn:

- At nearly same permeability contrast (1:1.1), regular acid preferred to flow through the high permeability cores.
- For high and low permeability cores, at an injection rate of 1 cm^3/min, in-situ gelled acid plugged the two cores faces.
- For low permeability contrast (1:2), in-situ gelled acid was able to divert the acid with permeability enhancement in both cores.

- For high permeability contrast (1: 20 up to 25), in-situ gelled acid was able to divert the acid only at injection rate less than 10 cm^3/min.
- At higher injection rates, in-situ gelled acid was not able to build enough pressure that could force the regular acid into the low permeability core.
- Increasing the injection rate from 1 to 10 increased the volume of in-situ gelled acid required to achieve diversion. However, it reduced the permeability reduction due to gel.
- For high permeability contrast (1: 20 up to 25), wormhole length of the high permeability core increased, as the in-situ gelled acid injection rate was increased.

Finally, the reaction of 5 wt% in-situ HCl gelled acid with Pink Dessert limestone was measured over a temperature range between 100-250^oF and different rotational speeds (100-1800 rpm) using the rotating disk apparatus. Based on the results obtained, the following conclusions can be drawn:

- The reaction of in-situ gelled acid with calcite is mass transfer limited up to a rotational speed of 1000 rpm and a surface reaction limited above this value at 150^oF.
- The HCl effective diffusivity in 5 wt% in-situ gelled acid is equal to $2.163*10^{-5}$ cm^2/s at 150^oF. The acid diffusivity for in-situ gelled acid is less by 63% and 40% in comparison to the diffusivity in regular and gelled acid, respectively.

- The reaction of in-situ gelled acid was measured at 1500 rpm over a temperature range between 100-250^{o}F and a power-law model was used to determine the reaction kinetics. The reaction rate constant was reported at each temperature. The kinetic parameters of the surface reaction were determined over the investigated range of temperature. The reaction activation energy was found to be 3.25 kcal/gmol and the pre-exponential factor was determined to be $1.341*10^{-2}$ $gmol^{0.681}/cm^{1.043}.s$
- The presence of cross-linker (Fe^{+3}) decreased the rate of calcite dissolution in both mass transfer and surface reaction limited regions. The cross-linker retarded the reaction by reducing the acid diffusivity and by forming a gel layer on the rock surface that reduced the area exposed to the acid, which decreased the overall acid dissolution rate.

Currently, in-situ-gelled acids are used at acid concentrations up to 28 wt% HCl. They can be prepared using aquifer water or seawater. However, on the basis of the results obtained from this study, it is strongly recommended to use polymer-based in-situ-gelled acids at 3 to 5 wt% HCl and prepare these acids in fresh or low-salinity waters. Iron contamination should be minimized by cleaning the mixing tank or bickling the tubing before acid pumping.

Acid injection rate should be determined based on the expected shear rate in the formation. The data obtained in this study can be used as a guideline for injection rate

selection. A core flood experiment is recommended to confirm optimum injected rate. Flow back the well to minimize the residual gel inside the formation.

NOMENCLATURE

$\dot{\gamma}$	Shear rate, s^{-1}
[Hb+]	Acid concentration in the bulk solution, gmol, cm^{-3}
A_0	Initial disk surface area, cm^2
C	Solute concentration, $gmol.cm^{-3}$
C_b	Reactant concentration in the bulk solution, $gmol.cm^{-3}$
C_s	Reactant concentration at the surface, $gmol.cm^{-3}$
D	Diffusivity, $cm.s^{-2}$
d[Ca]/dt	Calcium dissolution rate, $gmol.cm^{-2}.s^{-1}$
E	Young modulus, Pa
Ea	Reaction activation energy, $kcal.gmol^{-1}$
*G**	Complex modulus, Pa
G	Shear modulus, Pa
G'	Elastic or storage modulus, Pa
G''	Viscous or loss modulus, Pa
J_c	Creep compliance (strain/stress), 1/Pa
J	Mass flux, $gmol.cm^{-2}.s^{-1}$
K_m	Reactant mass transfer coefficient, $cm.s^{-1}$
K_o	Pre-exponential factor, $gmol^{(1-m)}.cm^{(3m-2)}.s^{-1}$
K_r	Reaction rate constant, $gmol^{(1-m)}.cm^{(3m-2)}.s^{-1}$
M	Reaction rate order,

N	K/ρ, $cm^2.s(n^{-2})$
$\dot{\gamma}_o$	Maximum shear rate, s^{-1}
R	Rate of reaction, $gmol.cm^{-2}.s^{-1}$
R_d	Initial calcium dissolution rate, $gmol.cm^{-2}.s^{-1}$
Re	Reynolds number
Rs	Radius of the disk, cm
Sc	Schmidt number
Sh	Sherwood number,
T	Time, s
U	Velocity, cm.s-1
α	Cone angle, °
δ	Phase shift or loss angle, °
ε	Shear strain
ε_o	Maximum strain, %
μ*	Complex viscosity, Pa.s
μ’	Elastic component of complex viscosity, Pa.s
μ”	Dynamic viscosity, Pa.s
P	Density, $g.cm^{-3}$
σ	Applied stress, Pa
τ	Stress, Pa
τ’	Elastic component of stress, Pa
τ”	Viscous component of stress, Pa

τ_o	Maximum component of stress, Pa
τ_o'	Maximum component of elastic stress, Pa
τ_o''	Maximum component of viscous stress, Pa
τ_s	Shear stress, Pa
ω	Frequency, Hz
Ω	Disk rotational speed, s^{-1}
$\Phi'(n)$	Function depends on n,

REFERENCES

Abdel Fatah, W., Nasr-El-Din, H.A., Moawad, T., and Elgibaly, A. 2008. Effects of Crosslinker Type and Additives on the Performance of In-Situ Gelled Acids. Paper SPE 112448 presented at the SPE International Symposium and Exhibition on Formation Damage Control, Lafayette, Louisiana, 13–15 February.

Al-Ghamdi, A.H., Mahmoud, M.A., Hill, A.D., and Nasr-El-Din, H.A. 2009. Diversion and Propagation of Viscoelastic Surfactant-Based Acid in Carbonate Cores. Paper SPE 121713 presented at the SPE International Symposium on Oilfield Chemistry held in The Woodlands, Texas, 20–22 April.

Al-Nakhli, A.R., Nasr-El-Din, H.A., and Al-Baiyat, A.A. 2008. Interactions of Iron and Viscoelastic Surfactants: A New Formation-Damage Mechanism. Paper SPE 112465 presented at the SPE International Symposium and Exhibition on Formation Damage Control, Lafayette, Louisiana, 13–15 February.

Amro, M.M. 2006. Extended Matrix Acidizing Using Polymer-Acid Solutions. Paper SPE 106360 presented at the Technical Symposium of Saudi Arabia Section, Dhahran, Saudi Arabia, 21-23 May.

Barron, A.N., Hendrickson, A.R., and Wieland, D.R. 1962. The Effect of Flow on Acid Reactivity in a Carbonate Fracture. *Journal of Petroleum Technology* **14**(4):409-415.

Bazin, B. 2001. From Matrix Acidizing to Acid Fracturing: A Laboratory Evaluation of Acid/Rock Interactions. *SPE Production & Facilities* **16**(1): 22-29.

Bazin, B., Roque, C. and Bouteca, M. 1995. A Laboratory Evaluation of Acid Propagation in Relation to Acid Fracturing: Results and Interpretation. Paper SPE 30085 presented at the SPE European Formation Damage Conference, The Hague, Netherlands, 15-16 May.

Bazin, B., Roque, C., Chauveteau, G.A., and Boute, M.J. 1999. Acid Filtration Under Dynamic Conditions To Evaluate Gelled Acid Efficiency in Acid Fracturing. *SPE Journal* **4**(4): 360-367.

Boles, J.L., Metcalf, A.S., and Dawson, J.C. 1996. Coated breaker for cross-linked acid. US Patent No. 5,497,830.

Brezinski, M.M. 1999. Chelating Agents in Sour Well Acidizing: Methodology or Mythology. Paper SPE 54721 presented at the SPE European Formation Damage Conference, The Hague, Netherlands, 31 May–1 June.

Buijse, M.A. 2000. Understanding Wormholing Mechanisms Can Improve Acid Treatments in Carbonate Formations. *SPE Production & Facilities* **15**(3):168-175.

Chang, F., Qu, Q., and Frenier, W. 2001. A Novel Self-Diverting Acid Developed for Matrix Stimulation of Carbonate Reservoirs. Paper SPE 65033 presented at the SPE International Symposium on Oilfield Chemistry, Houston, Texas, 13–16 February.

Chang, F.F., Nasr-El-Din, H.A., Lindvig, T., and Qiu, X.W. 2008. Matrix Acidizing of Carbonate Reservoir Using Organic Acids and Mixture of HCl and Organic Acids. Paper SPE 116601 presented at the SPE Annual Technical Conference and Exhibition, Denver, Colorado, 21–24 December.

Chang, F.F., Qiu, X., and Nasr-El-Din, H.A. 2007. Chemical Diversion Techniques Used for Carbonate Matrix Acidizing: An Overview and Case Histories. Paper SPE 106444 presented at the International Symposium on Oilfield Chemistry, Houston, Texas, 28 February–2 March.

Conway, M.W., Asadi, M., Penny, G., and Chang, F. 1999. A Comparative Study of Straight/Gelled/Emulsified Hydrochloric Acid Diffusivity Coefficient Using Diaphragm Cell and Rotating Disk. Paper SPE 56532 presented at the SPE Annual Technical Conference and Exhibition, Houston, Texas,3–6 October.

Coulter, G.R. and Jennings, A.R. 1999. A Contemporary Approach to Matrix Acidizing. *SPE Production & Facilities* **14**(2): 144-149.

Crowe, C.W. 1985. Evaluation of Agents for Preventing Precipitation of Ferric Hydroxide From Spent Treating Acid. *Journal of Petroleum Technology* **37**(4): 691–695.

Daccord, G., Lenormand, R. and Liétard, O. 1993. Chemical Dissolution of a Porous Medium by a Reactive Fluid. *Chemical Engineering Science* **48**(1): 169–186.

Daccord, G., Touboul, E. and Lenormand, R. 1989. Carbonate Acidizing: Toward a Quantitative Model of the Wormholing Phenomenon. *SPE Production Engineering* ***4****(1):* 63–68.

de Rozieres, J., Chang, F.F., and Sullivan, R.B. 1994. Measuring Diffusion Coefficients in Acid Fracturing Fluids and Their Application to Gelled and Emulsified Acids. Paper SPE 28552 presented at the SPE Annual Technical Conference and Exhibition, New Orleans, Louisiana, 25–28 September.

Dick, M.A., Heinz, T.J, Svoboda, S.F., and Aston, M..2000. Optimizing the Selection of Bridging Particles for Reservoir Drilling Fluids. Paper SPE 58793 presented at the SPE International Symposium on Formation Damage, Lafayette, Louisiana, 23–24 February.

Economides, M and Boney, C. 2000. *Reservoir Stimulation*. 3rd edition, Englewood Cliffs, New Jersey; Prentice Hall.

Ellision, B.T. 1969. Mass Transfer to a Rotating Disk. PhD Dissertation, University of California, Berkeley, California.

Fredd, C.N. and Fogler, H.S. 1998a. Alternative Stimulation Fluids and Their Impact on Carbonate Acidizing. *SPE Journal* **13**(1): 34-41.

Fredd, C.N. and Fogler, H.S. 1998b. Influence of Transport and Reaction on Wormhole Formation in Porous Media. *AIChE J.* **44**(9):1933–1949.

Fredd, C.N. and Fogler, H.S. 1998c. The Kinetics of Calcite Dissolution in Acetic Acid Solutions. *Chem. Eng. Sci.* **53**(22): 3863–3874.

Frick, T.P., Mostofizadeh, B., and Economides, M.J. 1994. Analysis of Radial Core Experiments for Hydrochloric Acid Interaction with Limestones. Paper SPE 27402 presented at the SPE International Symposium on Formation Damage Control, Lafayette, Louisiana, 7-10 February.

Halder, S., Nainwal, S.P., De, S.K., and Karmaker, G.P. 2004. In-situ Cross-linking Acid Diverting Agent (ISCADA): A New Solution to Stimulate Multi-Layered Reservoirs. Paper SPE 88591 presented at the Asia Pacific Oil and Gas Conference and Exhibition, Perth, Australia, 18-20 October.

Hansford, G.S., and Litt, M.1968. Mass Transport from a Rotating Disk into Power-Law Liquids. *Chemical Engineering Science* **23**(8): 849-864.

Hill, A.D., and Rossen, W.R. 1994. Fluid Placement Diversion in Matrix Acidizing. Paper SPE 27982 presented at the Centennial Petroleum Engineering Symposium, Tulsa, Oklahoma, 29–31 August.

Hill, A.D., Zhu, D., and Wang, Y. 1995. The Effect of Wormholing on the Fluid-Loss Coefficient in Acid Fracturing. *SPE Production & Facilities* **10**(4): 257-264.

Hill, D.G. 2005. Gelled Acid. US Patent Application No. 20050065041.

Hoefner, M.L. and Fogler, H.S. 1988. Pore Evolution and Channel Formation During Flow and Reaction in Porous Media. *AIChE J.* **34**(1): 45–54.

Huang, T., Hill, A.D. and Schechter, R.S. 1997. Reaction Rate and Fluid Loss: The Keys to Wormhole Initiation and Propagation in Carbonate Acidizing. Paper SPE 37312 presented at the SPE International Symposium on Oilfield Chemistry, Houston, Texas, 18-21 February.

Jones, A.T. and Davies, D.R., 1996. Quantifying Acid Placement: The Key to Understanding Damage Removal in Horizontal Wells. SPE 31146. Intl. Symposium on Formation Damage Control, Lafayette, Louisiana, 14-15 February.

Jones, A.T. Dovle, M., and Davies, D.R. 1996. Improving the Efficiency of Matrix Acidizing with a Succinoglycan Viscosifier. *SPE Production & Facilities* **11**(3): 144-194.

Kalfayan, L.I., and Martin, A.N. 2009. The Art and Practice of Acid Placement and Diversion: History, Present State and Future. SPE 124141 presented at the Annual Technical Conference and Exhibition, New Orleans, Louisiana, 4-7 October.

Kreiba, A. 2005. The Rheological Properties of Aqueous Polyacrylamide Solutions. M.S. Thesis, Concordia University, Montreal, Quebec, Canada.

Lakatos, I. and Lakatos, J. 2004. Diffusion of H^+, H_2O and D_2O in polymer/silicate gels. *Journal of Colloids and Surfaces A: Physicochemical and Engineering Aspects*, **246**(1): 9-19.

Levich, V.G. 1962. *Physicochemical Hydrodynamics*. Englewood Cliffs, New Jersey: Prenctice-Hall.

Liu, J. and Seright, R.S. 2001. Rheology of Gels Used for Conformance Control in Fractures. *SPE Journal* **6**(2):120-125.

Lund, K., Fogler, H.S., and McCune, C.C. 1973. Acidization I: The Dissolution of Dolomite in Hydrochloric Acid, *Chemical Engineering Science* **28**(3): 681-700.

Lund, K., Fogler, H.S., McCune, C.C., and Ault, J.W. 1975. Acidization II: The Dissolution of Calcite in Hydrochloric Acid. *Chemical Engineering Science* **30**(8): 825-835.

Lynn, J.D. and Nasr-El-Din, H.A. 2001. A Core Based Comparison of the Reaction Characteristics of Emulsified and In-Situ Gelled Acids in Low Permeability, High Temperature, Gas Bearing Carbonates. Paper SPE 65386 presented at the SPE International Symposium on Oilfield Chemistry, Houston, Texas, 13–16 February.

Macosko, C.W. 1994. *Rheology Principles: Measurements, and Applications*. New York: Wiley-Vch.

MaGee, J., Buijse, M.A., and Pongratz, R. 1997. Method for Effective Fluid Diversion when Performing a Matrix Acid Stimulation in Carbonate Formations. Paper SPE 37736 presented at the Middle East Oil Show, Bahrain, 15-18 March.

Metcalf, S., Lopez, H., Hoff, C., and Woo, G. 2000. Gas Production from Low Permeability Carbonates Enhanced Through Usage of a New Acid Polymer System. Paper SPE 59756 presented at the SPE/CERI Gas Technology Symposium held in Calgary, Alberta, Canada, 3-5 April.

Metzner, A. B., 1961. *Handbook of Fluid Dynamics*. *Streeter.* New York: McGraw-Hill Book Co.

Meyers, M.A. and Chawla K.K., 1999. *Mechanical Behavior of Materials*. New Jersey: Prentice Hall Upper Saddle River.

Mirza, A., and Turton, S. 1995. Selective Stimulation of Varying Characteristic Carbonate Reservoir Using Acid Activated Gel Diverter. Paper SPE 29824 presented at the Middle East Oil Show, Bahrain, 11-14 March.

Mohamed, S.K., Nasr-El-Din, H.A., and Al-Furaidan, Y.A. 1999. Acid Stimulation of Power Water Injectors and Saltwater Disposal Wells in a Carbonate Reservoir in Saudi Arabia: Laboratory Testing and Field Results. Paper SPE 56533 presented at the SPE Annual Technical Conference and Exhibition, Houston, Texas, 3–6 October.

Mostofizadeh, B. and Economides, M.J. 1994. Optimum Injection Rate from Radial Acidizing Experiments. Paper SPE 28547 presented at the SPE Annual Technical Conference and Exhibition, New Orleans, Louisiana, 25-28 September.

Nasr-El-Din , H.A., Al-Mohammad, A.M., Al-Aamri, A.M. and Al-Fuwaires, O. 2008. Reaction of Gelled Acids with Calcite. *SPE Production & Operations* **23**(3): 353-361.

Nasr-El-Din, H.A., Al-Mutairi, S.H., and Al-Driweesh, S.M. 2002b. Lessons Learned From Acid Pickle Treatments of Deep/Sour Gas Wells. Paper SPE 73706 presented at the International Symposium and Exhibition on Formation Damage Control, Lafayette, Louisiana, 20–21 February.

Nasr-El-Din, H.A., Taylor, K.C., and Al-Hajji, H.H. 2002a. Propagation of Cross-Linkers Used in In-Situ Gelled Acids in Carbonate Reservoirs. Paper SPE 75257 presented at the SPE/DOE Improved Oil Recovery Symposium, Tulsa, Oklahoma 13–17 April.

Newman, J. 1966. Schmidt Number Correction for the Rotating Disk. *J. of Physical Chemistry* **70**(4): 1327-1328.

Nierode, D.E., and Williams, B.B. 1971. Characteristics of Acid Reactions in Limestone Formations. *SPE Journal*,**11**(4): 406-418.

Roberts, L.D. and Guin, J.A. 1974. The Effect of Surface Kinetics in Fracture Acidizing. *SPE Journal* **14**(4): 385-395.

Rojas, M. R., Müller, A. J., A., and Sáez, E. 2008. Shear Rheology and Porous Media Flow of Wormlike Micelle Solutions Formed By Mixtures of Surfactants of Opposite Charge. *Journal of Colloid and Interface Science* **326**(1): 221–226.

Rosato, D.V., Rosato, D.V., and Rosato, M.G. 2001. *Plastics Design Handbook*. Boston: Kluwer Academic Publishers.

Schechter, R.S. 1992. *Oil Well Stimulation*. New Jersey: Prentice-Hill Inc.

Schramm, G. 2000. *A Practical Approach to Rheology and Rheometry*. 2nd Edition, Germany: Gebrueder HAAKE GmbH, Karlsruhe, Federal Republic of Germany.

Taylor, K.C. and Nasr-El-Din, H.A., 2003. Laboratory Evaluation of In-Situ Gelled Acids for Carbonate Reservoirs. *SPE Journal* **8**(4) 426-434.

Taylor, K.C., Al-Ghamdi, A.H., and Nasr-El-Din, H.A. 2004. Effect of Additives on the Acid Dissolution Rates of Calcium and Magnesium Carbonates. *SPE Production & Operations* **19**(3): 122-127.

Taylor, K.C., and Nasr-El-Din, H.A. 2002. Core Flood Evaluation of In-Situ Gelled Acid. Paper SPE 73707 presented at the International Symposium and Exhibition on Formation Damage, Lafayette, Louisiana, 20–21 February.

Taylor, K.C., Nasr-El-Din, H.A., and Al-Alawi, M.J. 1999. Systematic Study of Iron Control Chemicals Used During Well Stimulation. *SPE Journal* 4 (1): 19–24.

Wang, Y., Hill, A.D. and Schechter, R.S. 1993. The Optimum Injection Rate for Matrix Acidizing of Carbonate Formations. Paper SPE 26578 presented at the SPE Annual Technical Conference and Exhibition, Houston, Texas. 3-6 October.

Welton, T.D. and van Domelen, M.S. 2008. High-Viscosity-Yield Acid Systems for High-Temperature Stimulation. *SPE Production & Operations* **23** (2): 177-183.

Wineman, A.S., and Rajagopal, K.R. 2000. *Mechanical Response of Polymers – An Introduction.* United Kingdom: Cambridge University Press, Cambridge.

Woo, G.T., Lopez, H., Metcalf, A.S., and Boles, J.1999. A New Gelling System for Acid Fracturing. Paper SPE 52169 presented at the Mid-Continent Operations Symposium, Oklahoma City, Oklahoma, 28-31 March.

Yeager, V. and Shuchart, C. 1997. In-Situ Gels Improve Formation Acidizing. *Oil & Gas Journal* **95** (3): 70–72.

APPENDIX A

The developed model can be divided into two parts connected in parallel as it shown in **Fig. 3.2**. The first part is a modeled as a spring and a dashpot in series with each other (Maxwell Model). Therefore, the stress-strain relationship for this arrangement can represent by Maxwell model:

$$\left(\frac{d/dt}{E} + \frac{1}{\mu} \right) \sigma_1 = \frac{d\,\varepsilon}{dt} \quad \text{.....(A.1)}$$

While the second part is only a dashpot, which the stress-strain relationship can be represent by Eq. A.2

$$\sigma_2 = \mu_1 \frac{d\,\varepsilon}{dt} \quad \text{.....(A.2)}$$

Based on the parallel rearrangement for two parts: the total strain achieved for overall system is equal to the strain achieved in part1 which is equal to the strain achieved in part 2. The total applied stress, σ, will be equal to stress in part 1 plus stress in Part 2.

$$\sigma = \sigma_1 + \sigma_2 \quad \text{.....(A.3)}$$

In order to introduce the total stress σ, stresses σ_1 and σ_2 must have the same differential operator coefficient. This arranged by multiplying Eq. A.2 with $\left(\frac{d/dt}{E} + \frac{1}{\mu} \right)$, giving:

$$\left(\frac{d/dt}{E} + \frac{1}{\mu} \right) \sigma_2 = \left(\frac{d/dt}{E} + \frac{1}{\mu} \right) \mu_1 \, d\varepsilon/dt \quad \text{.....(A.4)}$$

Eqs. A.1 and A.4 can now be added, giving

$$\left(\frac{d/dt}{E} + \frac{1}{\mu} \right) (\sigma_1 + \sigma_2) = \left(\frac{d/dt}{E} + \frac{1}{\mu} \right) \mu_1 \frac{d\varepsilon}{dt} + \frac{d\varepsilon}{dt} \quad \text{.....(A.5)}$$

Finally, Eq. A.5 can be written as

$$\frac{1}{E} \frac{d\sigma}{dt} + \frac{\sigma}{\mu} = \frac{\mu_1}{E} \frac{d^2\varepsilon}{dt^2} + \left(\frac{\mu_1}{\mu} + 1 \right) \frac{d\varepsilon}{dt} \quad \text{.....(A.6)}$$

Applying Creep test behavior on Eq. A8, where σ = constant, dσ/dt = 0, and $J = \varepsilon/\sigma$ will lead to Eq. A.7.

$$\frac{\mu_1}{E} \frac{d^2 J}{dt^2} + \left(\frac{\mu_1}{\mu} + 1 \right) \frac{dJ}{dt} - \frac{1}{\mu} = 0 \quad \text{.....(A.7)}$$

Eq. A.7 is a second order linear non-homogenous ordinary differential equation with constant coefficients that can be written as

$$\frac{d^2 J}{dt^2} + \left(\frac{(\mu_1 + \mu)E}{\mu\mu_1} \right) \frac{dJ}{dt} - \frac{E}{\mu\mu_1} = 0 \quad \text{……………………………..…………..…(A.8)}$$

Using the solving procured for second order linear non-homogenous ODE, the Solution obtained is:

$$J(t) = C_1 - \frac{E}{\mu\mu_1} + C_2 e^{-\left(\frac{(\mu_1 + \mu)E}{\mu\mu_1} \right) t} \quad \text{…………………………..……..………..…(A.9)}$$

The following conditions were used to determine the constants C_1, and C_2

$J(0) = 0$ $\quad\quad\quad\quad$ $t = 0$

$J(\infty) = 1/E$ $\quad\quad\quad\quad$ $t = \infty$

$$J(t) = \frac{1}{E} \left(1 - e^{-\left(\frac{(\mu_1 + \mu)E}{\mu\mu_1} \right) t} \right) \quad \text{……………………..……..…(A10)}$$

VITA

Name: Ahmed Mohamed Mohamed Gomaa

Address: 507 Richardson Building, Petroleum Engineering Department, Texas A&M University, College Station, Texas, 77840-3116

Email: Ahmed.gomaa@pe.tamu.edu

Education: B.S., Petroleum Engineering, Cairo University, 2004

M.S., Petroleum Engineering, Cairo University, 2007

Ph.D., Petroleum Engineering, Texas A&M University, 2011